STRUCTURE-FUNCTION STUDIES ON A BACTERIAL METALLOISOMERASE: *ESCHERICHIA COLI* GLYOXALASE I

by

Susan Louise Clugston

A thesis
presented to the University of Waterloo
in fulfilment of the
thesis requirement for the degree of
Doctor of Philosophy
in
Chemistry

Waterloo, Ontario, Canada, 2000

The University of Waterloo requires that signatures of all persons using or photocopying this thesis. Please sign below, and give address and date.

ABSTRACT

STRUCTURE-FUNCTION STUDIES ON A BACTERIAL METALLOISOMERASE: *ESCHERICHIA COLI* GLYOXALASE I

The glyoxalase system removes cytotoxic α-ketoaldehydes from the cell. The first enzyme in this system, glyoxalase I (GlxI), is a metalloenzyme which catalyzes the isomerization of the nonenzymatically formed hemiacetal of methylglyoxal and glutathione to *S*-D-lactoylglutathione. Our investigations have focused on the bacterial GlxI enzyme isolated from ***Escherichia coli***. We have previously demonstrated that *E. coli* GlxI is a homodimeric protein, which is maximally active in the presence of Ni^{2+} and shows no activity with Zn^{2+}. This is in marked contrast to GlxI from *Homo sapiens*, *Saccharomyces cerevisiae*, and *Pseudomonas putida* that are active with Zn^{2+}. To extend our knowledge of glyoxalase I and the factors affecting this unexpected metal activation in *E. coli* GlxI, numerous kinetic analyses, structural studies, and sequence comparisons have been performed.

Examination of the kinetic parameters for *E. coli* GlxI indicated that the K_m remains relatively constant in the presence of several catalytic metal ions. However, the activity of the enzyme is significantly altered. Maximal activity is observed in the Ni^{2+}-reconstituted GlxI enzyme, with decreasing activity seen with the following metals; Co^{2+}, Mn^{2+}, Fe^{2+}, and Cd^{2+}. No activity was observed in the presence of Zn^{2+}, Cu^{2+}, Mg^{2+}, or Ca^{2+}. Metal analyses and isothermal titration calorimetry (ITC) were utilized to determine that the enzyme binds one mole of metal per mole of dimeric enzyme, including Zn^{2+} and Cu^{2+} which produce an inactive enzyme. The ITC analyses also indicated that the metal ions are very tightly bound to the enzyme with association constants (K_a) greater than 10^7-10^8 M^{-1}, with the exception of Mn^{2+} which has a K_a of approximately 10^6 M^{-1}. Metal competition studies suggested that exchange of the metal ion can occur, the rate of which is dependent upon the concentration, incubation temperature, and nature of the competing metal ions. Differential scanning calorimetry indicated that the metal-bound enzyme is significantly more stable than the apoenzyme, with the melting temperatures increasing 7-21°C in the presence of a metal ion.

Extensive structural studies were performed on *E. coli* GlxI. The chemical shift from a ^{113}Cd NMR study on Cd^{2+}-GlxI was consistent with oxygen and nitrogen ligands around the metal, as predicted based on sequence similarity to the *H. sapiens* GlxI enzyme. Electron paramagnetic resonance (EPR) analysis of Mn^{2+}-GlxI indicated an octahedral metal environment. X-ray absorption spectroscopy (XAS) on Ni^{2+}-GlxI confirmed these findings. However XAS analysis of the Zn^{2+}-substituted enzyme suggested the metal was penta-coordinate. These findings were confirmed by extensive protein crystallographic studies. The structure of *E. coli* GlxI is composed of βαβββ motifs, which serve to place GlxI as a member of a structural superfamily. The metal ligands in the *E. coli* GlxI active site were identified as His5, Glu56, His74, and Glu122. Two water molecules complete the octahedral coordination around Ni^{2+}, Co^{2+}, and Cd^{2+}. Interestingly, in *E. coli* Zn^{2+}-GlxI, the metal has only one water molecule and hence a trigonal bipyramidal coordination. It appears that an octahedral metal environment is required to produce an active enzyme.

The first metal ligand, His5, was changed by site-directed mutagenesis to a glutamine, the ligand found in the *H. sapiens* enzyme. Surprisingly, the metal affinity of this mutant *E. coli* GlxI enzyme was greatly decreased. Although the activities were reduced, the enzyme was still most active with Ni^{2+}, but low levels of activity were observed in the presence of Zn^{2+}. This ligand evidently appears to affect the metal binding properties of the enzyme, but is not the sole factor determining the metal selectivity in this enzyme.

To extend our knowledge of the sequence variation in glyoxalase I and to identify putative GlxI enzymes in other organisms, the sequence of *E. coli* GlxI was utilized to search the National Center for Biotechnology Information sequence databases. Twenty-eight putative GlxI sequences were identified, including nineteen from pathogenic organisms. Comparative analysis of these sequences revealed consistent alterations between the bacterial GlxI sequences and the *H. sapiens* GlxI sequence. One such alteration results in the active site of *E. coli* GlxI being much more open compared to the *H. sapiens* GlxI enzyme, as evident in the crystal structures.

The DNA postulated to encode GlxI enzymes from *Yersinia pestis* and *Pseudomonas aeruginosa* were isolated and placed in overexpression vectors. Preliminary studies indicated these sequences do indeed encode enzymes with GlxI activity. Furthermore, addition of $NiCl_2$ but not $ZnCl_2$ was observed to increase the activity of these enzymes.

ACKNOWLDGEMENTS

I would like to express my sincere appreciation and gratitude to Dr. John Honek. He has been a superb research supervisor, an excellent teacher, mentor, and friend. For this I am forever grateful.

I am also thankful to Dr. Elisabeth Daub for construction of the GlxI expression plasmids, and advice on SeMet incorporation and site-directed mutagenesis studies. Betsey has been a valued friend, and of course I am grateful to her for Toby.

I would like to acknowledge the members of the Honek lab, in particular Peter Sampson, Mark Vaughan, and Jennifer Steere for their friendship, chemistry advice, and coffee breaks. There are several undergraduate students who I would like to thank for their contributions to this work, including Hoa Ly, who synthesized the transition state analogue inhibitors, Rieko Yajimi for performing initial kinetic characterization of *E. coli* Co^{2+}-, Cd^{2+}- and Mn^{2+}-GlxI, and Grace Konrath for preliminary studies on Cu^{2+}- and Fe^{2+}-GlxI.

Thanks to the Biological Mass Spectrometry Laboratory for ESMS analyses, and in particular Amanda Doherty-Kirby. Dr. Patricia Schulte's assistance and advice on the use of PHYLIP and the construction of the phylogenic tree was invaluable. Tracy Fowler in the Solutions Analytical Lab is thanked for metal analysis, and Dr. Harold Frey for DSC studies.

I am also indebted to our numerous collaborators for their insightful contributions to our understanding and knowledge of GlxI, including Drs. Molly He and Brian Matthews for crystallographic analyses. Gerard Davidson and Dr. Michael Maroney for XAS studies, Dr. Doug Markham for EPR analysis. Valerie Robertson for ^{113}Cd NMR data acquisition, and Ellen Stokvis and Dr. Albert Heck for analysis of non-covalent complexes of GlxI by ESI-MS.

I also thank my committee members, Drs. Gary Dmitrienko, Guy Guillemette, and Janet Wood. The financial support from the University of Waterloo and the Natural Sciences and Engineering Research Council is gratefully acknowledged.

Finally, I thank Eugene and my parents for their constant love, support, and understanding, and of course thanks to Georgie and Toby for watching over me.

TABLE OF CONTENTS

LIST OF TABLES

Chapter 2

Chapter 3

Chapter 4

Chapter 5

Appendix A

Appendix C

Appendix D

Appendix F

LIST OF FIGURES

Chapter 1

Chapter 2

Chapter 3

Chapter 4

Chapter 5

Appendix B

Appendix C

Appendix E

Appendix F

LIST OF ABBREVIATIONS

Å	Angstrom
AA	Atomic absorption
Amp	Ampicillin
bp	Base pair
Carb	Carbenicillin
CD	Circular dichroism
Da	Dalton
DHAP	Dihydroxyacetone phosphate
DMSO	Dimethyl sulfoxide
DNA	Deoxyribonucleic acid
DTNB	5,5'-dithiobis-2-nitrobenzoic acid
EDTA	(Ethylenedinitrilo)tetraacetic acid
EPR	Electron paramagnetic resonance
ESI-TOF	Electrospray ionization time-of-flight
ESMS	Electrospray mass spectrometry
ESR	Electron spin resonance
EXAFS	Extended x-ray absorption fine structure
FPLC	Fast protein liquid chromatography
ΔG	Gibb's free energy change
G3P	Glyceraldehyde-3-phosphate
gloA	DNA encoding *E. coli* glyoxalase I
GlxI	Glyoxalase I (*S*-lactoylglutathione methylglyoxal lyase (isomerizing))
GlxII	Glyoxalase II (*S*-2-hydroxyacylglutathione hydrolase)
GlxIII	Glyoxalase III
Gly-Gly	Glycylglycine
GSH	Glutathione (reduced) (γ-L-glutamyl-L-cysteinylglycine)
h	Hour
ΔH	Enthalpy change
HEPES	4-(2-Hydroxyethyl)-1- piperazine ethane sulphonic acid
HMQC	Heteronuclear multiple quantum coherence
IC_{50}	Inhibitor concentration at which enzymatic activity is reduced by 50%
ICP	Inductively coupled plasma
IEF	Isoelectric focusing
IPTG	Isopropyl-β-D-thiogalactopyranoside
ITC	Isothermal titration calorimetry
K_a	Association constant
K_d	Dissociation constant
K_i	Inhibition constant
LB	Luria-Bertani growth media
LB_{Amp}	Luria-Bertani media supplemented with ampicillin

LB_{Carb}	Luria-Bertani media supplemented with carbenicillin
M	Molar
M9	Minimal media
MAD	Multiwavelength anomalous diffraction
MES	2-(*N*-Morpholino)ethanesulfonic acid
MG	Methylglyoxal
min	Minute
MIR	Multiple isomorphous replacement
MOPS	3-(*N*-Morpholino)propanesulfonic acid
m/z	Mass to charge ratio
NCBI	National Center for Biotechnology Information
nm	Nanometer
NMR	Nuclear magnetic resonance
OD	Optical density
PDB	Protein Databank
PCR	Polymerase chain reaction
pGL10	Inducible plasmid containing the *E. coli* glyoxalase I DNA
pGL11	Plasmid containing the DNA encoding the H5Q mutant *E. coli* GlxI
pGL12	Plasmid containing the DNA encoding the C-terminal truncated *E. coli* GlxI
PMSF	Phenylmethanesulfonyl fluoride
psi	Pounds per square inch
rpm	Revolutions per minute
s	Second
ΔS	Entropy change
SDS-PAGE	Sodium dodecylsulfate polyacrylaminde gel electrophoresis
SeMet	Selenomethionine
TIM	Triosephosphate isomerase
TOCSY	Total correlated spectroscopy
TOH	Tritium enriched water
Tris	Tris(hydroxymethyl)aminomethane
TSA	Transition state analogue
V	Volt
W	Watt
XANES	X-ray absorption near-edge structure
XAS	X-ray absorption spectroscopy

Note: The standard 3 letter and 1 letter codes for the amino acids and 1 letter base short forms for DNA have been utilized throughout this thesis.

CHAPTER 1

INTRODUCTION

1.1 The Glyoxalase System

The glyoxalase system converts 2-ketoaldehydes into their corresponding 2-hydroxycarboxylic acids (Vander Jagt, 1989; Thornalley, 1998). The first enzyme in this system, glyoxalase I (GlxI; *S*-D-lactoylglutathione methylglyoxal lyase (isomerizing), EC 4.4.1.5) is a metalloenzyme that catalyzes the isomerization of hemithioacetals formed non-enzymatically from glutathione (γ-L-glutamyl-L-cysteinylglycine; GSH) and cytotoxic α-ketoaldehydes into α-hydroxythioesters. Glyoxalase II (GlxII; *S*-2-hydroxyacylglutathione hydrolase, EC 3.1.2.6) then hydrolyzes the α-hydroxythioesters to the corresponding non-cytotoxic α-hydroxycarboxylic acids, regenerating GSH. The natural substrate *in vivo* for the glyoxalase reaction is believed to be methylglyoxal (MG) and hence the final product is D-lactate (Figure 1.1; Vander Jagt, 1989).

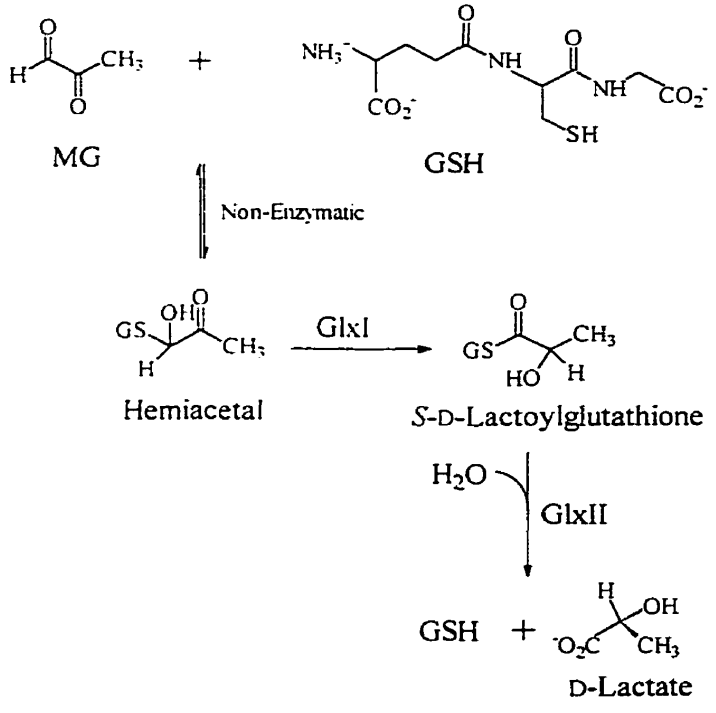

Figure 1.1: The reactions catalyzed by the two component glyoxalase system.

1.2 Historical Perspective

First identified in 1913, the glyoxalase system was believed to be involved in glycolysis due to the production of lactate (Dakin and Dudley, 1913a; Dakin and Dudley, 1913b; Neuberg, 1913a; Neuberg, 1913b). However, following the finding that glycolysis could occur in the absence of GSH, an essential cofactor in the glyoxalase reaction, and that D-lactate was generated, not L-lactate found in glycolysis, the physiological role of the glyoxalase system remained unknown (Lohmann, 1932; Racker, 1954). Furthermore, intermediates were found in the conversion from methylglyoxal to lactate suggesting the involvement of more than one enzyme in this system (Jowett and Quastel, 1933; Yamazoye, 1936; Racker, 1951). By 1948, two independent enzymes were identified, GlxI and GlxII (Hopkins and Morgan, 1948). Although the reaction catalyzed by glyoxalase I is an isomerization, GlxI was classified by the Enzyme Commission as a lyase based on the early knowledge of the reaction mechanism (Davis and Williams, 1969). Initially it was believed that GlxI used GSH and MG as substrates, rather than the non-enzymatically formed hemiacetal now known to be the single substrate in the reaction (Davis and Williams, 1969; Kurasawa et al., 1976).

The function of the glyoxalase system has been the focus of much speculation. Szent-Györgyi and coworkers had postulated that a derivative of methyglyoxal may be the so called "retine" or growth retarder, while glyoxalase I was "promine" or a growth promoter by removal of growth inhibitory MG (Együd and Szent-Györgyi, 1966a; Együd and Szent-Györgyi, 1966b). A great deal of effort was invested in examining retine and promine from various tissues, their effect on cell growth and division, and any possible link to cancer (Szent-Györgyi, 1965; Szent-Györgyi et al., 1967). Methylglyoxal was already known to be cytotoxic, as discussed below, and it was postulated that the presence of MG suppressed cell growth (Együd and Szent-Györgyi, 1966a). When damage occurred, glyoxalase I was released to remove MG and hence cell division was no longer inhibited. It is now known that the factors controlling cell growth and division are much more complicated with numerous controlling factors. As such, MG and the glyoxalase system are no longer believed to be the retine/promine pair or a direct cancer link (Reviewed by Kalapos, 1999). However, there does appear to be a definite trend in the levels of MG and GlxI in certain types of cancer cells,

making this a target for anticancer agents, as discussed below. Based on the current understanding, it is now believed that the primary function of the glyoxalase system is to remove toxic MG, as discussed in the following section.

1.3 Methylglyoxal

1.3.1 Sources

One of the major sources of methylglyoxal in the cell is believed to be from a side product in the triosephosphate isomerase (TIM; EC 5.3.1.1) catalyzed reaction (Figure 1.2; Iyengar and Rose, 1981). TIM generally catalyzes the conversion of dihydroxyacetone phosphate (DHAP) to glyceraldehyde-3-phosphate (G3P) in glycolysis. However, the phosphoenediolate intermediate produced by this enzyme has been found to eliminate phosphate, breaking down to MG rather than G3P (Pompliano et al., 1990; Richard, 1991). Although only 1 of 100,000 turnovers of TIM produces methylglyoxal, the physiological concentrations of TIM and triose phosphates suggest that approximately 0.4 mM of MG would be produced in each cell every day (Richard, 1991).

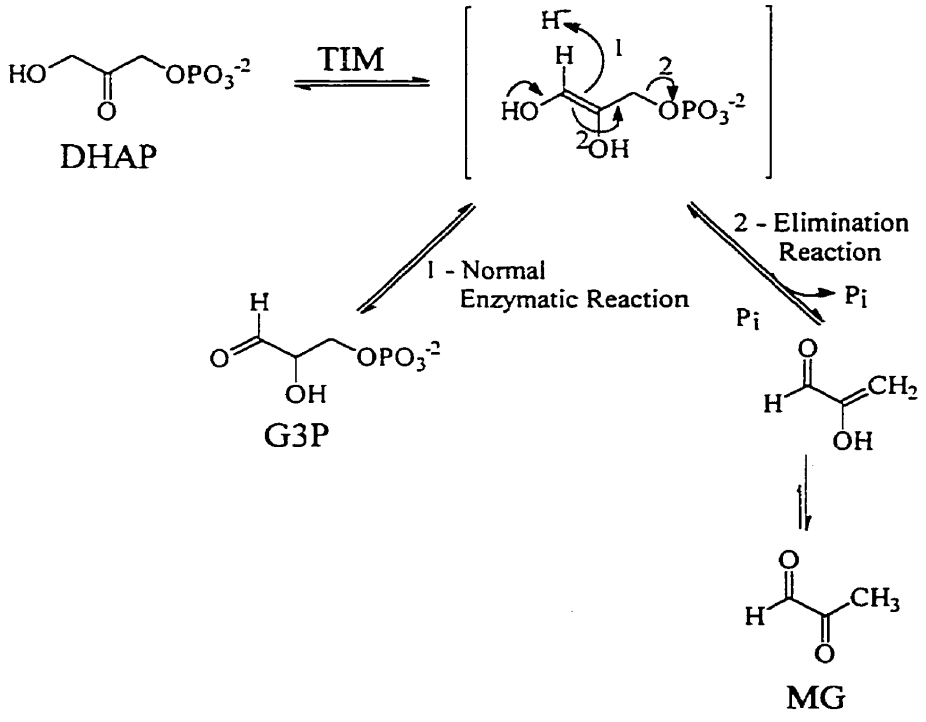

Figure 1.2: The normal reaction catalyzed by triosephosphate isomerase and the side reaction which produces methylglyoxal.

Methylglyoxal is also produced by a number of other cellular sources (Figure 1.3; For a review see Inoue and Kimura, 1995). Methylglyoxal synthase (EC 4.2.99.11) converts dihydroxyacetone phosphate (DHAP), a glycolytic intermediate, into MG (Hopper and Cooper, 1971; Hopper and Cooper, 1972). As such it has been suggested that the glyoxalase system provides a glycolytic bypass imparting a non-phosphorylated route for the conversion of triose phosphates to pyruvate (Cooper, 1984). Further support for the involvement of MG synthase in this postulated bypass is evident by the inhibition of the enzyme by inorganic phosphate and relief of this inhibition by DHAP (Hopper and Cooper, 1971). In fact, examination of MG synthase deficient cells suggests production of MG from DHAP is important for survival and adaptation for bacterial growth under certain conditions, alleviating the stress from the accumulation of phosphorylated intermediates (Ferguson et al., 1998; Tötemeyer et al., 1998).

MG synthase from *Escherichia coli* has been the best studied (Hopper and Cooper, 1971; Hopper and Cooper, 1972; Tötemeyer et al., 1998), with a 1.9 Å crystal structure having recently been released (Saadat and Harrison, 1999). The structure confirmed mechanistic predictions based on site-directed mutagenesis studies that a conserved aspartate residue in the active site appears to function as the catalytic base (Saadat and Harrison, 1998). The reaction mechanism is believed to be similar to that of TIM. The substrate for each is DHAP and they are both thought to form an enediol(ate) phosphate intermediate. The MG synthase reaction mechanism would be similar to that illustrated by route 2 in Figure 1.2, the phosphate elimination side reaction of the TIM reaction. The crystal structure of MG synthase is a homohexamer composed of interacting five-stranded β/α proteins, dissimilar to the α/β barrel characteristic of TIM. As such it has been proposed that these two enzymes are related by convergent evolution, having dissimilar sequences and structures but catalyzing similar mechanisms (Saadat and Harrison, 1999).

In addition, MG is produced by monoamine oxidase (EC 1.4.3.4) from the deamination of aminoacetone, a product of the oxidation of L-threonine by threonine dehydrogenase and spontaneous decarboxylation (Elliott, 1959; Green and Elliott, 1964; Lyles and Chalmers, 1995; Murata et al., 1986b; Ray and Ray, 1987). Acetone has been suggested to be an additional cellular source of MG by the action of acetol dehydrogenase or an acetone-inducible monooxygenase on 1-hydroxyacetone (acetol) (Inoue and Kimura,

1995). MG has also been found to form non-enzymatically from triose phosphates (Phillips and Thornalley, 1993).

1.3.2 Routes of Degradation

As mentioned, the glyoxalase system is believed to be the primary route for the removal of methylglyoxal from the cell. However, there are other routes for its degradation (For reviews see Cooper, 1984; Murata et al., 1989; Inoue and Kimura, 1995). Methylglyoxal reductase (EC 1.1.1.78) has been studied primarily from microbial sources with a few reports on mammalian sources such as goat and porcine liver (Ray and Ray, 1984; Saikusa et al., 1987). The *E. coli* enzyme appears to have a relatively broad substrate specificity, accepting several 2-oxoaldehydes, including glyoxal, methylglyoxal, phenylglyoxal, and 4,5-dioxovalerate, in addition to aldehydes such as glycoaldehyde and acetaldehyde (Saikusa et al., 1987). The enzyme from rat and goat liver also has very broad substrate specificity, unlike the *S. cerevisiae* and *H. mrakii* enzymes. In addition, the *E. coli* and goat liver MG reductase enzymes can utilize NADPH or NADH, whereas those from *S. cerevisiae*, *H. mrakii*, and *A. niger* require NADPH (Murata et al., 1989; Inoue and Kimura, 1995).

MG is also converted to pyruvic acid in an NAD^+- or $NADP^+$-dependent manner by the action of α-ketoaldehyde dehydrogenase (EC 1.2.1.23 and 1.2.1.49; Ray and Ray, 1982), and to acetol by the NADPH-dependent aldose reductase (Vander Jagt et al., 1992), well reviewed by Inoue and Kimura (1995). Figure 1.3 summarizes the sources of MG and the routes of MG degradation.

Although other routes for the removal of MG exist, the glyoxalase system is believed to be the primary means of metabolism. In 1983 Penninckx and coworkers demonstrated that when *S. cerevisiae* was grown on glycerol GlxI was induced (Penninckx et al., 1983). As glycerol is a source of DHAP that can be converted to MG, it was postulated that the increased GlxI activity detected was in response to increase levels of this toxic electrophile. Similar results were observed when MG was added directly to the growth media (Penninckx et al., 1983). Furthermore, a *S. cerevisiae* cell line deficient in GlxI production secreted MG into the media and then died when the cells were exposed to growth on glycerol (Penninckx et al., 1983). A contradictory report was presented in 1996 however (Inoue and Kimura, 1996). In this work both wild-type yeast and that without a functional GlxI enzyme survived when

grown on glycerol. Introduction of the GlxI gene on a multicopy plasmid did increase the resistance of the *S. cerevisiae* cells to added MG however (Inoue and Kimura, 1996). The observed cellular survival when grown on glycerol in this study is most likely due to removal of MG by alternate routes, as described above. It is also important to note that the conditions in which the yeast cells were grown in the laboratory setting may not accurately depict the stresses that may be applied to cells in a natural environment. Hence the importance of a functional glyoxalase system may be more evident under other conditions.

Recently, additional support has been presented indicating the essential role glyoxalase I plays in removing toxic methylglyoxal (Ferguson et al., 1998; MacLean et al., 1998; Tötemeyer et al., 1998). As we have demonstrated in our own work (Clugston et al., 1998a), increased expression of GlxI in *E. coli* leads to increased tolerance to methylglyoxal (MacLean et al., 1998). Furthermore, a mutant cell line lacking a functional GlxI displays a low rate of MG detoxification and its viability quickly decreases when exposed to MG (MacLean et al., 1998).

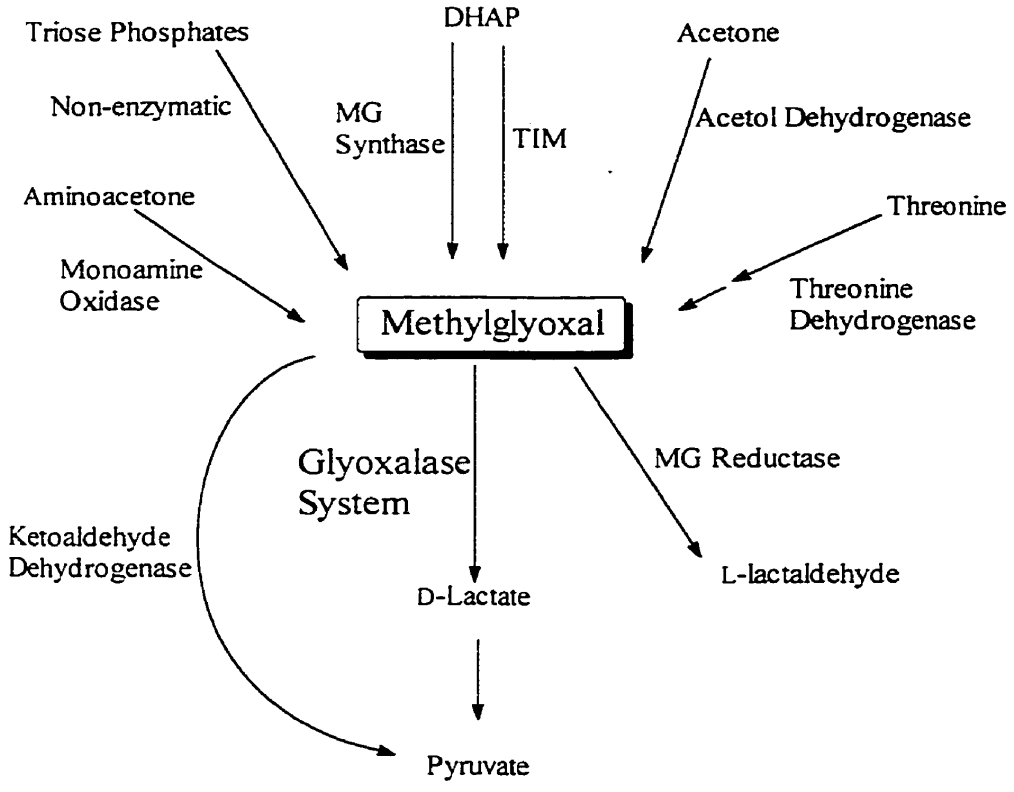

Figure 1.3: Summary of the primary sources of methylglyoxal with routes of degradation.

1.3.3 Toxic Effects

It has been known for many years that methylglyoxal can inhibit cell growth (French and Freedlander, 1958; Együd and Szent-Györgyi, 1966a; Vander Jagt, 1975). MG has been demonstrated to be cytostatic to *E. coli* K12 cells at a level of 1 mM (Vander Jagt, 1975). Due to its electrophilic nature, MG can covalently modify cellular macromolecules which results in cell death (Ferguson et al., 1998; Thornalley, 1998). The synthesis of DNA, RNA, and protein is inhibited by MG (White and Rees, 1982; Hou et al., 1995). MG has been shown to inhibit translation by reacting with the 7-methylguanosine cap structure of mRNA (Kozarich and Deegan, 1979). In addition, MG binds and modifies arginine, lysine, and cysteine residues in proteins (Lo et al., 1994b; Westwood and Thornalley, 1995; Uchida et al., 1997; Westwood et al., 1997). The reaction of MG with proteins has also been found to produce what is termed advanced glycation end products (AGEs) (Papoulis et al., 1995; Ahmed et al., 1997; Oya et al., 1999). The formation of AGEs *in vivo* has been linked to aging and complications associated with diabetes (Oya et al., 1999 and references therein). The relationship between MG, GlxI, and various disease states will be further examined in the following section.

1.4 The Role of Glyoxalase I in Disease States and as a Drug Target

As the function of the glyoxalase system is to remove cytotoxic methylglyoxal, this system has long been a target of interest for inhibitor design (Kermack and Matheson, 1957; Vince and Daluge, 1971; Vince et al., 1971; Barnard and Honek, 1989; Barnard et al., 1994, for example). Selective inhibition of GlxI can block the metabolism of MG and take advantage of the toxic effects of MG to restrict cell growth. A great deal of effort has been placed on developing new potential anticancer agents that target the glyoxalase system (Creighton et al., 2000). It has also been proposed that GlxI inhibitors may be useful antimalarial agents (Vander Jagt et al., 1990; Barnard et al., 1994; Thornalley et al., 1994) and similarly, selective inhibition of bacterial GlxI enzymes might be advantageous for antibacterial therapy. In addition the glyoxalase system appears to be involved in the complications associated with diabetes mellitus, as a result of increased MG levels (Thornalley, 1998). Our current understanding of the roles GlxI and MG play in these disease states is briefly reviewed below. Further knowledge of the glyoxalase system and its

mechanism of action could aid in the understanding and/or the possible treatment of these diseases.

1.4.1 Glyoxalase I Inhibitors as Anticancer Agents

Consideration of the glyoxalase system as an anticancer target was recognized as early as 1969, and is recently receiving renewed interest (Vince and Wadd, 1969; Vince and Daluge, 1971; For a recent review see Creighton et al., 2000). As a result, numerous studies have focused on developing better inhibitors, particularly for GlxI (Reviewed in Douglas and Shinkai, 1985; Thornalley, 1995; Creighton et al., 2000). Inhibition of GlxI could lead to a build up of toxic methylglyoxal in the cell, resulting in cell death. Although there are other pathways for the removal of MG, the glyoxalase system is believed to be the primary route.

Rapidly dividing cells have increased flux through glycolysis. Therefore as would be expected, tumor tissues have been reported to have an abnormally high rate of glycolysis and hence increased production of MG (Ranganathan et al., 1995; Thornalley, 1998). Furthermore, although some reports are contradictory, variation in the level of both GlxI and GlxII in certain types of cancer cells has been observed (Ayoub et al., 1993; Di Ilio et al., 1995; Tew et al., 1996). In general, GlxI activities appear higher in tumor samples compared to normal tissue (Ranganathan et al., 1995; Davidson et al., 1999). This may be due to the requirement to remove increased levels of MG. In contrast, GlxII activity is lower in some types of cancer cells compared to non-cancerous tissues (Ayoub et al., 1993). Therefore the hydrolysis of GSH analogue-based GlxI inhibitors should be slower in tumor tissues. As such this is thought to be a means of selectively inhibiting GlxI in cancerous cells. However, since the inhibitor will be slowly broken down by GlxII, high levels or steady administration of the inhibitor may be required to reach toxic levels.

Many inhibitors of GlxI initially studied did not appear to be effective anticancer agents. Problems with delivery of the drugs into the cells were most likely the cause. Glutathione monoethyl esters were shown to be transported into many types of cells more readily than GSH itself (Anderson et al., 1985). In 1992 it was found that the [glycyl, glutamyl] diethyl ester of a known GlxI inhibitor, *S*-bromobenzylglutathione, diffused into leukemia cells and underwent deesterification by intracellular esterases to yield the active inhibitor (Lo and Thornalley, 1992). Preparation of effective inhibitors in this ethyl ester

prodrug form has proved successful for delivery into the cells where GlxI inhibition can occur (Hamilton and Creighton, 1992; Murthy et al., 1994; Thornalley et al., 1996a; Thornalley et al., 1996b; Kavarana et al., 1999). A recent report has presented a new method to deliver GlxI enzyme inhibitors into the cell (Hamilton et al., 1999). The ethylsulfoxide form of a GSH-based inhibitor was shown to enter cells by an acyl interchange with intracellular GSH, which is catalyzed by GSH transferase. This method is much more efficient than the diffusion of ethyl ester derivatives across cell membranes, hence the intracellular concentrations reach higher levels making the inhibitors more potent *in vivo*.

We have reported the synthesis and kinetic analysis of our own transition state analogue inhibitor (Ly et al., 1998). Figure 1.4 illustrates the structure of the inhibitors tested and the postulated reaction intermediate they were designed to mimic. The replacement of the sulfur with a carbon should ensure GlxII can not hydrolyze the inhibitor, which would lower its effective concentration in the cell. Although effective inhibitors against GlxI from *S. cerevisiae* (K_i = 1.9 μM when R_1 = H and R_2 = CH_3), and *E. coli* (Chapter 2), they were not potent anticancer agents (Ly et al., 1998). The ethyl ester derivatives were also synthesized to improve transport into the cells but unfortunately this did not significantly enhance their anticancer effectiveness.

A

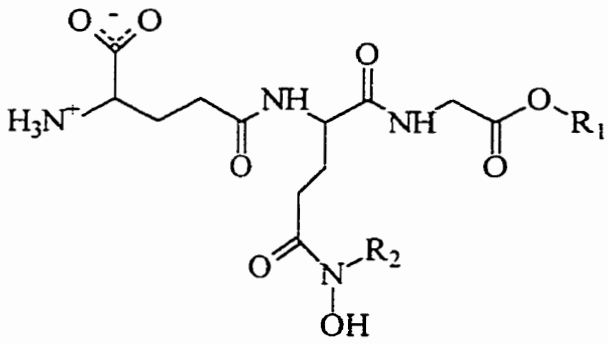

B

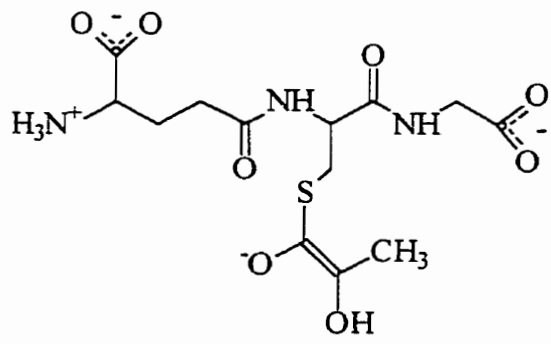

R_1 = H or CH_2CH_3
R_2 = H or CH_3

Figure 1.4: Structure of (A) the transition state analogues and their ethyl ester derivatives tested as GlxI inhibitors (Ly et al., 1998) and (B) the intermediate in the GlxI reaction these inhibitors were designed to mimic.

There has been a recent report of successful tumor treatment with a competitive inhibitor of GlxI. *S*-(*N*-*p*-Chlorophenyl-*N*-hydroxycarbamoyl)glutathione, an enediol analogue, was administered to mice as the [glycyl, glutamyl]diethyl ester prodrug and was found to inhibit the growth of solid tumors (Sharkey et al., 2000). This recent finding demonstrates that GlxI inhibitors may have the potential to be anticancer agents.

It was demonstrated that human leukemia cells which are resistant to antitumor drugs have higher expression of glyoxalase I than non-resistant leukemia cells (Sakamoto et al., 2000). Furthermore, treatment of these resistant cells with a known GlxI inhibitor, *S*-*p*-bromobenzylglutathione, in the cyclopentyl diester form, in conjunction with the antitumor agent etoposide, resulted in apoptosis (Sakamoto et al., 2000). A similar increase in apoptosis was not observed in leukemia cells not normally drug resistant. It is possible that the resistance is as a result of MG detoxification by GlxI but there may be other unidentified factors involved. Not only does this study implicate GlxI as a drug resistance factor but provides a means of overcoming some drug resistances observed in cancer treatment. This finding is even more significant given that GlxI could also be used as a cellular marker to identify drug resistant tumors.

1.4.2 Glyoxalase I as an Antimalarial Target

There are four known species of malaria parasites that infect humans, *Plasmodium vivax*, *Plasmodium ovale*, *Plasmodium malariae*, and *Plasmodium falciparum* (Knell, 1991). The protozoan, *P. falciparum*, is the most common malarial parasite in Africa and causes the most serious illness (Kreier, 1980; Knell, 1991). This parasite has been shown to have a very high glycolytic rate (Sherman, 1979; Homewood and Neame, 1980). Increased flux through glycolysis suggests higher levels of MG may be produced in the parasite than in the human erythrocyte cells. Analysis of the activities of the glycolytic enzymes as well as GlxI and GlxII in both the *P. falciparum* and the host erythrocyte indicated a marked increase in these enzymes in the parasite (Vander Jagt et al., 1990). Furthermore the production of both D- and L-lactate was increased in parasite-infected erythrocytes. Thus it has been concluded that higher levels of the glyoxalase enzymes are responsible for production of D-lactate, most likely to remove toxic MG resulting from increased glycolysis. Kinetic properties of both

GlxI and GlxII suggest that the parasite is not simply using the glyoxalase system of the host cell, but encodes its own glyoxalase enzymes (Vander Jagt et al., 1990).

Based on these findings, it has been suggested that inhibitors of the glyoxalase system may be effective antimalarial agents (Vander Jagt et al., 1990). Examination of the effect of known GlxI inhibitors on *P. falciparum* suggests this is a valid assumption. *S-p*-bromobenzylglutathione, was demonstrated to induce toxicity in this parasite when administered in its diethyl ester form (Thornalley et al., 1994). Several additional GSH analogues have also been shown to have antimalarial activity at the micromolar levels (Barnard et al., 1994). Our recently reported hydroxamate-based transition state analogue inhibitors (Figure 1.4) displayed moderate antimalarial activity with IC_{50} values in the range of 5-20 μM (Ly et al., 1998). Based on these results further development of effective GlxI inhibitors should be investigated.

It was initially suggested that GlxII could also be a target for antimalarial agents (Vander Jagt et al., 1990). The detoxification of MG would be restricted and *S*-D-lactoylglutathione would accumulate, potentially depriving the parasite of essential GSH. It has since been observed that the malaria parasite has a very high level of GSH synthesis and ability to reduce GSSG (glutathione disulfide; Atamna and Ginsburg, 1997; Ayi et al., 1998). This provides the parasite with effective protection against oxidative injury, unlike the host cell in which GSH levels are reduced (Atamna and Ginsburg, 1997). This observation implies that inhibitors of GlxII would not be able to rapidly deprive the parasite of GSH to cause cell death.

1.4.3 The Role of MG and Glyoxalase I in Diabetes

Modifications in the glyoxalase system during hyperglycemia have focused attention on the role MG and GlxI may play in diabetes (For a review see Thornalley, 1995; Thornalley, 1998). As mentioned, advanced glycation endproducts (AGEs) have been associated with several disease states, including complications associated with diabetes (Thornalley, 1998). The effect of the glycation of proteins within the cell is reduced by the high turnover of intracellular protein. In contrast, long lived extracellular proteins accumulate these adducts over time. Although generally thought to be caused primarily by glucose, it has been demonstrated that reactive α-oxoaldehydes, particularly methylglyoxal, can also cause

glycation under physiological conditions (Thornalley et al., 1999). Combining this information with the observation that MG concentrations are found to be elevated in the kidney cortex and medulla, lens, and blood of diabetic rats, and the levels of MG, *S*-D-lactoylglutathione, and D-lactate are elevated in the blood of diabetic humans, suggests that the role of MG in diabetes requires further investigation (Phillips et al., 1993; McLellan et al., 1994). Furthermore, aminoguanidine, an agent used to prevent diabetic complications, was demonstrated to scavenge methylglyoxal thereby preventing modification of human plasma proteins under physiological conditions (Lo et al., 1994a).

It has also been observed that GlxI and GlxII levels were higher in insulin-dependent diabetics suffering from diabetic complications (Ratliff et al., 1996), yet MG levels were still elevated. Partial inhibition of GlxI in endothelial cells by a GSH-based competitive inhibitor led to increased AGE formation under high glucose conditions (Shinohara et al., 1998). When incubated with high levels of glucose, a two-fold increase in both MG and D-lactate was observed for normal cells, whereas for those with increased GlxI production, the level of MG was not increased but D-lactate production was ten-fold higher (Shinohara et al., 1998). This clearly illustrates the increased production of MG during hyperglycemia and the requirement for its removal by GlxI. The observation that overexpression of GlxI completely prevented hyperglycemia-induced AGE formation provides a definitive link between the detoxification of MG and diabetic complications (Shinohara et al., 1998). Differences in the levels and activity of the glyoxalase enzymes may provide a clue to the differences observed in diabetic patients and their susceptibility to developing complications.

1.5 Glyoxalase I Properties and Distribution

Glyoxalase I has been identified in numerous organisms, from *E. coli* to *H. sapiens* (Vander Jagt, 1989; Ranganathan et al., 1993; Clugston et al., 1998a). Given its widespread existence it is expected to play a key role in the cell, and currently it is believed that the detoxification of methylglyoxal is that role. As such, GlxI has been proposed as a novel anticancer, antimalarial, and putative antibacterial target by taking advantage of the toxic effects of MG. To target GlxI with specific inhibitors, molecular details of the enzyme structure and reaction mechanism must be known. The current knowledge regarding the few

well studied glyoxalase I enzymes is outlined below, in addition to a listing of the known features of additional GlxI enzymes which have been identified.

1.5.1 Homo sapiens Glyoxalase I

Identification and Sequence Variation

The GlxI enzyme studied in the most detail to date is that from *Homo sapiens*. Although the sequence of the 184 amino acid protein was not reported until 1993, a great deal was already known about this enzyme (Kim et al., 1993; Ranganathan et al., 1993). Early work indicated that this homodimeric enzyme had a stoichometry of one zinc per enzyme subunit and that removal of the zinc eliminated catalytic activity (Aronsson et al., 1978). Furthermore, two alleles of GlxI appeared to exist in humans, inherited in an autosomally co-dominant fashion, giving rise to three kinetically indistinguishable enzymes, which could be separated by ion-exchange chromatography (Aronsson et al., 1979; Schimandle and Vander Jagt, 1979). The alteration has since been ascribed to a change in one amino acid residue; position 111 is either alanine or glutamic acid (Kim et al., 1995). A trend in the population genetics of these alleles was identified (Thornalley, 1991). The frequency of the alanine containing GlxI allele is highest in native Alaskan-Eskimo and Indian populations. The frequency of this allele was found to decrease geographically to the south and east, with minimum levels in the Papua New Guinea native tribes as well as Australian populations. Large variations in the levels of this allele in regions of the United States and Europe could be attributed to the immigrant populations in these areas (Thornalley, 1991). The glutamic acid containing allele is proposed to be the ancestral gene and the second allele is proposed to have arisen following mutation of position 111 to alanine. Attempts were made to link the frequency of this allele to the occurrence of insulin-dependent diabetes mellitus but no trend was observed (Thornalley, 1991).

Metal Ion Requirement

The catalytic activity of *H. sapiens* GlxI is inhibited by metal chelators, and metal analysis has indicated the presence of one metal per enzyme subunit (Aronsson et al., 1978). Although the metal measured in these studies was Zn^{2+}, it was originally believed that the natural metal was Mg^{2+} as enzymatic activity was most easily restored by reconstitution with

Mg^{2+}. Activity was also observed with Co^{2+} and Mn^{2+}, and although inactive the *H. sapiens* GlxI enzyme also binds Cd^{2+} and Cu^{2+} (Sellin et al., 1983a and references therein). Although no direct report of the enzymatic activity of *H. sapiens* GlxI in the presence of Ni^{2+} is available, the rat erythrocyte enzyme was found to be active with Ni^{2+}, although only 40% of the activity observed with Mg^{2+} (Han et al., 1977). It is generally assumed that the same activation would be observed for the *H. sapiens* enzyme (Sellin et al., 1983a). As our studies on the *E. coli* GlxI enzyme illustrate (Clugston et al., 1998a), this may not be a safe assumption.

The dissociation constants (K_d) of various divalent metals for *H. sapiens* GlxI were evaluated by a modification of equilibrium dialysis utilizing nitrilotriacetic acid as a metal buffer to establish low levels of the divalent metal under analysis. From this study it was determined that Zn^{2+} had the highest affinity, followed by Co^{2+}, Mn^{2+}, and finally Mg^{2+} with K_d approximately 10^4-fold lower than that of Zn^{2+} (Sellin and Mannervik, 1984). This evidence combined with the metal analysis, which detected Zn^{2+} in the purified enzyme led to the conclusion that Zn^{2+} was in fact the native metal in *H. sapiens* GlxI.

Spectroscopic studies on *H. sapiens* GlxI reconstituted with various metals also indicated that the metal ion may play a vital role in the enzymatic catalysis as outlined below. Hence the essential metal is catalytic rather than just a structural element in glyoxalase I.

Structural Studies

Replacement of the bound Zn^{2+} with Mn^{2+} in *H. sapiens* GlxI permitted analysis of the environment around the metal by electron paramagnetic resonance (EPR) studies and the nuclear relaxation rate of water protons (Sellin et al., 1982a; Sellin et al., 1982b; Sellin et al., 1983a). These studies, in the presence of the reaction product, *S*-D-lactoylglutathione, suggested that the metal was not close enough for direct interaction. This led to the hypothesis that the substrate binds outside of the first coordination sphere of the metal and that there are one or two water molecules coordinated in the active site, interacting with the metal and substrate. Addition of the competitive inhibitor, *p*-bromobenzylglutathione, appeared to occlude one of the exchangeable water ligands (Sellin et al., 1982a). Further EPR studies were performed with *H. sapiens* GlxI reconstituted with Co^{2+}, as well as the inactive Cu^{2+} form (Sellin et al., 1983b; Sellin et al., 1987). The results of these analyses indicated

that the metal was in an octahedral environment with at least one nitrogen-containing ligand. X-ray absorption spectroscopy (XAS) on the Zn^{2+} site in *H. sapiens* GlxI was also consistent with an octahedral environment around the metal (Garcia-Iniguez et al., 1984).

H. sapiens GlxI has been recently crystallized in several forms. The native enzyme containing Zn^{2+} was cocrystallized with each of the following glutathione analogues, *S*-benzylglutathione, a putative transition state analogue, and a proposed product analogue. In addition a mutant form of the enzyme was crystallized (PDB 1FRO, 1QIN, 1QIP, 1BH5 respectively; Cameron et al., 1997; Ridderström et al., 1998; Cameron et al., 1999a). The structure of the native *H. sapiens* GlxI enzyme with *S*-benzylglutathione bound is illustrated in Figure 1.5. Each monomer of this homodimeric enzyme consists of two domains, linked by a 20 amino acid connector region. In addition, each subunit has an N-terminal arm that wraps around the other subunit but does not directly interact with another region of the protein. Each of the four domains of the protein has a general βαβββ topology, forming a mixed β-sheet. Although the sequence homology is quite low, the N- and C-terminal domains of each subunit share a similar structural fold, the βαβββ motif, leading the authors to suggest that 3D domain swapping has occurred in this protein structure (Cameron et al., 1997). Based on this βαβββ topology, glyoxalase I represents a member of a previously unidentified structural superfamily (Armstrong, 1998; Bergdoll et al., 1998; Laughlin et al., 1998), as discussed in Chapter 5.

The two active sites in *H. sapiens* GlxI are located at the interface of the subunits with each active site containing a catalytic metal, Zn^{2+}. There are four residues from the protein, Gln34, Glu100, His 127, and Glu173, two from each subunit, and one water molecule coordinated to the metal, in a square pyramidal arrangement (Cameron et al., 1997). The geometry appears to be octahedral with one ligand missing. Presumably a second water ligand is precluded due to the presence of the benzylglutathione in the active site. Crystallization of the enzyme in the presence of a glutathione analogue, *S-p*-nitrobenzyloxycarbonylglutathione, designed to mimic the reaction product complex reveals two water molecules around the active site zinc, as does the structure of the Q33E/E172Q double mutant cocrystallized with hexylglutathione (Ridderström et al., 1998; Cameron et al., 1999a), supporting this assumption. This apparent octahedral geometry is consistent with the earlier spectroscopic studies outlined.

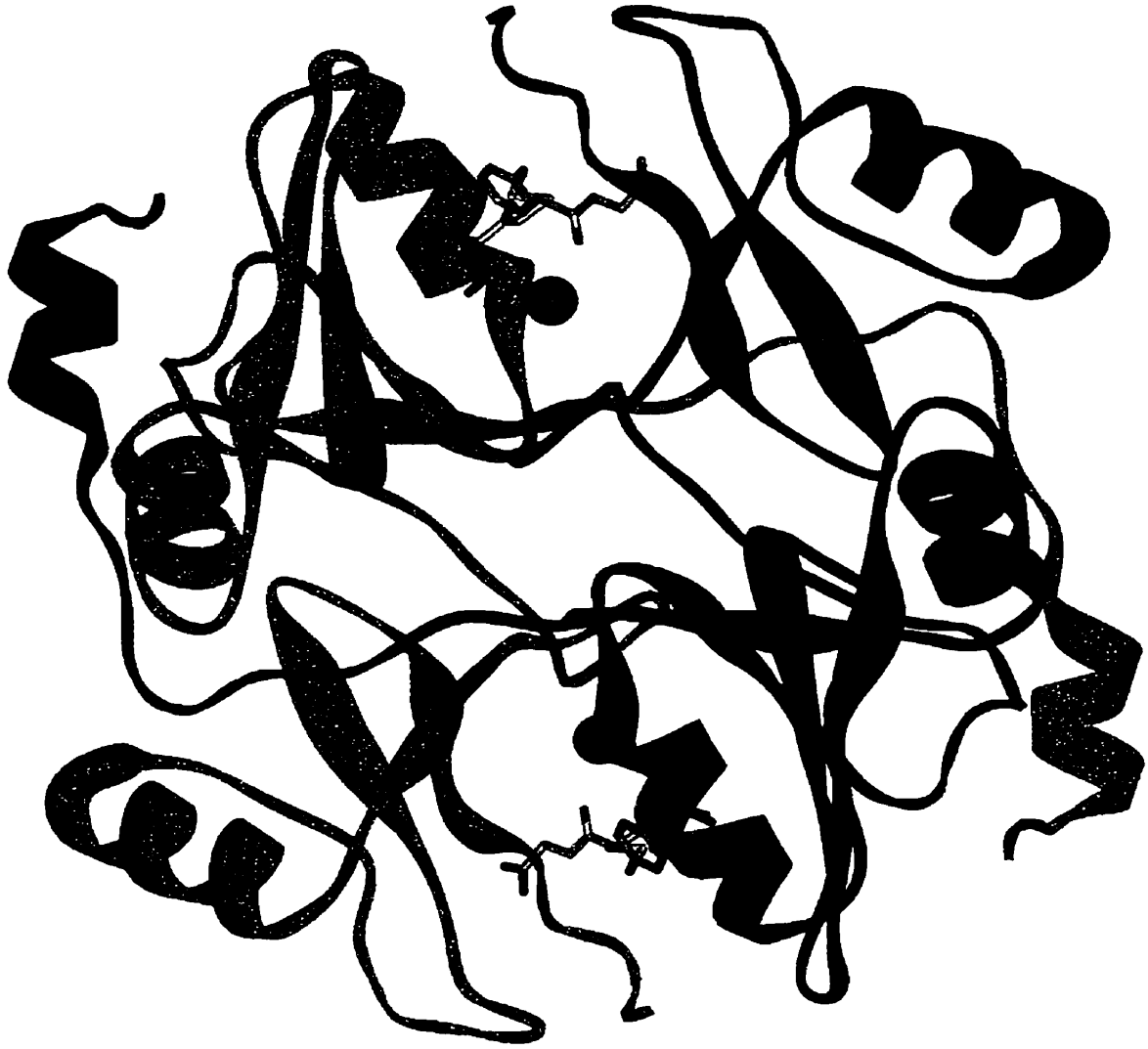

Figure 1.5: Structure of *H. sapiens* glyoxalase I (PDB 1FRO; Cameron et al., 1997). Subunit A is illustrated in green, B in blue, the zinc atom in black space fill, and the benzylglutathione cocrystallized in the active site is displayed as sticks. (Prepared with WebLab Viewer Pro ver 3.7, Molecular Simulations Inc.)

The results of the crystallization of the native enzyme with a putative transition state analogue and product mimic, as well as the mutant form of the enzyme are discussed further in relation to the proposed mechanism of action (Section 1.6).

It should be noted that the N-terminal methionine is not present in the active form of the enzyme and hence is not in the crystal structure. The numbering of the full *H. sapiens* GlxI sequence, including the N-terminal methionine, will be utilized throughout this thesis.

1.5.2 Pseudomonas putida Glyoxalase I

Sequence Analysis

The sequence encoding glyoxalase I from *P. putida* was first reported in 1988 and updated in 1994 (Rhee et al., 1988; Lu et al., 1994). The gene encodes a 173 amino acid protein with a subunit molecular weight of 19.4 kDa, following the loss of the N-terminal methionine in the active 172 amino acid enzyme (Lu et al., 1994). We have shown that the GlxI protein sequence from *P. putida* is 55% identical to that from *H. sapiens*, with an additional approximately 10% sequence similarity (Clugston et al., 1997). Interestingly, this bacterial GlxI more closely resembles the eukaryotic sequences than the other known and predicted GlxI sequences from bacterial sources (Lu et al., 1994; Clugston, 1997; Clugston et al., 1997).

Metal Requirement

For several years the metal usage in *P. putida* GlxI was unclear as published reports were contradictory. The addition of Zn^{2+} was reported to inhibit the activity of the enzyme by 75% at 0.1 mM and completely at 1.0 mM (Rhee et al., 1986). On the other hand, 1.0 mM of Mg^{2+}, Mn^{2+}, Ca^{2+}, Ni^{2+}, Cu^{2+}, or Hg^{2+}, had no apparent effect on the enzyme activity in this study. Furthermore, the addition of the metal chelator EDTA had no effect on the activity (Rhee et al., 1986). This led to the assumption that *P. putida* GlxI did not require a metal ion for catalytic activity. Within two years however, the same research group reported the expression and purification of *P. putida* GlxI and indicated that 0.9 mole of zinc was detected per mole of enzyme (Rhee et al., 1988). When the DNA was resequenced in 1994 and the possible role of a catalytic loop in the enzyme examined, there was no report on the metal content in the enzyme leaving this issue unresolved (Lu et al., 1994; Lan et al., 1995). The

recent report on the structural features of *P. putida* GlxI clarified this by confirming that the enzyme did require zinc and that there were two zinc ions in the active, dimeric enzyme (Saint-Jean et al., 1998), similar to that observed in *H. sapiens* GlxI. There was however, no report of any investigation into the activation with other metals at this point.

Structural Studies

The characterization of *P. putida* GlxI appears to have been plagued with discrepancies, from the DNA sequencing to the metal requirement as well as the structural properties. Contrary to initial reports that indicated that *P. putida* GlxI was monomeric, the active form of the enzyme is a homodimer with two zinc atoms bound (Rhee et al., 1986; Saint-Jean et al., 1998). Furthermore, the proposal that there exists a "catalytic loop" near the active site of the enzyme, similar to that observed in triosephosphate isomerase (TIM) does not appear to be valid (Joseph et al., 1990; Pompliano et al., 1990; Lan et al., 1995). Circular dichroism and fluorescence studies were performed with *H. sapiens* and *P. putida* GlxI in the presence of an enediol analogue and *S*-D-lactoylglutathione. These analyses suggested that a small conformational change occurs upon binding, consistent with the movement of such a catalytic loop region (Lan et al., 1995). Proteolytic cleavage experiments pointed to a region with moderate sequence homology to the catalytic loop in TIM, including a glutamate residue which functions as the catalytic base in TIM. Mutation of the corresponding glutamate in *P. putida* GlxI (Glu93) led to inactivation of the enzyme. Based on these results it was concluded that Glu93 is the catalytic base in the glyoxalase I reaction. However, no metal analysis was performed on the enzyme at any stage. We now know, based on the structure of the homologous *H. sapiens* GlxI (Cameron et al., 1997), that this glutamate is actually a ligand to the catalytic Zn^{2+}. Therefore the loss of activity upon mutation of this residue was most likely due to loss of the metal ion.

A more detailed analysis of the structural features of *P. putida* GlxI has recently been reported, revealing the dimeric nature of this enzyme, and confirming the binding of two zinc ions to the active dimer (Saint-Jean et al., 1998). In addition, structural studies were performed utilizing circular dichroism and size exclusion chromatography. This work displays an interesting feature of this protein, which has been proposed to have undergone 3D domain swapping, based on the structure of the *H. sapiens* GlxI enzyme (Cameron et al.,

1997). It was found that although the most active form of the *P. putida* enzyme is a dimer with two zinc atoms bound, a monomeric form containing only one zinc atom can be observed under particular conditions. Treatment of the dimer with glutathione produces a monomeric enzyme with a k_{cat} approximately one-fifth that of the dimeric enzyme and k_{cat}/K_m about fifteen-fold lower (Saint-Jean et al., 1998). Removal of the GSH results in slow dimerization of the protein.

Three-dimensional (3D) domain swapping is described as a means for stable dimeric proteins to evolve from monomeric proteins. For this to occur the two domains of the monomer covalently linked by a flexible hinge, open at the hinge permitting dissociation followed by reassociation of the domains from different monomers (Saint-Jean et al., 1998 and reference therein). The result is a two-fold symmetrical dimer. It is proposed that the monomeric form of *P. putida* GlxI is simply an alternate conformation of the protein, with the same characteristic active site. The domains are believed to be the βαβββ motifs observed in the *H. sapiens* GlxI crystal structure (Cameron et al., 1997; Section 1.5.1). Figure 1.6 summarizes the proposed evolution of the 3D domain swapped GlxI, which supports the evolutionary development of this superfamily described in Chapter 5.

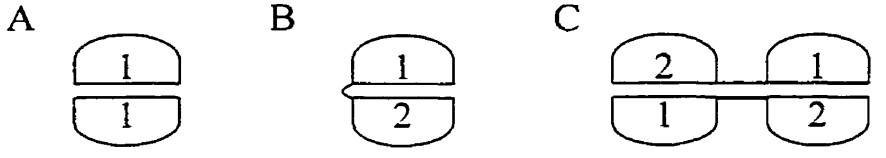

Figure 1.6: Various schematic representations of the structures of glyoxalase I during its proposed evolution. (A) Homodimer of a single domain protein, (B) monomer of a 2-domain protein, believed to be the structure of the monomeric *P. putida* GlxI observed, and (C) general arrangement of the 3D domain swapped dimer with two intermolecular domain-domain interfaces, as observed in the dimeric *H. sapiens* and *P. putida* GlxI enzymes. The numbers are used to represent the structural symmetry in the various forms of the enzyme. (Adapted from Saint-Jean et al., 1998)

1.5.3 Saccharomyces cerevisiae Glyoxalase I

Enzyme Characterization and Metal Effects

Numerous reports are available for the inhibition of yeast glyoxalase I, as this enzyme is commercially available (Ekwall and Mannervik, 1970; Vince et al., 1971; Ray and Ray, 1987; Barnard and Honek, 1989; Ly et al., 1998, for example). Fewer accounts however have been published describing the characteristics of the enzyme itself. Early reports indicated that the enzyme was inhibited by EDTA suggesting it is also a metalloenzyme (Aronsson et al., 1978; Murata et al., 1986c). However it initially appeared that the *S. cerevisiae* GlxI enzyme was not reactivated by the addition of divalent metals (Aronsson et al., 1978). Further studies revealed that partial reactivation of the yeast enzyme could be achieved with Mg^{2+}, Ca^{2+}, and to a small extent with Mn^{2+} (Murata et al., 1986c). However, Ni^{2+}, Co^{2+}, and Fe^{2+} had no effect on the inactive apoenzyme. Comparative studies with *H. sapiens* GlxI have indicated that both enzymes contain zinc in their native form (Aronsson et al., 1978; Marmstål et al., 1979; Murata et al., 1986c). Unlike the *H. sapiens* enzyme, *S. cerevisiae* GlxI contains only one zinc per active enzyme, but the *S. cerevisiae* GlxI enzyme is monomeric, whereas the *H. sapiens* GlxI enzyme is dimeric (Aronsson et al., 1978; Marmstål and Mannervik, 1978). Furthermore, equilibrium dialysis revealed binding of only one competitive inhibitor, *S-p*-bromobenzylglutathione, to the monomeric yeast enzyme, reconfirming the suggestion that only one active site exists in GlxI from *S. cerevisiae* (Marmstål and Mannervik, 1979).

Sequence Similarity and Analysis

Interestingly, although the *S. cerevisiae* GlxI enzyme has been studied for many years its sequence was not available until 1995 (NCBI Accession # CAA89948) and not published until the following year (Inoue and Kimura, 1996). The DNA encodes a 326 amino acid protein with a molecular weight of 37.2 kDa (Inoue and Kimura, 1996). As mentioned, *S. cerevisiae* GlxI is a monomeric enzyme. The monomer however is double the size of each subunit in the dimeric *H. sapiens*, *P. putida*, and *E. coli* GlxI enzymes. Analysis of the sequence of the *S. cerevisiae* GlxI enzyme with the other known and postulated GlxI sequences led to the proposal that this enzyme is the result of a gene duplication event forming a fused dimer gene product (Ridderström and Mannervik, 1996; Clugston, 1997;

Clugston et al., 1997). The N- and C-terminal halves of this large GlxI sequence are homologous to each other as well as to the sequences of the monomeric GlxI enzymes. Putative GlxI sequences which also appear to be the result of a similar gene duplication event have also been identified in *Schizosaccharomyces pombe*, and the plants, *Brassica oleracea*, and *Sporobolus stapfianus* (Clugston et al., 1998b). As the dimers are now joined, and the active site of the *H. sapiens* GlxI enzyme is known to be at the dimer interface the enzyme may not be able to form a second functional active site. It is possible that only one metal and inhibitor binding site exists because the protein can not reach the correct confirmation in the second site due to the linkage of the dimers. Additionally, not all of the metal ligands are completely conserved in each of the halves of the sequences. Based on alignment with the *H. sapiens* GlxI enzyme, and knowledge of the ligands to the metal identified in the *H. sapiens* GlxI crystal structure (Cameron et al., 1997), the putative metal ligands have been identified (Clugston, 1997; Clugston et al., 1998b). The first metal ligand, a glutamine in the *H. sapiens* GlxI enzyme but a histidine in most of the other sequences, is either a Gln or His in each of the halves of these duplicated proteins. The second ligand is universally conserved as a glutamate. The third and fourth ligands however are not conserved in the C-terminal halves of the *S. stapfianus* or *B. oleracea* sequences, being a glutamine versus histidine for the third ligand, and a valine rather than a glutamate for the final ligand (Clugston, 1997; Clugston et al., 1998b). Although these sequences are just postulated to encode GlxI at this stage, examination of these enzymes will most likely reveal that they only bind one metal ion as seen in the *S. cerevisiae* GlxI enzyme.

A similar duplication event was observed in the biphenyl-cleaving extradiol dioxygenase enzyme (Han et al., 1995) in which there is low sequence homology between the two halves but great structural similarity. Additionally, only the C-terminal domain binds iron as not all of the metal ligands have been conserved in the second site. This enzyme is now known to be a member of the βαβββ structural superfamily of which GlxI is a member (Bergdoll et al., 1998). The evolutionary development of these two groups of enzymes is believed to have involved divergent evolution from a common structural motif, a βαβββ module. This is further discussed in Chapter 5.

1.5.4 Other Sources of Glyoxalase I

We have identified numerous putative GlxI sequences in a vast array of organisms (Clugston et al., 1997; Clugston et al., 1998b; Clugston and Honek, 2000; Chapter 5). However, these must only be considered as putative GlxI enzymes before experimental evidence indicates they encode a protein with glyoxalase I activity. Nevertheless, in addition to the knowledge of the three GlxI enzymes outlined and our studies on the *E. coli* enzyme, numerous other GlxI enzymes have been identified and studied to a more limited extent. Several of these enzymes are outlined below.

Plant Sources

The expression of glyoxalase I was examined in *Lycopersicon esculentum* (tomato) and it was observed that stress from treatment with NaCl, mannitol or abscisic acid resulted in an increase in both the mRNA and protein levels in the roots, stem, and leaves (Espartero et al., 1995). It was suggested that a higher demand for ATP in the salt-stressed plant resulted in an enhanced rate of glycoylsis and hence increased levels of methylglyoxal. As a result the expression of GlxI was increased to remove the toxic MG (Espartero et al., 1995).

The 185 amino acid protein from *L. esculentum* has a molecular weight of 20.7 kDa. It was not indicated whether the quaternary nature of the protein was examined. The homology to other dimeric GlxI sequences (Clugston et al., 1997) suggests it would also be dimeric.

Characterization of GlxI from *Glycine max* (soybean) indicates expression is enhanced during cell division, as reported in other plants (Paulus et al., 1993; Skipsey et al., 2000). The purified GlxI enzyme, with a predicted mass based on the sequence of 21 kDa, migrated as a 24 kDa monomer on SDS-PAGE, but as a 38 kDa homodimeric protein with gel permeation chromatography (Skipsey et al., 2000). This is contrary to the initial claim that this enzyme was a 60 kDa heterodimer (Paulus et al., 1993). Although cell growth and expression of *G. max* GlxI in the presence of supplemental $ZnSO_4$ (1.0 mM) produced a protein with higher activity, and three moles of Zn^{2+} per mole of protein subunit, the metal was lost upon dialysis with GSH yet retained full activity. It was suggested that the metal is required for correct assembly of the protein but not required for catalysis (Skipsey et al., 2000). Given the high degree of homology to other known GlxI enzymes and the conservation of the metal ligands

in the protein, it is likely that a metal is required but was not detected in conditions used in these analyses. As the primary thiol in *G. max* is homoglutathione (γ-glutamyl-cysteinyl-β-alanine) rather than glutathione (γ-glutamyl-cysteinylglycine), the analysis of glutathione-utilizing enzymes from this organism has been of interest (Skipsey et al., 2000 and references therein). Kinetic analysis of the purified enzyme indicated no preference for homoglutathione substrate adducts over glutathione adducts (Skipsey et al., 2000).

Recently, the sequence, expression, and crude purification of GlxI from *Triticum aestivum* (wheat bran) have been reported (Johansen et al., 2000). The 37 kDa protein is monomeric with high homology to the GlxI sequence from *S. stapfianus*, indicating GlxI from this source is also the result of a gene duplication event.

Although the sequence has not yet been reported, GlxI isolated from *Aloe vera* was found to be a monomeric 44 kDa protein (Norton et al., 1990), suggesting it too is the result of a gene duplication event producing a fused dimer gene product, resembling the yeast and some of the plant sequences reported. This GlxI enzyme also resembles the *S. cerevisiae* enzyme in its metal activation properties. Full enzyme inhibition was found by treatment with EDTA, however the enzyme could not be reactivated (Norton et al., 1990).

Analysis of the levels of GlxI in *Zea mays* (corn) demonstrated that there is 20-30 times more GlxI in the leaves compared to the roots, consistent with the higher rate of glycolysis and photosynthesis in green tissues, and hence the increased requirement for GlxI to remove toxic MG (Spano et al., 1998). Furthermore, the levels were increased in leaves when subjected to cold stress, whereas no change was detected in the root levels (Spano et al., 1998). No characterization of the GlxI enzyme itself has been reported.

The expression, purification, and characterizaton of *Brassica juncea* (mustard) GlxI has been reported (Deswal and Sopory, 1991). As observed with other plant GlxI enzymes, the apparent mass of the GlxI enzyme based on a denaturing gel is higher than that predicted based on the sequence alone. In fact, the protein with a predicted weight of 24 kDa appears as two bands at 27 and 29 kDa, suggesting the enzyme may undergo posttranslational modification resulting in a heterodimeric enzyme (Deswal and Sopory, 1998; Veena et al., 1999). Further analysis revealed this is a Zn^{2+} enzyme but the apoenzyme can be reactivated by addition of Mn^{2+}, Mg^{2+}, Zn^{2+}, and Ca^{2+} (Deswal and Sopory, 1991; Deswal and Sopory, 1998). As reported for other plant GlxI enzymes, *B. juncea* GlxI expression is upregulated in

response to stresses such as salt and heavy metal (Veena et al., 1999). Recently, it has also been suggested that the activity of *B. juncea* GlxI is regulated by Ca^{2+} and calmodulin (Deswal and Sopory, 1999). This observation is intriguing, as GlxI expression is upregulated by stress and the Ca^{2+}/calmodulin signaling pathway is important in cell division and Ca^{2+} is also involved in stress signaling (Deswal and Sopory, 1999 and references therein). The exact nature of this interaction requires further investigation however.

Microbial Sources

GlxI purified from the yeast *Hansenula mrakii* was shown to be a monomeric 38 kDa protein, although the sequence is not yet known. Interestingly, no inhibition was seen upon addition of EDTA (Inoue et al., 1991). Further analysis of this enzyme is required to confirm this property.

The sequence postulated to encode GlxI from *Neisseria meningitidis* has been identified (Kizil et al., 2000). This 138 amino acid sequence encodes a protein with a calculated molecular weight of 15.7 kDa and high sequence homology to other known and postulated GlxI sequences. An *E. coli* cell line containing a plasmid expressing this protein displayed increased resistance to exogenously supplied methylglyoxal.

GlxI expression imparts increased resistance to methylglyoxal. We exploited this characteristic to identify the multicopy plasmid containing the gene encoding GlxI from a *Salmonella typhimurium* cDNA library (Clugston et al., 1997). This 135 amino acid protein has high homology to the other known and postulated GlxI sequences, including 91% identity to the sequence of the *E. coli* GlxI protein (Clugston, 1997).

Mammalian Sources

Purification and partial characterization of GlxI has been reported for numerous mammalian sources. A selection of these are briefly outlined.

Porcine erythrocyte GlxI has an apparent molecular weight of 52 kDa, is inhibited by EDTA, but could be reactivated by Mg^{2+}, Mn^{2+}, and Ca^{2+} (Mannervik et al., 1972). In addition, the kinetics and inhibition of GlxI from rat liver has been examined and a 43 kDa GlxI enzyme was isolated from mouse liver (Kester and Norton, 1975; Kurasawa et al., 1976).

Purification of GlxI from monkey intestinal mucosa revealed the protein is a homodimer with a native molecular weight of 48 kDa (Baskaran and Balasubramanian, 1987).

Active site modifications on this enzyme revealed the importance of numerous residues on enzymatic activity, and included tryptophan, lysine, and glutamate or aspartate residues. Interestingly, these results also suggested that histidine residues were not important for activity (Baskaran and Balasubramanian, 1987). Although the sequence is unknown it would be expected that the ligands to the metal would be conserved, including at least one histidine.

1.5.5 Escherichia coli Glyoxalase I

We have reported the sequencing and identification of glyoxalase I from *Salmonella typhimurium* (Clugston et al., 1997). However, the research presented in this thesis has focused on the characterization of the highly homologous GlxI enzyme from *Escherichia coli* (Clugston et al., 1998a). With the exception of an early report in which a crude preparation of glyoxalase I isolated from *E. coli* was analyzed for comparative kinetics with the enzyme from yeast sources (Vander Jagt, 1975), there have been no analyses of *E. coli* GlxI available prior to our studies. As outlined in Chapter 2, we have constructed a system for the efficient overexpression and purification of large quantities of apo *E. coli* GlxI (Clugston, 1997; Clugston et al., 1998a). We have shown this microbial glyoxalase I to be a homodimer, contrary to initial reports which suggested all microbial glyoxalase I enzymes were monomeric like that of *S. cerevisiae* (Ridderström and Mannervik, 1996). Furthermore, analysis of the metal activation of *E. coli* GlxI has indicated that unlike other GlxI enzymes reported, *E. coli* GlxI is maximally active in the presence of Ni^{2+} and shows no activity with Zn^{2+}. The structural and mechanistic implications of this unexpected activation are examined in the work presented herein.

1.6 Mechanistic Considerations

The mechanism of the glyoxalase I reaction and the role the metal ion may play in this process has been of interest for many years. Numerous studies have focused on the substrate specificity of the enzyme as well as the role the catalytic metal ion may play in the process.

1.6.1 Substrate Specificity

Although glyoxalase I from various sources has been shown to accept several α-ketoaldehydes and glutathione adducts as hemiacetal substrates, including phenylglyoxal and glyoxal and GSH analogues such as homoglutathione, the *in vivo* substrate is believed to be

the non-enzymatically formed hemiacetal of methylglyoxal and glutathione (Vander Jagt et al., 1972; See Vander Jagt, 1989 for a review). Two stereoisomers of the substrate can be formed, yet the product of the GlxI reaction is not a mixture of isomers but *S*-D-lactoylglutathione. It was initially presumed that the enzyme accepted only one isomer as its substrate. Initial reports appeared to support this theory (Brown et al., 1981). However, it has since been demonstrated by several groups that glyoxalase I actually accepts both isomers of the hemiacetal substrate (Griffis et al., 1983; Creighton et al., 1988; Landro et al., 1992; Rae et al., 1994). Using ^{3}H-labelled GSH, a series of pulse-chase isotope trapping experiments were performed. This work indicated that both diasteriomers were used by GlxI from yeast and porcine erythrocytes (Griffis et al., 1983). An expansion on this work using measured and calculated rate and equilibrium constants for several stages of the glyoxalase reactions, from formation of the hemiacetal substrate, GlxI conversion to *S*-D-lactoylglutathione product, and GlxII catalyzed hydrolysis, support the suggestion that both isomers are utilized by the enzyme with approximately equal efficiency (Creighton et al., 1988). The most definitive example involved the use of a stereochemically "locked" substrate (Figure 1.7). Rather than having GSH combine non-enzymatically with MG, *R*- and *S*-glutathiolacetaldehyde were synthesized and used as the substrate for the GlxI catalyzed reaction. The stereoisomers of the natural hemiacetal substrate of GSH-MG have an estimated interconverion rate of 10-40 s^{-1}. In contrast, the "locked" substrate have a very slow interconversion rate between the isomers. The rate is slow enough that the conversion to the product of the GlxI reaction is favoured (Landro et al., 1992). ^{1}H NMR was utilized to monitor the reaction catalyzed by *H. sapiens* GlxI. It was found that both isomers of the substrate are converted to product, glutathiohydroxyacetone in this case. The isomers are not accepted equally however. The *R*-isomer was converted at a rate of 0.8 s^{-1}, compared to 0.4 s^{-1} for the *S*-isomer (Landro et al., 1992). This work appears to demonstrate that GlxI accepts both isomers of the substrate.

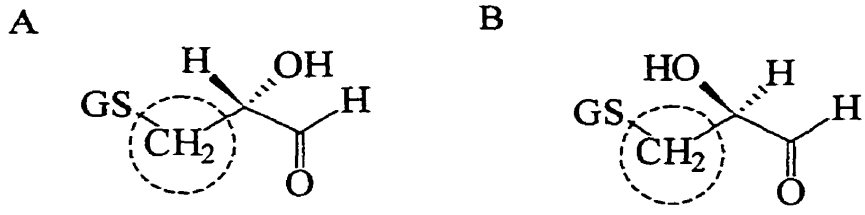

Figure 1.7: Stereochemically "locked" substrate analogue; (A) *R*- and (B) *S*-glutathiolactaldehyde. The methylene group circled is the only structural difference in this analogue compared to the normal substrate, making the proton of interest more difficult to remove and hence the rate of interconversion of the two isomers is greatly reduced. 'GS' represents the glutathione moiety.

1.6.2 Hydride Migration versus Enediol Intermediate

In the GlxI reaction the hemiacetal of MG and GSH is converted to *S*-D-lactoylglutathione. In this process the proton from the C-1 carbon must be removed and the C-2 carbon protonated. There are two ways this could proceed in the reaction mechanism, either by an intramolecular hydride migration (Figure 1.8), or by removal of the proton, endiol(ate) formation, followed by reprotonation at C-2 (Figure 1.9). To distinguish between these two possibilities, isotope exchange experiments were performed. Initially the reaction was performed in tritiated water (TOH) with yeast GlxI. Very little exchange of tritium (less than 4%) into the product was observed, suggesting that the hydride migration was occurring (Rose, 1957). However, the issue was later re-examined utilizing deuterium and a change in the temperature of the reaction with yeast GlxI, monitoring the production of labelled product by NMR (Hall et al., 1976; Hall et al., 1978). Under these conditions a small increase in the incorporation of the deuterium was observed, 15% incorporation at 25°C versus 22% at 35°C (Hall et al., 1976). The low levels of incorporation and lack of evidence in the initial experiment may be due to the active site conformation resulting in a shielded proton transfer. These results confirmed that the reaction did not proceed through a 1,2-hydride shift as originally believed but that an enediol intermediate was formed.

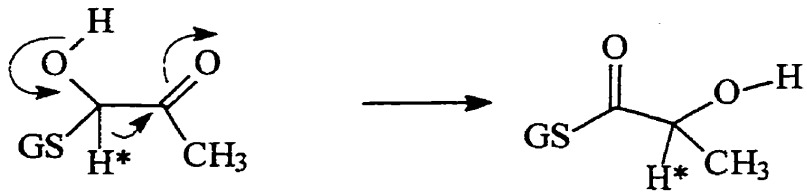

Figure 1.8: A previously proposed mechanism for the glyoxalase I removal of the C-1 hydrogen from the hemiacetal via a hydride migration.

Based on this knowledge a general mechanism has been proposed for the glyoxalase I reaction, summarized in Figure 1.9. The base responsible for the initial deprotonation was not elucidated at this stage, nor was the role of the essential metal ion.

1.6.3 Proposed Mechanism

Solution of the first crystal structure of a glyoxalase I enzyme (Cameron et al., 1997) not only provided a great deal of information regarding the protein structure in general, but also provided valuable knowledge about the catalytic metal site. Examination of the region surrounding the metal in the active site of the *H. sapiens* GlxI enzyme revealed an unexpected finding. There are no suitable residues close enough to function as a catalytic base. This led to the assumption that the metal bound water molecules may be important, as previous studies suggested, or that one of the ligands to the metal has a dual role (Sellin et al., 1982a; Sellin et al., 1982b).

Mannervik and coworkers were of the belief that one of the metal ligands also served as the catalytic base in this reaction, and proceeded to test this hypothesis. Initially methionine 158, in the active site of the enzyme, was mutated to establish any role this residue might play in the catalytic reaction (Ridderström et al., 1997). Analysis of this mutant form of the *H. sapiens* GlxI enzyme confirmed that Met158, a threonine in the *E. coli* enzyme, plays no role in the enzymatic catalysis but rather is involved in substrate binding. Further mutagenesis studies were directed towards the metal ligands. The two glutamate ligands (100 and 173) to the zinc in the enzyme active site were each replaced by glutamines. These two single mutants were found to have minimal enzymatic activity, which could be correlated to the lack of a catalytic metal in the enzyme as determined by inductively coupled plasma atomic emission spectroscopy (Ridderström et al., 1998).

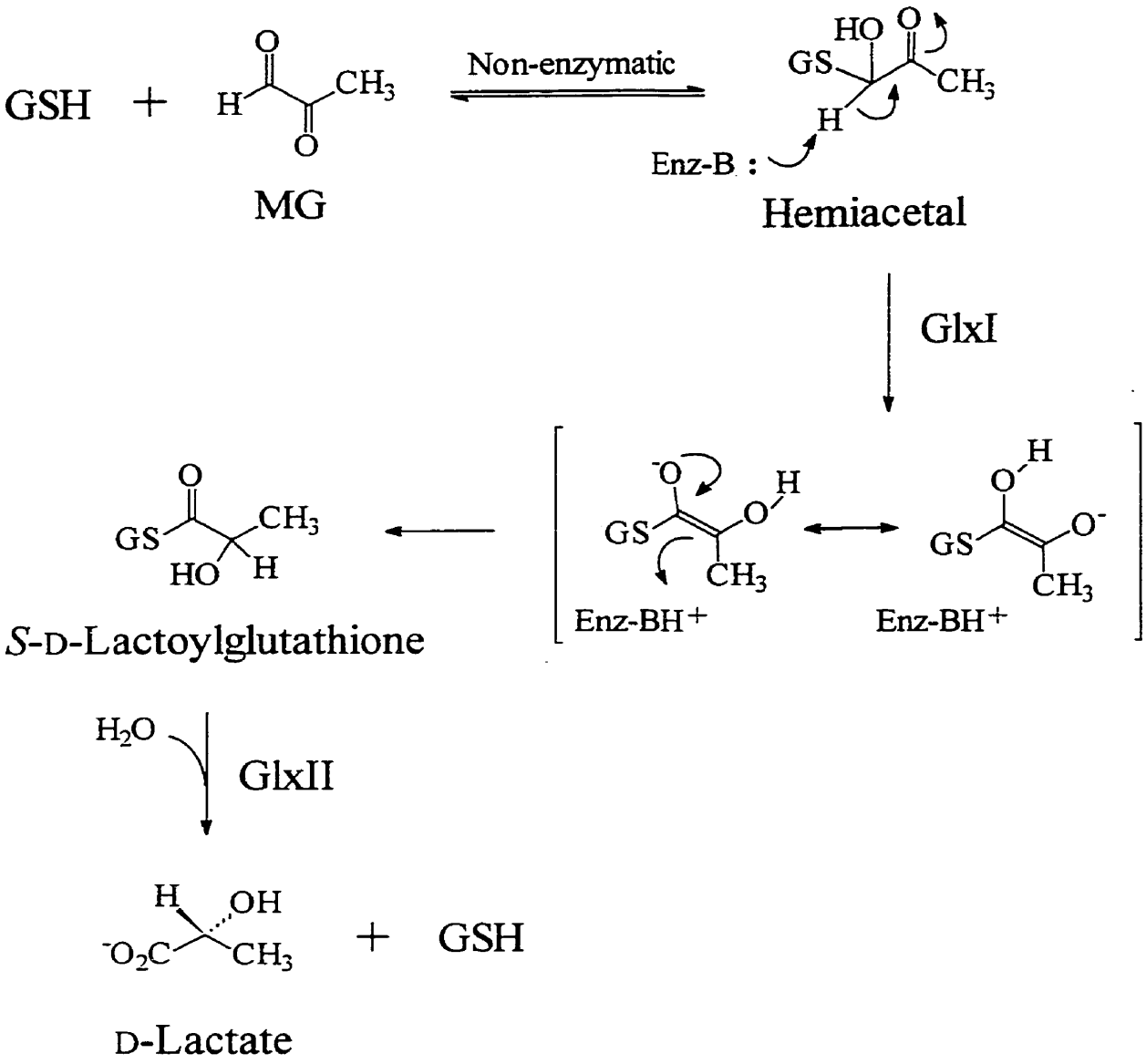

Figure 1.9: The reactions catalyzed by the glyoxalase system, with an enediol intermediate in the GlxI catalyzed reaction.

To compensate for the loss of a charged amino acid in the metal ligands, double mutants were constructed in which glutamine 34 was simultaneously mutated to a glutamate. The full metal complement of one mole of zinc per mole of enzyme subunit was found for the Q34E/E173Q double mutant however no catalytic activity could be detected. (Note: Numbering of the residues in the *H. sapiens* GlxI enzyme corresponds to the sequence including the N-terminal methionine, whereas some published reports refer to the residue numbers following removal of this methionine.) The Q34E/E100Q mutant however only retained 0.3 mole of zinc per mole of subunit and only 1.5% of the activity measured for the wild-type enzyme. It should be noted however that the activities of these enzymes were measured without the addition of supplemental metal to the assay solution. It is possible that the enzymatic activities would be higher had more metal been present. If the affinity of the enzyme for the metal is reduced the enzyme may not be able to bind the metal under the given conditions to reveal enzymatic activity. The crystal structure of the inactive Q34E/E173Q double mutant was determined and revealed no significant alteration in the enzyme active site or metal binding. Based on these results it was concluded that the metal ligand glutamate 173 is directly involved in the catalytic mechanism of the glyoxalase I reaction, perhaps serving as the catalytic base for removal of the C-1 proton from the substrate (Ridderström et al., 1998). Analysis of the crystal structure of the wild-type GlxI enzyme from *H. sapiens* and modeling of the structure revealed that glutamate 173 may lie as close as 4 Å to this carbon suggesting this dual role is possible (Cameron et al., 1997).

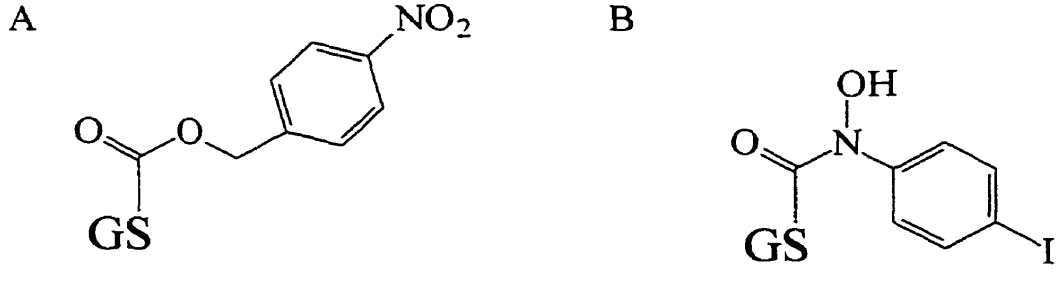

Figure 1.10: (A) A product analogue (NBC-GSH), and (B) putative transition state analogue (HIPC-GSH), cocrystallized with *H. sapiens* GlxI. The 'GS' indicates the glutathione moiety of the molecules.

The crystallographic studies with the *H. sapiens* GlxI enzyme have recently been expanded to include analyses of the enzyme with a putative transition state analogue, *S*-(*N*-hydroxy-*N*-*p*-iodophenylcarbamoyl)glutathione (HIPC-GSH) which is designed to mimic the enediol intermediate believed to form during the reaction. As well a glutathione analogue proposed to mimic the reaction product, *S*-*p*-nitrobenzylcarbonylglutathione (NBC-GSH), was also studied (Cameron et al., 1999a; Figure 1.10).

The structure with the putative transition state analogue bound to the enzyme revealed that the hydroxycarbamoyl group was directly coordinated to the zinc ion, and the one or two water molecules seen around the metal ion in other forms of the *H. sapiens* GlxI crystal structure were not present in this complex (Cameron et al., 1999a). Based on this observation and the results of the mutant forms of the enzyme a detailed mechanism for the GlxI reaction was proposed (Figure 1.11). It is suggested that when the substrate is bound in the enzyme active site the metal bound waters are replaced by the oxygens of the substrate, and glutamate 173 is also displaced. This would result in the 6-coordinate zinc becoming 5-coordinate for the duration of the reaction and the metal ion directly coordinated to the substrate, contrary to previous spectroscopic studies which suggested the presence of intervening water molecules. The glutamate is now able to function as the catalytic base and may be able to abstract the proton from the C-1 carbon of the substrate. The enediolate intermediate which is formed then may be reprotonated at the C-2 carbon, forming the product of the reaction which is then released from the active site (Cameron et al., 1999a).

However, this mechanism does not account for the apparent use of both isomers of the hemiacetal substrate. Although a similar mechanism utilizing glutamate 100 as the catalytic base could be proposed for the *R*-isomer of the substrate, the data does not support this. The position of this residue in relation to the reaction intermediate does not appear to allow reprotonation to form the D-lactoylglutathione isomer required, only the L-isomer would result based on the current analysis (Cameron et al., 1999a). The strengths and weaknesses of this mechanism are further discussed in Chapter 3, as are other possible mechanisms for the GlxI reaction.

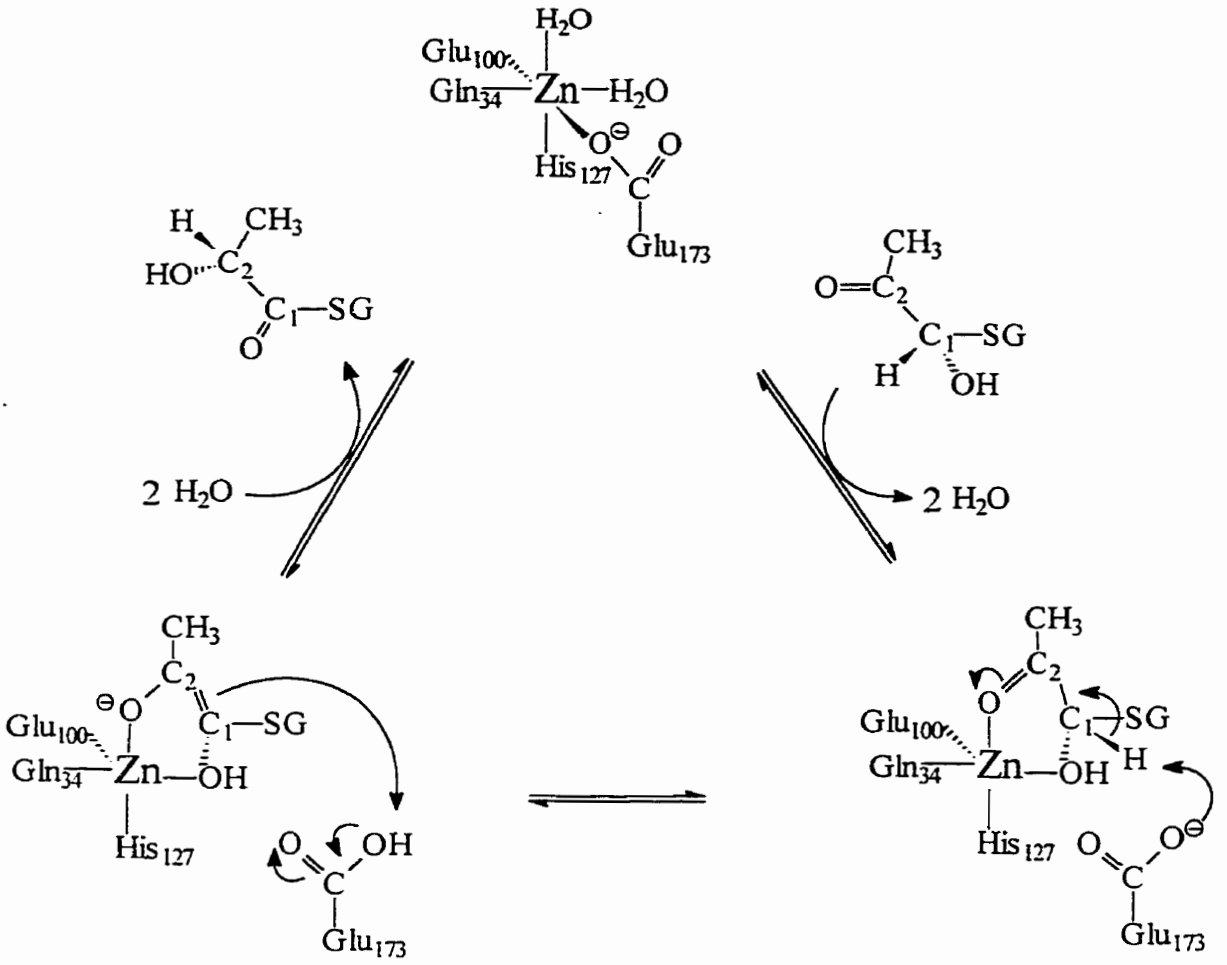

Figure 1.11: The mechanism of the glyoxalase I reaction, proposed based on mutagenesis and crystallographic studies on the *H. sapiens* enzyme (Ridderström et al., 1998; Cameron et al., 1999a).

1.7 Glyoxalase II

The second enzyme in the glyoxalase system, glyoxalase II (GlxII) hydrolyzes the product of the GlxI reaction, *S*-D-lactoylglutathione, to D-lactate and regenerates GSH. GlxII has been purified and studied from several sources. GlxII enzymes from three yeast sources, *Candida albicans*, *Hansenula mrakii*, and *Saccharomyces cerevisiae* were purified and found to be monomeric with molecular weights ranging between 22-32 kDa (Murata et al., 1986a; Talesa et al., 1990; Inoue and Kimura, 1992; Bito et al., 1997). The substrate of the GlxI reaction, the condensation product of GSH and MG, was inhibitory to these enzymes. This hemiacetal substrate is also inhibitory to the GlxII enzyme from mouse liver (Oray and Norton, 1980).

The gene encoding *Arabidopsis thaliana* GlxII was recently cloned, the protein purified and characterized by two independent groups (Crowder et al., 1997; Maiti et al., 1997; Ridderström and Mannervik. 1997). This monomeric enzyme had a molecular weight of 28.8 kDa and an isoelectric point of 6.2 (Crowder et al., 1997; Ridderström and Mannervik, 1997). It was also determined that there were two moles of Zn^{2+} bound per mole of monomeric enzyme (Crowder et al., 1997). Sequence analysis of the *H. sapiens* and *A. thaliana* enzymes indicated high homology between the proteins and led to the observation that a 15 amino acid region, containing several histidine residues is highly conserved. This region is also conserved in two other hydrolase families, the metallo-β-lactamases and a group of arylsulfatases (Crowder et al., 1997; Melino et al., 1998).

GlxII has also been identified in a wide range of additional species and tissues, from rat erythrocyte to pigeon spleen (Vander Jagt, 1989 and references therein). However, the available knowledge regarding GlxII expanded rapidly in recent years with the expression and characterization of the enzyme from *H. sapiens* (Ridderström et al., 1996; Cameron et al., 1999b). The 780 base pairs coding for the GlxII gene, yields a monomeric 28.9 kDa protein with an isoelectric point of 8.5. Limited proteolysis of *H. sapiens* GlxII combined with secondary structure predictions suggested that the monomeric enzyme is composed of two domains made up of different secondary structures (Aceto et al., 1998). This was confirmed by the recent solution of the crystal structure of *H. sapiens* GlxII (Cameron et al., 1999b). The 1.9 Å structure reveals that GlxII is composed of a four-layered β sandwich domain

similar to that observed in metallo-β-lactamase enzymes, and a second domain, unique to GlxII, which is composed mainly of α-helices (Figure 1.12; Cameron et al., 1999b). The active site contains a binuclear zinc-binding site, also observed in some metallo-β-lactamases. Examination of the ligands around the two zinc ions indicated the presence of a water molecule coordinated between the two metals. As such it is believed to exist as a hydroxide ion (Cameron et al., 1999b).

This enzyme was also cocrystallized with a substrate that is slowly hydrolyzed by the enzyme, *S*-(*N*-hydroxy-*N*-bromophenylcarbamoyl)glutathione (HBPC-GSH). Fortuitously, one molecule of the asymmetric unit contained this molecule while the second was found to contain glutathione, the product of the hydrolysis reaction. The hydroxide ion bound to the two metal ions was found to be only 2.9 Å from the substrate carbonyl carbon suggesting that it may act as nucleophile in the hydrolysis reaction. This has led to the postulated mechanism outlined in Figure 1.13 (Cameron et al., 1999b).

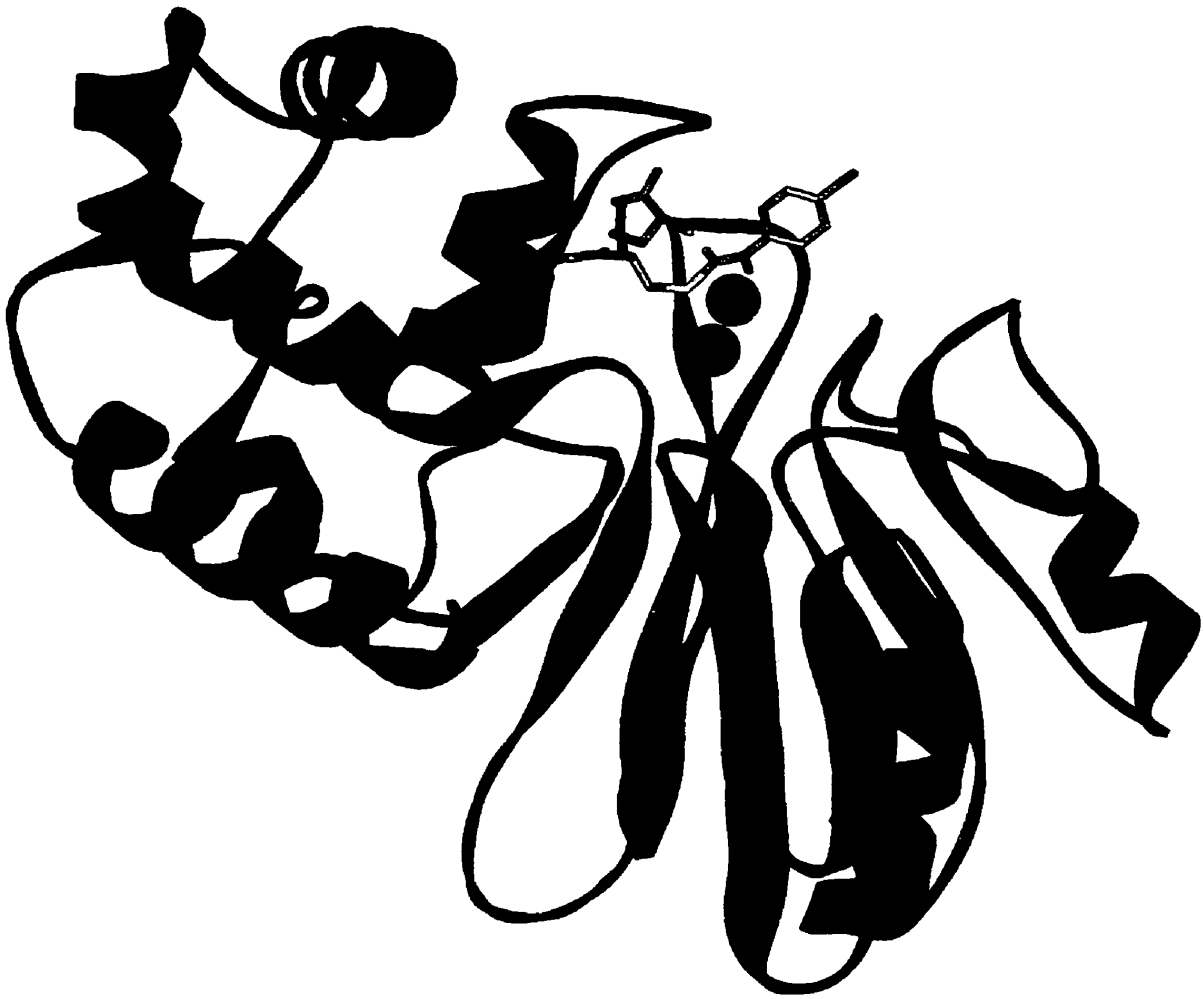

Figure 1.12: Structure of *H. sapiens* glyoxalase II (PDB 1QH5; Cameron et al., 1999b). The zinc atoms are in black space fill, and the HBPC-GSH cocrystallized in the active site is displayed as sticks. (Prepared with WebLab Viewer Pro ver 3.7, Molecular Simulations Inc.)

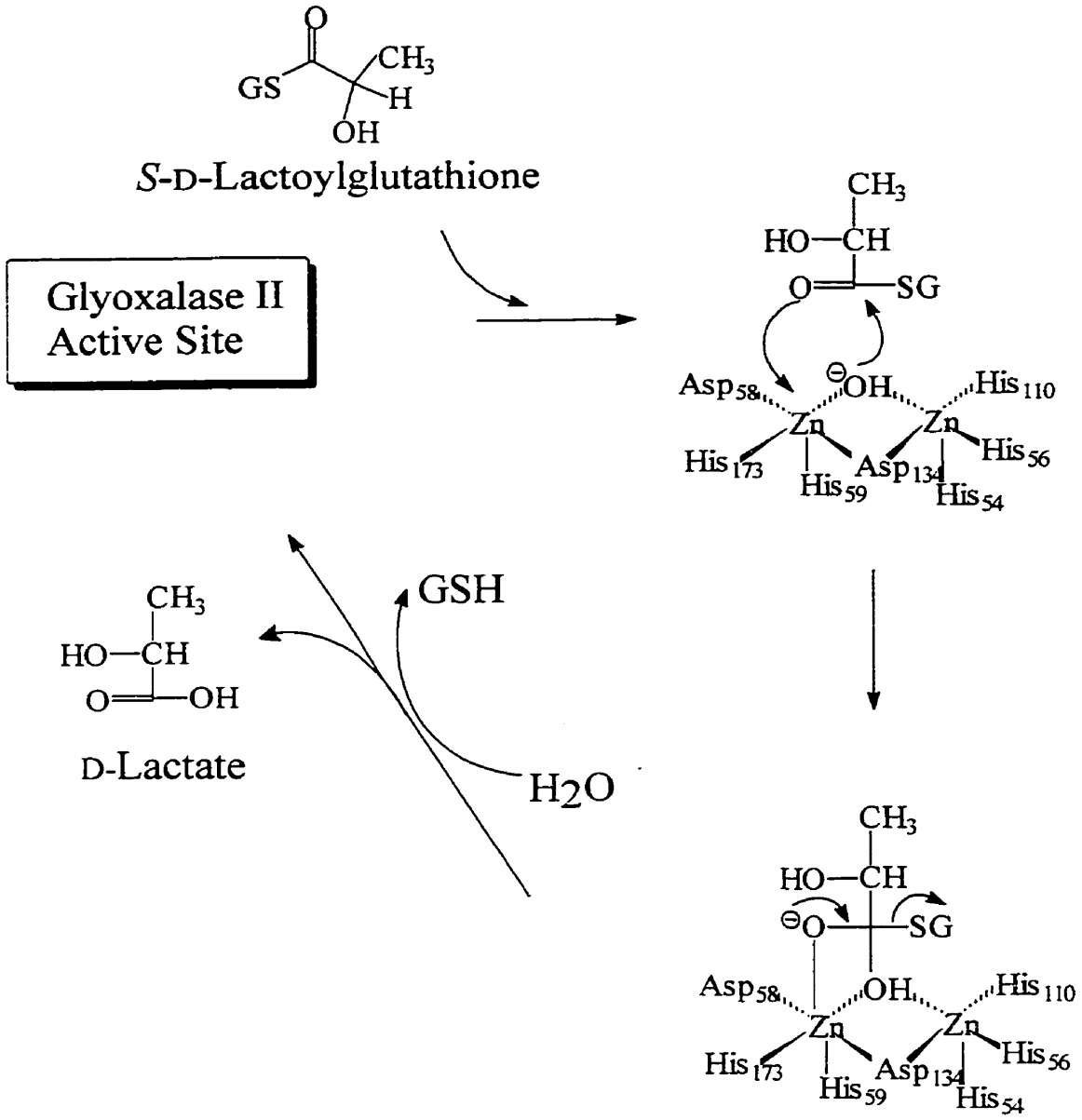

Figure 1.13: Proposed reaction mechanism for glyoxalase II. The amino acids observed in the crystal structure to be metal ligands are indicated with the corresponding residue numbers. (Adapted from Cameron et al., 1999b).

1.8 Glyoxalase III

In 1995 a unique glyoxalase enzyme was identified, capable of converting methylglyoxal directly to D-lactate, in a glutathione independent fashion (Misra et al., 1995). This enzyme, named glyoxalase III, was shown to be dimeric with a native molecular weight of approximately 82 kDa. Unlike GlxI which will accept a range of α-ketoaldehydes, to varying degrees, glyoxalase III prefers methylglyoxal and phenylglyoxal only, with the latter utilized at only 15% the rate of methylglyoxal (Misra et al., 1995). The purified protein was confirmed to be free of contaminating GlxI or GlxII activity by monitoring any production or consumption of *S*-D-lactoylglutathione. Neither was detected, nor was any GSH present. Furthermore, addition of GSH to the enzyme did not affect enzyme activity (Misra et al., 1995). Therefore, the activity observed is clearly due to a novel enzyme.

Surprisingly, in the five years since this unique enzyme was reported there have been no further publications regarding glyoxalase III in any organism. MacLean and coworkers (1998) reported that the activity of glyoxalase III in *E. coli* cells was tested during their analysis of MG resistance in cell lines expressing GlxI and GlxI null mutant cell lines. However, the only information gained was the observation that the activity of glyoxalase III was not enhanced in cells lacking a functional GlxI enzyme. Hence there appears to be no inherent compensation mechanism (MacLean et al., 1998).

1.9 Nickel and *E. coli*

As *E. coli* GlxI is maximally active in the presence of Ni^{2+} it is worth examining the levels of nickel available in the cell and other nickel-utilizing enzymes. It should be noted at this point however, that although we have detected maximal enzymatic activity with Ni^{2+}, and shown that addition of Ni^{2+} to the growth media enhances the activity of the expressed GlxI protein, indicating the Ni^{2+} is transported into the cell and taken up by the enzyme, we have not unequivocally established that Ni^{2+} is the native metal in *E. coli* GlxI outside a laboratory setting (Clugston, 1997; Clugston et al., 1998a). That being said, our report on the maximal activation of *E. coli* GlxI by nickel ions has attracted much interest and has been included in current reviews on nickel enzymes (Maroney, 1999; Watt and Ludden, 1999).

1.9.1 Nickel Transport

Although nickel is an essential trace metal, the levels of free nickel in cells must be tightly controlled. Toxicity can result from nickel binding non-specifically to biomolecules, or by displacing the natural metal from the binding site in proteins required for cell growth and survival (Ankel-Fuchs and Thauer, 1988; Drake, 1988; Wu et al., 1994; Chivers and Sauer, 2000). The cellular proteins requiring nickel will be discussed in the following section after an examination of the means by which nickel is transported into the cell. As our investigations deal with a bacterial enzyme, only the transport at the level of a single cell will be examined. A review of the transport in multicellular organisms, from plants to vertebrates can be found elsewhere (Drake, 1988).

Nickel can be transported into the cell in a passive or facilitated manner. Nickel can diffuse into the cell where is it incorporated into intracellular molecules. As such the nickel will essentially accumulate against a concentration gradient, if the intracellular form is different from the extracellular form. Facilitated nickel transport in microbial cells has been found to occur both by a high-affinity and low-affinity transport system. Three distinct Mg^{2+} transport systems have been identified in *S. typhimurium*, CorA, MgtA, and MgtB (Snavely et al., 1989). These magnesium transport systems have been demonstrated to also translocate nickel, as well as Co^{2+} and Zn^{2+} although with lower affinity than for Mg^{2+} (Drake, 1988; Snavely et al., 1989; Silver, 1996; Watt and Ludden, 1999).

High-affinity Ni^{2+} transport has been identified in several microbial organisms. There are two main classes, the single component and the multicomponent ATP-dependent group (Reviewed by Watt and Ludden, 1999). Examples of the single component class include HoxN, a nickel permease identified in *Alcaligenes eutrophus* (Eitinger et al., 1997). This integral membrane protein does not appear to require additional protein components to import nickel. Another integral membrane protein, NixA, has been identified in *Helicobacter pylori* as a high affinity nickel import protein (Fulkerson et al., 1998). A high-affinity nickel-specific transport system was also identified in *E. coli*. Unlike HoxN or NixA, the 'Nik' transport system is encoded by an operon of five genes. These genes are believed to encode an ATP-binding cassette transport ATPase (Figure 1.14; Navarro et al., 1993). The transcription of this operon appears to be highly regulated. An oxygen-sensitive transcriptional factor, the fumarate nitrate regulatory protein (Fnr) acts as an activator, and

NikR acts as a repressor when intracellular concentrations of Ni^{2+} are high (Chivers and Sauer, 2000). It has also been demonstrated recently that NikR is dimeric with two high affinity nickel binding sites and a low affinity site that regulates the DNA binding affinity of this protein. When NikR binds nickel it recognizes and binds to the operator DNA, repressing expression from the *nikABCDE* operon (Chivers and Sauer, 2000). Therefore, maximal expression of the five genes in the *nik* operon is observed when the intracellular nickel concentration is very low and the growth conditions are anaerobic.

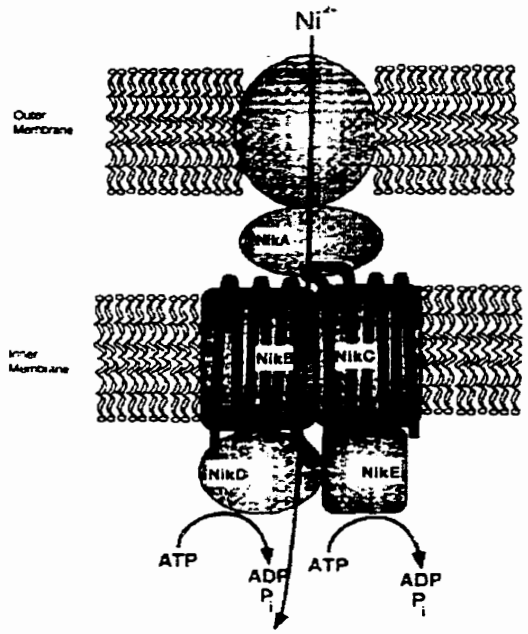

Figure 1.14: The ATP-dependent NikABCDE permease in *E. coli*. (From Silver, 1996)

1.9.2 Nickel Enzymes

As more nickel-dependent enzymes are identified the biological importance of this once ignored micronutrient are becoming clear (Ankel-Fuchs and Thauer, 1988; Drake, 1988). Although numerous metalloenzymes are active upon addition of Ni^{2+} or replacement of the native metal with Ni^{2+} (For example see Pallen and Wang, 1986; Angleton and Van Wart, 1988; Omburo et al., 1992; Ragusa et al., 1998), some even to levels greater than or comparable to the native enzyme activity, very few enzymes actually utilize nickel as the natural catalytic metal ion. The enzymes known to be nickel-dependent include: urease,

hydrogenase, carbon monoxide dehydrogenase, methyl-*S*-coenzyme M reductase, and one group of superoxide dismutase enzymes (For reviews see Hausinger, 1987; Volbeda et al., 1996; Hausinger, 1997; Maroney et al., 1998; Ragsdale, 1998; Maroney, 1999; Watt and Ludden, 1999). Other proteins that may prove to be nickel enzymes include peptide deformylase, cis-trans isomerase, and *E. coli* GlxI. In general, nickel-utilizing enzymes can be divided into two groups, those involving redox chemistry, and non-redox enzymes. The enzymes catalyzing redox reactions are briefly described first.

Superoxide dismutase (SOD) enzymes protect the cell from oxidative damage by catalyzing the disproportionation of superoxide to peroxide and molecular oxygen. This enzyme has been found to require a redox active metal and classes of SODs have been found to bind manganese, iron, copper, and the recently identified nickel-containing SOD (Kim et al., 1996; Youn et al., 1996). Spectroscopic studies on the nickel site indicate the metal is five-coordinate with three S-donor ligands, one N-donor, and one additional N or O-donor (Choudhury et al., 1999).

Hydrogenases catalyze the reversible activation of hydrogen, either oxidizing H_2 to generate reducing equivalents, or producing H_2 during fermentation when protons are the terminal electron acceptor in the electron transport chain. Although three groups of hydrogenases exist, based on their cofactors, the largest group contains nickel and iron. The nickel is coordinated by sulfur ligands from four cysteine residues (Maroney et al., 1998; Maroney, 1999 and references therein).

Carbon monoxide dehydrogenase catalyzes the oxidation of carbon monoxide to carbon dioxide. Growth of *Clostridium thermoaceticum* in the presence of ^{63}Ni was utilized to establish that nickel in the growth media was taken up by the bacteria and incorporated into the dehydrogenase (Drake et al., 1980). The nickel center has sulfur donor ligands and is linked to an iron-sulfur cluster (Diekert, 1988; Watt and Ludden, 1999). Carbon monoxide dehydrogenase is a bifunctional enzyme in acetogenic (anaerobes that produce acetate from autotropic growth on CO_2 and H_2 or a product of sugar fermentation) and methanogenic (convert acetate to methane and CO_2, coupled to ATP synthesis) bacteria (Watt and Ludden, 1999). The second active site catalyzes acetylcoenzyme A synthesis and also appears to contain a nickel site linked to an iron-sulfur cluster (Maroney, 1999; Watt and Ludden, 1999).

Methyl-*S*-coenzyme M reductase catalyzes the last step of methane production in methanogenic Archaea, often called methanogens (Wackett et al., 1988). Nickel is not directly bound by the enzyme but rather contained in a yellow chromophoric tetrapyrrole called F_{430} (Wackett et al., 1988; DiMarco et al., 1990; Hausinger, 1994; Watt and Ludden, 1999, and references therein).

One of the most extensively studied nickel enzymes is urease (Reviewed by Hausinger, 1994; Mobley et al., 1995; Hausinger, 1997; Maroney et al., 1998; Watt and Ludden, 1999). Urease catalyzes the hydrolysis of urea to form ammonia and carbamate via a non-redox reaction. The structure of *Klebsiella aerogenes* urease is a trimer of trimers with three dinuclear active sites. In addition to water ligands, one nickel has two histidine ligands, the second two histidine ligands in addition to an aspartate ligand. One of the key features however is the carbamylated lysine that bridges the two nickels (Jabri et al., 1995). Identification of this ligation pattern helped to explain why apourease regained very low levels of activity upon addition of nickel, unless CO_2 was also supplied (Park and Hausinger, 1995). The carbamate ligand is not specifically required, but a bidentate carboxylate-like bridging ligand is essential for proper positioning of the nickel ions.

The assembly of a functional urease enzyme has been shown to require numerous proteins. Four accessory proteins and three structural proteins have been identified in the urease gene cluster. Although the role of all the accessory proteins has not yet been clearly established, UreE is believed to be the accessory protein responsible for delivering Ni^{2+} to the apourease enzyme (Brayman and Hausinger, 1996; Colpas and Hausinger, 2000). An extensive number of reports have been presented on the analysis of the nickel insertion into apourease. The particulars of the currently proposed model can be found in great detail in several reports (Mobley et al., 1995; Watt and Ludden, 1999).

The hydrogenase and carbon monoxide dehydrogenase enzyme also appear to have associated gene products involved in delivery of nickel (Reviewed by Watt and Ludden, 1999).

Of these known nickel enzymes, only urease and hydrogenase enzymes have been identified in *E. coli* (Mobley et al., 1995; Silver, 1996; Maroney, 1999; Watt and Ludden, 1999). In addition to these known nickel enzymes, several other proteins require further investigation to determine if they are naturally nickel enzymes. A preliminary report has been

presented outlining the purification of an *E. coli* cis-trans isomerase that is proposed to bind nickel (Wülfing et al., 1994). Although the natural metal has not yet been established, peptide deformylase isolated from *E. coli* shows activity with Ni^{2+} and has been purified and studied as an Fe^{2+} and Ni^{2+} enzyme (Groche et al., 1998; Ragusa et al., 1998). Similarly *E. coli* GlxI is maximally active with Ni^{2+}, and the enzyme incorporates Ni^{2+} during protein expression in media containing Ni^{2+} (Clugston et al., 1998a), and may indeed be a Ni^{2+}-dependent enzyme. However, determination of the native metal awaits further investigation.

1.10 Summary and Research Objectives

The potential for the glyoxalase system to be an effective drug target, taking advantage of the toxic effects of methylglyoxal, is receiving renewed interest particularly in the area of anticancer agents. Alterations between eukaryotic GlxI enzymes and those from bacterial sources such as *E. coli* could also be targeted for novel antibacterial agents. As such, improvements in our understanding of the mechanism of action of this enzyme are critical. Our knowledge of the glyoxalase system has advanced significantly in recent years with many insights into the reaction mechanism, the solution of the first crystal structure of a glyoxalase I and glyoxalase II enzyme from *H. sapiens*, our identification of the unique metal activation properties of *E. coli* GlxI, and identification of many putative GlxI sequences in other organisms.

In this work we sought to gain a more detailed understanding of the structural and mechanistic enzymology of glyoxalase I. Our investigations have focused specifically on the metal binding site and properties of *Escherichia coli* GlxI. To begin, the kinetics of the enzyme activation with various metal ions was examined in addition to the relative affinity of the enzyme for the divalent metals. These characteristics are compared to a mutant form of the enzyme in which one of the metal ligands is altered. Structural features of the overall enzyme and details of the active site metal environment were examined primarily with spectroscopic and crystallographic techniques revealing interesting insights into the variation in metal activation of this enzyme. In addition, numerous putative GlxI sequences have been identified, including nineteen from pathogenic organisms. Analysis of these postulated sequences in comparison to the GlxI sequences from *H. sapiens*, *P. putida*, and *S. cerevisiae* allowed the identification of consistent alterations in the bacterial sequences. Furthermore,

the DNA encoding two of the putative GlxI sequences has been placed in an overexpression system, and the metal activation of the produced protein examined.

As *E. coli* GlxI is maximally active in the presence of Ni^{2+}, our improved knowledge of this enzyme enhances our understanding of the glyoxalase system and the role of the metal ion in the GlxI reaction. This work also provides further insight into the factors that may control metal selectivity by an enzyme and the effect of various metal ions on the enzymatic activity with structural explanations for such differences. Furthermore, analysis of *E. coli* glyoxalase I containing Ni^{2+} ameliorates our knowledge of protein-nickel interactions in general.

CHAPTER 2

ESCHERICHIA COLI GLYOXALASE I:

KINETIC STUDIES AND DETAILED METAL ANALYSES

2.1 Introduction

To increase our knowledge regarding the detoxification enzyme, glyoxalase I (GlxI), and to obtain information on a representative bacterial form of the enzyme, we pursued the isolation and characterization of *Escherichia coli* glyoxalase I. We have previously reported the creation of an expression and purification system and several unique properties of this enzyme (Clugston, 1997; Clugston et al., 1998a). This work, performed during my M.Sc. studies, is outlined in the following section. The results of this work led to the current investigations presented in this thesis in which we have examined the enzyme kinetics, as well as the numerous properties of the metal substituted forms of the enzyme, from activation levels to enzyme affinity for the metals and stability of the enzyme. This work has provided fascinating insights into the characteristics of glyoxalase I.

2.1.1 E. coli Glyoxalase I

Protein Expression and Purification

The DNA encoding *E. coli* glyoxalase I, *gloA* (Figure 2.1), was placed under the control of the *ptac* promoter in the plasmid, pTTQ18 (Stark, 1987). The resultant expression system, *E. coli* MG1655/pGL10, consistently produces 150-200 mg of protein per litre of cell growth in rich media. A two-step purification protocol was developed, yielding homogeneous apoenzyme for use in extensive kinetic and structural studies (Figure 2.2). Our initial studies on this enzyme revealed interesting properties of the enzyme, some of which are quite different from the properties of previously studied GlxI enzymes, such from *H. sapiens* or *S. cerevisiae*.

```
TGGCGGCGCGGAAGGCTATACCGATTACCCGACGTTGTAATCCAACATTGCGAGCGGCGT 126
                                    -35

AAAGCCGCCGCTATACTAAAACAACATTTTGAATCTGTTAGCCATTTTGAGGATAAAAAG 186
          -10                HinfI                SD

ATGCGTCTTCTTCATACCATGCTGCGCGTTGGCGATTTGCAACGCTCCATCGATTTTTAT 246
 M  R  L  L  H  T  M  L  R  V  G  D  L  Q  R  S  I  D  F  Y   20

ACCAAAGTGCTGGGCATGAAACTGCTGCGTACCAGCGAAAACCCGGAATACAAATACTCA 306
 T  K  V  L  G  M  K  L  L  R  T  S  E  N  P  E  Y  K  Y  S   40

CTGGCGTTTGTTGGCTACGGCCCGGAAACCGAAGAAGCGGTGATTGAACTGACCTACAAC 366
 L  A  F  V  G  Y  G  P  E  T  E  E  A  V  I  E  L  T  Y  N   60

TGGGGCGTGGATAAATACGAACTCGGCACTGCTTATGGTCACATCGCGCTTAGCGTAGAT 426
 W  G  V  D  K  Y  E  L  G  T  A  Y  G  H  I  A  L  S  V  D   80

AACGCCGCTGAAGCGTGCGAAAAAATCCGTCAAAACGGGGGTAACGTGACCCGTGAAGCG 486
 N  A  A  E  A  C  E  K  I  R  Q  N  G  G  N  V  T  R  E  A  100

GGTCCGGTAAAAGGCGGTACTACGGTTATCGCGTTTGTGGAAGATCCGGACGGTTACAAA 546
 G  P  V  K  G  G  T  T  V  I  A  F  V  E  D  P  D  G  Y  K  120

ATTGAGTTAATCGAAGAGAAAGACGCCGGTCGCGGTCTGGGCAACTAATCTCCTGCCGGG 606
 I  E  L  I  E  E  K  D  A  G  R  G  L  G  N                 135

CGTGAACTCATCGCGCCCGCATCTTTACTGCATCGACAAGTAATATTTGTCATAATGCGC 666
                                                    BssHII

GC                                                             668
```

Figure 2.1: *E. coli* glyoxalase I DNA sequence and corresponding protein sequence. The sites utilized in the construction of the expression plasmid, pGL10, are shown for reference. Details of the plasmid construction have been presented previously (M.Sc. work; Clugston, 1997; Clugston et al., 1998a).

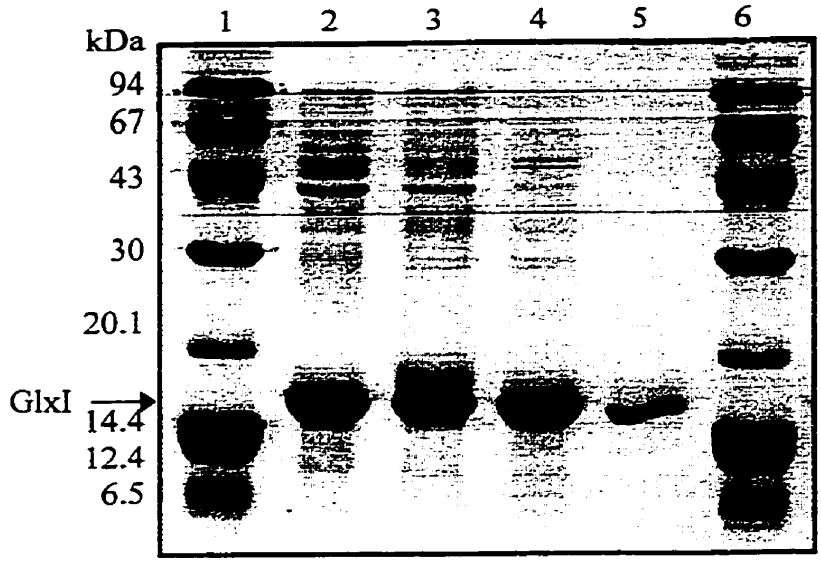

Figure 2.2: Stages in the purification of *E. coli* glyoxalase I. (15% SDS-PAGE with Coomassie staining; From Clugston, 1997; Clugston et al., 1998a).

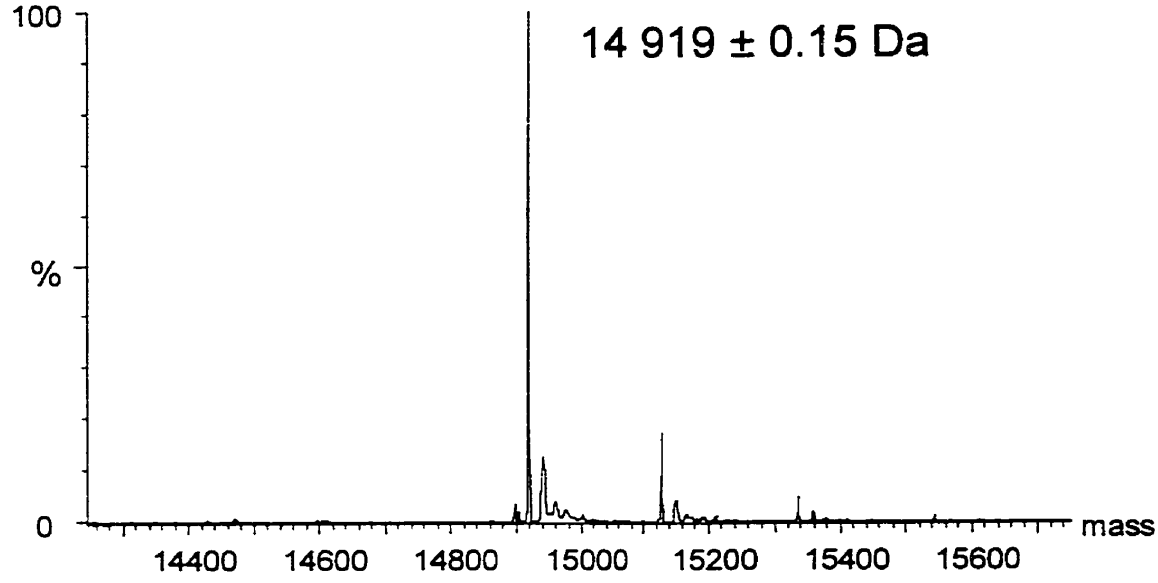

Figure 2.3: Reconstructed electrospray mass spectrum of purified *E. coli* glyoxalase I, indicating the observed subunit molecular mass in Daltons (Calculated = 14 919). Other small peaks corresponding to non-covalent adducts with sodium, potassium, and MOPS buffer are evident. No other peaks were observed in the spectra over a mass range of 1000-100 000 Da.

Characteristics of E. coli Glyoxalase I

We have demonstrated that *E. coli* glyoxalase I is a metalloenzyme that functions as a homodimer with a subunit molecular weight of 14 919 Da, confirmed by electrospray mass spectrometry (Figure 2.3). The addition of metal does not appear to affect the overall structure of the enzyme, based on circular dichroism studies, nor does it influence the dimeric nature of the enzyme. Gel filtration studies indicated the enzyme to be dimeric both in the presence and absence of metal ions (Clugston, 1997; Clugston et al., 1998a).

Metal Activation

For the *Homo sapiens*, *Saccharomyces cerevisiae*, and *Pseudomonas putida* GlxI, the essential metal has been shown to be zinc (Aronsson et al., 1978; Ridderström and Mannervik, 1996; Saint-Jean et al., 1998). In contrast, however, GlxI from *E. coli* is completely inactive in the presence of zinc. Maximal activity is found in the presence of Ni^{2+}, with reduced activity with Co^{2+}, Cd^{2+}, and Mn^{2+} (Figure 2.4; Clugston, 1997; Clugston et al., 1998a). In addition, maximal activity was observed with one mole of metal per mole of dimeric enzyme (Figure 2.5), compared to the two equivalents seen for the dimeric *H. sapiens* GlxI enzyme. This was confirmed by metal analyses which indicated that active Ni^{2+}-GlxI contained only one equivalent of metal. This was especially puzzling given the relatively high amino acid sequence homology between the *E. coli* and *H. sapiens* enzymes (36% identity plus and additional 14% similarity; Cameron et al., 1997; Clugston, 1997; Clugston et al., 1998a).

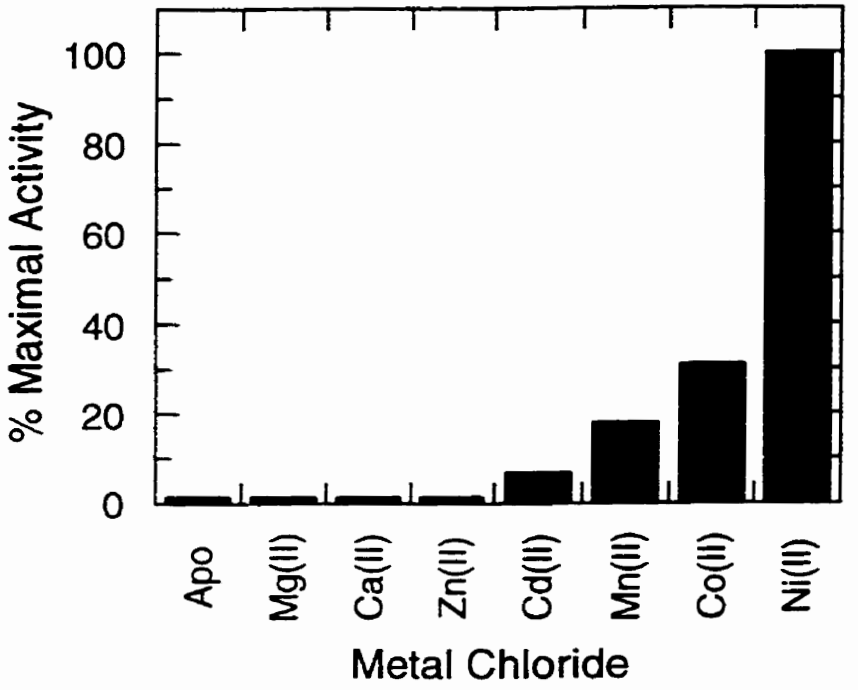

Figure 2.4: Activation of apo *E. coli* GlxI by various metal ions (10x mole equivalence; Clugston, 1997; Clugston et al., 1998a).

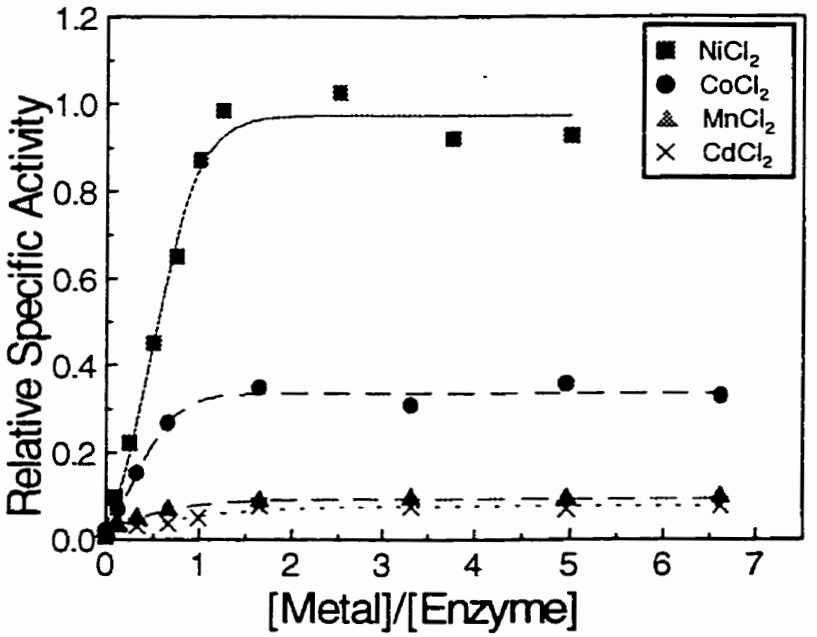

Figure 2.5: Titration of apoGlxI with four activating metals (Clugston, 1997; Clugston et al., 1998a). Activities are shown relative to the Ni^{2+}-activated enzyme with the lines indicating the trend in the data.

2.1.2 Kinetic Analyses

To further examine the role the metal ion plays in the activity of *E. coli* GlxI, a detailed kinetic study has been undertaken. The kinetic parameters of the enzyme activated with several metal ions have been examined. In addition, the effect of pH on the enzymatic function of Co^{2+}-GlxI has been compared to the previous work with Ni^{2+}-GlxI (Clugston, 1997; Clugston et al., 1998a), which indicated the K_m for the MG-GSH hemiacetal adduct substrate was significantly increased above a pH of 8.0. As our preliminary analysis indicated that *E. coli* GlxI reaches maximal enzymatic activity with only one mole of metal supplied per mole of dimeric enzyme (Figure 2.5), it appeared that the affinity of the enzyme for metal was also quite high. To determine how tightly the metal is bound, and whether any exchange of the bound metal ion can occur, a series of metal competition experiments were performed.

2.1.3 Metal Binding

In an effort to characterize the metal binding in *E. coli* GlxI we have examined two particular aspects, the amount of metal bound to the enzyme and the affinity of the protein for specific metal ions.

Quantitative Metal Analysis: Inductively Coupled Plasma Analysis (ICP)

Elemental analysis is often employed to determine the amount of metal in a given sample. Two common techniques to analyze the levels of metals in a solution are atomic absorption (AA) and inductively coupled plasma (ICP) spectroscopy. The basic principle behind these techniques is that every element produces its own characteristic spectrum when excited. When energy is supplied to an atom, one of the valence electrons can move from its low energy state, or ground state, to a higher orbital, or excited state and the absorbed radiation is termed the resonance line (Robinson, 1996). The principle difference between these two analytical techniques is that atomic absorption spectroscopy is concerned with the absorption of energy when the electron is excited, whereas ICP analysis is within the field of atomic emission spectroscopy. The transition of an electron from an excited state to any lower excited state, even the ground state, produces a photon of energy and this emission is the basis for ICP analysis (Robinson, 1996). Discrete energy levels exist and therefore the difference between these levels can be defined and the absorbed or emitted energies, which

are particular wavelengths of light, are characteristic for each element (Robinson, 1996). The intensity of the light emitted, in the case of emission spectroscopy, is related to calibration curves to determine the concentration of the particular metal in the sample. The radiant energy absorbed or emitted is generally in the ultraviolet (UV) range, as opposed to x-ray radiation utilized in techniques such as x-ray absorption spectroscopy (XAS) in which core or inner shell electrons are excited (Chapter 3). For both absorption and emission spectroscopy free atoms must be generated prior to excitation. This is generally accomplished with a flame or thermal atomizer. In ICP emission a plasma torch, generally argon, is utilized to generate and excite the atoms. Although there are several differences between AA and ICP spectroscopy, well described by Robinson (1996), for our purposes the key feature was that in AA analysis one individual element is examined at a time. In ICP emission spectroscopy numerous elements can be analyzed simultaneously.

We were interested in determining the types of metals present in our protein solutions and their quantities. Therefore, ICP analysis was employed. To determine the amount of metal bound to each GlxI dimer, metal analysis was performed on the enzyme that had been reconstituted with several different metal chlorides. In addition we were interested in determining the amount of metal incorporated into the enzyme during bacterial expression of the protein. *E. coli* expressing GlxI, was grown in the presence of $NiCl_2$, $ZnCl_2$, or no additional metals and metal analyses performed on the partially purified enzymes to determine if the metal was transported into the cell and bound by the enzyme.

Binding Affinity: Isothermal Titration Calorimetry (ITC)

There are many techniques available for the analysis of the interactions of a protein with various ligands, several of which are briefly outlined below and have been reviewed elsewhere (Hensley, 1996; Doyle and Hensley, 1997; Loo, 1997; Fersht, 1999).

Equilibrium dialysis has been widely utilized for analysis of binding interactions. This involves dialyzing a solution of the enzyme plus ligand against ligand alone, separated by a semipermeable membrane. The semipermeable membrane will allow passage of the ligand but not the protein. Following equilibration, the amount of bound and free ligand in the protein compartment is determined and compared to the amount of free ligand in the other chamber (Hughes and Klotz, 1956; Fersht, 1999). Analysis of the ratio of bound to free

ligand at various concentrations of ligand is performed to determine the dissociation constant. Traditionally ligands that are radioactive are employed due to the ability to perform these measurements on small quantities of protein. Various methods are available to quantify the metal of interest (Hughes and Klotz, 1956). Equilibrium dialysis has been extensively employed in the analysis of metal dissociation rates and dissociation constants for carbonic anhydrase (Kiefer et al., 1995; Huang et al., 1996; Hunt and Fierke, 1997). A 'PAR assay' was developed by Hunt and coworkers (Hunt et al., 1984) in which 4-(2-pyridylazo)resorcinol (PAR) is utilized to detect the enzyme-bound zinc colorimetrically, following the chromatographic removal of the free metal after dialysis.

Fluorescence spectroscopy is also commonly utilized to detect and quantify changes that may occur when a macromolecule and ligand bind. This technique is dependent upon either the macromolecule or ligand undergoing a change in its fluorescence upon interaction. In principle, increasing amounts of ligand are added to the protein solution and the change in fluorescence monitored (Fersht, 1999). This methodology has also been applied in some cases to systems in which there may not be a change in fluorescence upon binding, but an absorbance change can be monitored (Fersht, 1999).

Analytical ultracentrifugation has also been applied to this problem (Hensley, 1996). The absorbance of the bound and free forms of the macromolecule are monitored by ultraviolet spectroscopy during the sedimentation process. The higher molecular weight complexes will sediment more rapidly and hence a moving boundary in the absorbance measurements is observed (Fersht, 1999).

As described in the following section in which the association of various inhibitors for GlxI is examined, electrospray mass spectrometry (ESMS) is also gaining acceptance for the analysis of non-covalent complexes (Loo, 1997).

A method that is just beginning to become widely used, as more instruments are available, is surface plasmon resonance (SPR). In this technique, the macromolecule is immobilized on a surface and the ligand solution flows over the immobilized partner. Any changes in the refractive index, associated with the interaction of the two molecules, are measured in real time (Szabo et al., 1995; Doyle and Hensley, 1997). From these measurements the association rate constant, k_a, and dissociation rate constant, k_d, can be measured, and the corresponding dissociation constant K_d, calculated from these results. An

obvious source of error or interference with this method is the requirement for immobilization of one of the ligands. This may modify or alter the interaction (Loo, 1997).

The technique chosen for the investigation of the interaction between *E. coli* GlxI and various metal ligands was isothermal titration calorimetry (ITC). This thermodynamic technique measures the heat of binding, either endothermic or exothermic, when two molecules interact. By exact measurement of this heat a binding isotherm can be constructed from which thermodynamic parameters of the interaction can be determined (Doyle, 1997; Ladbury and Chowdhry, 1998). This is becoming a widely used technique as it has many advantages over other methods. For example, ITC does not require immobilization of the protein as in SPR, no specific labels are required on either the ligand or macromolecule, and no spectroscopic change is required to monitor the interaction. ITC is also useful for numerous applications, from the interaction between two proteins, to protein-ligand interactions, DNA-protein or DNA-ligand interactions (Brandts et al., 1990; Ladbury and Chowdhry, 1996).

In a typical ITC titration the sample cell contains the macromolecule, equilibrated to the desired temperature. Aliquots of the ligand are then added in precise amounts by a motor driven syringe. The heat change upon each addition is monitored compared to the reference cell and appears as a peak on the binding isotherm. As the binding sites on the macromolecule are filled with ligand the heat change decreases with each addition until only the heat of dilution of the ligand is observed, producing the binding isotherm (Ladbury and Chowdhry, 1996). The area under each peak in the binding isotherm is determined to quantitate the heat from the titration. Figure 2.6 illustrates the general design of an isothermal chamber and the specific setup of the CSC calorimeter utilized in our analyses.

From this data the stoichiometry (n) of the interaction can be determined from the molar ratio of the macromolecule and ligand at the equivalence point. In our case this was the number of metal ions bound to each dimeric protein molecule. In addition the thermodynamics are measured, namely the change in enthalpy (ΔH) and association constant (K or K_a). From this information the entropy change (ΔS) and the Gibbs free energy change (ΔG) can be calculated according to the following equation:

$$\Delta G^\circ = -RT \ln K = \Delta H^\circ - T\Delta S^\circ$$

where R is the gas constant and T the absolute temperature in Kelvin.

The variables are often referred to with a 'B' (eg $\Delta_B G^\circ$) to indicate they are derived from binding studies. The ITC analysis of a particular system can be expanded to include analyses performed at various temperatures (Ladbury and Chowdhry, 1996; Ladbury and Chowdhry, 1998), which can be used to determine the change in heat capacity ($\Delta_B C_p$) according to the following:

$$\Delta C_p = (\Delta H^\circ_{T2} - \Delta H^\circ_{T1})/(T_2 - T_1)$$

where T_1 and T_2 are the two temperatures at which the experiment was performed.

The amount of protein required is dependent upon the amount of heat produced for the given interaction. Sufficient levels are required to ensure the heat being measured is above baseline levels. It has been found that 3-12 mg of protein is generally required in each titration. As a general guide, it is recommended that sufficient protein be used such that the product of the molar protein concentration and the binding constant (K) is between 1 and 1000 (arbitrary units; Brandts et al., 1990).

In this work, the interaction of apo *E. coli* GlxI with Ni^{2+}, Zn^{2+}, Co^{2+}, Cd^{2+}, Mn^{2+}, Mg^{2+}, and Ca^{2+} has been examined by isothermal titration calorimetry.

A

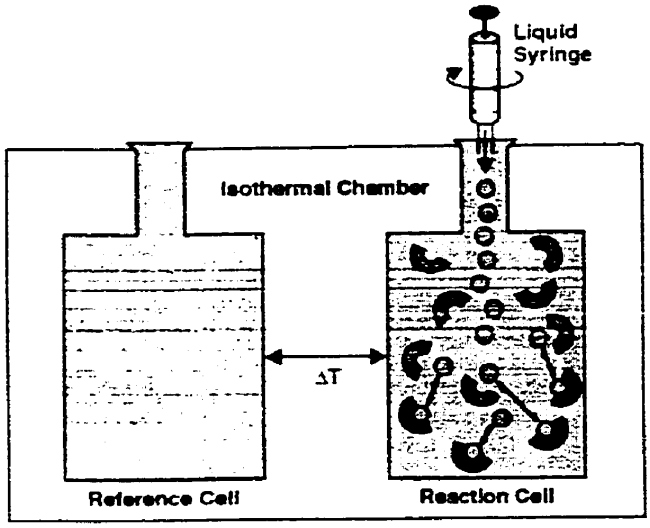

B

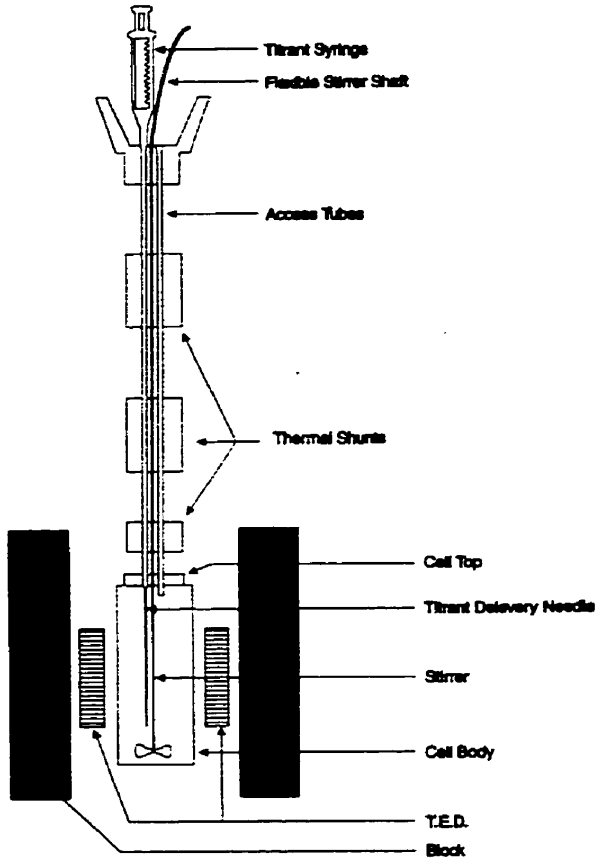

Figure 2.6: (A) General concept in ITC illustrating the binding of a ligand to a macromolecule (From Doyle and Hensley, 1997). ΔT is the temperature difference between the sample and reference cell measured during the titration. (B) Schematic of the CSC ITC (From CSC 4200 ITC User's Manual). T.E.D. refers to the thermo electric device which are the semiconductor thermopile heat flow sensors.

2.1.4 Thermal Stability

A widely used technique to determine the thermal stability of an enzyme is differential scanning calorimetry (DSC). This thermodynamic method measures the conformational energy in macromolecules. The sample, protein in this instance, is heated over a temperature range and the difference in heat between the sample and reference cells are monitored. At a particular stage in the temperature scan, the melting temperature (T_m), the sample will undergo a physical change. For proteins this is generally denaturation, or thermal unfolding (Ladbury and Chowdhry, 1998; Fersht, 1999). Protein unfolding is an endothermic process, hence there is an uptake of heat in the sample cell. Differences in the T_m give an indication of any variations in the stability of various forms of the protein. The experiments can be further expanded to examine the thermal denaturation curves with variations in the buffer pH. With this information the change in the heat capacity (ΔC_p) between the folded and unfolded states can be determined and further thermodynamic parameters, such as ΔH can be calculated (Ladbury and Chowdhry, 1998; Fersht, 1999). Detailed reviews of these calculations can be found elsewhere (Ladbury and Chowdhry, 1998; Fersht, 1999).

In this preliminary DSC study, the transition or melting temperature was examined for *E. coli* GlxI reconstituted with different metal ions as well as the apoenzyme. Comparison of the T_m values provides an indication of the variation in stability of the enzyme with the particular metal ion present.

2.1.5 Analysis of Inhibitor Binding Affinity by Mass Spectrometry and Comparative Kinetics

Traditional screening of potential inhibitors can be a labour-intensive process involving the examination of the enzyme kinetics in the presence of various levels of the inhibitor under examination. The increased availability of plate-readers has allowed for more rapid determination of enzyme kinetics and inhibition levels on smaller quantities of material. However, an alternative technique to the standard spectrophotometric assays is gaining wider acceptance, the use of mass spectrometry for determining the binding affinity of an inhibitor to the protein of interest (Przybylski and Glocker, 1996; Loo, 1997; Roepstorff, 1997). Many inhibitor molecules act by non-covalent binding to the enzyme, usually at the active site of the enzyme. Such non-covalent interactions are thus of crucial importance in biochemistry, not

only in enzyme-substrate and enzyme-inhibitor interactions, but also in the area of protein-protein interactions. Over the last several years biomolecular mass spectrometry has evolved into a potential alternative technique for the investigation of these complexes, with its speed and sensitivity as significant advantages (Loo, 1997). For example, using mass spectrometry enzyme substrate and/or inhibitor interactions have been studied even for rather large combinatorial peptide libraries (Camilleri and Haskins, 1993; Gao et al., 1996; Potier et al., 1997). Electrospray mass spectrometry has also been used to investigate specific molecular protein-protein and protein-ligand interactions (Ayed et al., 1998; Jorgensen et al., 1998; Nettleton et al., 1998; Rostom et al., 1998). With this in mind, we have examined the non-covalent protein-protein interactions and binding affinities of several *S*-substituted glutathione analogues, a putative transition state analogue (Ly et al., 1998) and a flavonoid towards *E. coli* glyoxalase I by nanoflow electrospray time-of-flight mass spectrometry (nanoESI-TOF-MS), in collaboration with Dr. A. J. R. Heck and E. Stokvis at Utrecht University (Utrecht, the Netherlands). The relative affinity of the inhibitors for the protein are compared to the level of inhibition measured by standard enzyme kinetics (Stokvis et al., 2000).

2.2 Materials and Methods

2.2.1 Reagents and Materials

The following reagents were obtained from Sigma Chemical Company (St. Louis, MO): albumin (bovine), ampicillin (trihydrate), *S*-(*p*-azidophenacyl)-glutathione, carbenicillin (disodium salt), Coomassie brillinant blue R, cupric chloride (dihydrate), diethanolamine (bis[2-hydroxyethyl]amine), DTNB (5,5'-dithiobis-(2-nitrobenzoic acid), ethylenediamine-tetraacetic acid (EDTA), glutathione (reduced), glutathione-sulfonic acid, *S*-hexylglutathione, *S*-lactoylglutathione, *S*-methylglutathione, methylglyoxal (40% aqueous solution), MES (2-(*N*-morpholino)ethanesulfonic acid), MOPS (3-(*N*-morpholino)propanesulfonic acid), myricetin, *S*-(*p*-nitrobenzyl)-glutathione, *S*-octylglutathione, *S*-propylglutathione, and Tris (hydroxymethyl)aminomethane.

S-{2-[3-(Hexyloxy)benzoyl]-vinyl}glutathione, *N*-methyldiethanolamine, and nickel (II) chloride (hexahydrate, 99.9999% pure) were obtained from Aldrich (Oakville, ON).

Ammonium chloride, calcium chloride (dihydrate), DMSO (dimethyl sulfoxide), hydrochloric acid, orthophosphoric acid, magnesium chloride (hexahydrate), potassium acetate, potassium chloride, potassium hydroxide, sodium chloride, sodium hydroxide, sulfuric acid, and yeast extract powder were obtained from BDH (Toronto, ON). Each was analytical reagent grade material.

Agarose was obtained from ICN (Cleveland, Ohio). Tryptone (Bacto®) was from Difco Laboratories (Detroit, MI). IPTG was obtained from Diagnostic Chemicals Ltd. (Charlottetown, PEI), and Coomassie brilliant blue G-250 from Eastman Kodak Co. (Rochester, NY). Chelex® 100 resin and RotoLytes® were obtained from Bio-Rad (Mississauga, ON). Bacto® tryptone was obtained from Difco (Detroit, MI).

"Baker-Analyzed" reagent grade, manganous chloride (tetrahydrate), cobalt chloride (hexahydrate), cadmium chloride, and zinc chloride were purchased from J.T. Baker (Toronto, ON). Chromium chloride and iron (II) chloride was from Alfa Aesar (Ward Hill, MA).

ACS certified reagent grade acetic acid (glacial), glycerin, nickel chloride (hexahydrate), and nitric acid were obtained from Fisher Scientific (Nepean, ON), in addition

to potassium phosphate mono and dibasic, sodium phosphate mono and dibasic. Acetone (HPLC grade) was from Fisher or EM Science (Gibbstown, NJ).

Restriction enzymes were obtained from Roche Diagnostics (previously Boehringer Mannheim, Laval, QC) and New England Biolabs (Beverly, MA), and used according to the manufacturer's instructions. T4 DNA ligase and *Pwo* DNA polymerase were from Roche.

2.2.2 General Equipment

Incubators

Cell cultures were grown in a Gyrotory® Water Bath Shaker Model G76, at a speed of approximately 5, or in a Series 25 Controlled Environment Incubator Shaker, 200 rpm shaking rate, New Brunswick Scientific (Edison, NJ). For cell growth on plates or standing liquid cultures, two models of oven incubators were utilized, a Precision® Gravity Convection Incubator, Precision Scientific, Inc. (Chicago, IL), and a Lab-Line® L-C Incubator, Lab-Line Instruments, Inc. (Melrose Park, IL).

Centrifuges

Large scale centrifugation (>20 ml) was performed using a Beckman Avanti J-25I centrifuge, Beckman Instruments, Inc. (Mississauga, ON), at 4°C or a Beckman J2-21 centrifuge. Amicon Centricon concentrators were spun in a IEC clinical centrifuge, International Equipment Co. (Needham Heights, MA). Samples in microcentrifuge tubes were spun in either a Biofuge A (Heraeus Sepatech GmbH, Germany), or a Bechman GS-15R centrifuge.

Cell Disruption Equipment

Cell suspensions were disrupted utilizing either sonication with a Sonicator™ Cell Disruptor Model W225, converter model #2 and standard tapered microtip, output control set at 5, Heat Systems-Ultrasonics, Inc. (Plainview, NY), or French Press, Carver Laboratory Press at 10,000 – 12,000 psi (Fred S. Carver Inc., Summit, NJ).

Chromatography

Fast Protein Liquid Chromatography (FPLC®) was performed with a Pharmacia Biotech system (now Amersham Pharmacia Biotech, Uppsala, Sweden), with the following components; LCC-500 controller, two P-500 pumps, MV-7 motor valve, UV-M monitor, and a REC-482 chart recorder. The Q-Sepharose® Fast Flow and Superdex® 75 columns were also obtained from Pharmacia. Buffers for use with the FPLC columns were filtered through a 0.22 μm filter (Millipore, Bedford, MA).

Protein Concentration

Protein samples were concentrated using either an Amicon Centricon® YM10 or a Diaflo® Ultrafiltration Membrane PM10 in a 200 ml Amicon stirred cell (Millipore, Beverly, MA).

Absorbance Measurements

Spectrophotometric assays were performed with a Varian Cary 3 spectrophotometer, software version 3.04 (Mississauga, ON).

2.2.3 General Experimental Protocols

The following section outlines protocols utilized throughout many aspects of the work in this thesis. Any changes for a particular experiment are noted in the appropriate section.

Glyoxalase I Enzymatic Assay

The standard glyoxalase I assay was performed as described by Bergmeyer (1983). MG and GSH were preincubated in 50 mM degassed potassium phosphate buffer, pH 6.6, for approximately 15 minutes at room temperature to allow the hemimercaptal substrate to form non-enzymatically. The free GSH concentration was maintained at 0.1 mM to avoid enzyme inhibition (Cliffe and Waley, 1961). The hemimercaptal concentration was calculated using a K_{diss} of 3.1 mM (Vince et al., 1971), and the following equilibrium equation:

$$K_{diss} = [MG_{total} - MG_{complex}]\,[GSH_{total} - GSH_{complex}] / [MG\text{-}GSH_{complex}]$$

$$\text{Note: } [GSH_{free}] = [GSH_{total} - GSH_{complex}] = 0.1 \text{ mM}$$

The rate of formation of the glyoxalase I reaction product, *S*-D-lactoylglutathione, was monitored at 240 nm in 10 mm pathlength quartz cuvettes using an extinction coefficient (ε) of 2860 $M^{-1}cm^{-1}$ (Vander Jagt et al., 1972). One unit of enzyme is defined as the amount of enzyme that produces 1 μmol of *S*-D-lactoylglutathione per minute.

Calibration of Methylglyoxal Solution

Methylglyoxal (MG; 40% aqueous solution) was distilled at atmospheric pressure, to remove any contaminants and polymers, collecting the distillate between 92 - 96°C (Vince et al., 1971). This distilled stock solution was kept at 4°C for up to six months.

Calibration of the distilled MG stock solution was performed based on a modification of the standard glyoxalase I assay (Bergmeyer, 1984). In 1 ml matched cuvettes, 0.5-1.0 mM GSH, and ~0.1 units GlxI (purified *E. coli* GlxI or yeast GlxI grade IV from Sigma) was added to 100 mM potassium phosphate buffer, pH 6.8. The reaction was initiated with the addition of MG to a concentration of 0.2-1 mM, from a sample of the distilled stock MG that was diluted 50-150 fold. The GSH is added in excess to ensure all MG is consumed in the reaction. Distilled stock concentrations varied between 4-8 M.

The concentration of the MG stock solution was calculated based on the amount of product formed (ΔA_{240}), using the standard extinction coefficient for *S*-D-lactoylglutathione (2860 M^{-1} cm^{-1}).

Glutathione Calibration

For most general assays the concentration of a freshly prepared GSH solution can be calculated based on the weight of the GSH powder and the volume of the solution. However, for determination of kinetic parameters the exact concentration of the solution was determined by titration based on the method by Ellman (1959). A 50 mg/ml GSH stock was prepared in the buffer employed in the reaction under analysis. A sample of the stock solution was diluted 60-fold with 100 mM potassium phosphate buffer, pH 7.4, and basified to a pH of 7.5-8.0 with Na_2CO_3. To a cuvette containing 1 ml of potassium phosphate buffer, pH 7.4, a sample of the diluted GSH (~0.05 mM final concentration) was added. An aliquot of DTNB (5,5'dithio-bis(2-nitrobenzoic acid); 2 mg/ml stock in methanol) was added to both the sample and reference cuvettes and the absorbance at 412 nm monitored. Further aliquots of DTNB were added, until there was no further change in the absorbance. The concentration of the

stock GSH was calculated based on the overall absorbance change (ε = 14, 150 $M^{-1}cm^{-1}$; Collier, 1973).

DNA Methods

Plasmid isolation and all standard DNA manipulations were performed according to Sambrook et al. (1989).

Protein Electrophoresis

A Pharmacia PhastSystem™ with commercially available gels and precast buffer strips was utilized for SDS-PAGE (sodium dodecylsulfate polyacrylamide gel electrophoresis) analysis of protein samples. Unless otherwise indicated 20% homogeneous gels were used for analysis of GlxI samples. Samples were mixed in a 1:1 ratio with loading buffer (150 mM Tris Base, 2% SDS, 1% beta-mercaptoethanol, 10% glycerol, 0.1% Bromophenol blue pH 8.0) and boiled for 10 minutes.

Gels were also stained in the PhastSystem development unit. The three steps of the Coomassie staining consisted of staining with 0.1% Coomassie brilliant blue R, 30% methanol, and 10% acetic acid, followed by three destaining steps of 30% methanol and 10% acetic acid, and a final preservation with 5% glycerol and 10% acetic acid.

Protein Concentration Determination

The Bradford method (Bradford, 1976) was utilized for determination of protein concentrations with bovine albumin as a standard. The Bradford dye reagent, 0.01% w/v Coomassie brilliant blue G-250, 95% ethanol, 10% phosphoric acid (85% w/v), was filtered through Whatmann #1 paper and stored at 4°C for up to one month.

In addition, the accuracy of this method was confirmed by utilizing the theoretical extinction coefficient of the denatured protein (6.0 M guanidine hydrochloride) predicted for *E. coli* GlxI (ε = 15 930 $M^{-1}cm^{-1}$ for a single subunit), calculated by PC/Gene® 6.85 software (IntelliGenetics Inc., Mountain View, CA), based on the method of Gill and von Hippel (1989). Also, because of the presence of a single Cys residue in each subunit of the homodimeric protein, quantitation of the Cys in the denatured GlxI protein by DTNB based on the method of Riddles et al. was performed (Riddles et al., 1983). A sample of protein was added to potassium phosphate buffer (100 mM, pH 7.4), containing guanidinium chloride (6

M) and EDTA (1 mM), and the absorbance at 412 nm monitored following the addition of DTNB (25-50 µl of a 3 mM stock in buffer). The concentration of thiol was calculated using a molar extinction coefficient of 13 700 $M^{-1}cm^{-1}$ under these conditions (Riddles et al., 1983; Creighton, 1989).

Preparation of Metal-Free Buffers and Plasticware

To remove extraneous metals from buffers and water, the solutions were passed over Chelex 100 resin (Na^+ form) prior to use (~5 ml resin/litre of buffer or less) using a Pharmacia peristaltic pump P-1. To 'Chelex-treat' a protein sample, <5 ml metal substituted protein was passed over ~3 ml resin. As the Chelex treatment removes divalent metals from solution, replacing them with Na^+, the solution may become somewhat basic following treatment and therefore the pH was monitored, particularly in solutions of low buffer concentration.

All Chelex-treated solutions, and apoenzyme samples were stored in plasticware presoaked in acid to minimize leaching of metals into the solution. Buffers were stored in Nalgene bottles and protein samples in scintillation vials (ensuring there was no metal liner in the lids). Plasticware was soaked in 10% nitric acid for 15 min then rinsed with copious amounts of Chelex-treated MilliQ-H_2O. To minimize the level of metal leaching from the quartz cuvettes during the kinetic measurements of apoGlxI, the cuvettes were soaked in 1:1 nitric acid:sulfuric acid for 15 min prior to use.

Electrospray Mass Spectrometry (ESMS)

The integrity of each protein sample was monitored by ESMS, provided by the Biological Mass Spectrometry Laboratory (BMSL), University of Waterloo. A Micromass Quattro II triple-stage quadrupole mass spectrometer equipped with an electrospray ionization source was utilized. Samples were introduced in an eluant of 1:1 H_2O/CH_3CN (containing 1% formic acid). The data was analyzed with the Masslynx software (version 2.0) and the multiply charged distribution profile subjected to the MaxEnt algorithm in order to determine the true molecular mass and its associated errors.

2.2.4 Protein Expression and Purification

The cell growth and protein purification conditions have been previously reported in detail in my M.Sc. work (Clugston, 1997; Clugston et al., 1998a). The final conditions used throughout this work are summarized here.

Cell Growth Conditions

Cell cultures were generally grown in Luria-Bertani (LB) broth (1% w/v tryptone, 0.5% yeast extract, 0.5% NaCl, ± 1.25% agar, pH 7.4 with NaOH), supplemented with ampicillin (Amp) or Carbenicillin (Carb), at a concentration of 100 μg/ml in LB agar plates, 50 μg/ml in LB broth, or 30 μg/ml in minimal media where indicated.

To express *E. coli* GlxI a starter culture of LB_{Carb} was inoculated with *E. coli* MG1655/pGL10 and the culture left standing at 37°C overnight. After approximately 14 hours, the culture was shaken at 37°C for ~30 minutes, to ensure the cells would be in a stage of rapid growth. A large scale culture of LB_{Carb} plus 1 mM $NiCl_2$, was then inoculated with 10 ml starter culture/1L media. When the OD_{600} reached approximately 0.5 (~4 h) the culture was induced with 0.5 mM IPTG (isopropyl-β-D-thiogalactopyranoside) for an additional 6 hours, at 37°C. The cells (~3.5 g/L) were then collected (10,000 rpm JA-14 or 15 300 g, 15 min), washed with 20 mM Tris pH 7.0, repelleted (10,000 rpm JA-25.5 or 12,100 g, 15 min), frozen in liquid N_2, and stored at -80°C.

Cell Disruption

Frozen *E. coli* MG1655/pGL10 cells were thawed on ice in 20 mM Tris pH 7.0. (10 ml/gram of frozen cells for sonication or ~5 ml/g for French Press disruption). The cell suspension was disrupted by two rounds of sonication using short pulses (~10 s) with intermittent cooling on ice (~30 s) or by two passes through the French Press at 10,000-12,000 psi. PMSF (phenylmethylsulfonyl fluoride; 1mM) and glycerol (30% v/v) were immediately added to the solution and the cell debris removed by centrifugation (20,000 rpm JA-25.5 or 48 300g, 15 min). As the solution was too viscous to effectively filter, the supernatant was respun in a clean centrifuge tube to remove any additional debris.

Protein Purification

The crude extract was applied to a Q-Sepharose Fast Flow column (HR 10/30), equilibrated with 20 mM Tris, 30% glycerol, pH 7.0 at 1-2 ml/min and eluted with a linear (1%/min) gradient to 1 M KCl, in the same buffer. The fractions containing GlxI activity (30-50% KCl) were pooled and dialyzed overnight (2 x 1 L 10% glycerol/H_2O, 4°C) with SPECTRA/POR® molecularporous membrane tubing, molecular weight cutoff 12,000-14,000, (Spectrum Medical Industries, Inc. Los Angeles, CA) with frequent additions of PMSF (1.5 mM initially, an additional 1.0 mM after 3 hours and after 8 hours from the start of the dialysis the dialysis solution was changed and 1.5 mM PMSF added). The pH of the glycerol/H_20 was adjusted to between 6-9 using KOH after each PMSF addition.

The dialyzed protein sample was further purified by preparative isoelectric focusing (IEF; Bio-Rad Rotofor®, Mississauga, ON). Prior to protein loading, the IEF was loaded with MilliQ-grade water and a constant power of 3-5 W was applied for 20 minutes to remove any contaminating ions from the system. To separate GlxI, a pH gradient of 4.5-5.0 was established with Bio-Rad RotoLytes® (final concentration of 100 mM each MES and Gly-Gly). Following a 6 hour separation at 12 W constant power, the active fractions were pooled and concentrated by ultrafiltration (10 kDa cutoff) with a buffer change to 50 mM MOPS pH 7.0 (Chelex treated). The protein under these conditions was stable to storage at 4°C for at least six months.

2.2.5 Enzyme Kinetic Studies

Determination of Kinetic Parameters

Determination of the Michaelis constant, K_m, and the maximal enzyme velocity, V_{max}, for *E. coli* GlxI activated with various metal chlorides involved measurement of the initial reaction rate utilizing 10 substrate concentrations ranging between 0.005 and 2.0 mM. The enzyme stock was diluted with 50 mM MOPS, pH 7.0, and 2.5 mole equivalence of metal to dimeric enzyme added unless otherwise noted. The data was fit by non-linear regression analysis using GraFit 3.01 (Erithacus Software Ltd.).

As the iron (II) chloride readily oxidizes, care had to be taken to prevent exposure to air. The metal powder and prepared solutions were handled under a flow of argon. All

buffers and solutions were degassed and sparged with argon prior to use. The Fe^{2+}-activated GlxI was introduced with a standard pipetman, keeping a layer of argon over the enzyme solution and bubbling argon through the substrate solution in the cuvette immediately prior to addition of the enzyme.

To ensure that the metal chlorides did not affect the stability of the *S*-D-lactoylglutathione product or the hemithioacetal substrate, each was incubated separately with the metals in the assay buffer, in the absence of GlxI and the absorbance at 240 nm was monitored over time.

pH Profile

A profile of the effect of pH on the activity of the Co^{2+}-activated enzyme was performed by altering the pH between 5.0 and 8.2, as previously described for Ni^{2+}-GlxI (Clugston, 1997). This is within the range that the dissociation constant for the substrate formation is valid (3.1 mM; Vince et al., 1971; Vander Jagt et al., 1972). The ionic strength was maintained at 0.2, half from the buffer and half from potassium chloride (0.1 M). Potassium acetate buffer (0.1 M) was utilized for pH 5.0 and 5.5, potassium phosphate between pH 5.85 and 8.0 (0.0807 M at pH 5.85, 0.062 M at pH 6.2, 0.0465 M at pH 6.9, 0.0381 M at pH 7.4, 0.0343 M at pH 8.0), *N*-methyldiethanolamine (0.146 M) for pH 8.2, and diethanolamine (0.133 M) for pH 8.4. When higher concentrations of substrate (>0.5 mM) were added to the buffer the pH decreased up to 0.1 units, particularly with the lower concentration phosphate buffers. To compensate the phosphate buffers were prepared 0.1 pH units higher than the final desired value.

Metal Competition

To determine if the metal bound to GlxI can be replaced by another metal in solution, metal competition studies were performed. One mole equivalent metal chloride (Ni^{2+} or Zn^{2+}) was added to dimeric apoGlxI and the activity determined. Five- and one hundred-fold equivalents of the competing metal (Ni^{2+} or Zn^{2+}, Co^{2+}, Cd^{2+}, Mn^{2+}, Cu^{2+}) were then added and the solutions kept at 4°C. The activities were tested with 0.5 mM substrate, 1 min, 1 hour, 1 day, and 7 days after addition of the competing metal. Similar competitions were performed with GlxI reactivated with each of Co^{2+}, Cd^{2+}, Mn^{2+}, and Cu^{2+} versus Ni^{2+} and Zn^{2+} as the competing metal, with the exception of Zn^{2+} versus Cu^{2+} as both are inactive and

hence no exchange could be monitored by activity assays. To avoid a decrease in the enzymatic activity during storage at low concentrations, all incubations were performed at a protein concentration of 2 mg/ml. Immediately prior to determination of the activity an aliquot of the protein-metal solution was diluted 20-fold to permit activity measurement of low quantities of enzyme. Two controls were also monitored for each metal. In one case water was added in place of the competing metal and in the second, the metal added in excess matched the original activating metal to ensure there was no further activation beyond that observed with one equivalent.

Further analysis was performed with incubation of the solutions at 37°C. To ensure the enzyme is stable under these conditions, the activity of GlxI activated with one mole equivalent $NiCl_2$ to dimeric enzyme was monitored over a 2 day period. Complete metal competitions were performed by adding one equivalent metal then five-and one hundred-fold equivalents of the competing metal, incubating at 37°C and monitoring the activity over a 2 hour period. Each of the metal combinations described for the tests at 4°C were repeated at 37°C. As this is a time-dependent experiment each time point was measured once but each of these sets of measurements was performed in duplicate.

Inhibitor Studies

Purified apoenzyme was diluted in 50 mM MOPS, pH 7.0 and one mole equivalent of $NiCl_2$ added to produce an active dimeric enzyme. IC_{50} measurements were performed at 6-9 different inhibitor concentrations with a substrate concentration of 0.04 mM, maintaining a free GSH concentration of 0.1 mM to avoid enzyme inhibition, assuming a K_d of 3.1 mM for methylglyoxal and GSH (Cliffe and Waley, 1961; Vince et al., 1971). Every point was measured in triplicate and each set of measurements was performed at least twice. The inhibitors studied were dissolved in the assay buffer, 50 mM potassium phosphate, pH 6.6, with the exception of the transition state analogue (TSA), which was dissolved in water and *S*-{2-[3-(hexyloxy)benzoyl]vinyl}glutathione, dissolved in DMSO (dimethyl sulfoxide). The IC_{50} curves were fit using GraFit 3.01 (Erithacus Software Ltd.) according to the following equation: $y = a/(1+(x/IC_{50})^s)$, or by a standard linear fit ($y = mx + b$) when the solubility and low inhibition level of several compounds limited testing over a wide concentration range.

2.2.6 Metal Binding

Inductively Coupled Plasma (ICP) Analysis

For inductively coupled plasma (ICP) analyses of the *E. coli* GlxI protein, the purified protein was prepared in metal free solutions. For the various metal substituted forms of the enzyme analyzed, apoGlxI was reconstituted with 2.5 mole equivalents of metal chloride ($NiCl_2$, $ZnCl_2$, $CoCl_2$, $CdCl_2$, $MnCl_2$, $CuCl_2$, $MgCl_2$, $CaCl_2$) and the solution dialyzed overnight versus 2 x 500 ml 50 mM MOPS, pH 7.0 (Chelex treated) to remove any unbound metal ions. Initially samples and controls were passed through Chelex 100 resin to remove loosely bound metals, and acidified to below pH 2 with high purity nitric acid. As this was not found to be necessary subsequent samples were not passed over Chelex resin prior to acidification. To ensure that the Chelex treatment was not removing bound metal from the enzyme or affecting the activity in any other manner, the activity of the sample was tested before and after passage through the Chelex resin as well as before and after the dialysis. Attempts were made to also test the binding of $FeCl_2$ to apoGlxI, however precipitation of Fe^{3+} occurred during the dialysis, preventing passage of the unbound metal from the dialysis tubing and hence the results were invalid.

To determine the metal content of *E. coli* GlxI grown in the presence of $ZnCl_2$ (0.1 mM), the enzyme was purified with the Q-Sepharose Fast Flow anion exchange column, and dialysis, but not subjected to isoelectric focusing, as this removes any bound metal. This was to determine if Zn^{2+} added to the media is taken up by the cells and incorporated into *E. coli* GlxI. The effect of added Ni^{2-} to the growth media and the effect of no metals added on the metal content of GlxI has previously been reported (Clugston, 1997; Clugston et al., 1998a). Concentrations of 0.1 mM $ZnCl_2$ or 1 mM $NiCl_2$ added to the growth media was found not to be detrimental to *E. coli* MG1655/pGL10 cell growth.

Metal analyses were performed at the Solutions Analytical Laboratory (previously called the Water Quality Laboratory, Department of Earth Sciences, University of Waterloo). Inductively coupled plasma analyses were performed using a Thermo Instruments IRIS Plasma Spectrometer (ICP). The following metals were tested for: Al, As, B, Ba, Ca, Cd, Co, Cr, Cu, Fe, Li, Mg, Mn, Mo, Ni, P, Pb, S, Se, Si, Sr, Ti, V, and Zn. Commercial standards were prepared in house in duplicate.

Isothermal Titration Calorimetry (ITC)

ITC titrations were carried out in a Calorimetry Sciences Corporation (CSC; Spanish Fork, UT) 4200 Isothermal Titration Calorimeter, with Hastelloy stainless steel cells, at a constant temperature of 25°C, 297 rpm stirring rate. Titrations were performed with purified apoGlxI and several metal chlorides ($NiCl_2$, $ZnCl_2$, $CoCl_2$, $CdCl_2$, $MnCl_2$, $MgCl_2$, $CaCl_2$). The enzyme concentration in each titration was between 0.06-0.14 mM dimeric apoGlxI in 50 mM MOPS pH 7.0 (Chelex treated), or 3.6-8.4 mg of protein per run to fill the 1.260 ml cells plus the access portals. Metal concentrations were between 1-2 mM in matching buffer, prepared in the same buffer stock used for protein storage (must be exactly identical). The reference cell was filled with MilliQ-grade water. Titration with each metal into apoGlxI was performed a minimum of three times, with the exception of Mg^{2+} and Ca^{2+} which were only measured twice.

Titration data was collected with the "shell" software provided with the instrument. The area under the peaks in the binding isotherm, corresponding to the heat absorbed or released when the ligand interacted with the protein, was analyzed with ITC Data Works™ Version 1.0, and the thermodynamic parameters determined utilizing BindWorks™ version 1.0. The heat of dilution was calculated by determination of the area under each peak at the end of the titration following saturation. This value was added or subtracted to each value during the titration. A sample titration of each metal into buffer was first performed to ensure the heat of dilution was not concentration dependent.

Prior to analysis of protein-metal interactions, the ITC was calibrated utilizing the internal electrical heater to ensure the heat measured by the thermo electric device is properly converted into μWatts. In addition a chemical calibration was performed (Briggner and Wadso, 1991) titrating barium chloride (Aldrich) into 18-crown-6 (Aldrich) and the exact cell volume found to be 1260 μl. Test titrations were also performed with 2'CMP and RNase A (Sigma). The thermodynamic parameters determined were within acceptable limits of the published values (Wiseman et al., 1989) confirming the instrument was functioning properly and the techniques utilized to setup the titration were suitable.

2.2.7 Protein Stability Studies

Differential scanning calorimetry (DSC) was performed by Dr. H. Frey in Professor J. Lepock's laboratory (Department of Physics, University of Waterloo), on a Calorimetry Sciences Corporation (CSC) Nano DSC. GlxI samples (1 mg/ml in Chelexed 50 mM MOPS pH 7.0) were prepared by adding 2.5 mole equivalence metal chloride to dimeric apoenzyme concentration. The samples were scanned at 1°C per minute and each sample was rescanned to determine the denaturation reversibility. Data was analyzed with Microcal™ Origin™ version 5.0 software (Microcal Software, Inc., Northampton, MA).

2.2.8 Mass Spectrum Analysis of the Non-covalent Interactions between Glyoxalase I and Various GSH Analogues

For mass spectrum analyses purified apoenzyme, following isoelectric focusing, was concentrated and the buffer changed to 5 mM ammonium acetate buffer, pH 7.0 using an Amicon Centricon (YM10). Aliquots of the enzyme were stored in microcentrifuge tubes, which had been presoaked with 10% nitric acid to remove any extraneous metals and well rinsed with Chelex treated water. The samples were then lyophilized and stored at -80°C.

Mass spectrometry (MS) studies on the non-covalent interactions between *E. coli* GlxI and various GSH analogues were performed by Dr. A. J. R Heck and E. Stokvis at Utrecht University (Utrecht, The Netherlands). The buffer solutions used in the MS studies generally consisted of aqueous 5 mM ammonium acetate, acidified with acetic acid to a pH of 5.0. For the pH dependence studies 5 mM ammonium acetate solutions were adjusted using acetic acid or ammonium hydroxide to pH values of 2.5, 3.0, 4.0, 5.0, 7.0, 8.0, and 10.0. GlxI was dissolved in a 25 mM ammonium acetate buffer (pH 5.0). The transition state analogue (TSA), *S*-methylglutathione and *S*-propylglutathione were directly dissolved in the buffer. Stock solutions of *S*-hexylglutathione, *S*-octylglutathione, *S*-D-lactoylglutathione, *S*-(*p*-nitrobenzyl)-glutathione, *S*-{2-[3-(hexyloxy)benzoyl]vinyl}glutathione, glutathionesulfonic acid, and *S*-(*p*-azidophenacyl)-glutathione were first dissolved in DMSO and placed overnight in an ultrasonic bath. A myricetin stock solution was prepared in absolute ethanol. These solutions were diluted to the selected concentrations with buffer. The final solutions contained only marginal quantities of organic solvent (DMSO or ethanol). No loss of enzymatic activity was observed under these conditions.

Nanoflow ESI-TOF (electrospray ionization time-of-flight) mass spectra of GlxI and the potential inhibitors were acquired using a Micromass Q-TOF hybrid tandem mass spectrometer equipped with a Z-spray ionization source, using gold-coated glass capillaries. The capillary was typically loaded with a few microlitres of the buffered solution. Experimental ion source parameters were optimized for detection of non-covalent complexes as described previously (van Berkel et al., 2000; van Dongen and Heck, 2000). The potential between the nanospray needle and the orifice of the mass spectrometer was approximately 1700 V; the optimal cone voltage was approximately 60 V. The first quadrupole was used in the RF-only mode. TOF spectra were measured over a m/z range of 800 to 4000. The data were recorded and processed using the MassLynx software. Mass calibration of the spectrometer was performed using horse heart myoglobin.

2.3 Results and Discussion

2.3.1 Kinetic Analyses

Determination of Enzyme Kinetic Parameters in the Presence of Various Metal Ions

The detailed kinetic studies on *E. coli* GlxI in the presence of various metals reinforced our preliminary findings (Figure 2.7). The enzyme is maximally active with Ni^{2+} and exhibited lower levels of activity with Co^{2+}, Cd^{2+}, and Mn^{2+}. In addition, activity was found upon addition of Fe^{2+} but not with Cu^{2+}. Table 2.1 summarizes the results of the kinetic analysis. During these experiments several difficulties were encountered. One obvious problem was the oxygen sensitivity of Fe^{2+}. Initial attempts to introduce the Fe^{2+}-activated GlxI into the cuvette with a gas-tight Hamilton syringe proved problematic. The enzyme appeared to be activated by contact with the syringe needle. As these needles are made of stainless steel, which contains nickel, it is likely that this is the source of the enzyme activation. As a result the Fe^{2+}-activated enzyme solution had to be introduced with a standard pipettor. The enzymatic assay is monitored for only a few minutes and the substrate solution was sparged with argon to minimize possible oxidation of the metal Fe^{2+} to Fe^{3+}. Using this technique it was possible to obtain the V_{max} and K_m for Fe^{2+}-activated GlxI. Attempts by an undergraduate thesis student, G. Konrath, to perform an activity titration for Fe^{2+} into apoGlxI was hampered by iron oxidation. The maximal activity appeared to be reached between one and two mole equivalents of metal to dimeric enzyme, rather than 1 equivalent seen previously for the other metals (Figure 2.5). With one equivalent of Fe^{2+} the activity was only approximately 75% of the fully active form. It is likely that there was some oxidation of the iron solution upon preparation lowering the effective concentration used in the titration. As the kinetic analysis presented in Table 2.1 were performed with 2.5 equivalents of metal in each case, there was sufficient Fe^{2+} available for the analysis.

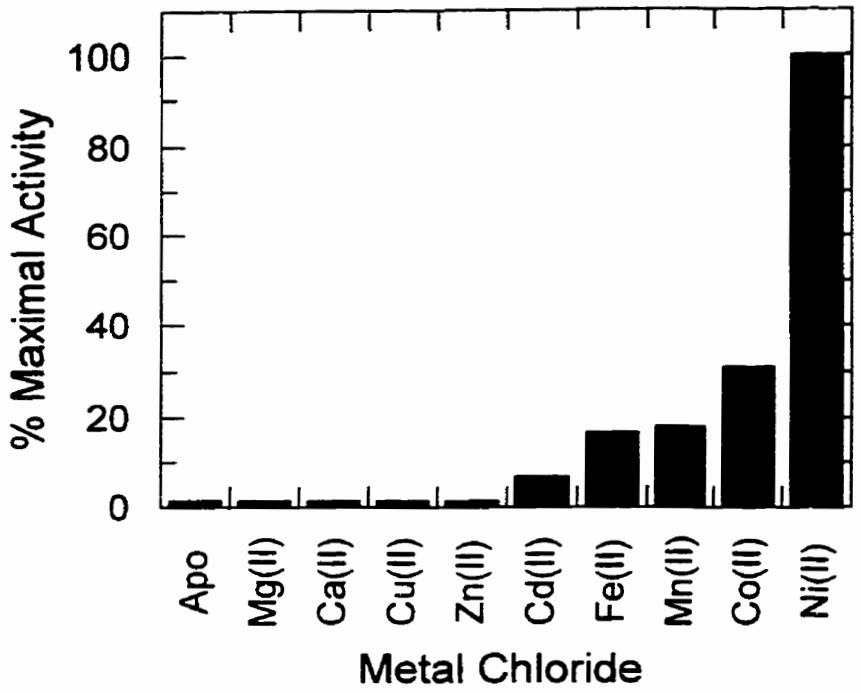

Figure 2.7: Activation of apo *E. coli* GlxI by various metal ions (10x mole equivalence; Clugston, 1997; Clugston et al., 1998a, and this work).

Table 2.1: Kinetic analyses of *E. coli* glyoxalase I with various activating metals*.

Metal Chloride	V_{max} (μmol/min/mg)	K_m (μM)	k_{cat} (s^{-1})	k_{cat}/K_m (M^{-1} s^{-1})
Ni^{2+}†	676 ± 17	27 ± 0.4	338	12 x 10^6
Co^{2+}	213 ± 33	12 ± 2	106	9.1 x 10^6
Mn^{2+}	121 ± 9.8	9.6 ± 2	60.2	6.3 x 10^6
Fe^{2+}	112 ± 19	10 ± 3	55.7	5.5 x 10^6
Cd^{2+}	43.1 ± 4.6	8.9 ± 0.4	21.4	2.4 x 10^6

†From Clugston et al., 1998a

*10 substrate concentrations were measured in triplicate with ~0.4 μg of enzyme per assay, and each set of kinetic measurements performed 2-3 times for each metal.

A second problem that was encountered was in the analysis of Mn^{2+}-GlxI. After addition of the metal activated enzyme to the substrate solution, the activity appeared to slowly decrease during the course of the reaction. It was found that addition of excess metal to the substrate solution reduced the rate of this decrease, suggesting that the metal was being lost in the reaction mixture. Analysis of the enzyme activity using MES as the assay buffer rather than phosphate eliminated this problem. The pH was maintained at 6.6 so as not to alter the equilibrium for the MG-GSH substrate. This loss of metal was also observed, and to a much greater extent, for the H5Q mutant form of GlxI discussed in Chapter 4. Although it has a very low affinity, phosphate does bind metals, whereas MES-based buffers do not have detectable metal binding properties (Price, 1996). As this problem was only encountered with the Mn^{2+}-activated enzyme it suggests that the affinity of the enzyme for Mn^{2+} is slightly lower than for the other metals. This was in fact proven in the metal binding analysis presented in the following section. The kinetic parameters for Ni^{2+}-GlxI were measured using MES for the assay buffer and there were no significant effects on the enzyme activity. Hence, all subsequent Mn^{2+} activity assays were performed in MES. This buffer effect may also explain why the V_{max} reported in this work is somewhat higher than the apparent V_{max} (~ 65 μmol/min/mg) reported from our previously metal titration study (Clugston, 1997).

As evident from Table 2.1, there is a slight alteration in the Michaelis constant, K_m, with the various metal ions, suggesting the alteration of the active site metal is not greatly affecting the substrate binding. The value for the Ni^{2+}-activated enzyme is somewhat higher than that measured for the other forms of the enzyme, but is still within the same order of magnitude. For the five metal activated forms of *E. coli* GlxI, the primary alteration in their kinetics is seen in the V_{max} or k_{cat}. There is approximately a 15-fold difference in the activity range of these five active forms of the enzyme.

In comparison, the Zn^{2+}-active forms of GlxI from *S. cerevisiae*, *H. sapiens*, and *P. putida* have k_{cat} values of 1120 s^{-1}, 1500 s^{-1}, and 500 s^{-1} respectively (Vander Jagt and Han, 1973; Ridderström et al., 1997; Saint-Jean et al., 1998). However, the k_{cat}/K_m values from these sources are similar to that of the *E. coli* GlxI, being 3.5 x 10^6 $M^{-1}s^{-1}$, 23 x 10^6 $M^{-1}s^{-1}$, and 1.3 x 10^6 $M^{-1}s^{-1}$ from *S. cerevisiae*, *H. sapiens*, and *P. putida*, respectively (Vander Jagt and Han, 1973; Ridderström et al., 1997; Saint-Jean et al., 1998). The k_{cat}/K_m values indicate that the *E. coli* GlxI is very efficient, functioning at close to a diffusion-controlled rate. Recent

studies on the kinetic properties of the yeast GlxI enzyme utilizing various viscosometric methods supports the suggestion that GlxI functions at a diffusion-controlled rate, under physiological conditions (Shih et al., 1997).

pH Profile

The activity of *E. coli* GlxI was analyzed at various pHs to determine the effect of pH on enzyme activity. We previously reported that Ni^{2+}-GlxI was active between pH 5-8 with no significant effect on the catalytic activity (Clugston, 1997; Clugston et al., 1998a). At pH 8.4 V_{max} was not reached precluding determination of the Michaelis constant at this value. However, between pH 8.0-8.4 a significant increase in the K_m was noted. There was also an increase in the K_m below pH 5.8. A similar pH profile analysis has been performed on the Co^{2+}-activated enzyme (Figure 2.8). As illustrated, the K_m is also increased above pH 8 but not as significantly as observed for Ni^{2+}-GlxI. Like the Ni^{2+} form, the maximal activity of the Co^{2+}-activated enzyme could not be determined at pH 8.4. Also similar to the Ni^{2+}-GlxI, Co^{2+}-GlxI did exhibit an increase in the K_m at pH 5.5 but once the pH was reduced to 5.0 the maximal activity was no longer measurable. This is not observed for Ni^{2+}-GlxI. It is possible that at this lower pH the affinity of the enzyme for the metal is reduced and the activating Co^{2+} is lost. A decrease in the activity of the enzyme during the time frame of the assay suggested that the activity was not simply decreased at this pH but that there were other complicating factors, such as metal loss. Alteration in the ionization state of glutathione in this pH range has been considered to be unlikely from studies with yeast GlxI (Vander Jagt and Han, 1973). The sudden change in the K_m suggests that the protonation state of some residues involved in substrate binding may have been affected. Examination of the crystal structure of *E. coli* GlxI and comparison with the *H. sapiens* GlxI structure cocrystallized with a GSH-analogue, allows for the identification of potential active site residues that may be affected (Chapter 3; Cameron et al., 1997; He et al., 2000). Although the active site environment may alter the pK_a value, in general histidines have been found to have a pK_a value in the range of 5-8 in proteins, cysteines between 8-11, and the carboxy of aspartate or glutamates have been observed to have pK_a value between 2-5.5 in proteins (Fersht, 1999 and references therein). The ligands to the catalytic metal in *E. coli* GlxI are histidines (5 and 74) and glutamates (56 and 122) and therefore may be affected by the change in pH above 8 or

below 5. However, as the enzyme was still able to reach maximal enzymatic activity until pH 8.4 this is not expected to be the cause of the increase in K_m. In the *H. sapiens* GlxI enzyme, the aromatic ring of phenylalanine 68 lies above the peptide linkage in glutathione. In the *E. coli* enzyme this residue is tyrosine 39. Although tyrosines generally have pK_a values between 9-12 in proteins (Fersht, 1999), it may be affected above a pH of 8 in the *E. coli* enzyme. Aside from the glutamate residues involved in metal ligation, glutamate 49 may be involved in substrate binding, although it is rather distant from the active site. In *H. sapiens* GlxI this residue corresponds to leucine 93, which is 4.3 Å from the benzyl ring of the benzylglutathione bound in the active site. Arginine 38 in the *H. sapiens* enzyme was observed to form a salt bridge with the carboxylate of the GSH. Although the pK_a values for arginine is generally in the range of 12, this residue is conserved in the *E. coli* enzyme and therefore may be important in substrate binding. The role of these residues in substrate binding in *E. coli* GlxI is speculative at best given our current knowledge. The active site of the *E. coli* enzyme is much more open than in the *H. sapiens* enzyme (Chapter 3) and therefore there may be alterations in the binding of substrate. Upon completion of the data analysis of *E. coli* GlxI cocrystallized with a GSH-analogue, the determination of the residues involved in substrate binding that might be affected by a change in pH may be identified.

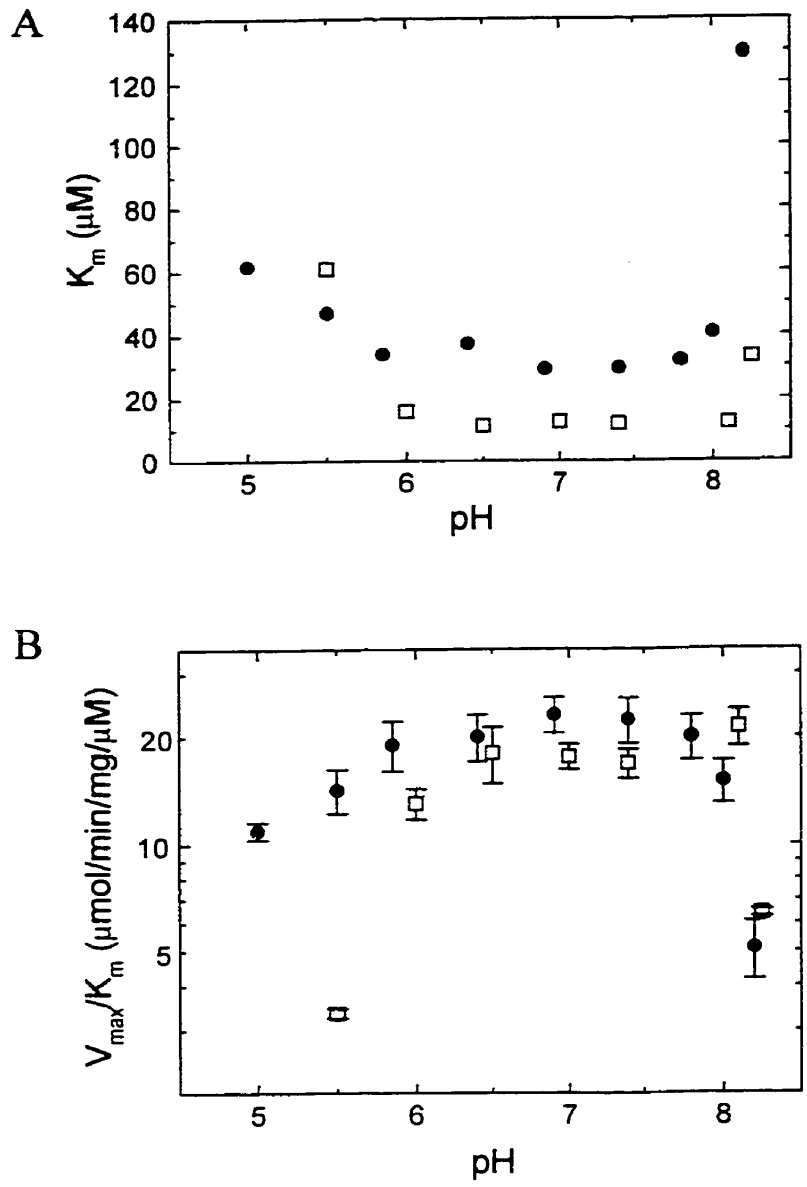

Figure 2.8: Comparison of the effect of pH changes on (A) the K_m and (B) activity (log plot of V_{max}/K_m) of *E. coli* glyoxalase I activated with Ni^{2+} (•) and Co^{2+} (□).

Metal Competition Studies

As maximal enzymatic activity is achieved without an excess of metal present but only one equivalent of metal added to the apoenzyme, it appeared that *E. coli* GlxI has a high affinity for the metal ions. Therefore it was of interest to determine if any exchange of the bound metal could occur. To evaluate this possibility numerous metal competition studies were undertaken. Initially, the enzyme was activated with one mole equivalent of metal and 5 or 100 equivalents of the competing metal were added. The enzyme-metal solution was incubated on ice and the activity monitored. Figures 2.9 and 2.10 illustrate representative plots for Ni^{2+}-GlxI and Zn^{2+}-GlxI with Co^{2+}, Mn^{2+}, Cd^{2+}, Cu^{2+} and either Ni^{2+} or Zn^{2+} added in excess. If we assume that we are observing metal exchange then this exchange appears to occur very slowly. Similar trends were seen with GlxI reconstituted with each Co^{2+}, Mn^{2+}, Cd^{2+}, and Cu^{2+} and excess Ni^{2+} and Zn^{2+} added to attempt to compete for the metal binding site. In order to better analyze the potential metal exchange, the experiments were then repeated but with the enzyme solution incubated at 37°C. Ni^{2+}-activated GlxI was first incubated at 37°C and the enzyme activity monitored to ensure enzyme stability under these conditions. The enzymatic activity of *E. coli* GlxI in the presence of Ni^{2+} did not change over the course of 48 h when incubated at 37°C. Thus, these conditions could be employed for further competition studies. In all of the competition experiments the enzyme was incubated at a concentration of 2 mg/ml and diluted immediately prior to analysis. This ensured consistency in the incubation concentrations, and maintained the enzyme concentration at a high level to ensure enzyme stability.

A series of plots are illustrated in Figures 2.11 and 2.12 showing the alteration of enzyme activity over time in the presence of alternate metals. The activity change is related to the specific metal ion, in addition to the incubation temperature and metal concentration. In the case of the Zn^{2+}- and Cu^{2+}-substituted GlxI the enzyme activity increases upon addition of the competing metal. This increase is attributed to the activation by the competing metal. Conversely, for the Ni^{2+}-activated enzyme, the activity decreases with this possible metal exchange. The specific activity eventually levels out, and in most cases this occurs at the level of activation of the metal in excess, suggesting the bound metal may now be completely exchanged. As illustrated in Figure 2.9A and 2.11A, Mn^{2+} does not completely replace Ni^{2+}

with only 5 equivalents added (relative activity 0.5 rather than expected 0.2). Similarly competition with Cu^{2+} did not produce a completely inactive enzyme. A further reduction in activity was observed with 100 equivalents, which possibly indicated that more of the metal had exchanged. This suggests that the rate of exchange for Mn^{2+} and Cu^{2+} is lower than for other metals tested. In contrast, complete exchange with Cd^{2+}, based on a decrease in the relative activities to 0.08, suggests a more rapid exchange for this metal. The Mn^{2+}-GlxI was more rapidly activated with the addition of excess Ni^{2+} than Cd^{2+}-GlxI. Similar results were observed for the analysis with 5 equivalents of competing metal (data not shown), but the exchange appeared to occur at a slower rate.

One exception to these observations was the activation of Zn^{2+}-GlxI and Cu^{2+}-GlxI with excess Ni^{2+} (Figure 2.10 and 2.12A and E). Although the activity increases with time, it does not reach the maximal activity generally seen for Ni^{2+}-GlxI. Even when the activity of the sample incubated at 37°C was tested 24 hours later the activity had not reached its maximal level. This could mean there was incomplete exchange of the metal ions, or that the enzyme is less stable when incubated with Zn^{2+} or Cu^{2+} and the enzyme was becoming inactive prior to activation with the Ni^{2+}. Our recent differential scanning calorimetry results (Section 2.3.3) indicate this later suggestion is not likely for the Zn^{2+} sample, as the enzyme appears very stable in the presence of Zn^{2+}. ApoGlxI can be fully reactivated with the addition of metal, hence it is possible to achieve full activity after removal of the metal in *E. coli* GlxI. This is not the case for *S. cerevisiae* GlxI (Murata et al., 1986c). Without an analysis of the metal content of the enzyme following the incubation with excess metal it is not possible to speculate further on the reasons for the lack of complete re-activation.

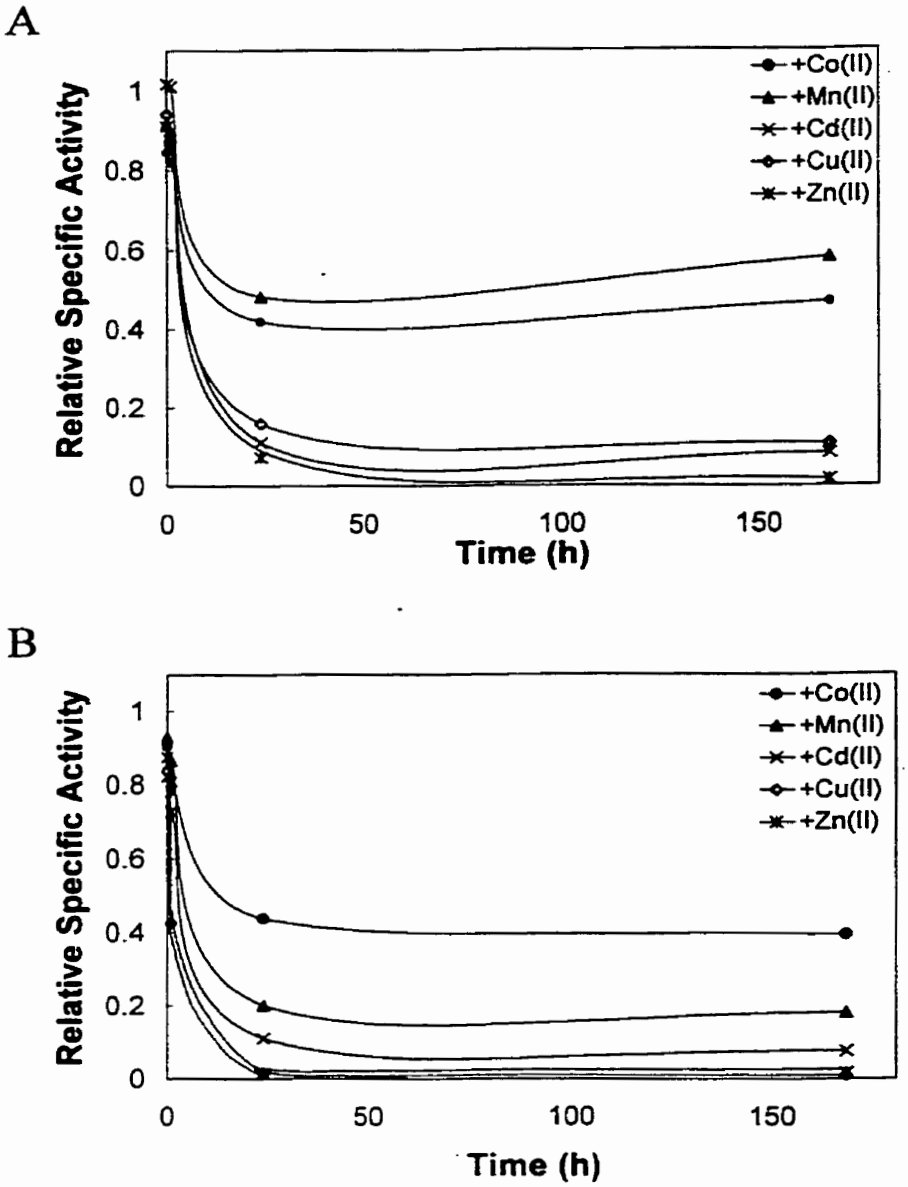

Figure 2.9: Ni^{2+}-GlxI metal competition. (A) 5 equivalents and (B) 100 equivalents of the indicated competing metal added and incubated at **4°C**. Activities are shown relative to fully active Ni^{2+}-GlxI. The lines are arbitrary fits to show the trend in the data.

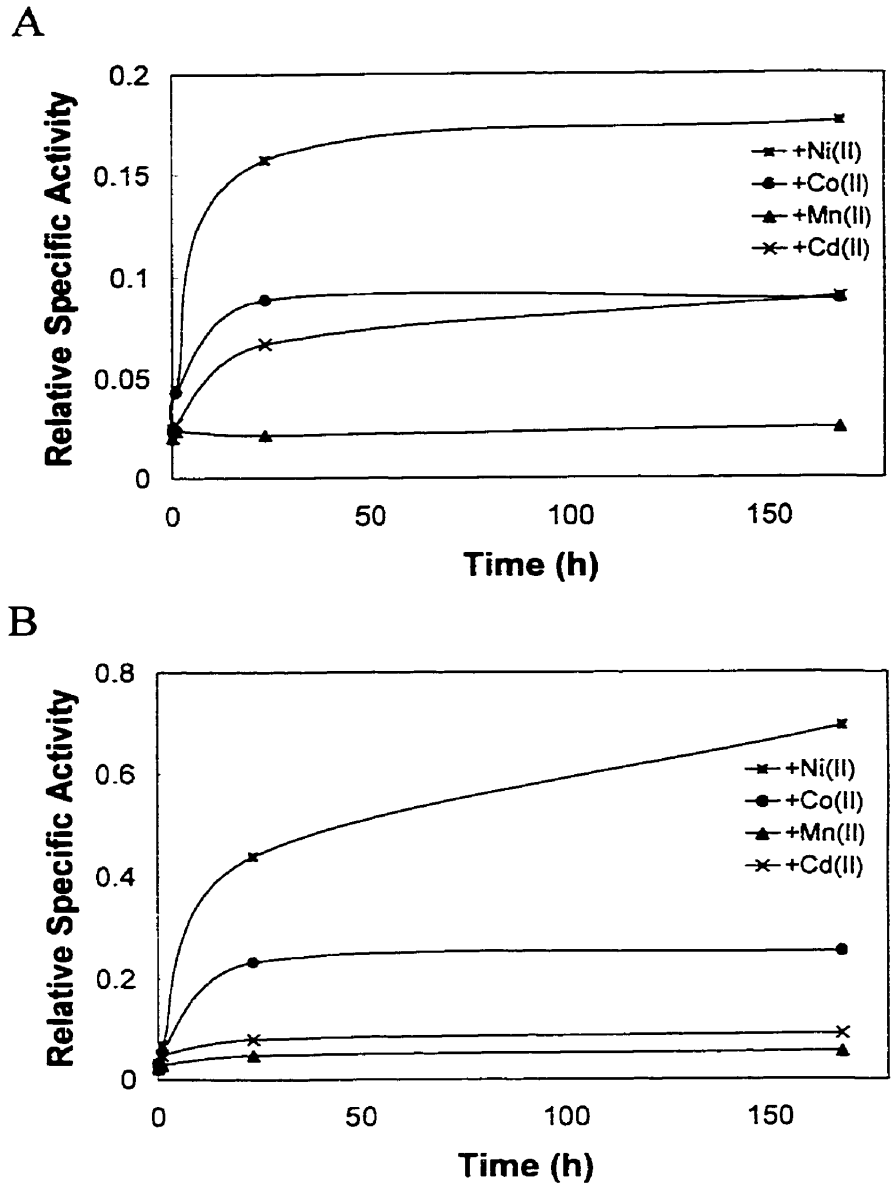

Figure 2.10: Zn^{2+}-GlxI metal competition. (A) 5 equivalents and (B) 100 equivalents of the indicated competing metal added and incubated at **4°C**. Activities are shown relative to fully active Ni^{2+}-GlxI. The lines are arbitrary fits to show the trend in the data.

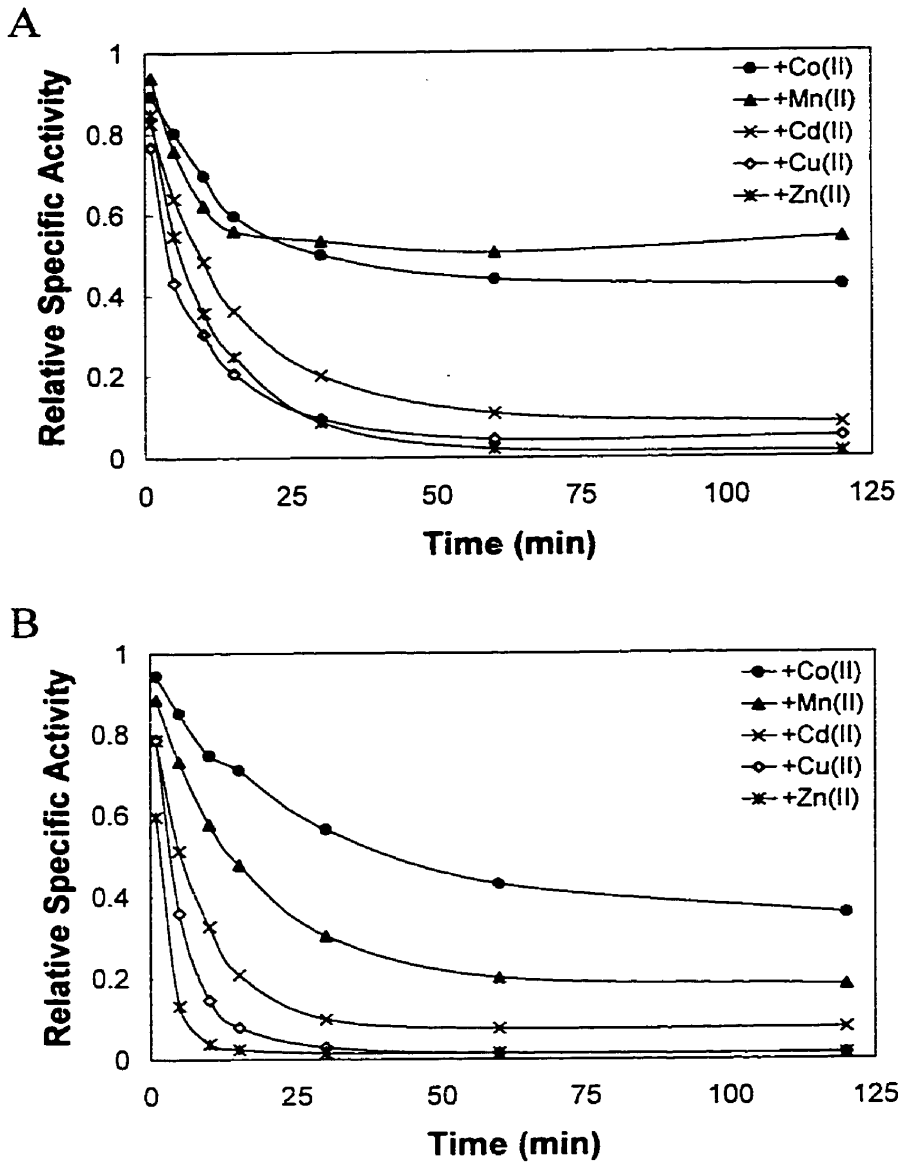

Figure 2.11: Ni^{2+}-GlxI metal competition. (A) 5 equivalents and (B) 100 equivalents of the indicated competing metal added and incubated at **37°C**. Activities are shown relative to fully active Ni^{2+}-GlxI. The lines are arbitrary fits to show the trend in the data.

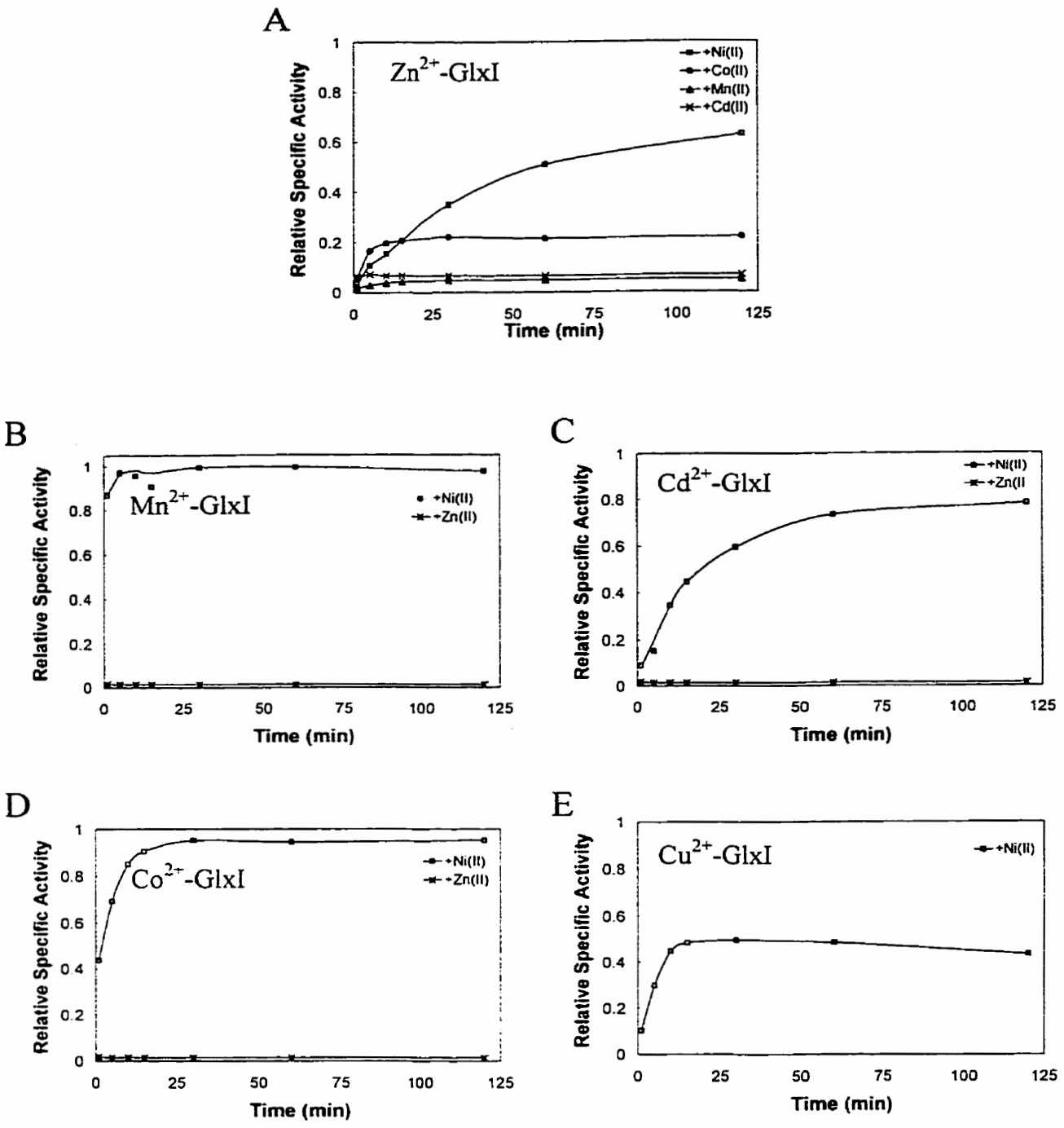

Figure 2.12: Metal competition with 100 equivalents of the indicated competing metal, incubated at **37°C**. ApoGlxI was first activated with one mole equivalent metal to reconstitute the enzyme in each of the following forms (A) Zn^{2+}, (B) Mn^{2+}, (C) Cd^{2+}, (D) Co^{2+}, and (E) Cu^{2+}. Activities are shown relative to fully active Ni^{2+}-GlxI. The lines are arbitrary fits to show the trend in the data.

2.3.2 Metal Binding

As our metal analysis indicated that *E. coli* GlxI is maximally active with one mole of metal per mole of dimeric enzyme (Figure 2.5) and analysis of the metal content confirmed only one Ni^{2+} ion per dimer in the active enzyme (Clugston, 1997; Clugston et al., 1998a), further analysis of the metal binding properties of *E. coli* GlxI was warranted.

Incorporation of Metal into E. coli GlxI During Protein Expression

Previous analysis of the metal content of *E. coli* GlxI, produced in *E. coli* MG1655 grown with no added metal ions as well as with $NiCl_2$ added to the growth media (M.Sc. work; Clugston, 1997), were expanded to include an analysis of the protein when grown in the presence of $ZnCl_2$. Appendix A, Table A.1 lists the results of the metal analysis for *E. coli* GlxI grown in the presence of $NiCl_2$ and $ZnCl_2$. Based on this combination of experiments, the following observations and general conclusions can be made for *E. coli* GlxI. When $NiCl_2$ was added to the growth media, Ni^{2+} was incorporated into the produced protein as determined by ICP analyses (Clugston, 1997). This indicates that Ni^{2+} is transported into the cells, most likely through the low-affinity Mg^{2+} transport system (Drake, 1988; Snavely et al., 1989; Silver, 1996), where it is taken up by the GlxI protein. In addition, the activity of the overproduced enzyme directly correlated with the amount of Ni^{2+} incorporated into the protein during cell growth (based on ICP and kinetic analyses). However, incorporation of Zn^{2+} (available from the growth media with and without supplementation with $ZnCl_2$) into the overproduced enzyme resulted in production of inactive holoenzyme. The amount of protein produced was not affected by the presence of Ni^{2-} or Zn^{2+} in the growth media. Because of the high efficiency of protein production from our construct (150-200 mg/L with a 6 h induction time), substantial amounts of apoenzyme (50-70%) were always produced. The remaining amount of apoenzyme could be converted to active holoenzyme upon addition of nickel to the protein solution. Addition of $ZnCl_2$ did not activate the apoenzyme even when incorporated during protein expression.

Number of Metal Ions Bound to E. coli GlxI

ICP analysis was also employed to determine if each of the activating metals bind in the same ratio as seen for nickel. This was also utilized to determine if the metals that do not

activate the enzyme, such as Zn^{2+} and Mg^{2+}, are bound by the enzyme, but in an inactive form. Table 2.2 summarizes the results of these analyses. For each of the activating metals, Ni^{2+}, Co^{2+}, Cd^{2+}, Mn^{2+}, one metal ion is detected per enzyme dimer. Interestingly, Zn^{2+} and Cu^{2+} do in fact bind to the enzyme in the same ratio but produce an inactive holoenzyme. Mg^{2+} and Ca^{2+} however do not appear to bind to *E. coli* GlxI, explaining the lack of activation. This is in contrast to the *H. sapiens* GlxI enzyme which is equally active with Zn^{2+} or Mg^{2+} (Sellin et al., 1983). *S. cerevisiae* GlxI has been found to contain Zn^{2+} as its natural metal but partial activity is recovered by addition of Mg^{2+} or Ca^{2+} to the apoenzyme (Murata et al., 1986c).

These results clearly indicate that one mole of metal is bound per mole of dimeric enzyme. This is in sharp contrast to what was expected. *H. sapiens* GlxI has been shown to be a homodimeric enzyme with two equivalent active sites each located at the dimer interface, with one Zn^{2+} ion in each site (Cameron et al., 1997). The *E. coli* GlxI protein sequence is 36% identical to that of *H. sapiens* including three of the four ligands to the metal, hence a similar structure and similar active site arrangement were expected. To confirm that our results are accurate, isothermal titration calorimetry (ITC) was performed in conjunction with the metal analyses. This analytical technique confirmed the ratio of bound metal ions to the apoenzyme in each case (Table 2.2). The protein concentration was determined by the Bradford method (Bradford, 1976) using albumin as a standard. To confirm the validity of this technique for *E. coli* GlxI the theoretical extinction coefficient of the denatured *E. coli* GlxI protein (ε = 15 930 $M^{-1}cm^{-1}$ for a single subunit) was employed. In addition, a cysteine titration with DTNB was performed. *E. coli* GlxI has 1 cysteine at position 86. The results of these methods were found to be in agreement with the determination of the protein concentration by the Bradford method, within experimental error. Therefore, our conclusion that *E. coli* GlxI reaches maximal activity with one metal ion bound per dimer appears to be accurate.

Table 2.2: Results of the isothermal titration calorimetry (ITC) and inductively coupled plasma (ICP) analyses of *E. coli* GlxI with various metal ions.

Metal Chloride	n (Binding sites)	ΔH (kJ/mol)	K_a* (M^{-1})	Moles Metal/ Dimeric Enzyme by ICP
Nickel	1.04 ± 0.11	-16.4 ± 0.9	$> 10^7$	1.2
Zinc	0.93 ± 0.05	-10.8 ± 0.4	$> 10^8$	0.80
Cobalt	0.92 ± 0.02	-10.9 ± 0.2	$> 10^7$	0.80
Manganese	0.90 ± 0.06	-14.0 ± 0.5	$3.9 \pm 1.0 \times 10^6$	0.84
Cadmium	1.00 ± 0.03	-31.8 ± 0.6	$> 10^8$	0.95
Magnesium	0	-	-	0
Calcium	0	-	-	0
Copper	N.D.†			1.2

*Only an approximate association constant could be determined except for Mn^{2-} binding. The values measured were quite variable when the best fit was calculated, even within the same titration data. The ranges are just presented as a guide to the relative binding affinity for each metal examined.
†Not determined.

It is possible, and expected, that a second putative metal binding site exists in *E. coli* GlxI. It may be that this second site has much weaker affinity for any of the metals tested. Addition of a very large excess of $NiCl_2$ to the enzyme (~1000 equivalents) did not increase the enzymatic activity above that observed when only one equivalent of $NiCl_2$ was added. Hence, any binding to a second site does not appear to affect the enzyme activity. ITC was also performed in which an excess of metal (20-fold) was titrated into the enzyme to determine if there was any evidence for a second binding site. Under the conditions examined no evidence for a second site was detected. However, ESMS analyses described in section 2.3.4 found that two inhibitor molecules could bind to the enzyme, indicating two active sites do exist. Nevertheless, our crystallographic results presented in Chapter 3 show one metal ion bound in each of two active sites, under the crystallization conditions used.

Affinity of E. coli GlxI for Various Metal Ions

The isothermal titration calorimetry studies not only provided information on the number of binding sites on the macromolecule, but also provided information regarding the

thermodynamic parameters of the interaction between the protein and metal ions. As seen in Table 2.2, the equilibrium binding constant or association constant (K_a) is very high for most of the metals analyzed. Unfortunately, the affinity is too high for accurate determination by calorimetry in most instances. Only a general range could be determined, for example Ni^{2+} appears to have a K_a greater than 10^7 M^{-1}, which corresponds to a dissociation constant (K_d) of 1^{-8} or in the nanomolar range. Figure 2.13 illustrates a sample titration of $NiCl_2$ into apoGlxI. Determination of an exact affinity at this level is difficult with any of the techniques listed in the introduction, not just isothermal titration calorimetry. What can be determined from these K_a values for each of the metals are the relative affinities.

The enzyme appears to have a lower affinity for Mn^{2+} allowing for more accurate determination of the association constant (3.9×10^6 M^{-1}). Ni^{2+} and Co^{2+} have affinities ($>10^7$ M^{-1}) intermediate between Mn^{2-} and the tightly bound Cd^{2+} and Zn^{2+} ($>10^8$ M^{-1}).

The enthalpy change (ΔH) for the interaction of each metal with apoGlxI is each in the same range, although ΔH for Cd^{2+} is somewhat lower. Without an accurate K_a value, further thermodynamic parameters of the interactions can not be determined (ΔG and ΔS for example).

A complication was encountered during the analysis of the metal binding. The cells in the ITC are made of Hastelloy stainless steel, which is ~60% nickel (Alfa Aesar 1999-2000 Research Chemicals, Metals and Materials Catalogue). As *E. coli* GlxI readily binds nickel there were problems with baseline stability during some of the titrations. While the apoenzyme was present in the ITC cell for approximately one hour equilibrating prior to the start of the titration, a small steady production of heat was observed. Even after the start of the titration, the baseline often had a positive slope. Once approximately one equivalent of metal chloride was added the baseline rapidly decreased and leveled out, suggesting the increase was due to binding metal in the system. A sample of protein was removed from the ITC after approximately 90 min in the stainless steel cell. The relative activity was about 10% that seen with fully active Ni^{2-}-GlxI, which may explain why in some instances the number of binding sites (n) was slightly below one. Prior to each titration, the cells were rinsed with Chelex treated MOPS buffer, a buffer that matched the protein solution buffer. Earlier trials involving a 15 min presoak of the cells with EDTA (1 mM) did not prove beneficial. Uninterpretable titration data resulted. It was speculated that the EDTA might

simply be binding to the walls of the cell rather than removing any free or loosely bound metals, even following extensive rinsing with buffer prior to addition of the enzyme. When the metal was titrated into the cell it might then bind to the apoenzyme and to the residual EDTA, effectively titrating the EDTA from the walls of the sample cell. During the same set of experiments it was found that buffer with 10% glycerol as a protein stabilizer could not be used in any titrations, even when matching buffer was utilized in the reference cell. As a result, it could not be determined how much of the problem was due to the EDTA rinse, or glycerol interference.

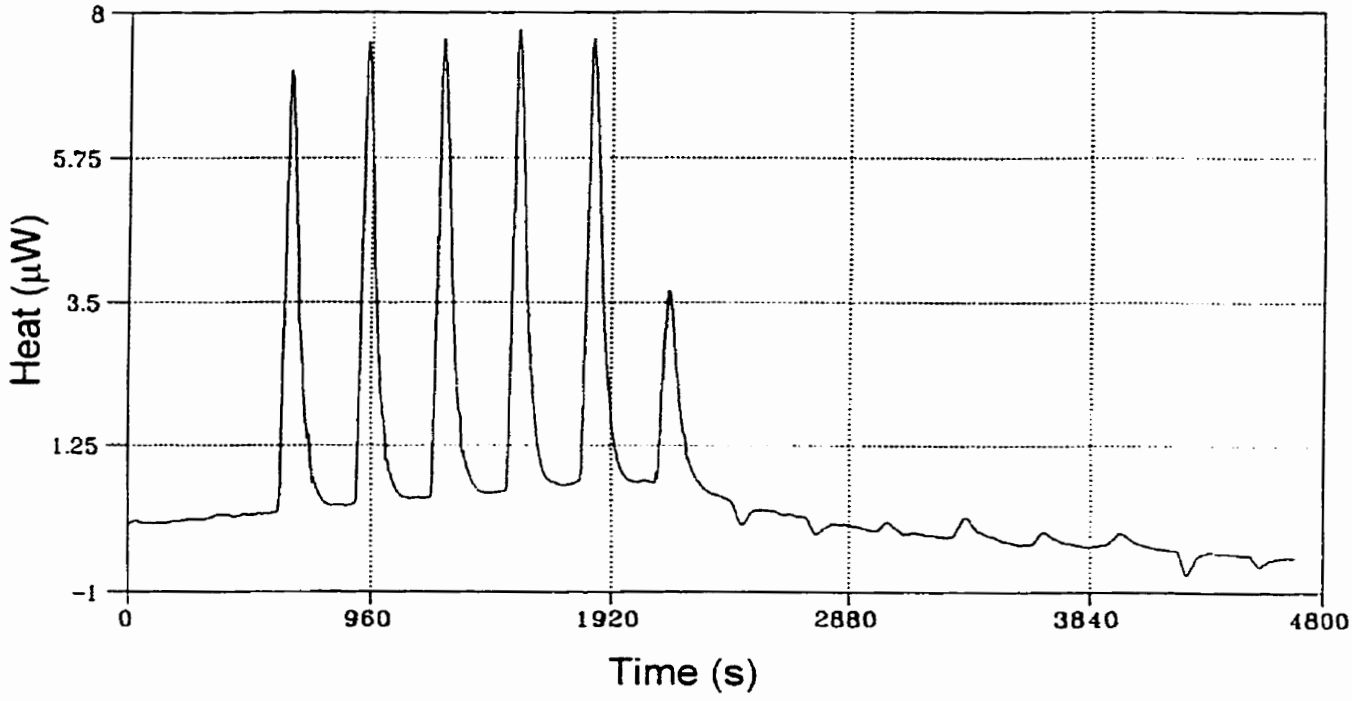

Figure 2.13: Representative binding isotherm of a titration of $NiCl_2$ into apo *E. coli* glyoxalase I.

2.3.3 Protein Stability Studies

Differential Scanning Calorimetry (DSC)

The stabilities of the various metal-substituted forms of wild-type *E. coli* GlxI were evaluated by differential scanning calorimetry (DSC). As seen in Figure 2.14, the results reveal a very interesting trend. Although the apoenzyme is quite stable (T_m = 67.0°C) there is a significant increase in stability upon addition of metal. The Ni^{2+}-substituted GlxI has a thermal denaturation temperature (T_m) of 83.8°C, whereas this increases even further in the presence of Zn^{2+}, to 88.4°C. The Co^{2+}-, Mn^{2+}-, and Cd^{2+}-substituted GlxI enzymes have thermal denaturations of 82.7°C, 74.2°C, 84.3°C respectively. The denaturation does not appear to be reversible for the enzyme in any form. Similar trends in enzyme stability upon addition of metal ions have been reported. The presence of zinc in *Aeromonas hydrophila* AE036 metallo-β-lactamase was found by DSC to stabilize the enzyme conformation, as evident in a 14°C increase in the T_m of the mono-Zn^{2+} form of the enzyme compared to the apoenzyme (Hernandez Valladares et al., 1997). Similarly, the single-stranded DNA binding protein, gene 32 protein (g32P) from bacteriophage T4, a zinc metalloprotein, has a T_m 6°C higher than the apoform of the enzyme (Keating et al., 1988). The T_m for this protein reconstituted with either Cd^{2+} or Co^{2+} was very similar to that observed for the Zn^{2+} form of the enzyme.

We have previously shown that *E. coli* GlxI remains dimeric in the absence of metal and circular dichroism indicated there were no major structural changes upon binding Ni^{2+} (Clugston, 1997; Clugston et al., 1998a). This suggests that the metal does not play a structural role but rather the metal binding site is intact in the enzyme, ready for the catalytic metal to bind. This was confirmed in our crystallographic analysis which revealed that apoGlxI had the same structure as the metal substituted forms of the enzyme and the four metal ligands from the protein were simply less rigid prior to metal binding (Chapter 3; He et al., 2000). However, the differences in the stability of the enzyme displayed here indicate the metal ion does have some effect on the structural integrity of the enzyme. It is interesting that although the enzyme is inactive with Zn^{2+}, the protein is slightly more stable in the presence of this metal than with Ni^{2+}. Our work has suggested that the affinity of the apoenzyme for Zn^{2+} is very high, and that excess Zn^{2+} can replace one of the activating metals in GlxI over

time. The significance of this increased stability in the presence of Zn^{2+} is not known at this time. As Zn^{2+} is readily available in the cell, it is possible however, that binding Zn^{2+} may be a way to sequester GlxI in the cell in an inactive yet stable form till needed.

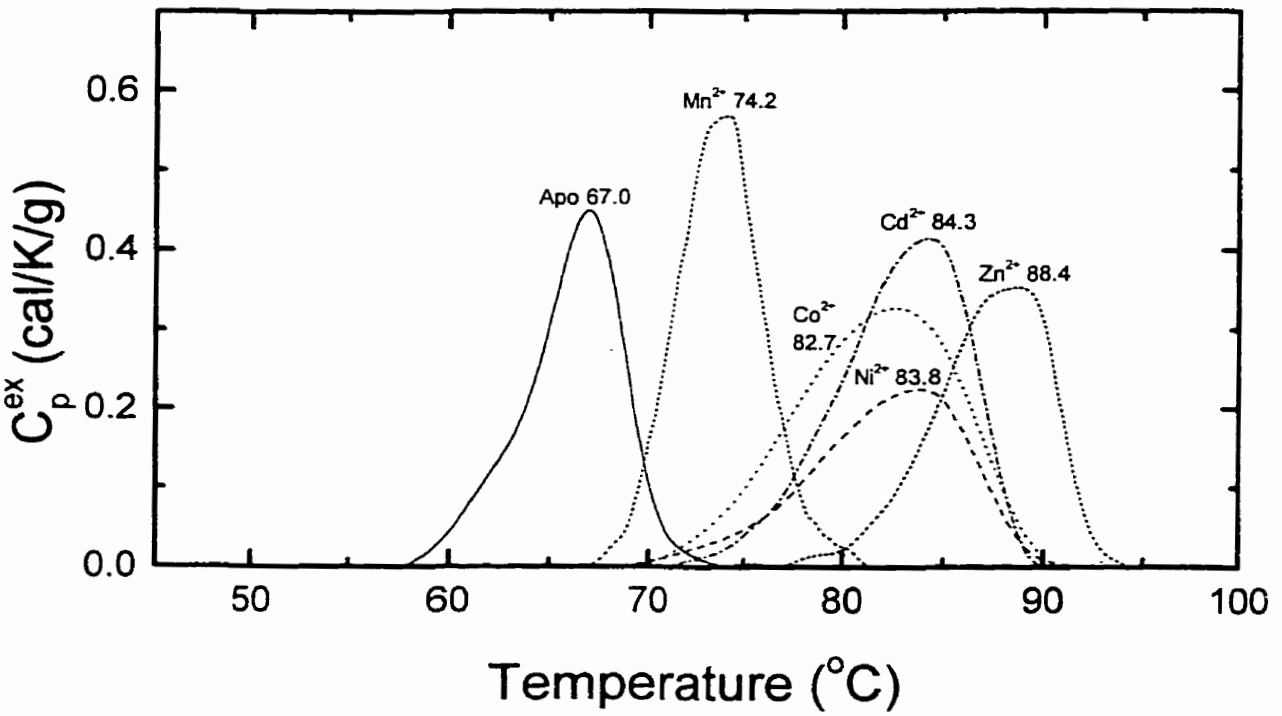

Figure 2.14: Illustration of the DSC results for apo *E. coli* GlxI and various metal substituted forms.

2.3.4 Inhibitor Binding Affinities of E. coli Glyoxalase I Determined by Mass Spectrometry of Non-covalent Complexes and Comparative Kinetic Analyses

Enzyme Topology and pH Influence

We have previously demonstrated by gel filtration chromatography, that the active form of *E. coli* GlxI is dimeric, however all of our mass spectral data on *E. coli* GlxI was collected under denaturing conditions and hence only the protein monomers were evident (Clugston, 1997; Clugston et al., 1998a). In order to determine whether a possible non-covalent dimer of the enzyme could be detected by ESI-MS (electrospray ionization mass spectrometry), and to probe the stability of this dimer, mass spectra of *E. coli* GlxI in buffers with a pH of 2.5, 3.0, 4.0, 5.0, 7.0, 8.0, and 10.0 were recorded. Figure 2.15 graphically illustrates the relative contribution of dimer species to the total ion signal as observed in the ESI spectra recorded at different pHs. As indicated, at pH values between 4 and 8 the mass spectra were dominated by ion signals originating from the dimer. Nevertheless at these pH values the mass spectrum still showed minor ion signals corresponding to the monomer. At the more extreme pH values, monomeric species were predominantly detected. It is predicted that the extremes in pH could disrupt the non-covalent quaternary structure and dissociate the subunits. It is interesting to note that this pH study resembles the pH activity profile of the enzyme in solution (Clugston, 1997; Clugston et al., 1998a; Figure 2.8). These results indicate that ESI-MS might be an extremely useful technique to give preliminary pH stability information on protein assemblies (Loo, 1997; Green et al., 1999; van Berkel et al., 2000).

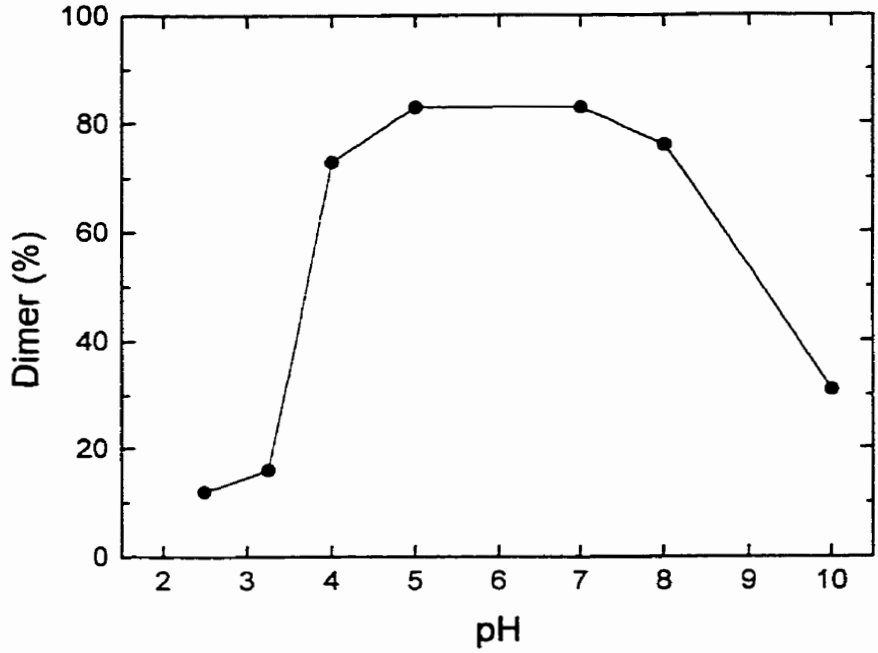

Figure 2.15: Percentage of dimer to dimer + monomer ions as determined from the mass spectra of *E. coli* GlxI as a function of the pH. Nanoflow ESI-TOF spectra were aquired on a Micromass Q-TOF hybrid tandem mass spectrometer, as described in the material and methods.

Role of Ni^{2-} in Enzyme Dimerization Examined by ESI-MS

It is known that GlxI requires a catalytic metal ion for bioactivity and *E. coli* GlxI is maximally active with Ni^{2-}. However, all the mass spectra were recorded on the apoenzyme. The results summarized in Figure 2.15 suggest that the *E. coli* glyoxalase I enzyme remains in its dimeric form even in the absence of Ni^{2-} ions. Our previous gel filtration study also confirmed that the enzyme is dimeric even in the absence of a bound metal ion (Clugston et al., 1998a). Circular dichroism has also indicated that there is no significant structural alteration in the enzyme upon metal binding (Clugston, 1997). Hence, it can be concluded that the Ni^{2-}-binding is not essential for dimerization of the *E. coli* enzyme, nor for the molecular structure of each subunit. This was reconfirmed by examination of the crystal structure of the apoenzyme (Chapter 3).

Enzyme Inhibitor Complex Topology

Enzyme inhibitors of GlxI are conventionally investigated by monitoring the enzymatic production of *S*-D-lactoylglutathione using UV difference spectroscopy. This method requires comparatively large quantities of enzyme and inhibitor per run, and is rather time-consuming. Additionally, it is rather difficult to obtain information about the enzyme-inhibitor complex topology/stoichiometry by UV difference spectroscopy on its own. ESI-MS was utilized as an initial inhibitor screen by determination of their relative binding affinities to the enzyme. For these studies a 2 μl mixture of 5 μM *E. coli* GlxI (10 pmol) with a fixed amount of inhibitor was incubated for an hour in an ammonium acetate buffer at neutral pH. An illustrative nanoflow ESI mass spectrum of *E. coli* GlxI and *S*-{2-[3-(hexyloxy)benzoyl]-vinyl}glutathione is shown in Figure 2.16. In addition to the ion signals originating from the unbound monomer (■) and unbound dimer (•), additional signals were observed (indicated by the arrows) which could be attributed exclusively to the dimer non-covalently bound to an inhibitor molecule. The data shown in Figure 2.16 clearly reveal that while the inhibitors bind strongly to the GlxI dimer, they do not bind to the monomer. These results suggest that the inhibitor binding sites, or active sites, are most likely formed by the two subunits. This is consistent with the observation that the active sites are at the dimer interface in the homologous *H. sapiens* GlxI (Cameron et al., 1997), and confirmed by our x-ray structural studies on the *E. coli* enzyme (Chapter 3; He et al., 2000).

Role of Ni^{2+} in Inhibitor Binding

As outlined, this mass spectrometric approach evaluates binding affinities rather than inhibition values. In order to determine whether the binding of an inhibitor to GlxI was influenced by the presence or absence of Ni^{2+}, mass spectra of GlxI and *S*-{2-[3-(hexyloxy)benzoyl]vinyl}glutathione in buffered solutions containing 0, 2.5 and 25 mole equivalents of Ni^{2+} were compared. No significant differences were observed and therefore it was assumed that indeed Ni^{2+} does not influence the binding affinities appreciably. In the presence of Ni^{2+} the mass spectrometric data became rather complicated as many additional ions were detected containing several Ni^{2+} and/or $NiCl^{+}$ adducts, making the assignment of the ion signals quite difficult. Therefore, we chose to carry out the mass spectrometric studies in the absence of nickel.

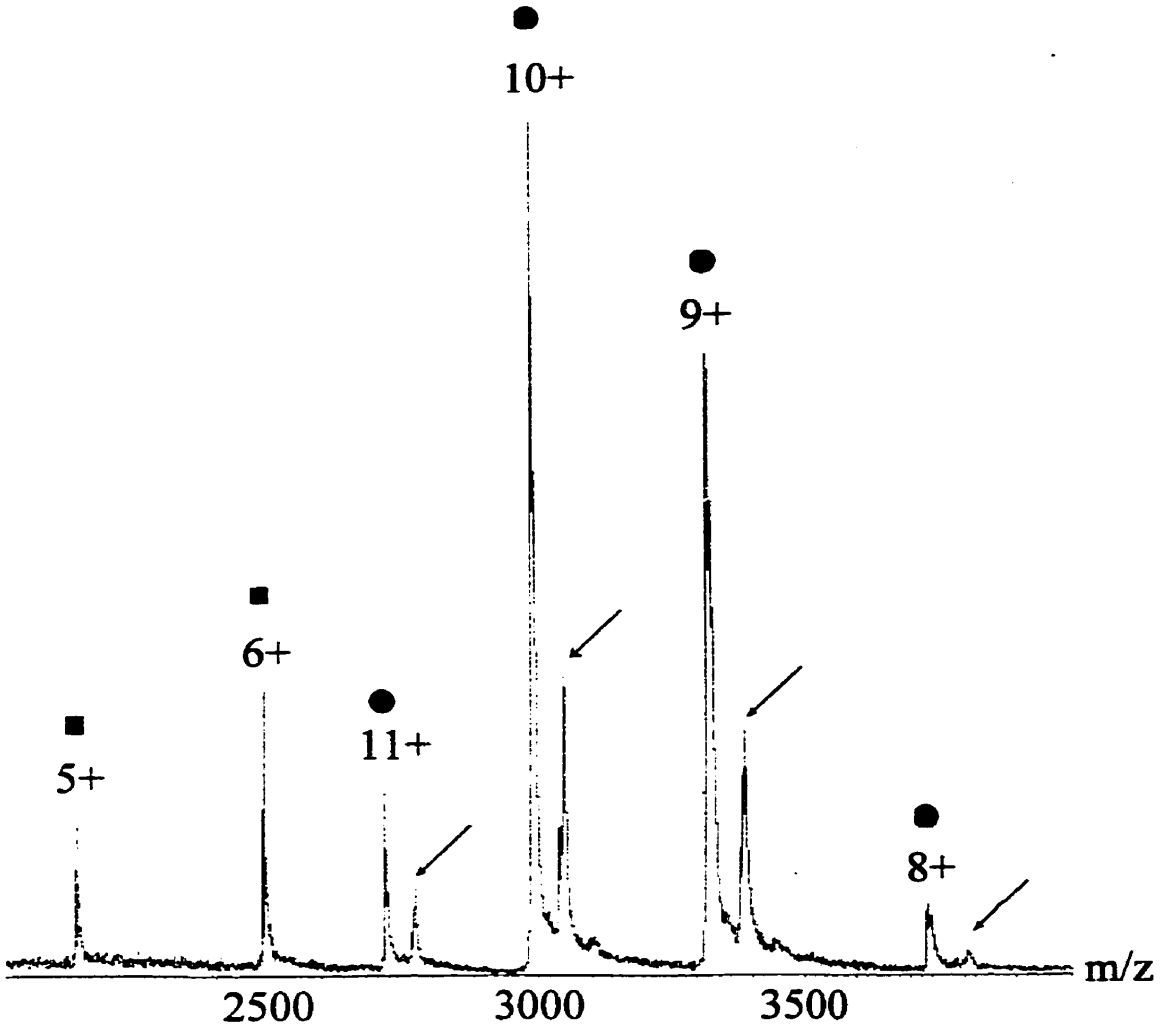

Figure 2.16: ESI mass spectrum of *E. coli* GlxI (5 μM) with *S*-{2-[3-(hexyloxy)benzoyl]-vinyl}glutathione (2.5 μM). ■indicate the GlxI monomer, ● the dimer, and the arrows indicate the binding of an inhibitor molecule.

Inhibitor Screening by Mass Spectrometry

The binding of a small library of inhibitors (Table 2.3) to *E. coli* GlxI was individually tested keeping the concentration of the different inhibitors constant (8 μM). If it is assumed that the relative intensities of the free and inhibitor-bound dimer are an indication of the relative affinity of the enzyme for inhibitor, then the mass spectra may be used to obtain relative binding affinities. This has been considered a reasonable assumption in previous ESI-MS protein-ligand bio-affinity studies (Jorgensen et al., 1998; van Dongen and Heck, 2000). From the mass spectral data it could be directly determined that *S*-methylglutathione (**a**) binds weakly compared to *S*-hexylglutathione (**c**). To derive more quantitative data the multiply charged distribution profiles were transformed to produce true molecular neutral spectra using the Masslynx NT software. From the peak integrals, relative affinities of inhibitors for binding to GlxI were established. The average number of bound inhibitor molecules (n) was calculated per dimer and is given in Table 2.3. 'n' was calculated from the mass spectra for all the studied inhibitors at constant enzyme and identical inhibitor concentrations. For comparison, solution IC_{50} values were determined for some selected inhibitors. Figure 2.17 shows an illustrative plot of the fractional enzyme activity as a function of the transition state analogue concentration, from which the IC_{50} value of the transition state analogue for GlxI from *E. coli* could be determined. The measured IC_{50} values have been included in Table 2.3. It should be noted again that in the ESI-MS studies only the interaction between the enzyme and the inhibitor is studied, in the absence of Ni^{2+}. For the enzyme kinetic analyses, Ni^{2+} had to be added, as the enzyme is otherwise not active. Regardless, the extent of inhibitor binding seems to show an accurate correlation with the determined IC_{50} values. The inhibition values confirm the mass spectrometric results and indicate that out of the 11-membered library only two are inhibitors in the micromolar range, the transition state analogue (**k**) and *S*-{2-[3-(hexyloxy)benzoyl]vinyl}glutathione (**e**). The agreement found in the ESI-MS affinity data and the IC_{50} data from kinetic analyses emphasizes that the absence/presence of Ni^{2+} has no significant effect on the binding affinity. The Ni^{2+} ions do affect the enzymatic catalysis rate, but the absence/presence of Ni^{2+} most likely does not lead to major conformational changes in the inhibitor binding site(s).

Table 2.3: Structures, inhibition values (IC_{50} with 0.04 mM substrate), and relative binding affinities (n) of the library of potential inhibitors of *E. coli* GlxI evaluated.

	Compound	Structure	IC_{50} (mM)	n
	S-Substituted GSH	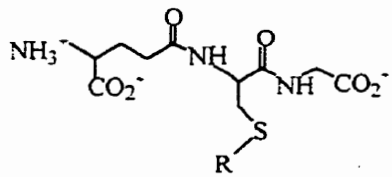		
(a)	*S*-methylglutathione	R = $-CH_3$	2.97 ± 0.45	0.32
(b)	*S*-propylglutathione	R = $-(CH_2)_2CH_3$	1.00 ± 0.08	0.53
(c)	*S*-hexylglutathione	R = $-(CH_2)_5CH_3$	1.18 ± 0.14	0.54
(d)	*S*-octylglutathione	R = $-(CH_2)_7CH_3$	0.52 ± 0.01	0.58
(e)	*S*-{2-[3-(hexyloxy) benzoyl]vinyl}glutathione	R = 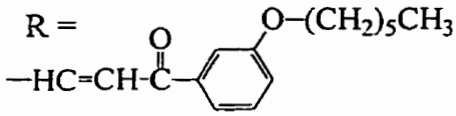	57.25 ± 2.47 μM	0.94
(f)	*S*-(*p*-azidophenacyl)-glutathione	R = 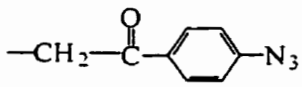	1.18 ± 0.10	0.50
(g)	*S*-lactoylglutathione (reaction product)	R = 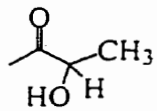	2.05 ± 0.16	0.28
(h)	*S*-nitrobenzylglutathione	R = 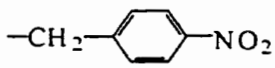	0.88 ± 0.04	0.53
(i)	Glutathionesulfonic acid	R = $-O_3^-$	> 5	0.42
(j)	Myricetin	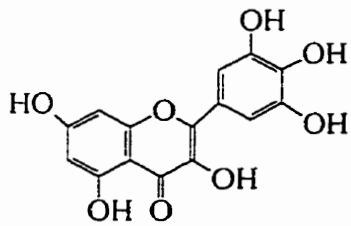	N.D.	0.13
(k)	Transition State Analogue (TSA)	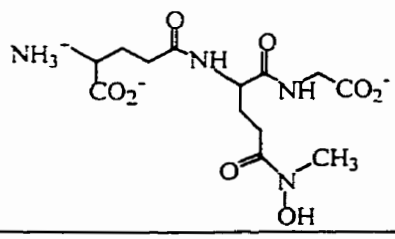	1.80 ±0.12 μM	1.33

Several glutathione analogues have been demonstrated to be competitive inhibitors of the *S. cerevisiae* and *H. sapiens* GlxI enzymes (Kermack and Matheson, 1957; Vince and Wadd, 1969; Aronsson et al., 1981; Cameron et al., 1997). It has been suggested that the binding pocket present in *S. cerevisiae* and *H. sapiens* glyoxalase I has a hydrophobic region (Aronsson et al., 1981; Cameron et al., 1997). In order to determine whether similar interactions are important in the *E. coli* enzyme we evaluated a series of increasingly hydrophobic glutathione analogues (**a** to **d** in Table 2.3). Both our mass spectrometric data and IC_{50} data indicate that the inhibition potency increases with increasing alkyl chain length (Table 2.3). However, none of these alkyl-glutathione analogues reach the high inhibition level previously demonstrated for the *S. cerevisiae* enzyme (e.g. IC_{50} of octyl-GSH = 59 μM; Barnard and Honek, 1989), suggesting a significant alteration in the binding pocket of the *E. coli* enzyme. If similar alterations exist between the active sites of *E. coli* and *H. sapiens* glyoxalase I, determination of such differences in the binding pocket could be targeted for the development of novel antibacterial agents. Chapter 3 presents the recently determined crystal structure of *E. coli* GlxI (He et al., 2000). Comparison of the active site of this enzyme with that of the *H. sapiens* indicates that the active site is much more open, which may explain the difference in the response to these inhibitors.

Other GSH-based analogues containing aromatic groups (**f** and **h**) were evaluated. However, no major increase in potency was observed by the inclusion of an aromatic functionality. Neither the reaction product, *S*-D-lactoylglutathione (**g**), nor the negatively charged glutathionesulfonic acid (**i**) appear to bind particularly strongly to the enzyme. However, two compounds in our library exhibited particularly strong binding affinity, the transition state analogue (**k**) (Ly et al., 1998) and *S*-{2-[3-(hexyloxy)benzoyl]vinyl}glutathione (**e**) (Table 2.3). We previously demonstrated that the transition state analogue (**k**) is also a competitive inhibitor of *S. cerevisiae* GlxI (Ly et al., 1998) and hence binds in the enzyme active site.

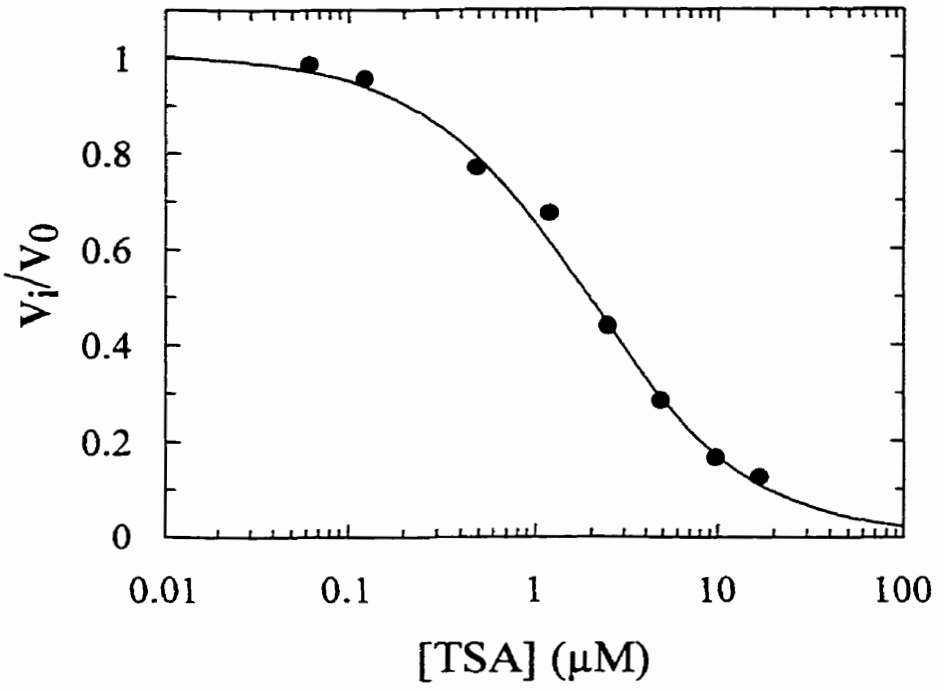

Figure 2.17: Representative plot of the fractional enzyme activity as a function of the transition state analogue inhibitor concentration, used to determine IC_{50} values. These curves were fit using GraFit 3.01 (Erithacus Software Ltd.) according to the following equation: $y = a/(1+(x/IC_{50})^S)$.

The mass spectrometric approach has apparent advantages in that it is much more rapid, it requires far less enzyme and inhibitor (i.e. as little as several picomoles of enzyme and inhibitor) and it does not suffer from problems associated with spectral interference. For instance the flavonoid myricetin (**j**), has been previously shown to inhibit the *S. cerevisiae* GlxI enzyme at a level of 50 μM (Barnard and Honek, 1989). However, because of the unfavorable effect of myricetin on the standard λ = 240 nm spectrophotometric assay, an alternate protocol is required for testing such a compound. Due to this difficulty and the very weak binding of myricetin to the *E. coli* glyoxalase I enzyme, illustrated in the ESI-MS study, myricetin was not tested in the present kinetic analyses. Also, several other compounds evaluated, such as *S*-(*p*-nitrobenzyl)glutathione (**k**) and the reaction product *S*-D-lactoylglutathione (**g**), contribute to the absorbance at λ = 240 nm, which limits the effective range of inhibitor concentrations that can be evaluated. Using electrospray mass spectrometry

to evaluate the relative binding of these compounds does not suffer from these disadvantages and may therefore provide a powerful alternative method for an initial screening of inhibitors for this enzyme.

Specific and Nonspecific Binding Evaluated by Titration Experiments

Other studies described previously have indicated that only one metal ion is required per dimer to produce a fully functional *E. coli* GlxI enzyme, suggesting only one functional active site. Therefore, a particularly interesting result from our present ESI-MS data is that it appears that the dimeric enzyme can bind two inhibitors. In order to determine whether this binding of a second inhibitor is indeed specific, GlxI was titrated in subsequent experiments with different amounts of inhibitor. These experiments were performed on *S*-hexylglutathione (**c**), myricetin (**j**), the transition state analogue (**k**) and *S*-{2-[3-(hexyloxy)benzoyl]vinyl}glutathione (**e**). Figure 2.18 shows illustrative examples of mass spectra obtained in titration experiments performed with the transition state analogue (**k**), with concentration ratios of enzyme to inhibitor of 0.20, 1 and 4. The numbers in the figure indicate the number of bound transition state analogue molecules to *E. coli* GlxI. From this figure it is clear that even below saturating conditions a second transition state analogue molecule binds to the GlxI dimer, indicating that the binding of two inhibitors is specific. Similar profiles were observed for the other inhibitors. In Figure 2.18C the possible binding of a third transition state analogue inhibitor molecule is observed. Since this binding was only observed at very high inhibitor concentrations, above saturation, this binding of the third molecule is believed to be much less-specific. Similar profiles were observed for the other inhibitors. Titration curves for the binding of four different inhibitors to *E. coli* GlxI (10 μM) determined by ESI-MS indicate that two inhibitor molecules bind specifically to the dimeric enzyme (Figure 2.19), suggesting that there are two intact binding sites. These titration curves again display the relative binding of the inhibitors to the dimeric enzyme. For example, even at very high inhibitor to enzyme ratios, myricetin (**j**) still does not reach saturation levels, unlike the transistion state analogue (**k**) and *S*-{2-[3-(hexyloxy)benzoyl]vinyl}glutathione (**e**).

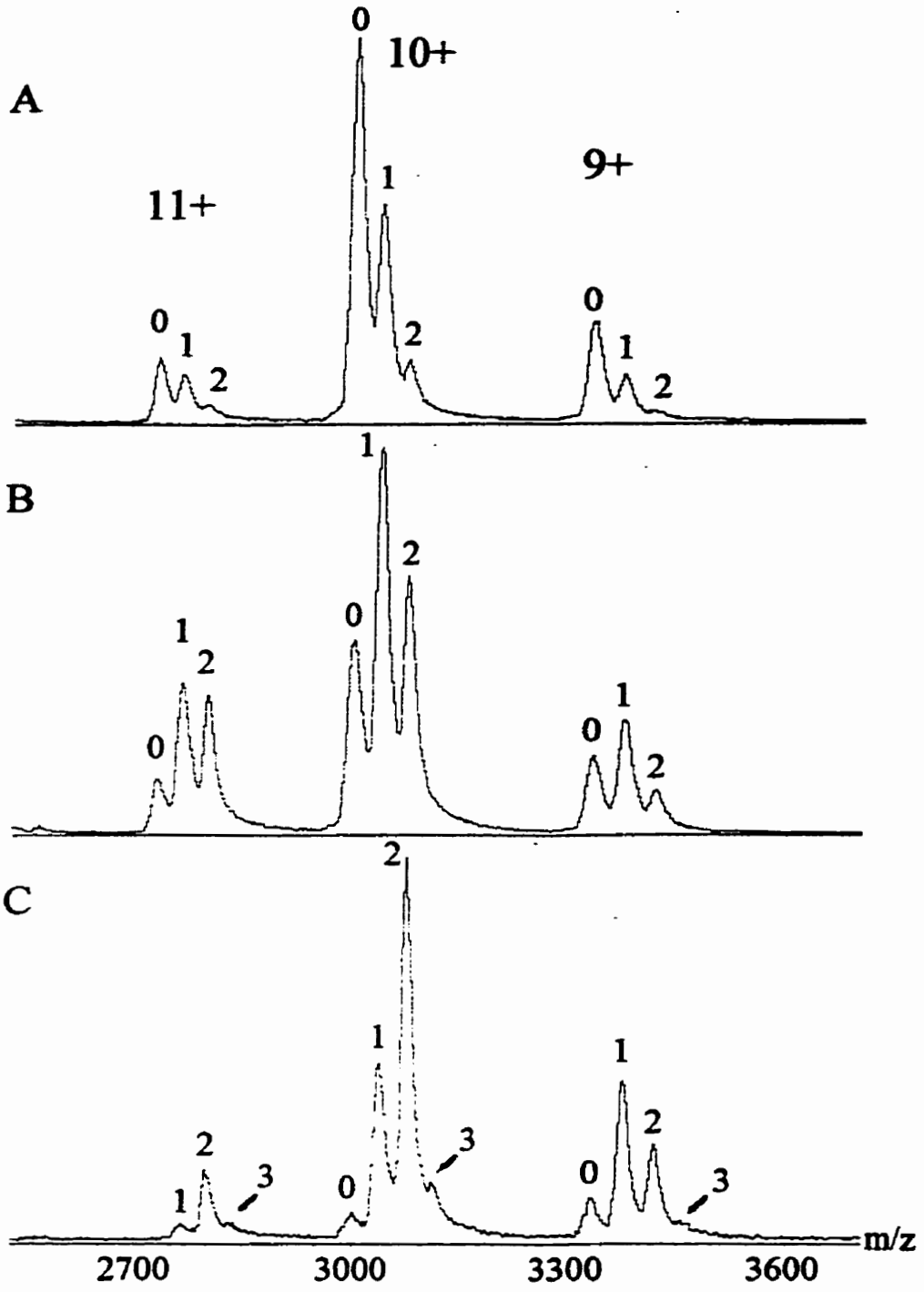

Figure 2.18: NanoESI-TOF mass spectrum of 5 μM *E. coli* glyoxalase I with (a) 1 μM, (b) 5 μM, and (c) 20 μM transition state analogue (**k**). The numbers in the figure indicate the number of bound transition state analogue molecules to *E. coli* GlxI.

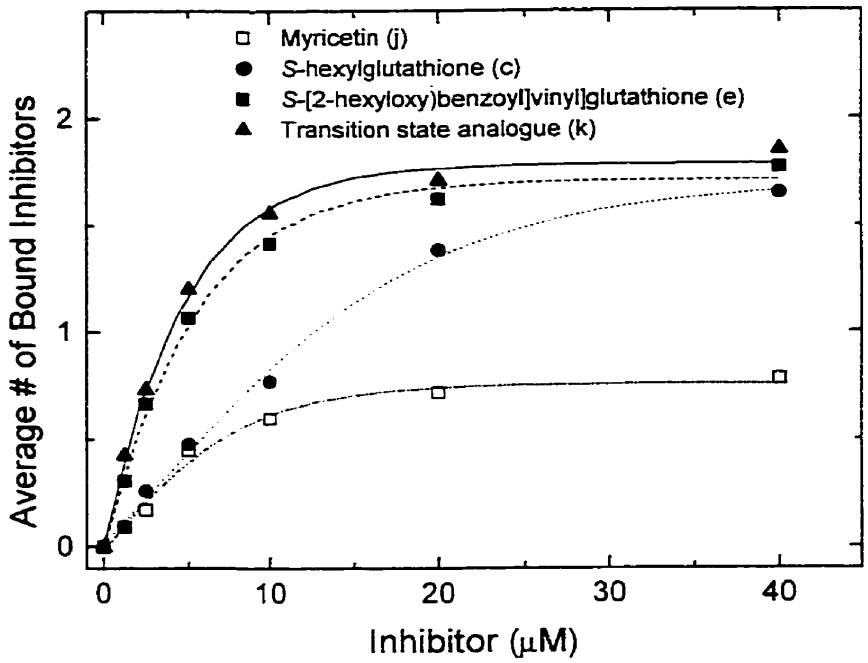

Figure 2.19: Titration curves for the binding of inhibitors to *E. coli* GlxI (10 μM) as measured by ESI-MS.

2.4 Conclusions

In the examination of the kinetics of *E. coli* GlxI we have identified several metals which activate the enzyme to varying levels, Ni^{2+}, Co^{2+}, Mn^{2+}, Fe^{2+}, and Cd^{2+}. Although the enzyme does bind Zn^{2+}, the metal ion found in the active forms of GlxI from *S. cerevisiae*, *H. sapiens*, and *P. putida*, the GlxI enzyme from *E. coli* is inactive with Zn^{2+} bound. Activity titrations, metal analysis, and isothermal titration calorimetry indicate that *E. coli* GlxI is active with one equivalent of metal bound to the dimeric enzyme. The same ratio of bound metal was found for the inactive forms of the enzyme containing Zn^{2+} and Cu^{2+}. In contrast, Mg^{2+} and Ca^{2+} do not appear to bind or activate the enzyme. Furthermore, ITC indicates that the metals are tightly bound to the active site, with the exception of Mn^{2+} which appears to have an affinity two orders of magnitude lower than the other metals. Interestingly, although Zn^{2+} produces an inactive enzyme, the association constant for this metal is quite high. Although the association constant is very high for these metals, dynamic exchange still appears to occur. Metal competition studies indicate that the rate of metal ion exchange is dependent not only on the identity of the metals, but also the temperature, and concentration of the competing metal. Increased temperature and increased levels of competing metal appeared to result in a more rapid replacement of the bound metal. In addition, the stability of the enzyme, as determined by differential scanning calorimetry, is greatly enhanced in its holoenzyme form over the apoenzyme. Zn^{2+}-GlxI has a melting temperature slightly higher than that of Ni^{2+}-GlxI. The significance of this is not currently understood.

Although maximally active with only one metal ion bound, the enzyme does have two active sites able to bind GSH-based inhibitors, as determined by analysis of non-covalent complexes by mass spectrometry. It is speculated that the affinity of the enzyme for a second metal ion is significantly lower than for the first metal bound and does not affect the level of enzyme activity.

CHAPTER 3

ENZYME STRUCTURAL STUDIES AND DETAILED ANALYSIS OF THE METAL BINDING SITE

3.1 Introduction

To gain further insight into the unique metal activation of the *E. coli* glyoxalase I enzyme, numerous structural studies were undertaken. To focus specifically on the metal center and the ligands to the metal ^{113}Cd NMR (nuclear magnetic resonance) studies were performed in collaboration with V. Robertson at the University of Guelph (Guelph, ON), EPR (electron paramagnetic resonance) analysis of the Mn^{2+}-substituted enzyme with Dr. G. D. Markham at the Fox Chase Cancer Center (Philadelphia, PA), and XAS (x-ray absorption spectroscopy) analyses of the Ni^{2+}- and Zn^{2+}-substituted enzyme in collaboration with Dr. M. J. Maroney and G. Davidson from the University of Massachusetts (Amherst, MA). To examine the entire protein structure and gain a detailed picture of the active site in the presence of several different metals, an x-ray crystallographic study was pursued in collaboration with Drs. B. W. Matthews and M. M. He at the University of Oregon (Eugene, OR). The results of these structural analyses provide extensive details regarding the active site metal environment and offer interesting insight into the differential metal activation of this metalloenzyme.

3.1.1 ^{113}Cd NMR

Cadmium (Cd^{2+}) has been found to readily replace numerous metals in proteins, including Zn^{2+}, Cu^{2+} and Ca^{2+} (Coleman, 1993; Summers, 1988 and references therein), and as such has been frequently utilized to probe the metal binding site of proteins, both structural and catalytic. There are two NMR active, ½ spin isotopes of cadmium, ^{111}Cd and ^{113}Cd. Each of these isotopes are present in natural abundance of approximately 12%, but for historical reasons ^{113}Cd tends to be utilized over ^{111}Cd (Coleman, 1993; Goodfellow et al., 1998). The detection sensitivity however is only 1% that of ^{1}H and 70% of ^{13}C. Hence, to

facilitate the analysis of metal binding sites in proteins, enriched $^{113}Cd^{2+}$ at 96% is commonly utilized. Even at this level, concentrations of 1-2 mM are required for measurable signal to noise ratio in a reasonable time frame.

Analysis of numerous proteins and small molecules has demonstrated that $^{113}Cd^{2+}$ has a chemical shift range over 1000 ppm, which makes it sensitive to small changes at the metal coordination site (Coleman, 1993). The deshielding from the coordinating ligands increases from O<N<S, with each S ligand increasing the chemical shift approximately 100 ppm. In addition, an increase in shielding for a given donor is noted with increased coordination number. However, a distortion from regular symmetry can change the chemical shift. The chemical shift ideally can be utilized to determine the type of ligands to the metal, their identity and geometry (Goodfellow et al., 1998). However, the geometry determination is not always reliable. As a result it is difficult to make accurate conclusions regarding the overall binding site simply from a one dimensional ^{113}Cd experiment. Recent studies using desulforedoxin and various mutant forms of this enzyme have attempted to establish a relationship between the metal site geometry and the chemical shift (Goodfellow et al., 1998). However, at this time the chemical shift can only be reliably used to indicate the type of ligands surrounding the metal. To identify the ligands surrounding the Cd^{2+}, two dimensional (2D) NMR studies have been performed, in which ^{113}Cd is coupled to ^{1}H signals. Two such methods have been employed in the analysis of the metal binding site of several proteins, heteronuclear multiple quantum coherence (HMQC) and heteronuclear cross-polarization TOCSY (total correlated spectroscopy; Live et al., 1985; Gardner and Coleman, 1994).

We undertook a ^{113}Cd NMR analysis of *E. coli* glyoxalase I to determine the type of ligands around the metal and the feasibility of performing detailed 2D NMR analyses.

3.1.2 Electron Paramagnetic Resonance (EPR)

Electron paramagnetic resonance (EPR), also called electron spin resonance (ESR) is similar to NMR but involves changes in the spin of unpaired electrons rather than nuclei. It can be utilized to detect changes in the environment of the electrons (Cantor and Schimmel, 1980; Campbell and Dwek, 1984).

EPR studies on *H. sapiens* GlxI with bound Co^{2+}, Cu^{2+}, and Mn^{2+} in combination with various inhibitors have been reported (Sellin et al., 1982a; Sellin et al., 1983; Sellin et al.,

1987). These studies have suggested that the metal ion is in an octahedral environment, with at least one nitrogen atom acting as a metal ligand from one or two histidines.

E. coli GlxI reconstituted with Mn^{2+} was analyzed in the presence and absence of various GSH-analogues, including the product of the glyoxalase I reaction, *S*-D-lactoylglutathione, and the postulated transition state analogue described previously (Section 1.4.1 and 2.3.4). It was hoped that if there was a difference in the ligation pattern around the metal center during some stage of the reaction this could be detected by comparison of the EPR results of the various samples.

3.1.3 X-Ray Absorption Spectroscopy (XAS)

X-ray absorption spectroscopy (XAS) is a widely used tool for the analysis of protein metal centers. This technique involves measurement of the transition of the metal center from its core electronic state to its excited electronic or continuum states (Hay, 1984; Yachandra, 1995). This is specifically known as x-ray absorption near-edge structure (XANES). The examination of the absorption cross section fine structure at energies above the electron release threshold is known as extended x-ray absorption fine structure (EXAFS). The information from these two analyses is complementary. From EXAFS data, information can be obtained regarding not only the type of atoms surrounding the metal but also the distance to within 0.02 Å (Hay, 1984). EXAFS however can not determine the bond angle and the determination of the number of ligands has a 20% error (Hay, 1984). XANES can provide the oxidation state of the metal in addition to the symmetry at the metal center (Yachandra, 1995).

To obtain this data, synchrotron radiation is utilized to photoionize the core electrons in the metal under analysis. When the energy of this incident ray is greater than the ionization energy of the 1*s* electron, this electron is excited to the ionization continuum. The EXAFS spectrum is produced by the interference of the outgoing photoelectron wave and the back-scattering of the wave from nearby atoms (Hay, 1984). The interference can be constructive or destructive producing oscillations in the collected data. Figure 3.1 illustrates this phenomena. The XANES data is obtained in the same spectrum. In the x-ray absorption spectrum, the XANES region preceeds the sudden increase in absorption or absorption edge resulting from the input of energy to produce a photoelectron. When the photoelectron comes from the 1*s* core level of the atom this is known as the K-edge (Hay, 1984; Yachandra, 1995).

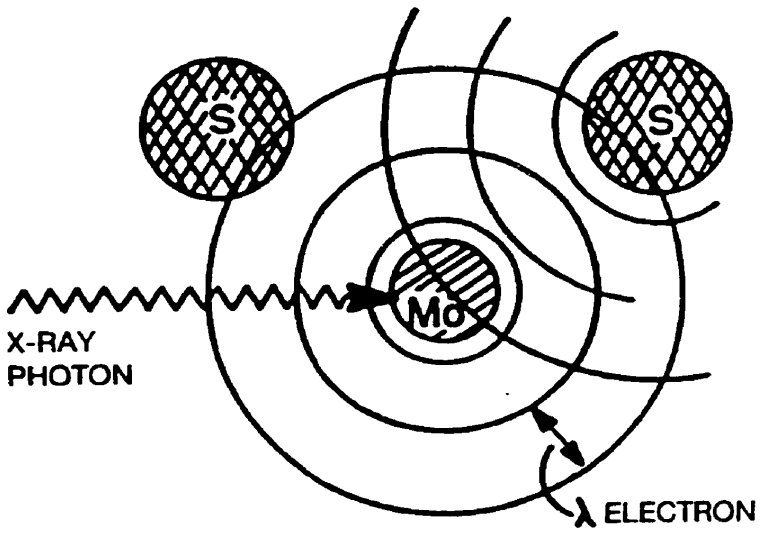

Figure 3.1: Illustration of the physical origins of EXAFS using molybdenum as the example (From Hay, 1984).

XAS analysis of *E. coli* GlxI with Ni^{2+} and Zn^{2+} bound were examined to determine if there was a difference in the ligation pattern surrounding the two metal centers given that Ni^{2+} produces an active enzyme and Zn^{2+} an inactive GlxI enzyme. A difference in metal ligation could provide clues to this difference in activation. In addition, the metal substituted enzyme was examined with various enzyme bound GSH-analogues, as performed for the EPR studies, to determine if a change in the metal ligation accompanies the binding of these molecules. These studies could provide clues to the mechanism of the GlxI catalyzed reaction.

3.1.4 Protein Crystallography

Determination of the x-ray crystal structure of a protein can be invaluable in protein characterization. The molecular details of the active site in addition to the overall shape and design of the protein structure can direct future experimental analyses. However, to solve the structure of a protein one must determine both the amplitude and phase of each diffracted wave in the diffraction data. The collected data however only provides the amplitude but not the phase, which is the angle for each reflection (Hendrickson et al., 1990; Rhodes, 1993). This is a very general description of the most difficult problem in crystallography, after successfully growing crystals, known as the "phase problem". To overcome this problem,

heavy atom derivatives of the protein are often utilized. Multiple isomorphous replacement (MIR), which involves soaking crystals of the protein with various heavy atoms such as mercury, can be employed to solve this problem (Rhodes, 1993). The heavy metal will scatter the x-rays more than the atoms of the protein. Examination of the change in intensity of the diffraction data from the heavy atom can be utilized to determine the phase. Another method employed is multiwavelength anomalous diffraction (MAD), which has been described as *in situ* isomorphous replacement (Smith, 1991; Hendrickson et al., 1990). Selenium is a heavy atom suitable for such replacements and selenomethionine is a frequently utilized heavy atom derivative. The replacement of methionines with selenomethionine (SeMet) in a protein would place the selenium heavy atom at a specific number of locations throughout the protein structure (Hendrickson et al., 1990; Doublie, 1997; Smith and Thompson, 1998). In fact, the incorporation of SeMet as a protein label in crystallographic studies utilizing MAD analysis accounts for two-thirds of all structures solved by MAD (Smith and Thompson, 1998). Other MAD analyses have employed heavy atoms such as mercury or gold introduced into the protein. SeMet was incorporated into *E. coli* GlxI to aid in the structure determination utilizing the technique of MAD analysis. The enzymatic characterization of SeMet-GlxI is presented in Chapter 4.

In order to aid in understanding the unusual metal activation observed in *E. coli* GlxI, a detailed crystallographic analysis of various metal substituted forms of this enzyme was also undertaken. In addition, the structure of *H. sapiens* GlxI has recently been reported (Cameron et al., 1997) and has been identified as a member of a $\beta\alpha\beta\beta\beta$ superfamily of metalloproteins (Bergdoll et al., 1998). Determination of the structure of *E. coli* GlxI provides the first structural information on a bacterial GlxI and adds to our knowledge of this superfamily. These analyses have identified the distinctions between the bacterial and eukaryotic GlxI structures and revealed differences in the environment around the metal, providing a clue to the differences in catalytic efficiency. The results suggest that it is the geometry of the metal coordination, rather than the metal ion itself, that correlates with the catalytic activity.

3.2 Materials and Methods

The pertinent details for the preparation of the enzyme samples for each technique are provided. As this work was performed in collaboration with other groups, a summary of some of the experimental details of their work in addition to data tables are included in an appendices to this thesis or in the indicated references.

The primary sequence of *H. sapiens* GlxI contains 184 amino acids (Ridderström and Mannervik, 1996), the N-terminal Met being lost in the active enzyme. All references to *H. sapiens* GlxI residue numbers refer to the intact 184 amino acid sequence.

3.2.1 ^{113}Cd NMR

Sample Preparation

ApoGlxI was concentrated to 0.82 mM utilizing an Amicon Centricon (YM10; Millipore, Bedford, MA) and the buffer changed to 22 mM MOPS, pH 7.0, Chelex treated. Immediately before NMR analysis, D_2O was added to 10%, and 0.9 mole equivalence of $^{113}CdCl_2$ (US Services Inc, Summit, NJ) was added, giving a final dimeric enzyme concentration of 0.72 mM, Cd^{2+} concentration of 0.65 mM, in 20 mM MOPS, 10% D_2O.

NMR Data Collection

NMR data acquisition was performed by Valerie Robertson at the University of Guelph. ^{113}Cd NMR was collected at 88.744 MHz utilizing a Bruker-Spectrospin 400 MHz NMR under direct observe, with a broad band multinuclear probe, at 23°C, in a 5 mm NMR tube (235). The acquisition time was 0.6161 s, relaxation time of 2 s, line broadening of 10 Hz. The ^{113}Cd signal and 90° pulse time was initially determined utilizing concentrated $Cd(ClO_4)_2$ (Sigma) in 100% D_2O, then the resonance of a 0.1 M $Cd(ClO_4)_2$ solution in 10% D_2O was employed as a reference to set the chemical shift at zero.

To ensure the signal measured from the enzyme sample was not due to free Cd^{2+}, a control sample of 15 mM $^{113}CdCl_2$ in 20 mM MOPS, 10% D_2O was prepared.

3.2.2 EPR

Sample Preparation

Four Mn^{2+}-GlxI samples were prepared by adding 2 mole equivalents of $MnCl_2$ (Baker Analyzed, J.T. Baker) to apoGlxI. Ultrafiltration was used to remove the excess metal and change the buffer to 50 mM HEPES (4-(2-hydroxyethyl)-1-piperazineethanesulfonic acid) pH 7.0, using a Centricon (YM10). The protein was concentrated to 1.2 mM (~40 mg/ml). The first 200 µl sample was enzyme plus metal alone, the second contained 5 mM *S*-octylglutathione, third 10 mM *S*-lactoylglutathione, and the final sample contained 10 mM transition state analogue (TSA; described in section 1.4.1). The samples were frozen in liquid nitrogen and shipped on dry ice to Dr. G. D. Markham for EPR analysis.

3.2.3 XAS

Sample Preparation

The samples of *E. coli* GlxI used in the XAS studies were prepared by reconstitution of recombinant apoGlxI with 1.5-2.5 equivalents of $NiCl_2$ or $ZnCl_2$. All enzyme samples were then concentrated to between 1.2-2.7 mM dimeric enzyme using a Centricon concentrator (YM10), the buffer changed to 50 mM MOPS, 25% glycerol and adjusted to pH 7.0 with tetraethyl ammonium hydroxide (10% solution in water), prior to loading into sample holders (Figure 3.2) and freezing on dry ice. Enzymatic activity was monitored throughout each sample preparation, and the final enzyme concentrations were determined by the Bradford method, as previously described (Section 2.2).

Figure 3.2: Schematic representation of the polycarbonate EXAFS sample holders. The shaded region in the top view represents a trough 0.75 mm deep into which the ~40 µl sample is placed. Drawn at ~115% actual size.

The enzyme activity of a representative sample was confirmed following x-ray exposure. Details of the XAS experimental procedures can be found elsewhere (Davidson et al., 2000a; Davidson et al., 2000b).

Preparation of Inhibitor Complexes

The enzyme-product complex was prepared by adding *S*-lactoylglutathione (final concentration of 5 mM) in 50 mM MOPS and 25% glycerol to one aliquot of the concentrated enzyme. An *S*-octylglutathione inhibitor complex was prepared by adding *S*-octylglutathione (5 mM final concentration) in 50 mM MOPS and 25% glycerol to a second aliquot. A second inhibitor complex was prepared by adding L-γ-glutamyl-*N*-hydroxy-*N*-methyl-L-glutaminylglycine (TSA; to 10 mM final concentration) in water to the third aliquot. Sample three was diluted by the addition of a solution of TSA in water, to give final concentrations of 40 mM MOPS and 20% glycerol. The concentrations of *S*-lactoylglutathione, *S*-octylglutathione, and TSA used in EXAFS samples were higher than the determined IC_{50} values of these compounds (2.05 mM, 0.52 mM, and 1.80 μM respectively; Chapter 2.3.4; Stokvis et al., 2000)

3.2.4 Crystallography

Sample Preparation

Native *E. coli* MG1655/pGL10 was grown, GlxI expressed, and the protein purified as previously described (Clugston et al., 1998a). The incorporation of selenomethione (SeMet) and the purification and characterization of SeMet-GlxI can be found in Chapter 4.

The precipitated protein following isoelectric focusing has the highest purity and was utilized for all crystallographic work. The protein was concentrated using an Amicon Centricon concentrator (YM10) and the buffer changed to 50 mM HEPES, pH 7.0 (Chelex treated buffer, Na^+ form). For the various metal substituted forms of the enzyme, 2-2.5 mole equivalents of metal ($NiCl_2$, $ZnCl_2$, $CdCl_2$, $CoCl_2$, or $MnCl_2$) were added to the dimeric apoenzyme, prior to concentration and the enzyme concentrated to between 12-37 mg/ml. Protein samples were frozen in liquid nitrogen and stored at –80°C in eppendorf tubes which had been soaked in 10% nitric acid for ~30 minutes to remove any extraneous metals followed by liberal rinsing with Chelex-treated water.

Crystallization of Ni^{2+}-, Co^{2+}-, Cd^{2+}-, Zn^{2+}-, Apo, and SeMet-Ni^{2+}-GlxI

The various metal-bound forms of native GlxI were readily crystallized by vapour diffusion in hanging drops with PEG 1000 and PEG 8000 as a precipitant. The protein solution (5 µl of 12-37 mg/ml) was mixed with an equal volume of well liquor containing 5-10% PEG 1000 and 5-10% PEG 8000. After approximately one week at room temperature, crystals of dimensions ~0.8 x 0.3 x 0.2 mm appeared. Although the apoGlxI protein gave crystals under similar conditions, they appeared to be less stable. More stable crystals with better morphology were obtained by placing the trays at 4°C for 2 weeks or longer. The crystals of SeMet-Ni^{2+}-GlxI could only be obtained when additional buffer (50 mM HEPES pH 7.0) was added to the hanging drops containing ~11 mg/ml protein and they differed in morphology from the native GlxI crystals. In addition, these crystals diffracted very poorly until subjected to one or more cycles of crystal annealing (Harp et al., 1998; Harp et al., 1999). The crystals were flash cooled in a stream of cold nitrogen and then transferred to mother liquor with 30% PEG 400 at room temperature. After a 1 min incubation the crystals were flash cooled again in the presence of 30% PEG 400.

Data Collection

The diffraction data for native Ni^{2+}- and apoGlxI were collected on beamline 9-1 at the Stanford Synchrotron Radiation Laboratory. The data for the crystals of Co^{2+}-, Cd^{2+}-, and Zn^{2+}-GlxI were recorded under cryo conditions on a Rigaku R-AXIS imaging plate mounted on a rotating anode source. Four data sets of SeMet-Ni^{2+}-GlxI crystals were collected at different wavelengths, maximizing the K-edge anomalous dispersion effects of selenium, on beamline 5-2 at the Advanced Light Source (Berkeley, CA).

Structure Determination, Model Building, Refinement, and Analysis

These analyses were performed by Dr. M. He and are included in Appendix D (He et al., 2000).

Presentation of the Protein Structures

The selection of graphical representations of the protein presented in the crystallographic section were prepared by Dr. M. M. He, using MOLSCRIPT, Render3D, and Bobscript (Kraulis, 1991; Esnouf, 1997; Merritt and Bacon, 1997).

3.3 Results and Discussion

3.3.1 ^{113}Cd NMR

We have demonstrated that Cd^{2+} binds and activates *E. coli* GlxI, readily facilitating ^{113}Cd NMR analysis of the metal binding site in this enzyme. This preliminary NMR study has been performed to determine the type of ligands around the metal and the practicality of further 2D NMR experiments with GlxI.

To measure the ^{113}Cd signal in a reasonable length of time, high concentrations in the range of 1 mM, or for *E. coli* GlxI approximately 30 mg/ml, are required even when utilizing the enriched cadmium. As approximately 500 µl is required for each NMR analysis, a significant amount of protein must be utilized. This is obviously a factor restricting extensive analyses. Using the Centricon spin columns high concentrations of GlxI were achieved for this experiment. Dilution of a sample of this enzyme to workable levels indicated that the enzyme was still active following this treatment.

The chemical shift observed for the sample of *E. coli* $^{113}Cd^{2+}$-GlxI (Figure 3.3) is consistent with a mixture of oxygen and nitrogen ligands, but no sulfur ligation as this would tend to shift the signal to above 300 ppm (Coleman, 1993). This is consistent with the prediction of histidine and glutamate ligands, based on the sequence comparison of *E. coli* GlxI to the *H. sapiens* enzyme (Figure 3.4). However, other types of non-sulfur ligands could certainly result in the observed ^{113}Cd NMR spectrum.

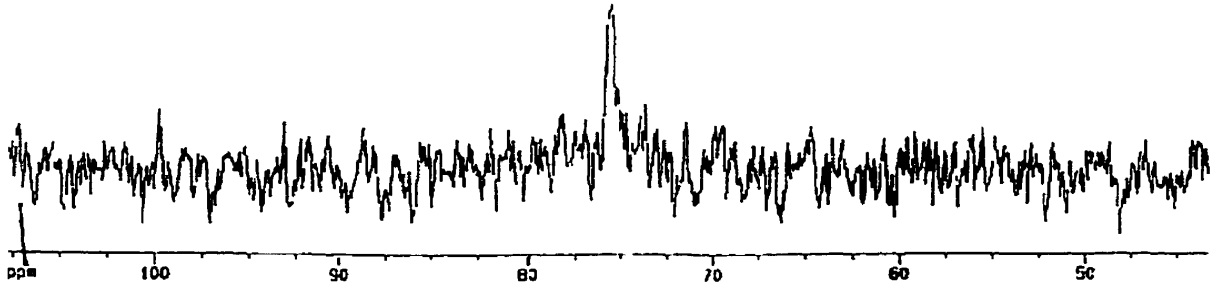

Figure 3.3: ^{113}Cd NMR spectrum of Cd^{2+} substituted *E. coli* GlxI.

Concentrated (15 mM) $^{113}CdCl_2$ was analyzed to ensure the signal detected was not solely due to free ^{113}Cd in solution. The peak observed had a chemical shift of approximately 25 ppm, significantly different from the 75 ppm for Cd^{2+}-GlxI.

V. Robertson also attempted to perform a 2D NMR analysis on this protein sample, coupling the ^{113}Cd signal to ^{1}H, however no signal was detected. ^{113}Cd-^{1}H heteroTOCSY pulse sequences used in analysis of the metal site in proteins have been described elsewhere (Live et al., 1985; Gardner and Coleman, 1994). Our lack of detection of a signal suggests that a more concentrated sample is required to facilitate these measurements. Also, it is still possible that the H^+ from the MOPS buffer may interfere with the analysis. Prior to further NMR analyses a different buffer system should be investigated, such as phosphate or deuterated MOPS. Phosphate however has the added complication of complexing with Cd^{2+} and precipitating as either the phosphate or hydroxide complex (Coleman, 1993), hence the levels of Cd^{2+} would have to be minimized.

The results of this analysis confirm the non-sulfur type of ligands, and our additional structural studies described later in this chapter confirm this and clearly identify each ligand. Future ^{113}Cd NMR studies could be directed towards any change in the chemical shift upon binding substrate analogues or inhibitors, which could indicate a change in ligation around the metal center. Comparative 2D NMR studies of these samples would provide even more details regarding the metal ligation. Although this does not provide a static picture as in crystallographic analysis, it does not require the crystallization of the protein with each of the inhibitor molecules that one wishes to examine, and the instrument and expertise are readily available. However, EXAFS and x-ray crystallographic studies of GlxI in the presence of inhibitors have yielded important data.

```
E. coli        ----------------------------MRLLHTMLRVGDLQRSIDFYTKVLGMKLLRT  31
H. sapeins     MAEPQPPSGGLTDEAALSCCSDADPSTKDFLLQQTMLRVKDPKKSLDFYTRVLGMTLIQK  60
                                          : * :***** * ::*:****:****.*::.

E. coli        SENPEYKYSLAFVGYG---------------PETEEAVIELTYNWG-----VDKYELG--  69
H. sapeins     CDFPIMKFSLYFLAYEDKNDIPKEKDEKIAWALSRKATLELTHNWGTEDDATQSYHNGNS 120
               .: *  *:** *:.*                . :.:*.:***:***     .:.*. *

E. coli        --TAYGHIALSVDNAAEACEKIRQNGGNVTREAGPVKGGTTVIAFVEDPDGYKIELIEEK 127
H. sapeins     DPRGFGHIGIAVPDVYSACKRFEELG--VKFVKKPDDGKMKGLAFIQDPDGYWIEILNPN 178
                  .:***.::* :. .**::::.: *  *.    * .*  . :**::***** **::: :

E. coli        DAGRGLGN  135
H. sapeins     KMATLM--  184
               . .  :
```

Figure 3.4: Protein sequence alignment of *E. coli* GlxI with *H. sapiens* GlxI generated by ClustalW 1.8. * indicates conserved residues; : highly homologous; . homologous residues. The metal ligands are in bold.

3.3.2 EPR

The EPR analysis indicated that the Mn^{2+} in the active site of *E. coli* GlxI was in an octahedral environment, as predicted based on the structure of the *H. sapiens* GlxI enzyme (Cameron et al., 1997). Unfortunately further details regarding the specific ligands could not be determined, nor could any notable difference be seen between the enzyme with an empty active site and those with bound GSH-analogues. Interestingly, the sample containing *S*-lactoylglutathione gave an EPR signal characteristic of free Mn^{2+} suggesting the metal had been lost from the enzyme active site. It is not known why this would happen when each of the four samples contained the same enzyme and metal concentration. The ITC data presented in the previous chapter indicated that the affinity of the enzyme for Mn^{2+} is lower than for the other metals tested. In fact it is approximately two orders of magnitude lower than for Ni^{2+} or Zn^{2+}. In addition during the kinetic analysis of the wild-type enzyme loss of the metal was observed for the Mn^{2+} reconstituted enzyme when analyzed in phosphate buffer (Section 2.3.1). The observation that the Mn^{2+} is also lost in this EPR analysis further

supports the weak binding nature of *E. coli* GlxI for Mn^{2+}. The Mn^{2+} bound to the enzyme was also lost during crystallographic studies.

Samples of the EPR spectra provided by Dr. Markham are included in Appendix B.

3.3.3 XAS

Metal Environment

Information regarding the coordination number and geometry of the Ni^{2+} site can be found in the XANES region of the spectrum. The region is sensitive to the number of ligands and the geometry of the ligands bound to the metal site and therefore provides a more reliable determination of the geometry and number of ligands than the EXAFS data. The Ni K-edge XANES spectrum of *E. coli* GlxI indicates a symmetric ligand environment. A four-coordinate planar geometry was eliminated as a possibility, indicating that the active site Ni is six-coordinate. See Appendix C for a table listing the data fits performed by G. Davidson and Dr. M. J. Maroney. Details of the data analysis can be found in the published article (Davidson et al., 2000a).

The EXAFS data indicates that the first coordination sphere of the active site Ni^{2+} is adequately fit by a single shell of O(N) scattering atoms at an average distance of 2.07 Å (fit Ni01 in Table C.1 of Appendix C). Modeling the first coordination sphere as a six-coordinate site composed of two shells of O/N donors (1-2 at 1.91 Å and 4-5 at 2.08 Å) slightly improves the fit (Ni02). Multiple scattering analyses of features near 3 and 4 Å are consistent with the coordination of two histidine ligands (fit Ni03). Addition of a shell of C atoms with multiple scattering parameters in the second coordination sphere at 2.98 Å, as might be expected from carboxylate donors, also improves the fit (Ni04). The best fits are obtained with 1-2 C atoms in this shell, indicating that at least one of the O/N donors is a carboxylate ligand.

The EXAFS of Zn^{2+}-GlxI is consistent with a five-coordinate Zn site with two shells of O/N donor ligands (2 at 1.90 Å and 3 at 2.05 Å, fit Zn02). Addition of one well-ordered histidine ligand, or two histidines with significant disorder (fit Zn03) in the atoms in the third coordination sphere, greatly improves the fit.

The structure of the Ni^{2+} site from this XAS analysis is consistent with that seen in the *H. sapiens* GlxI enzyme, with the substitution of the Gln ligand for a His in the *E. coli* enzyme. As discussed (Chapter 1), the crystal structure of *H. sapiens* GlxI confirmed

previous EXAFS and EPR suggestions that the metal is coordinated by six ligands (Sellin et al., 1982a; Sellin et al., 1982b; Sellin et al., 1983; Garcia-Iniguez et al., 1984;). The four protein residues in the *H. sapiens* enzyme were identified as ligands, Gln34 with a Zn^{2+}-O distance of 2.0 Å, Glu100 Zn^{2+}-O = 2.0 Å, His127 Zn^{2+}-N = 2.1 Å, and Glu173 Zn^{2+}-O = 2.0 Å. The final two ligands were identified as water molecules with Zn^{2+}-OH_2 distance of 2.1 Å and 2.8 Å (Cameron et al., 1997; Cameron et al., 1999a). The *E. coli* GlxI sequence has only 36% identity to the *H. sapiens*. Nonetheless, protein sequence alignments between the *E. coli* and *H. sapiens* GlxI enzymes suggest the conservation of three of the four metal ligands in the *E. coli* enzyme (Glu56, His74, and Glu122), with the fourth ligand tentatively corresponding to a histidine (His5; Figure 3.4).

The XAS data on *E. coli* GlxI support a six-coordinate $Ni(Glu)_2(His)_2(OH_2)_2$ site, whereas the EXAFS analysis for the Zn^{2+}-substituted *E. coli* GlxI is consistent with a $Zn(His)_2(Glu)_2OH_2$ site. As the *S. cerevisiae* and *P. putida* enzymes are active with Zn^{2+} bound (Aronsson et al., 1978; Saint-Jean et al., 1998) yet also have a His ligand rather the Gln seen in the *H. sapiens* GlxI this change in ligation is not expected to be responsible for the critical difference in the activity (See Chapter 4 for interesting results on the H5Q mutant GlxI). These results suggest that a six-coordinate metal may be required to produce an active enzyme and Zn^{2+} does not give that configuration in *E. coli* GlxI, whereas a six-coordinate Zn^{2+} does occur in *H. sapiens* GlxI producing an active enzyme.

Inhibitor Binding and the Mechanistic Implications

The results from Ni K-edge and XANES analysis combined suggest that addition of *S*-lactoylglutathione or *S*-octylglutathionine to Ni^{2+}-GlxI has no effect on either the redox level or the geometry of the Ni site. This confirms that the *S*-octylglutathionine does not directly interact with the metal. Crystallization of the *H. sapiens* GlxI enzyme in the presence of *S*-hexylglutathione also did not appear to significantly alter the metal ligand environment (Ridderström et al., 1998). In contrast, EPR and NMR studies on the *H. sapiens* GlxI enzyme suggested that the addition of *S*-lactoylglutathione removes one water ligand from the metal environment (Sellin et al., 1982a). There is no evidence for this in the *E. coli* Ni-GlxI, under the given conditions.

Interestingly, the Ni^{2+}-GlxI TSA complex is more consistent with a five-coordinate geometry suggesting a trigonal bipyramidal geometry, as determined by XANES analysis. This would suggest that a ligand associated with the Ni^{2+} site in the native sample could be lost upon addition of hydroxamate.

The crystal structure of *H. sapiens* GlxI with a transition state analogue inhibitor (*S*-(*N*-hydroxy-*N*-*p*-iodophenylcarbamoyl)glutathione) added indicates that two water molecules and Glu173 are replaced by two O atoms from the inhibitor (Cameron et al., 1999a). The EXAFS data for *E. coli* Ni^{2+}-GlxI are consistent with this result, although it is not clear whether the TSA displaces a carboxylate ligand in addition to the two water molecules. The XANES analysis showing a five-coordinate site is also consistent with a $Ni(His)_2(Glu)(TSA)$ structure. Such a structure appears to be consistent with the proposed reaction mechanism of the *H. sapiens* GlxI that features displacement of Glu173, which can then function as a catalytic free base (Cameron et al., 1999a).

3.3.4 Crystallography

Structure Determination

Initially attempts were made to determine the structure of *E. coli* GlxI using molecular replacement based on the previously reported *H. sapiens* GlxI structure (PDB 1FRO). As these efforts proved unsuccessful, the SeMet form of *E. coli* GlxI was prepared and crystallized for use in MAD analysis for the solution of the native enzyme structure. Further details regarding the analysis and interpretation of the crystallographic data can be found in Appendix D (He et al., 2000).

The five *E. coli* GlxI structures have been deposited in the protein database with the following codes: Ni^{2+}-GlxI, 1F9Z; Zn^{2+}-GlxI, 1FA5; Co^{2+}-GlxI, 1FA6; Cd^{2+}-GlxI, 1FA7; ApoGlxI, 1FA8.

Overall Structure

The 135 amino acid native *E. coli* GlxI protein structure is composed of two identical subunits and has an overall fold similar to that of the 184 amino acid *H. sapiens* enzyme (Cameron et al., 1997). Each subunit is itself made up of two domains (residues 3-60 and 72-126) that are linked by an intervening segment of 12 residues (Figure 3.5A). Each of these

domains is composed of a βαβββ motif forming a mixed β-sheet (Figure 3.5A). The sequence of the strands within the sheet is $\beta_1\beta_4\beta_3\beta_2$. Within their respective "core" regions, the two domains have quite similar structure (eg. The C^{α} atoms of residues 3-36 and 72-97 superimpose within 0.3 Å). The solvent-exposed loops connecting strands β_2 and β_3 (residues 36-38 and 104-107) and β_3 and β_4 (residues 47-51 and 115-119), however have very different conformations (Figure 3.6A).

In the dimer, the β_1 strand of the first domain from subunit A associates in an antiparallel manner with the β_1 strand from the second domain of subunit B. This leads to a curved 8-stranded β-sheet (Figure 3.5B). A reciprocal interaction between the second domain of subunit A and the first domain of subunit B leads to a second curved β-sheet. The two metal-binding sites per dimer are located within these curved β-sheets.

The two monomers are very close in structure (Figure 3.6B), with their C^{α} atoms being superimposable within 0.47 Å. To compare the conformation in the vicinity of the two active sites, the first domain from the first monomer plus the second domain from the second monomer was overlaid on to the second domain from the first monomer plus the first domain from the second monomer (Figure 3.6C). In this case, the RMS deviation of the C^{α} atoms is only about 0.54 Å with the largest difference in the loop regions from residues Gln91-Gly94 and Val103-Thr108. The C^{α} atoms in these two loops have B factors ranging from 40 to 70 $Å^2$, significantly higher than the average value of 19.5 $Å^2$ for the protein as a whole (Figure 3.7). Higher backbone B factors were also found for the same two loops in SeMet- Ni^{2+}-GlxI. The high B factors of the two loops in both crystal packing environments indicate their flexibility. The B factors of residues 91-94 in subunit A are about 25 $Å^2$ higher than those in subunit B for all the GlxI structures solved. This is consistent with the observation that residues 91-94 in subunit B are involved in crystal contacts while the same residues in subunit A are exposed to the solvent. Although the loop formed by residues 103-108, which is "above" the active site, is very mobile, the backbone in the vicinity of the metal-binding residues is among the most rigid part of the entire protein (Figure 3.7).

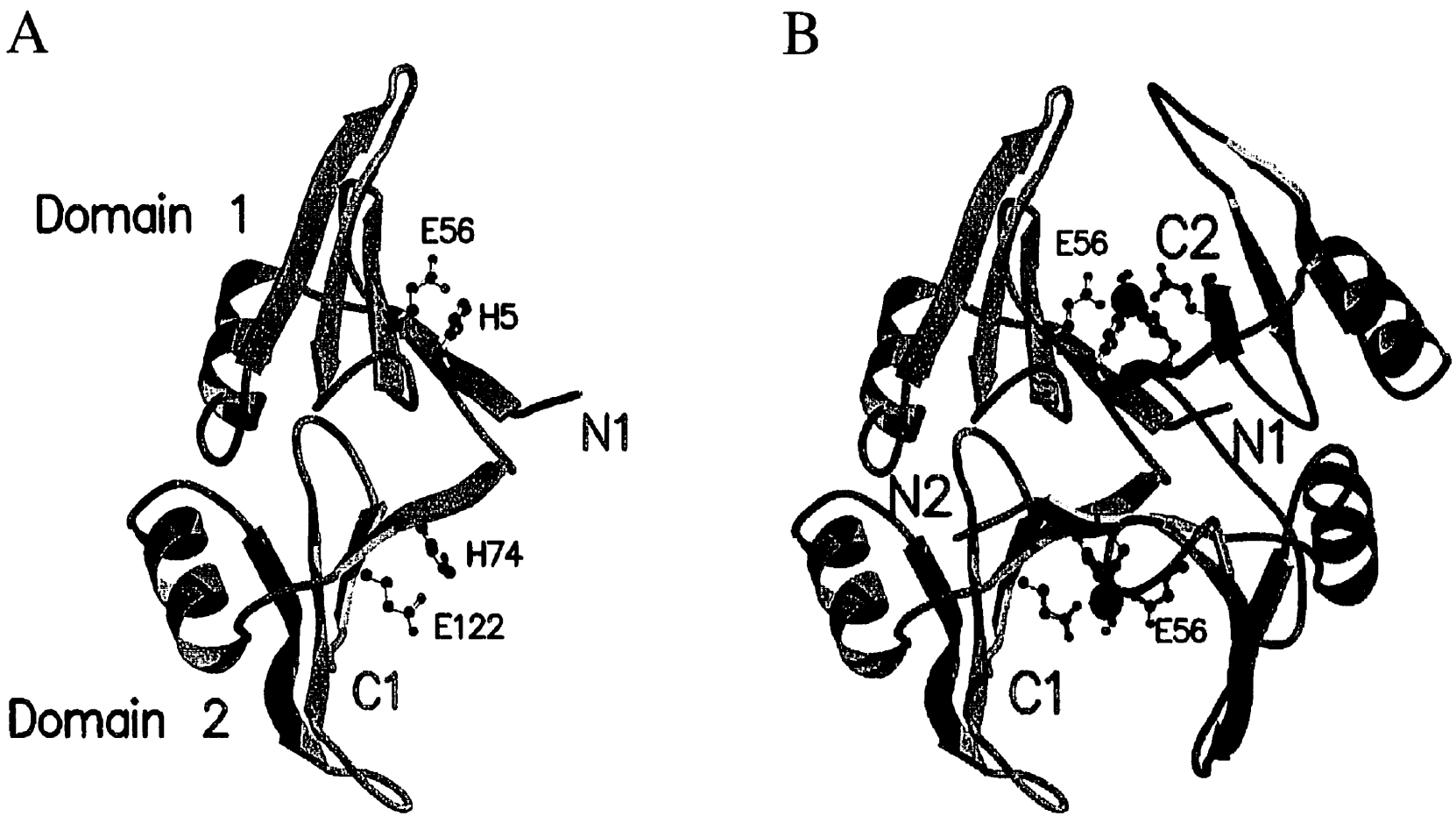

Figure 3.5: Schematic representation of *E. coli* GlxI, (A) monomer, and (B) dimer. The two monomers in the dimer are coloured orange and grey, respectively. The nickel (magenta) and its coordinating protein and water ligands are shown in ball and stick representation. The active site is situated within a curved β-sheet, which is formed on dimerization.

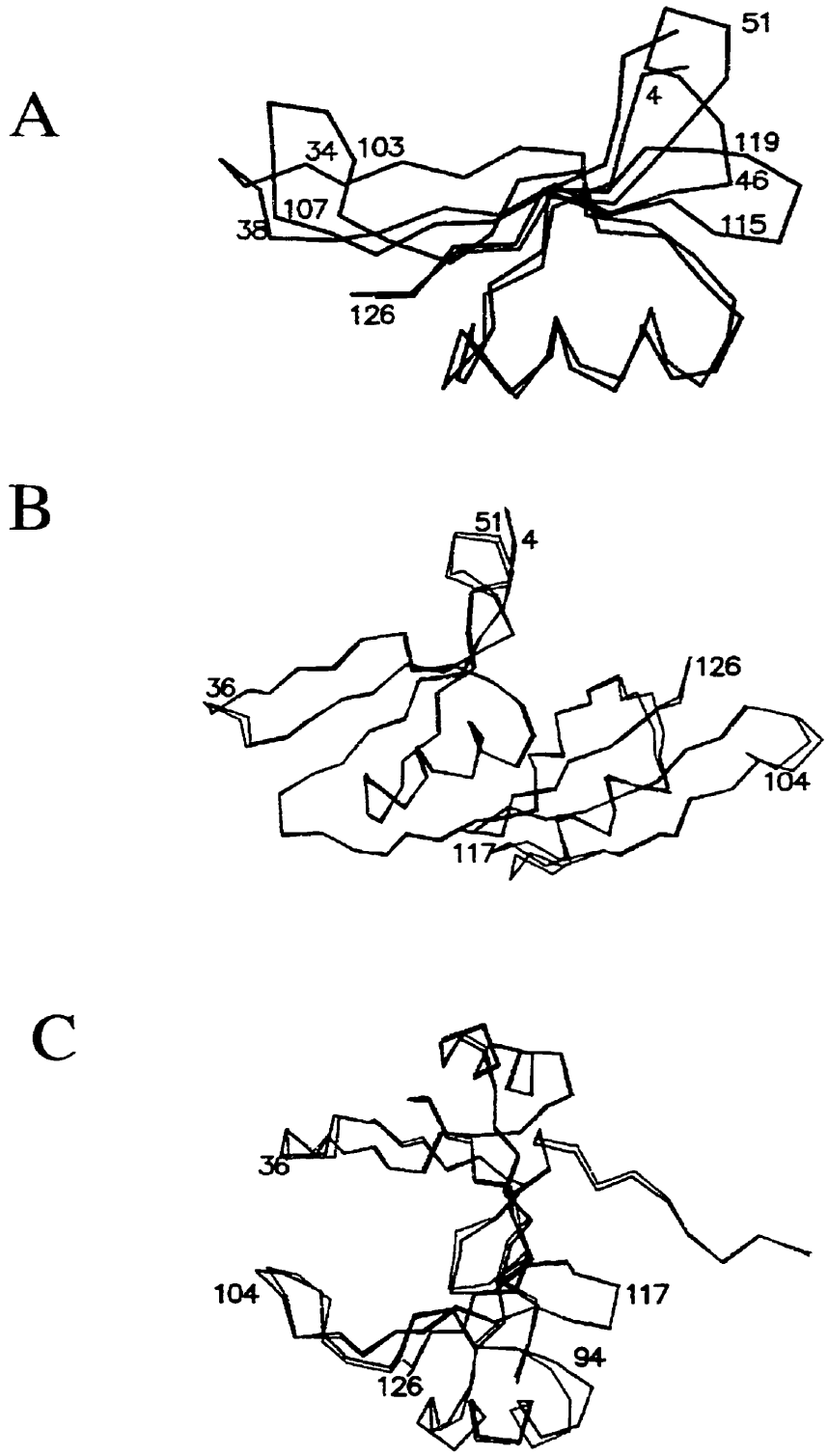

Figure 3.6: Superposition of (A) domain 1 (red) on domain 2 (light blue), (B) monomer 1 (magenta) on monomer 2 (green), and (C) superposition of the respective domains that constitute the active site of *E. coli* GlxI.

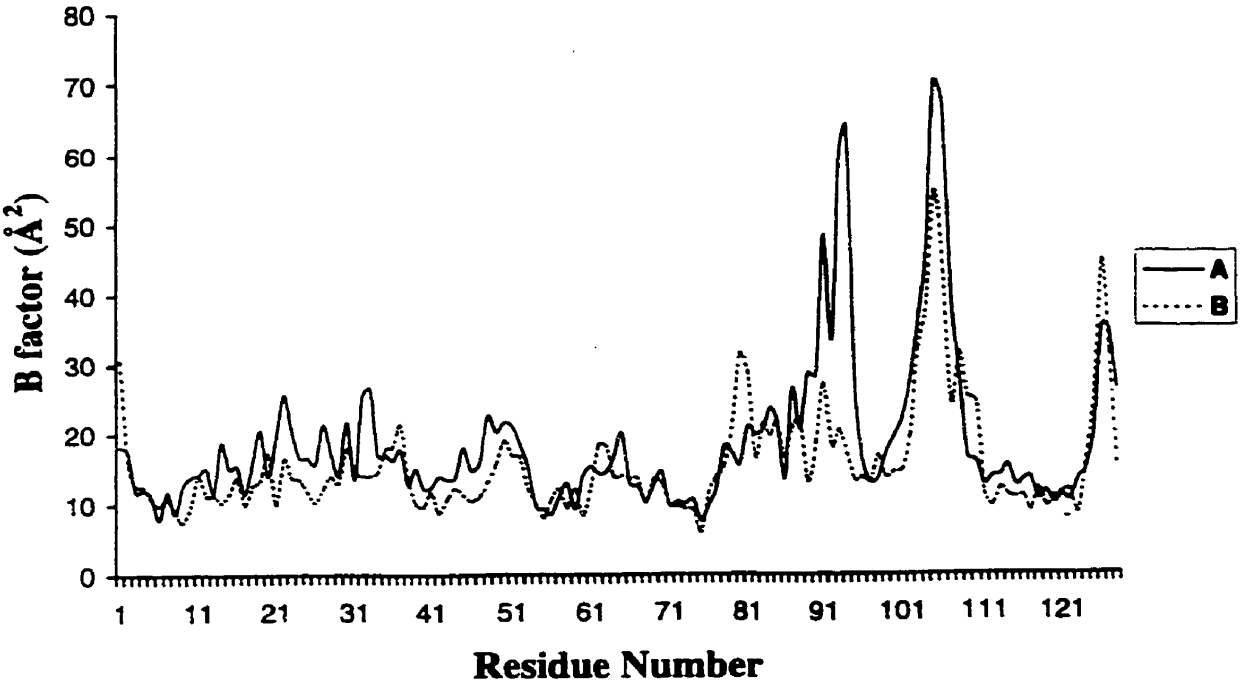

Figure 3.7: The B factors of the C^{α} atoms in subunit A (solid line), and subunit B (dotted line) of Ni^{2+}-GlxI.

Toward the carboxy-terminus of the molecule the electron density could be followed clearly until Glu126, at which point it became much weaker. It could, however, still be followed until it entered the active site of an adjacent molecule in the crystal. At this point, the density became much stronger and could be modeled as Gly134-Asn135, the two residues at the carboxy-terminus of the protein. The intervening electron density between Glu126 and Gly134 is long enough to account for the intervening seven residues, but was not sufficiently well defined to permit the inclusion of these residues in the final model.

Metal Coordination

Although biochemical data have indicated that only one metal ion per dimer is required to fully activate the protein (Chapter 2 and Clugston et al., 1998a), two such ions are seen at essentially equivalent positions (Figure 3.5B). In the native *E. coli* Ni^{2+}-GlxI structure

four protein residues (His5 and Glu56 from one monomer and His74 and Glu122 from the other) and two water molecules are coordinated to the nickel (Figure 3.8A). Very similar ligation is seen in the two active sites. As we have shown *E. coli* GlxI to be a homodimeric enzyme with high homology to the *H. sapiens* enzyme this would have been the expected result. However, these contradictory findings suggest that the two active sites may not be completely equivalent. If the second site has a much lower affinity for metal ions, it may not bind under the conditions of the kinetic analyses. The concentration of enzyme (12-37 mg/ml or 0.4-1.2 mM dimeric enzyme), and hence metal, required in the crystallization conditions are significantly higher than that employed in standard kinetic experiments. The enzyme is generally stored at a concentration of approximately 5 mg/ml and diluted prior to kinetic analysis, in which nanograms to micrograms of enzyme are used. Metal analysis were performed at enzyme concentrations of 0.5-1.0 mg/ml. These factors may contribute to the ability of the enzyme to bind the second metal in the crystallization conditions, explaining this anomaly. Several examples of oligomeric proteins of identical subunits with half-site reactivity have been observed (Beimann and Koshland, 1994; Koshland, 1996; Avaeva et al., 1997; Fersht, 1999; Izard, 1999), however at this time is it unclear how and if this relates to *E. coli* GlxI. Alternatively, it may be that the protein crystallizes better if both sites are symmetric and hence occupied by a metal ion.

The coordination geometry surrounding the nickel ion is octahedral with close to ideal geometry (Figure 3.9; Table 3.1 and 3.2). Nickel lies in the plane defined by N^{ε} of the two histidine residues and the two water molecules. Monodentate coordination is seen for each of the two axial carboxylates. Substitution of different metal ions in the active site of GlxI does not change the overall structure of the protein. The Co^{2+}, Cd^{2+}, and Zn^{2+} enzymes have a C^{α} RMS deviation not exceeding 0.3 Å when compared to Ni^{2+}-GlxI. The changes that do occur are localized to the immediate vicinity of the metal sites. As with the native nickel enzyme, the enzymatically active Co^{2+} and Cd^{2+} derivatives also exhibit octahedral coordination, albeit with somewhat longer coordination distances (Table 3.1), consistent with the increased radii of Co^{2+} and Cd^{2+} compared to Ni^{2+} (Pauling, 1960). In contrast, the inactive Zn^{2+} derivative displays trigonal bipyramidal coordination with the same four protein ligands plus a single water molecule (Figures 3.8B and 3.9B), as suggested by the EXAFS data (Section 3.3.3).

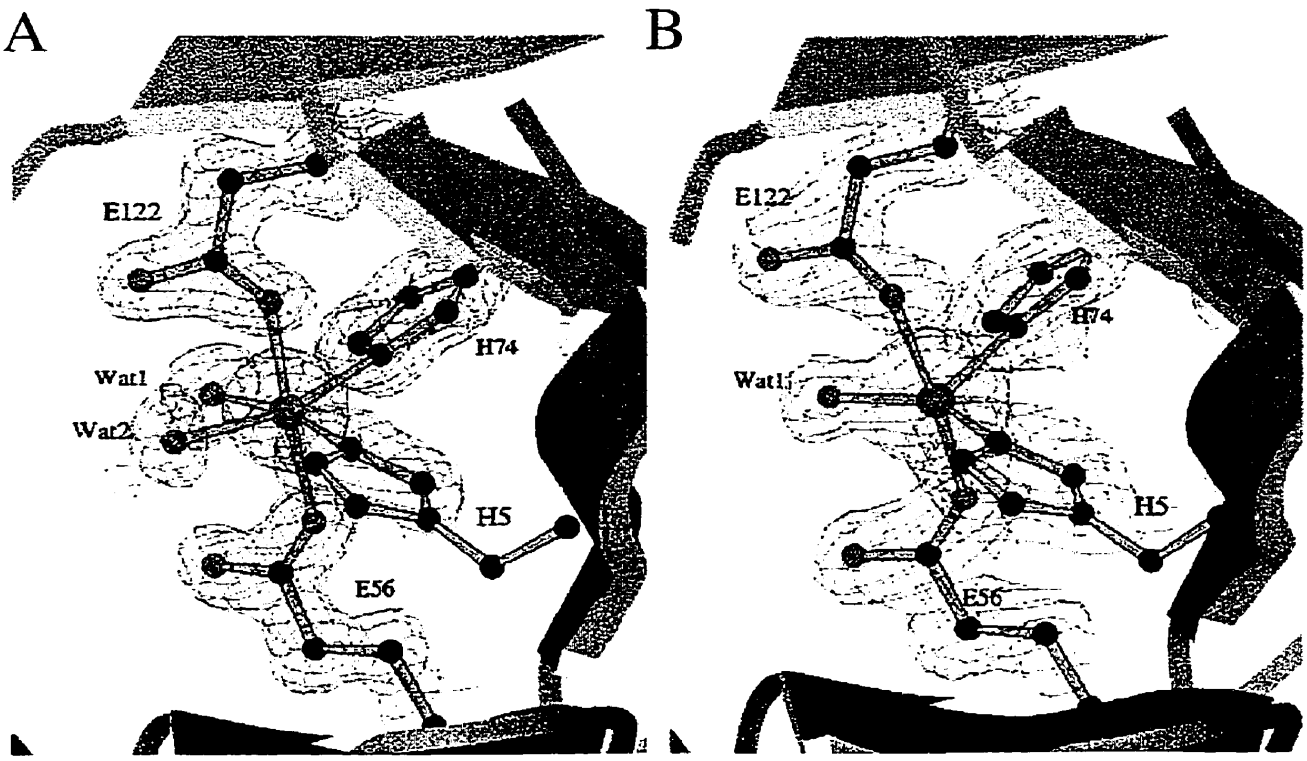

Figure 3.8: The active sites of (A) Ni^{2+}- and (B) Zn^{2+}-substituted GlxI. The resolution is 1.5 Å for the Ni^{2+} enzyme and 1.8 Å for the Zn^{2+} form. See appendix D or He et al., 2000 for details of the restraints used in the refinement of this figure.

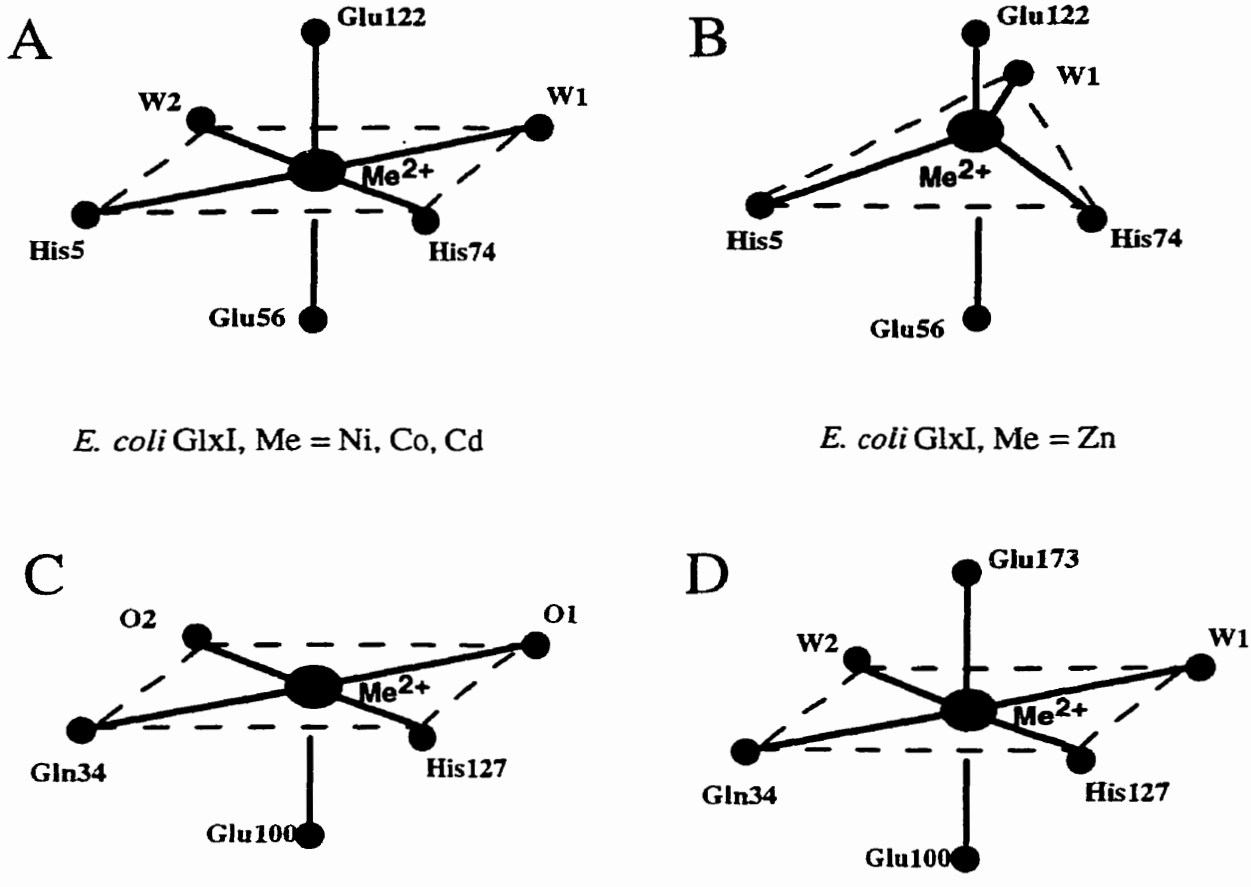

E. coli GlxI, Me = Ni, Co, Cd

E. coli GlxI, Me = Zn

Human GlxI, Me = Zn

Human GlxI, Me = Zn

Figure 3.9: Metal coordination in different GlxI structures. (A) Complexes of *E. coli* GlxI with Ni^{2+}, Co^{2+}, and Cd^{2+}. The two water ligands are labeled W1 and W2. (B) Complex of *E. coli* GlxI with Zn^{2+}. (C) Complex of *H. sapiens* Zn^{2+}-GlxI with *S*-(*N*-hydroxy-*N*-*p*-iodophenylcarbamoyl)glutathione. The two oxygen ligands from this hydroxamate inhibitor are labeled O1 and O2. (D) Complex of *H. sapiens* Zn^{2+}-GlxI with *S*-*p*-nitrobenzyloxycarbonylglutathione (Coordinates from PDB 1QIN and 1QIP; Cameron et al., 1997; Cameron et al., 1999a)

Table 3.1: Coordination distance for the metal ligands in *E. coli* glyoxalase I complexes.

	Ligand Distances (Å)							
	Ni^{2+}		Co^{2+}		Cd^{2+}		Zn^{2+}	
Ligand	Site 1	Site 2	Site 1	Site 2	Site 1	Site 2	Site 1	Site 2
His5 N^{ε}	2.2	2.1	2.3	2.2	2.4	2.3	2.2	2.1
W1	2.1	2.1	2.3	2.2	2.4	2.4	2.0	2.1
His74 N^{ε}	2.3	2.3	2.4	2.3	2.6	2.5	2.2	2.2
Glu56 O^{ε}	2.1	2.1	2.1	2.1	2.4	2.3	2.1	2.1
Glu122 O^{ε}	2.1	2.1	2.2	2.4	2.8	2.4	2.1	2.4
W2	2.2	2.2	2.4	2.4	2.4	2.6		

Table 3.2: Coordination geometry for the metal ligands in the four *E. coli* glyoxalase I metal substituted forms.

	Octahedral Bond Angles (deg)							Trigonal Bipyramidal Bond Angles (deg)		
		Ni^{2+}		Co^{2+}		Cd^{2+}			Zn^{2+}	
Atoms	Ideal	Site 1	Site 2	Site 1	Site 2	Site 1	Site 2	Ideal	Site 1	Site 2
O^{ε}122-Me-N^{ε}74	90	81	82	84	90	87	90	90	90	92
N^{ε}5-Me-O^{ε}122	90	99	95	91	79	79	95	90	88	88
O^{ε}56-Me-N^{ε}5	90	79	82	81	85	85	84	90	83	88
W1-Me-O^{ε}56	90	88	88	85	87	80	81	90	87	93
W1-Me-O^{ε}122	90	93	96	103	108	104	100	90	95	86
O^{ε}122-Me-O^{ε}56	180	179	176	172	163	164	179	180	169	173
W1-Me-N^{ε}5	180	163	165	161	163	161	161	120	143	131
N^{ε}74-Me-W1	90	91	92	90	91	92	89	120	101	112
N^{ε}74-Me-O^{ε}56	90	99	96	98	96	93	91	90	99	98
N^{ε}74-Me-N^{ε}5	90	100	99	105	104	102	102	120	116	116
W2-Me-N^{ε}5	90	92	93	93	90	93	95			
W2-Me-O^{ε}56	90	97	98	101	101	104	103			
W1-Me-W2	90	79	79	78	77	78	78			
W2-Me-O^{ε}122	90	83	84	79	77	79	76			
W2-Me-N^{ε}74	180	161	162	155	158	157	160			

The geometry of the two zinc ions is slightly different. In one active site the zinc-bound water superimposes on one of the two water ligands in the nickel complex and has close-to-perfect trigonal bipyramidal geometry. In the other active site, the water does not superimpose on either water ligands of the Ni^{2+} structure resulting in distorted trigonal bipyramidal coordination.

The overall structure of apoGlxI is very similar to that of the metal-bound forms. The RMS discrepancy of the C^{α} atoms relative to the nickel enzyme is 0.32 Å. This is consistent with the circular dichroism spectrum, which did not suggest any significant structural change upon addition of Ni^{2+} ions to the apoenzyme (Clugston, 1997). There are some changes in the immediate vicinity of the metal sites. In the apoenzyme, the metal ligands are somewhat more loosely packed, and the two glutamates are directed away from the vacant sites.

The structure of GlxI substituted with Mn^{2+} could not be determined. The enzyme was prepared in the same fashion as the other metal-substituted forms, and activity assays suggested the metal was retained throughout the enzyme preparation. However, x-ray analysis of the enzyme cocrystallized or soaked in up to 5 mM Mn^{2+} showed weak electron density at the metal binding sites, suggesting that the affinity for this metal ion in the crystal is low. This finding further supports the previous work that indicated the affinity of the protein for Mn^{2+} was weaker than for the other metals studied. The EPR analysis however did indicate that the Mn^{2+} was in an octahedral environment, consistent with the metal coordination environment found in this work for the other active metal forms.

Comparison with Human GlxI and Other Members of the βαββββ Superfamily

The overall structure of *E. coli* GlxI is similar to that found in the *H. sapiens* enzyme (Cameron et al., 1997), containing two βαββββ motifs in each monomer. This pattern has been suggested to result from gene duplication, and serves to place the GlxI enzymes as a member of a recently identified βαββββ superfamily of metalloenzymes (Bergdoll et al., 1998). Despite very low sequence homology and no similarity in enzymatic function, *H. sapiens* GlxI has been shown to be structurally related to the bacterial bleomycin resistance protein (BRP) from *Streptoalloteichus hindustanus* (Dumas et al., 1994), and 2,3-dihydroxybiphenyl 1,2-dioxygenase (DHBD) from *Burkholderia cepacia* (Han et al., 1995). The fosfomycin resistance protein (FosA), a Mn^{2+}-dependent glutathione-*S*-transferase, has

also been suggested to be a member of this superfamily (Bernat et al., 1997). A detailed analysis of the structural similarities and postulated evolution of this family of enzymes has been presented elsewhere by Bergdoll et al. (1998) and is further examined in Chapter 5. With the exception of FosA, which has not been structurally characterized, all members of the βαββββ family have overall structures that are much more similar to that of *E. coli* GlxI than to that of *H. sapiens* GlxI. Therefore, the determination of the structure of the *E. coli* enzyme provides a more representative member of the family as a whole.

Despite the expected overall similarity between the *E. coli* and *H. sapiens* GlxI structures there are several substantive differences, many of which we had previously predicted based on sequence alignments, presented in Chapter 5. A 29 amino acid N-terminal arm which wraps around the adjacent subunit in the *H. sapiens* protein is absent in the *E. coli* enzyme as well as in other members of the βαββββ family. This extended arm may help to stabilize the dimeric form of the *H. sapiens* enzyme, although its absence in the *E. coli* enzyme shows that such an arm is not essential for dimer formation. Since this arm lies mostly on the surface of the enzyme its absence is not expected to substantially perturb the rest of the structure.

Another difference is that *E. coli* GlxI has a significantly larger active site pocket than that of *H. sapiens* GlxI. In the *H. sapiens* enzyme, the active site consists of a largely hydrophobic pocket with a volume of about 70 $Å^3$. In contrast, the active site in the *E. coli* enzyme consists of a deep solvent channel about 10-15 Å in diameter (Figure 3.10). This increase in solvent accessibility is predominantly due to the deletion of a 15 amino acid segment that would lie approximately between residues 51-52 in the bacterial protein (See Chapter 5 for further analysis and figures). This deletion eliminates an α-helix and a loop that lies along the side of the active site in the *H. sapiens* enzyme. As a result, the active site of *E. coli* GlxI may have a very different response to inhibitors and substrates.

Two smaller regions (residues 107-111 and 120-123 in *H. sapiens* GlxI) not present in the *E. coli* enzyme correspond to small loops lying between the two βαββββ motifs. These differences are mirrored within the other known superfamily members and suggest the *E. coli* enzyme is more similar to the other known members of the superfamily than is the *H. sapiens* GlxI. Further analysis and figures displaying the regions missing in the *E. coli* GlxI enzyme are presented in Chapter 5.

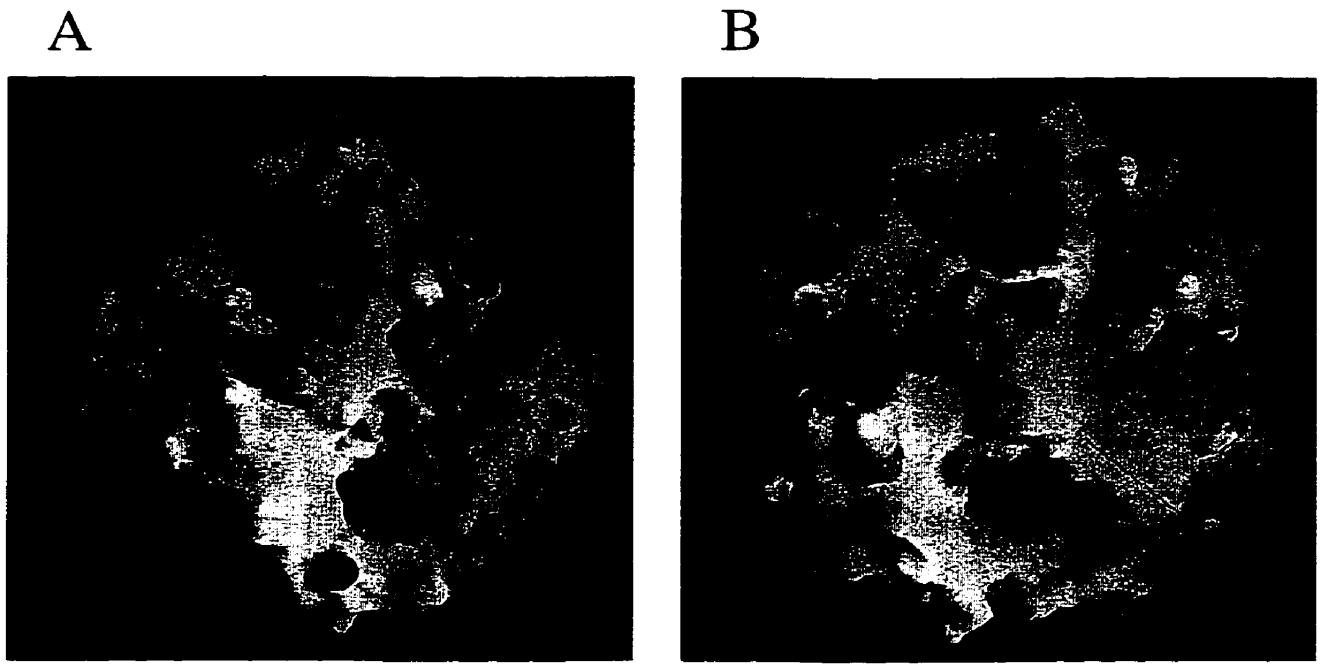

Figure 3.10: Molecular surfaces of the (A) *E. coli* and (B) *H. sapiens* GlxI proteins. Positive potential (> 15 mv) is coloured blue, neutral potential (0 mv) is coloured grey, and negative potential (< -15 mv) is coloured red. The molecules are shown in approximately the same alignment as Figure 3.5B. The electrostatic potentials were calculated and molecular surfaces displayed using the program GRASP (Nicholls and Honig, 1991).

Previous studies have shown that the four C-terminal residues of *E. coli* GlxI (Gly132-Asn135) can be proteolytically removed without affecting catalytic activity (Barnard, 1997; Clugston et al., 1998a). In the electron density map, the residues following Glu126 can not be traced accurately due to weak electron density, with the exception of the final two residues (Gly134-Asn135), which bind within the active site of an adjacent protein molecule in the crystal. The mobility of the C-terminal region explains its susceptibility to proteolytic degradation. Analysis of the B factors of the *E. coli* GlxI structure (Figure 3.7) reveals two regions with higher than average mobility, residues 91-94 and 104-106. The second region lies "above" the active site, suggesting a possible involvement in substrate binding. There is some evidence for this in the recent structure determination of the *H. sapiens* GlxI with a proposed transition state analogue, which indicates that C^{α} of Lys157 moves 3 Å toward the active site (Cameron et al., 1999a). This residue is located within a loop that corresponds to residues Pro102-Val103-Lys104-Gly105-Gly106-Thr107-Thr108-Val109 in the *E. coli* enzyme. Thus Lys104 in the *E. coli* enzyme may play a role similar to the Lys157 in the *H. sapiens* enzyme.

Comparative Analysis of the Metal Binding Site

High resolution structures of five different forms of the *E. coli* GlxI enzyme permits comparison of the various active enzymes and also allows for detailed analysis of the inactive Zn^{2+} enzyme and the metal-free apoenzyme. The structures presented here show that each of the active forms of *E. coli* GlxI has an octahedral metal coordination, with two participating water molecules. In addition, the EPR results (Section 3.3.2) on the Mn^{2+} substituted *E. coli* GlxI, indicated that the Mn^{2+} is also octahedrally coordinated. Examination of the metal binding site of the Zn^{2+} form of the enzyme reveals a significant difference in the coordination geometry around the metal compared with the active forms of the enzyme (Figure 3.9). Not only is there loss of one water ligand to the Zn^{2+} making this a five rather than six coordinate metal, the geometry around the metal has also changed. The octahedral environment seen around the active Ni^{2+}-, Co^{2+}-, and Cd^{2+}-GlxI, is modified to a trigonal bipyramidal arrangement for the Zn^{2+} enzyme.

Direct comparison with the metal coordination of the active Zn^{2+} *H. sapiens* enzyme is difficult as a crystal structure of the *H. sapiens* enzyme lacking an inhibitor has not yet been

reported. However, the available inhibitor complexes indicate that Zn^{2+} is coordinated by four protein ligands (Gln34, Glu100, His127, Glu173) plus one or possibly two water molecules with square pyramidal or octahedral geometry (Figure 3.9). Liganding with the inhibitor substitutes for the binding of the second water molecule in some cases (Cameron et al., 1997; Ridderström et al., 1998; Cameron et al., 1999a).

In the case of the *E. coli* enzyme, the two residues at the carboxy-terminus of one molecule bind within the active site of an adjacent molecule in the crystal. The location and mode of binding is similar to that of benzylglutathione cocrystallized in the active site of the *H. sapiens* enzyme (Figure 3.11). In particular, the O11 and N1 of benzylglutathione form hydrogen bonds with $N^{\delta 2}$ and $O^{\delta 1}$ of Asn104 that mimic those between the O and $N^{\delta 2}$ of Asn135 and Asn60 in the *E. coli* GlxI enzyme. The presence of these two amino acids in the active site does not, however, appear to contribute to or directly influence the ligation at the metal site.

Even though the *H. sapiens* and *E. coli* GlxI enzymes have similar amino acid sequences and similar three-dimensional structures, they do not have identical metal ligands, as indicated previously. Figure 3.9 and Figure 3.4 clearly shows that the Gln34 of the *H. sapiens* enzyme is replaced with a histidine in the *E. coli* enzyme. In the absence of structural information, this variability might have suggested that this is a nonessential amino acid. Even with the knowledge of the respective structures, it might suggest that the presence of the glutamine would correlate with the use of nickel. This is discounted, however, by the observation that the *S. cerevisiae* and *P. putida* GlxI enzymes which are active with zinc, maintain the same four metal ligands as the *E. coli* including the second histidine ligand (Chapter 5 and Clugston et al., 1997). The key factor responsible for activity, therefore, seems to be geometry.

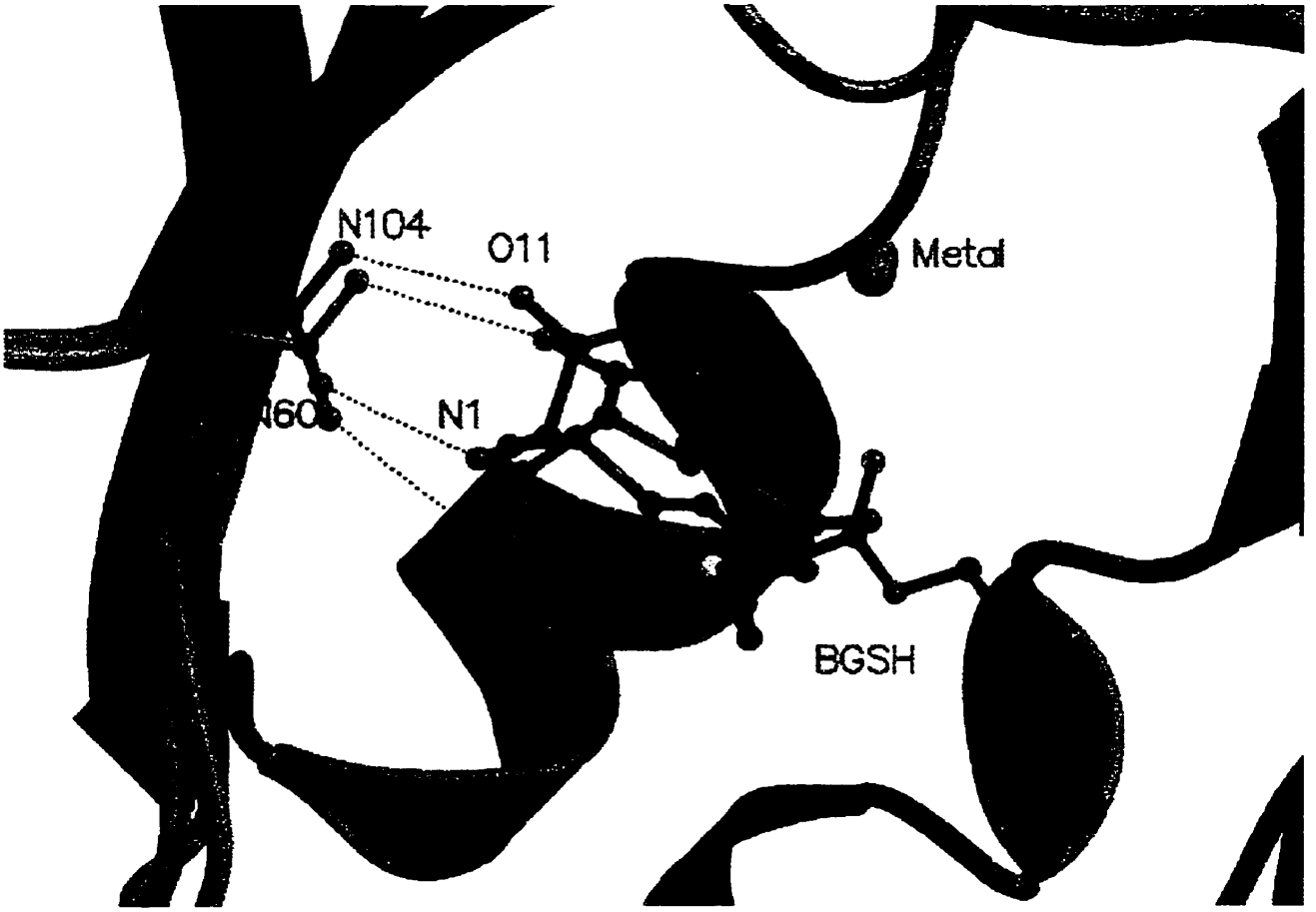

Figure 3.11: Superposition of the active site of *E. coli* GlxI (green) on *H. sapiens* GlxI (blue). Benzylglutathione, which is bound to the *H. sapiens* enzyme, is shown in blue with its hydrogen bonds to Asn shown as dotted lines. Gly134 and Asn135, which bind within the active site of the *E. coli* enzyme and make analogous hydrogen bonds to Asn60, are shown in green.

Previous studies of the zinc endopeptidase astacin have revealed a relationship between the geometry around the metal center and enzymatic activity of various metal-substituted forms of the enzyme (Gomis-Rüth et al., 1994). Trigonal bipyramidal ligation was observed for each of the three active forms of the enzyme, Zn^{2+}, Cu^{2+}, and Co^{2+}, whereas a second solvent water was present to form an octahedral coordination for the Ni^{2+} enzyme, and no water molecules existed with the tetrahedral Hg^{2+}-asticin, both of which were inactive. The results from studies on astacin suggest that the correct orientation of metal-liganded water molecules was necessary for catalytic activity. In the case of astacin, Zn^{2+} and Co^{2+} give the appropriate orientation while Ni^{2+} does not. The structural analysis of *E. coli* GlxI displays a similar correlation between geometry and activity except that in this case Ni^{2+}, Co^{2+}, and Cd^{2+} appear to have the correct orientation of bound water molecules, while Zn^{2+} does not. The orientation of the water ligands may be important in the reaction mechanism.

Reaction Mechanism

On the basis of solvent isotope exchange studies on the *S. cerevisiae* enzyme the overall mechanism of GlxI has been proposed to involve proton abstraction, formation of an enediol(ate), and reprotonation at the adjacent carbon (Hall et al., 1976). A specific mechanism has been proposed based on the recent crystallographic studies of *H. sapiens* GlxI in the presence of a putative transition state analogue (Cameron et al., 1999a). In this mechanism, it is proposed that the six-coordinate zinc, including two water ligands, becomes five-coordinate upon substrate binding. The two oxygen atoms of the substrate (seen with the enediol inhibitor) replace the two water ligands. The binding of the substrate is also proposed to displace the zinc ligand Glu173, which is then free to act as the catalytic base (Figure 3.12). Based on the present knowledge of the crystal structure of the *E. coli* enzyme, a related mechanism could be proposed, i.e. it could be envisaged that Glu122 in the *E. coli* enzyme, the counterpart of Glu173, would be displaced from the metal on substrate binding and act as the catalytic base. There are, however, a number of uncertainties. For example, while an incoming substrate might be envisioned to displace a glutamate from zinc, it would be less likely to do so for nickel (Gomis-Rüth et al., 1994). However, our recent EXAFS results (Section 3.3.3) suggest that this may in fact be the case for *E. coli* Ni^{2+}-GlxI also.

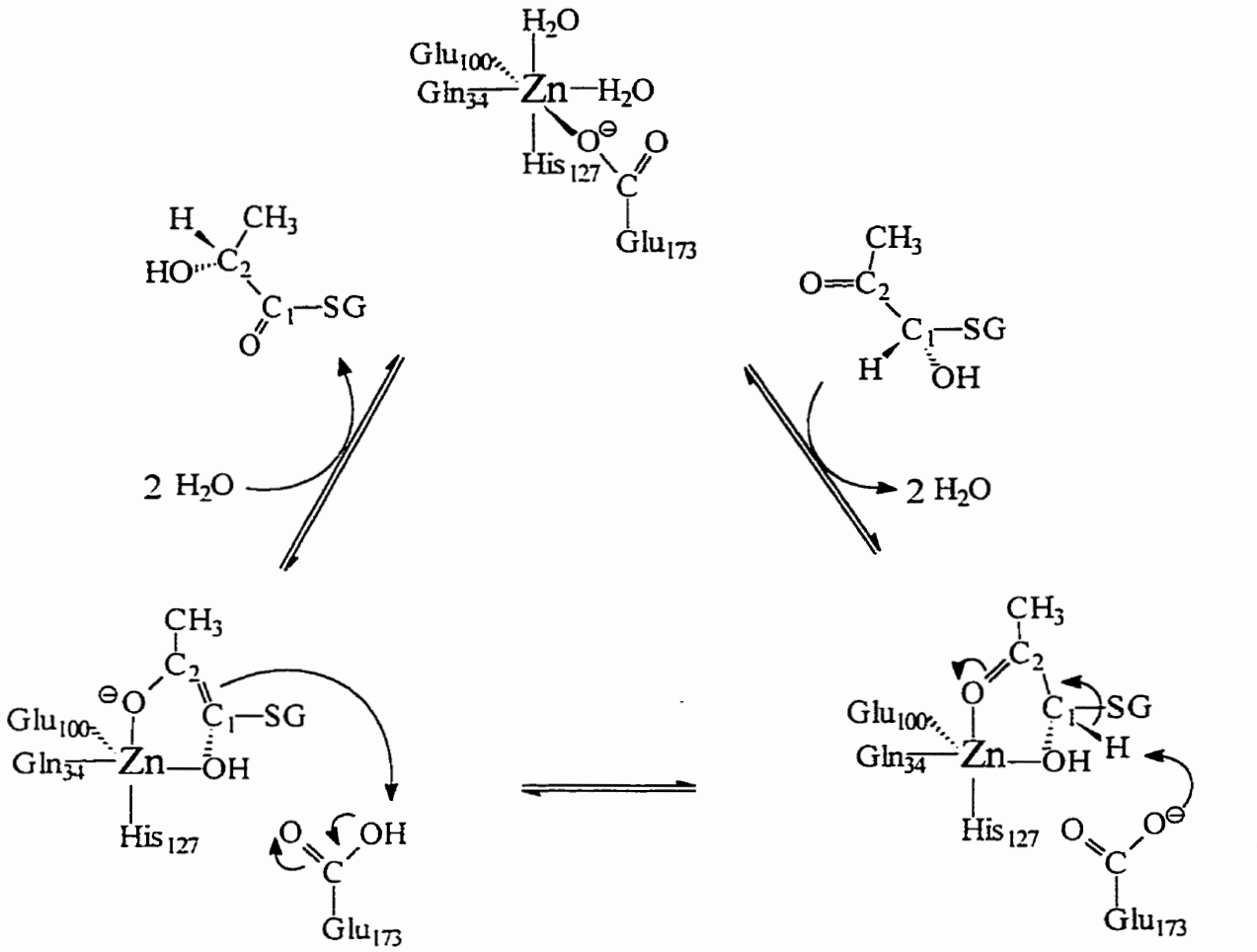

Figure 3.12: Postulated glyoxalase I reaction mechanism proposed based on the *H. sapiens* structural data (Adapted from Cameron et al., 1999a).

Although we have also utilized a hydroxamate in our own analysis (Ly et al., 1998; Sections 2.3.4, 3.3.2 and 3.3.3), it should be noted that the choice of a hydroxamic acid transition state inhibitor could be a double-edged sword. Hydroxamic acids have been successfully utilized as transition state/reactive intermediate analogues for studies on the enzyme triosephosphate isomerase (TIM; Davenport et al., 1991), an enzyme lacking a metal center but whose mechanism is believed to proceed via an enediol intermediate. As the GlxI reaction is also believed to involve an enediol, hydroxamic acids would appear a natural choice for transition state analogues and have been shown to be potent GlxI inhibitors (Murthy et al., 1994; Ly et al., 1998). However, hydroxamic acids are potent metal binding agents in general and this property has been utilized in the development of numerous metalloprotease inhibitors (Babine and Bender, 1997). In all cases the hydroxamic acid analogue has been found to bind directly to the metal center and yet these compounds themselves do not resemble the transition state for the protease mechanism. One must consider this metal affinity when using these analogues as representatives of the transition state. This is especially problematic in the case of the *E. coli* enzyme where, by analogy, one would postulate that the incoming substrate displaces the two water molecules around the nickel.

In principle, the following mechanisms might be pertinent to the *E. coli* GlxI, based on our current structural knowledge: (1) The substrate (or transition state) might displace one or both water molecules plus Glu122 to function as the catalytic base, analogous to that proposed for the *H. sapiens* enzyme (Figure 3.13). (2) On the basis of the octahedral geometry for all the activating metals for *E. coli*, a mechanism that utilizes the two water molecules to polarize and possibly serve in the proton abstraction could be proposed (Figure 3.14). Previous work on the *H. sapiens* enzyme has indicated the importance of two water molecules directly interacting with the substrate (Sellin et al., 1982a; Sellin et al., 1982b). (3) An additional unspecified specific or general base might participate, with either the water molecules on the metal polarizing the substrate (shown) or directly displaced by the two oxygen atoms in the substrate (Figure 3.15). However, the only putative general base present in the active site is Glu49 but this residue is approximately 8.0 Å distal from the metal center. Unless major structural changes occur in the *E. coli* GlxI active site upon substrate binding, Glu49 acting as a general base is doubtful.

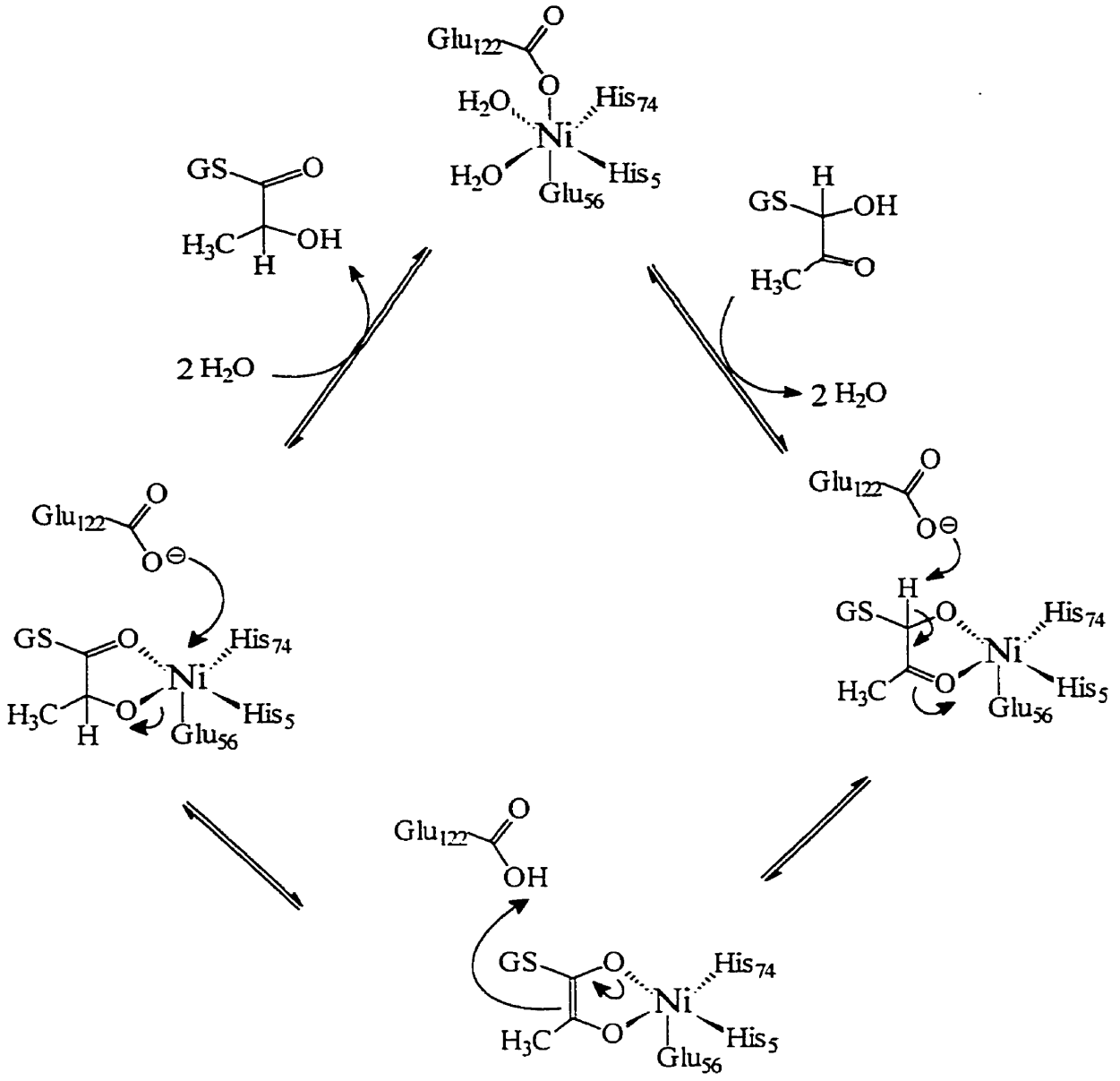

Figure 3.13: One postulated mechanism for the reaction catalyzed by glyoxalase I, similar to that proposed for the *H. sapiens* enzyme with a glutamate being displaced from the metal and acting as the catalytic base.

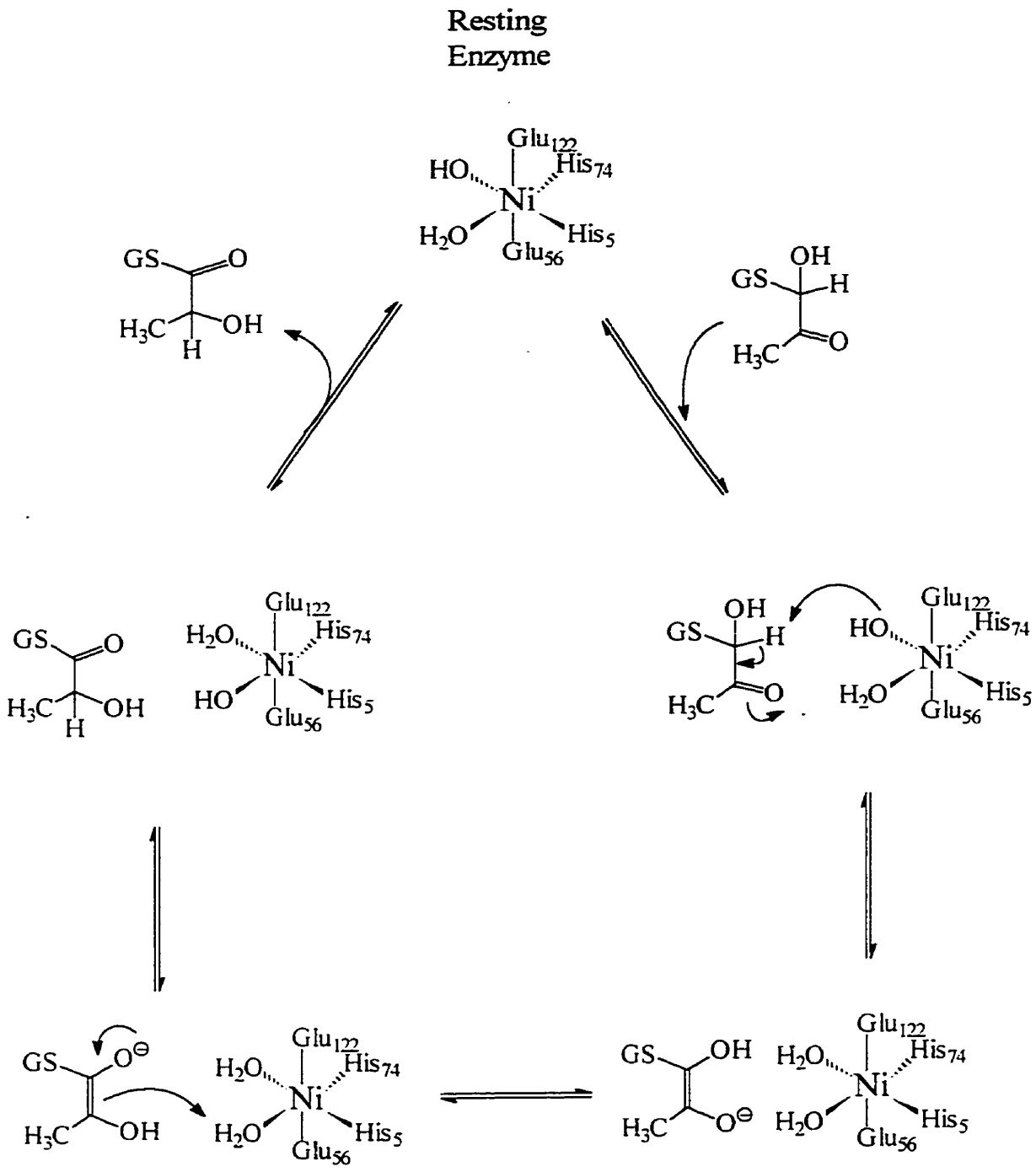

Figure 3.14: Illustration of a possible mechanism for the glyoxalase I reaction, in which the two water molecules serve to polarize and possibly abstract the proton.

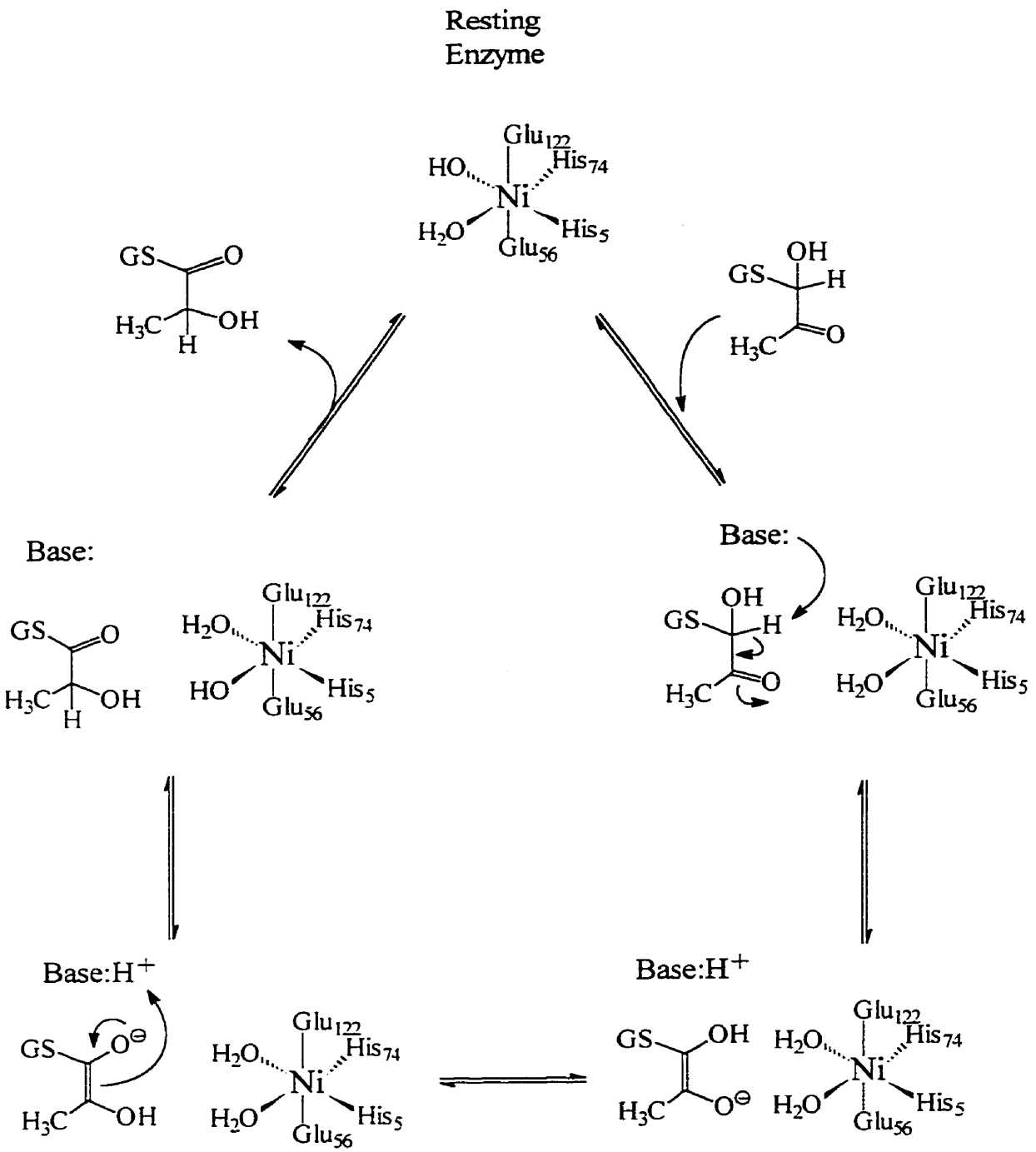

Figure 3.15: A third possible mechanism for the glyoxalase I reaction, in which the two water molecules either serve to polarize the substrate or are displaced by the substrate, and an unspecified base abstracts the proton.

As our EXAFS analyses (Section 3.3.3) suggested the possibility that one metal ligand also may be lost in the *E. coli* enzyme upon binding the hydroxamate TSA, analogous to that proposed for the *H. sapiens* GlxI, further crystallographic studies were required. To further elucidate the mechanism of the glyoxalase I reaction we have attempted to cocrystallize the enzyme in the presence of various inhibitors including the putative transition state analogue inhibitor used in our other analyses (Ly et al., 1998). Initial cocrystallization attempts were unsuccessful. It was speculated that the binding of the terminal two residues in the active site of the adjacent protein dimer prevented binding of the inhibitors. To circumvent this problem, a C-terminal truncated form of *E. coli* GlxI was constructed. As we have previously shown that the removal of the terminal four residues by proteolytic degradation still produced an active enzyme, and the structural data have indicated that these residues are mobile, these residues are not believed to be critical to the enzyme activity. As described in Chapter 4, a protein lacking the terminal nine residues was constructed. During the development of an effective protein production and purification protocol for this expression system, conditions were found for the successful crystallization of the wild-type GlxI enzyme cocrystallized with various inhibitors. As such the C-terminal truncated protein was no longer required. The diffraction data from these cocrystallization experiments is currently under analysis by Dr. M. He in Professor B. Matthews laboratory at the University of Oregon.

3.4 Conclusions

The most remarkable feature of these structural studies is the correlation between catalytic activity and the coordination at the metal binding site. Each of the protein-metal complexes that have octahedral (six-fold) geometry yields an active enzyme. This includes the complexes of the *E. coli* enzyme with Ni^{2+}, Co^{2+}, Cd^{2+}, and Mn^{2+} as well as the complex of the *H. sapiens* enzyme with Zn^{2+}. Conversely, the complex of the *E. coli* enzyme with Zn^{2+} has trigonal bipyramidal (five-fold) coordination and is inactive. It would seem clear that octahedral geometry is a prerequisite for activity. Two possible reasons can be suggested for this. First, it may be that a rather special geometry is required to have a glutamic acid (e.g. Glu173 in the *H. sapiens* enzyme) act as both a metal ligand and as a catalytic base (assuming it does, in fact, fulfill both roles). Second, it may be that the mechanism of action requires that two water molecules be bound to the metal ion either in the resting enzyme, or at some time during catalysis. Six-fold coordination would allow four protein ligands plus two such water molecules, but this would not be the case for five-fold metal ligation. Clarification of the GlxI reaction mechanism awaits further crystallographic analysis but it appears, based on the EXAFS studies, that the six-coordinate metal in the active enzyme becomes five-coordinate during the reaction.

Clearly the amino acid sequence similarity between the *E. coli* GlxI enzyme and other GlxI enzymes known to require zinc, would lead to an incorrect assumption with regard to the nature of the activating metal ion for this enzyme. This work on *E. coli* GlxI is an example of why caution must be exercised when drawing conclusions based on the analysis of sequence data alone and reaffirms the idea that comparisons made utilizing bioinformatic approaches also need to be tempered with biochemical analyses.

CHAPTER 4

MODIFIED *E. COLI* GLYOXALASE I ENZYMES

4.1 Introduction

Three modified forms of *E. coli* GlxI were prepared during this study to aid in the structure-function analyses of this enzyme. A selenomethionine containing GlxI was utilized in the crystallography studies previously described, a C-terminal truncated form of the enzyme was prepared to aid in cocrystallographic studies, and a mutation of one of the ligands to the metal was examined for its effect on the metal activation of the enzyme. The construction of the expression systems, purification, and characterization of each of these enzymes is described.

4.1.1 Selenomethionine Incorporation

The selenomethione (SeMet) derivative of *E. coli* GlxI was prepared to aid in the solution of the x-ray structure, as described in Chapter 3. This form of the enzyme contains SeMet in place of methionine at positions 1, 7, and 26 in the protein. Although they are frequently utilized for MAD analysis, the SeMet form of each protein should be characterized to ensure its properties are homologous to those of the native enzyme. Generally no change is seen in the protein activity. Interestingly however, the activity has been increased in a few enzymes by the incorporation of SeMet. Examples include interleukin-5 and tryptophanyl-tRNA synthetase (Doublie, 1997). It is thought that this change in activity may be due to the increase in the hydrophobicity or the larger van der Waals radius of selenium versus sulfur, 2.00 versus 1.85 Å repectively, in the enzyme active site (Doublie, 1997).

In addition, SeMet is readily oxidized to the selenomethionine seleno-oxide, under ambient temperatures (Smith and Thompson, 1998). This generally will not interfere with crystallization but will cause chemical and electronic changes at the Se atom. This has been found to cause difficulties in phase determination (Smith and Thompson, 1998). Therefore the oxidation state of the SeMet residues and overall activity and characteristics of SeMet-GlxI were monitored during its preparation for structural studies.

4.1.2 C-Terminal Truncated GlxI

Due to the difficulties encountered in the cocrystallization of *E. coli* GlxI with various inhibitors, possibly due to the binding of the C-terminal 2 residues (Gly134-Asn135) of an adjacent protein dimer in the active site of the enzyme (See Section 3.3.4), we chose to pursue the isolation of a truncated form of the enzyme. Previous studies demonstrated that the removal of the four terminal residues does not affect the enzymatic activity (Barnard, 1997; Clugston et al., 1998a).

4.1.3 His5→Gln Mutant E. coli Glyoxalase I

One of the unique characteristics of *E. coli* GlxI compared to GlxI from other sources is its activation with Ni^{2+} rather than Zn^{2+} (Clugston et al., 1998a). We were interested in analyzing the factors producing this altered metal activation. As one metal ligand in *H. sapiens* GlxI differs from that found in *E. coli* GlxI, the effect of this altered ligand was of interest. However, the metal ligands in the *S. cerevisiae* and *P. putida* GlxI enzymes, predicted by sequence homology, are the same as those found in the *E. coli* enzyme, even though these enzymes are active with Zn^{2+} (Aronsson et al., 1978; Saint-Jean et al., 1998). This led to the speculation that this altered metal ligand, His5 in *E. coli* versus Gln34 in *H. sapiens* GlxI, was not the key factor determining the different metal activation. To clearly establish the effect of the ligand change on the enzyme activity we mutated the His5 in the *E. coli* enzyme to a Gln and characterized the mutated protein.

4.2 Materials and Methods

See Chapter 2.2 for a description of the standard protocols employed in the construction and characterization of the mutated and modified enzymes described in this chapter, unless otherwise indicated. This includes the cell culture preparation and growth conditions, protein purification protocol, enzymatic assay, metal content determination, and ESMS analysis.

4.2.1 Selenomethionine Incorporation

The plasmid containing the DNA encoding *E. coli* glyoxalase I, pGL10, was transformed into an *E. coli* MG1655 methionine auxotrophic cell line, *E. coli* DH93 (MG1655 *metH*174::*Tn*5 *metE*::*Tn*10; laboratory collection), and its parental cell line *E. coli* RK4349 (*his metB metE*::*Tn*10).

Various modifications employed during the development of an efficient method of SeMet incorporation are described throughout the results and discussion. The final conditions found to effectively incorporate SeMet into GlxI are as follows. Minimal media (M9; Davis et al., 1980) supplemented with 0.4% glucose, 1 mM $MgSO_4$, 0.1 mM $CaCl_2$, 0.001% uracil, and 5 μM $NiCl_2$ was inoculated (1:100 dilution) with *E. coli* MG1655/pGL10 grown in LB_{Amp}. Expression was found to be best with 0.7 L in a 4 L flask, rather than a full 1 L used in native GlxI expression. When the culture reached an optical density (OD) of ~0.5 at 600 nm. L-selenomethionine (SeMet; 0.3 mM; Sigma) and $NiCl_2$ (to a total concentration of 12.5 μM) were added and the culture allowed to grow for an additional 30 min at 37°C. GlxI synthesis was then induced for 8 hours with IPTG (0.5 mM). The cells were harvested and the protein purified in the same manner as described for the native enzyme (Section 2.2). Incorporation of SeMet was monitored by electrospray mass spectrometry (ESMS).

4.2.2 C-terminal Truncated Glyoxalase I

Construction

Dr. M. M. He (University of Oregon) mutated the plasmid containing the wild-type GlxI gene, pGL10, to encode a protein in which Lys127 was mutated to a stop codon. After the QuikChange method, described in the construction of H5Q GlxI (Section 4.2.3) was found to be unsuccessful, the two-stage PCR method utilizing overlap-extension (Figure 4.1) was employed in the construction of this plasmid, named pGL12.

To amplify the *gloA* gene, external primers ('a' and 'd' in Figure 4.2) were prepared as well as internal primers with the unique *Psh*AI restriction site and the mutation (AAA→TAA; Figure 4.3; 'b' and 'c' in Figure 4.2). The final product from the two-stage PCR was digested with *Cla*I and *Psh*AI and ligated into the template vector, pGL10, which had been digested with the same enzymes and the resultant expression vector labelled pGL12.

Expression and Purification

The *E. coli* MG1655/pGL12 cells were grown and protein expression induced in the same manner as described for the wild-type enzyme (Section 2.2). Following difficulties with protein expression, the growth conditions were varied. The effect of $NiCl_2$ addition (1mM), increasing amounts of IPTG (0.5 mM versus 1.0 mM), variation of the length of the induction time (3-6 hours), and use of ampicillin versus carbenicillin were monitored.

The software program PC/Gene (Release 6.85, 1995), using the Physico-Chemical parameters subprogram was utilized to predict the isoelectric point (pI) of the truncated form of *E. coli* glyoxalase I. As the pI for the truncated protein was lower than that for the wild-type, full-length enzyme, 4.58 versus 4.71, the pH gradient in the preparative isoelectric focusing stage of the purification was modified to ensure the protein would focus in the center of the generated pH gradient. Rather than using a 50:50 mixture of RotoLytes (MES:Gly-Gly) which establishes a pH gradient of 4.5-5.0, the ratio was shifted to the acidic side, using 60 MES: 40 Gly-Gly. The remainder of the purification protocol was performed in the same manner as previously described for the wild-type enzyme (Section 2.2).

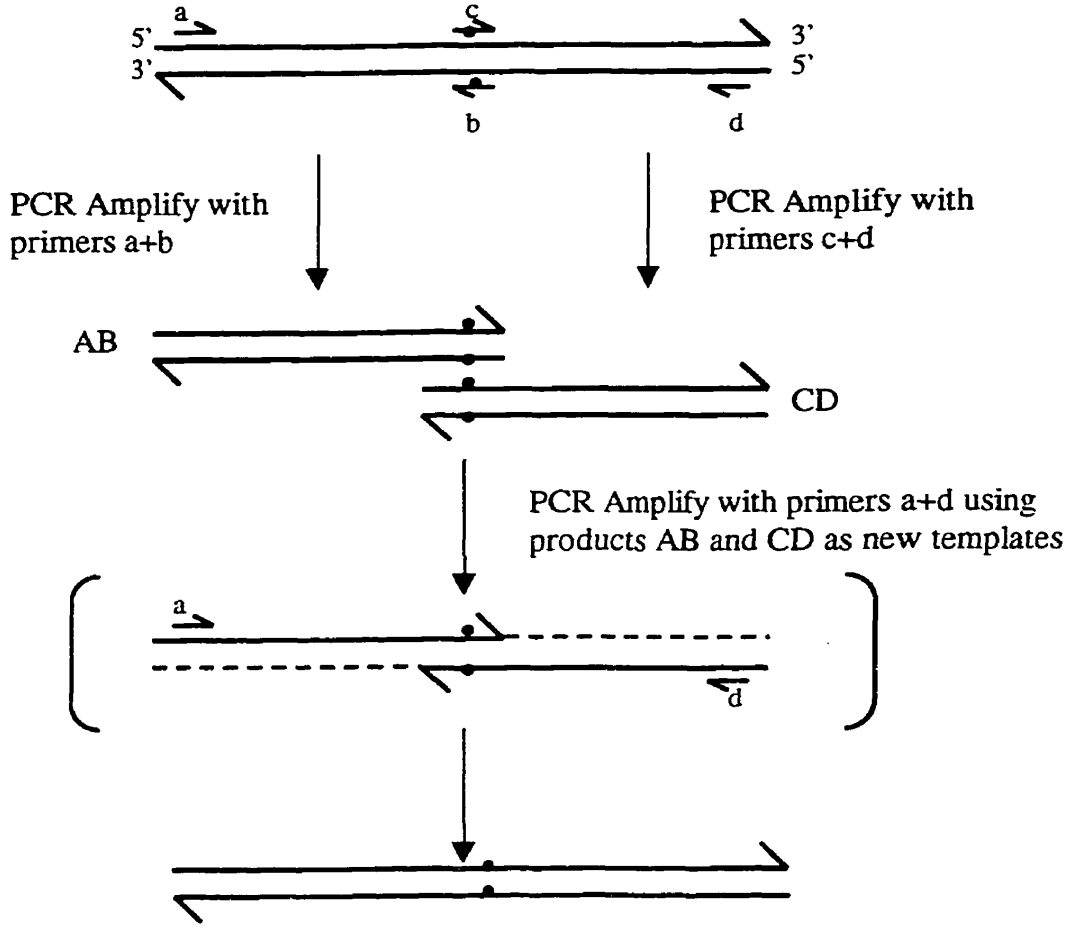

Figure 4.1: Overview of site-directed mutagenesis utilizing the method of overlap extension (Adapted from Ho et al., 1989). The DNA template and primers are shown as lines with the black dots representing the mutagenesis site. The brackets enclose a proposed intermediate believed to form during the reaction with the combined mutagenic products, AB and CD, as the new DNA templates. The dotted lines indicate the regions which will be amplified to create the full length fused product. Primers 'a' and 'd' are the external primers and 'b' and 'c' the internal mutagenic primers, sense and antisense primers, respectively.

'a' $^{5'}$CTGTTAGCCATTTTGAGG$^{3'}$

'd' $^{5'}$CGCGCATTATGACAAATATTACTTG$^{3'}$

'b' $^{5'}$CGAAGAG*TAA*GACGCCGGTCG$^{3'}$

'c' $^{5'}$CGACCGGCGTC*TTA*CTCTTCG$^{3'}$

Figure 4.2: Primers used for the two-stage PCR amplification with overlap extension of *gloA* and the surrounding region from pGL10. External primers 'a' and 'd' and internal mutagenic primers, 'b' and 'c' with the mutated codon in large italics.

N-terminal region of *gloA* insert:

'a' Start

GAATCTGTTAGCCATTTTGAGGATAAAAAG**ATG**CGTCTTCTTCATACCATGCTGCGCGTT

*Hinf*I

GGCGATTTGCAACGCTCC**ATCGAT**TTTTATACCAAAGTGCTGGGCATGAAACTGC.....

*Cla*I

C-terminal region of the *gloA* insert:

'b' and 'c' Stop

.....GTTAATCGAAGAG*AAA***GACGCCGGTC**GCGGTCTGGGCAAC**TAA**TCTCCTGCCGGGCG

*Psh*AI

'd'

TGAACTCATCGCGCCCGCATCTTTACTGCATCGACAAGTAATATTTGTCATAAT**GCGCGC**

*Bss*HII

Figure 4.3: N- and C-terminal regions of the *gloA* insert, with the sections homologous to the indicated primers underlined, mutated codon in large italics, and *Cla*I and *Psh*AI sites indicated in bold. The *gloA* insert was initially inserted between the *Hinf*I and *Bss*HII sites of pTTQ18, shown for reference (Clugston et al., 1998a). The start of the region coding GlxI is indicated in addition to the stop codon.

4.2.3 Construction of His5→Gln Mutant Glyoxalase I

Primer Synthesis and DNA Sequencing

The primers employed in the mutagenesis outlined below were obtained from MOBIX (McMaster University, Hamilton, ON). Sequencing of pGL11 was also performed by MOBIX.

To sequence the mutated *gloA* DNA, a primer complementary to the region upstream of the DNA insert region, part of the pTTQ18 plasmid, and a primer complementary to the region downstream of *gloA*, within the inserted DNA were also synthesized (Figure 4.4). These primers would be suitable for sequencing of other plasmid constructs based on pGL10, the pTTQ18 based plasmid for the expression of wild-type GlxI.

Mutagenesis

Primers homologous to the DNA encoding GlxI and the DNA upstream, within the *gloA* insert, were designed with a single base change to mutate His5 to Gln. (CAT→CAA; Figure 4.5). This one-step mutagenesis protocol is based on the QuikChange™ site-directed mutageneis protocol from Stratagene (La Jolla, CA), as outlined in Figure 4.6.

Six reaction conditions were prepared, varying the $MgSO_4$ concentrations between 0.2-2.5 mM. PCR amplification was performed with the following program. A "hot start" or "jump start" was performed in which the tubes were heated to 95°C for 1 min without the polymerase enzyme. Following the addition of the *Pwo* DNA polymerase enzyme (Boehringer Mannheim/Roche Diagnostics) the following cycle was performed 12 times: 95°C 30 s; 55°C 60 s; 68°C 10 min; ending with a 15 min incubation at 68°C to ensure all extensions were completed.

The PCR reaction product mixtures were incubated with *Dpn*I at 37°C for 1 hour to digest the methylated wild-type, template DNA. The plasmid containing the mutated *gloA* gene, pGL11, was first transformed into *E. coli* DH5α as this cell line is deficient in the restriction enzymes to degrade non-methylated DNA. Methylated pGL11 was then isolated from DH5α and transformed into *E. coli* MG1655 for effective protein expression.

A $^{5'}$CAA TTT CAC ACA GGA AAC AGC G$^{3'}$

B $^{5'}$CGA TGC AGT AAA GAT GCG GGC G$^{3'}$

Figure 4.4: Sequence of the primers utilized for sequencing of the *gloA* region of pGL11. (A) Primer homologous to pTTQ18 upstream of the insert region and (B) homologous to the region of the inserted DNA, downstream of *gloA*.

Start

$^{5'}$ G GAT AAA AAG **ATG** CGT CTT CTT *CAA* ACC ATG CTG CGC G $^{3'}$

Stop

$^{5'}$ C GCG CAG CAT GGT *TTG* AAG AAG ACG **CAT** CTT TTT ATC C $^{3'}$

Figure 4.5: Primers for the PCR mutagenesis of *E. coli* GlxI His5→Gln. Bold indicates the region homologous to the translation start codon and the mutated codon is in large italics.

Expression and Purification

E. coli MG1655/pGL11 was grown with 50 μg/ml ampicillin, not carbenicillin as for wild-type GlxI, as there was no effect on the growth or protein expression, and this antibiotic is more economical.

Centricon YM10, YM30, YM50, and YM100 were from Amicon (Millipore, Bedford, MA) and used according to the manufacture's specifications. Chelating Sepharose™ Fast Flow resin (Amersham Pharmacia Biotech, Sweden) was prepared in the Ni^{2+} form, and protein binding tested in 50 mM MOPS, 150 mM KCl, pH 7.0 (Chelex treated).

The purification protocol for the wild-type GlxI enzyme was utilized to purify the H5Q mutant GlxI with the following exception. Following the isoelectric focusing stage of the purification, the protein was subjected to separation on a Superdex 75™ HR 10/30 (Amersham Pharmacia Biotech, Uppsala, Sweden) gel filtration column, equilibrated with 50 mM MOPS pH 7.0 (Chelex treated). Samples of less than 500 μl were applied and the protein eluted with buffer at 0.5 ml/min for 60 min.

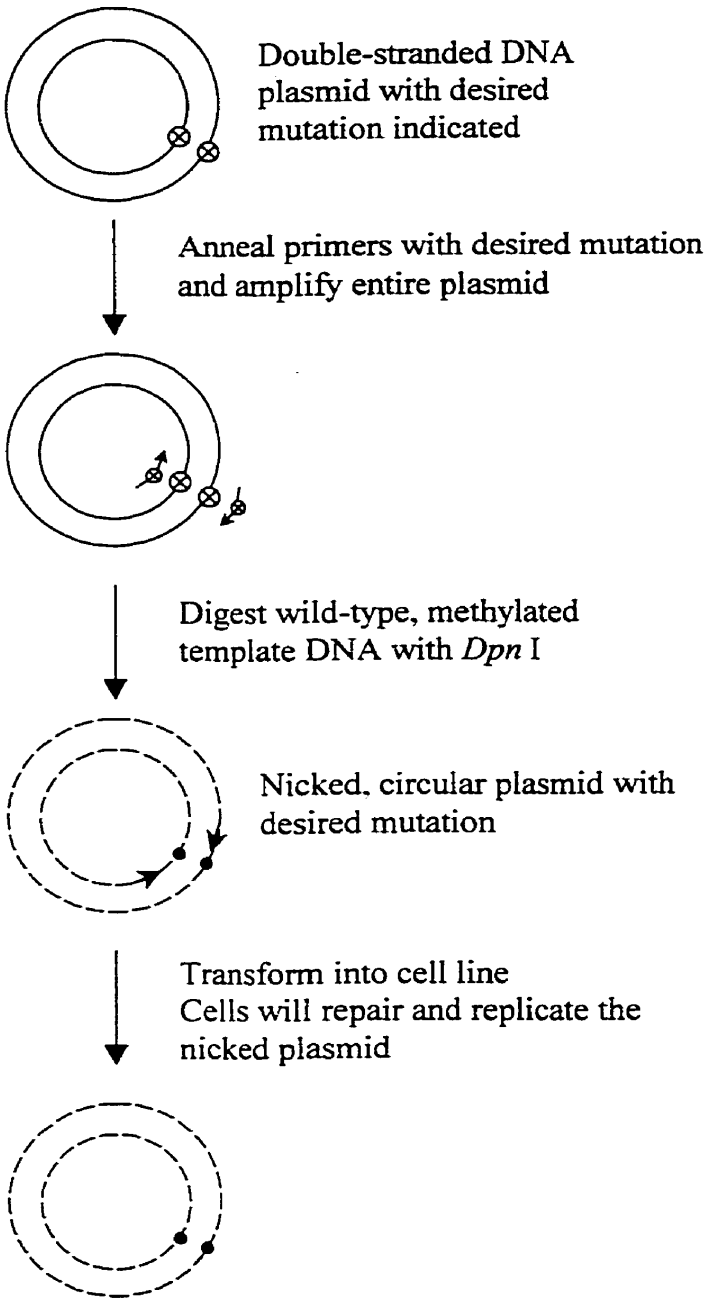

Figure 4.6: Outline of the QuikChange ™ site-directed mutagenesis protocol. ⊗ indicates site of desired mutation; • indicates mutation. (Adapted from Stratagene Cloning Systems QuikChange™ Site-Directed Mutagenesis Kit Instruction Manual)

Protein Characterization and Metal Effects

Kinetic assays were performed in 50 mM potassium phosphate buffer pH 6.6, according to the standard protocol (Section 2.2), or in 50 mM MES (2-(*N*-morpholino)ethanesulfonic acid), pH 6.6. For each metal tested, the desired metal chloride concentration was added directly to the substrate solution immediately before performing the assay. In addition, the enzyme was preincubated for a minimum of 10 minutes with the same metal concentration to ensure there was no differential concentrations or time dependence of metal binding.

Possible interference by metal ions was determined by performing a scan from 800-200 nm of 0.2 mM *S*-lactoylglutathione (reaction product) in water with and without the addition of the metal chloride, in the absence of GlxI. Hydrolysis of the product (0.2 mM in 50 mM MES pH 6.6) by the metal chlorides was monitored at 240 nm for 10 min. Similarly, breakdown of the substrate was investigated by monitoring the absorbance at 240 nm following addition of increasing amounts of metal, in the range of concentrations used in the kinetic assays for each metal.

As low levels of substrate breakdown were detected for $ZnCl_2$, these values (slopes over the time period of the enzyme catalyzed assay) were subtracted from the enzyme catalyzed reaction values.

4.3 Results and Discussion

4.3.1 Glyoxalase I Containing Selenomethionine

Attempts to Incorporate Selenomethionine Utilizing a Methionine Auxotroph

As wild-type *E. coli* cell lines are able to biosynthesize their own methionine, inhibition or mutation of this pathway is generally required for the incorporation of a methionine analogue into expressed proteins. Commonly, a methionine auxotroph cell line is employed. In this case the plasmid encoding GlxI, pGL10, was transformed into two methionine auxotrophic cell lines, *E. coli* DH93 and RK4349, for incorporation of SeMet. Numerous difficulties were encountered with these expression systems.

As DH93 is known to require uracil, the effect of added uracil (0.001%) in the minimal media was determined. It was found that although not essential for growth, uracil enhanced the growth of *E. coli* DH93/pGL10 cells and hence was added to the cultures for the remainder of the analyses.

During the initial studies no protein production was detected, even in the control culture with normal methionine added. DH93/pGL10 will grow in LB and express GlxI, indicating there was no problem with the expression system itself. The problem arose with growth on minimal media. Small scale (2 ml) cultures were utilized to test the effect of varied levels of Met (0.1-1.0 mM), IPTG (0.5 or 1.0 mM), presence of $NiCl_2$ (0-1.0 mM), and the carbon source (0.4% glucose versus 0.5% glycerol), on protein production. Cultures grown in LB then rinsed with M9 followed by growth in an M9 starter culture were used to inoculate the cultures. Although the cell cultures grew, minimal if any GlxI production was observed in each case, even when LB was re-inoculated as a control. The wild-type expression system, *E. coli* MG1655/pGL10, also produced no protein under these conditions.

To determine if there was an essential nutrient absent from these growth conditions the following supplements and combinations of each were tested in small scale cultures (5 ml) of each *E. coli* MG1655/pGL10 and DH93/pGL10: thiamine (2×10^{-4}%), biotin (2×10^{-4}%), casamino acids (1%), 2 x M9 salts, and LB_{Amp} alone. In each case the M9 was supplemented with glucose, $MgSO_4$, $CaCl_2$, uracil, and Amp, in addition to methionine for the DH93 strain. GlxI expression was detected in each case, as monitored by SDS-PAGE. The difference in

these later tests could not be accounted for by the addition of the supplements, as even the unsupplemented conditions were successful during these trials, unlike in the previous studies. The only difference was the culture utilized to inoculate the samples. This culture was taken directly from an LB starter culture and was not first grown in M9, hence there was a carry over of some rich LB media. The additional supplements during the initial growth in M9 must be sufficient for cell growth and protein production. In addition it was inadvertently discovered that if cold M9 media was inoculated, protein production was drastically decreased. For this reason, the media was always warmed to 37°C prior to being inoculated with the starter culture in LB.

Variation in the levels of added nickel revealed that levels as low as 20 μM $NiCl_2$ slowed the growth of *E. coli* DH93/pGL10 in M9, and >0.1 mM $NiCl_2$ inhibited growth almost completely. In contrast, *E. coli* MG1655/pGL10 was grown in LB with 1 mM $NiCl_2$ (Chapter 2). SeMet was also found to inhibit cell growth, hence it was not added until the induction of protein expression. Following addition of SeMet, the cells were allowed to grow for 30 minutes prior to induction of protein expression to allow time for transport of the SeMet into the cells, minimizing the likelihood of normal methionine being incorporated in the expressed protein.

E. coli RK4349 does not require supplemental uracil as does *E. coli* DH93 but it does require supplemental histidine (0.0015%). As conditions were found for the successful incorporation of SeMet utilizing MG1655/pGL10, further studies utilizing RK4349 were not pursued following the initial unsuccessful attempts.

Inhibition of Methionine Biosynthesis

An alternative to protein expression in a cell line deficient in the synthesis of methionine is to inhibit the pathways leading to methionine formation in the wild-type cell line (Doublie, 1997). This technique was also tested in the incorporation of SeMet into *E. coli* GlxI. The addition of high levels of lysine, threonine, phenylalanine, leucine, isoleucine, and valine inhibit methionine biosynthesis by the inhibition of aspartokinases enzymes involved in the biosynthesis of methionine (Doublie, 1997). This method produced the same level of protein expression and same efficiency of SeMet incorporation as expression without this inhibition; hence these supplements were not utilized in large scale growths.

Conditions for Successful Selenomethionine Incorporation and Protein Expression

Interestingly, the method for efficient incorporation of SeMet is surprisingly simple for *E. coli* GlxI. A starter culture grown in LB media is used to inoculate M9 minimal media and SeMet is added to the culture 30 minutes prior to induction of protein synthesis. ESMS confirmed that SeMet is incorporated into GlxI (15 060 Da full incorporation). However, a significant amount of SeMet-GlxI +27 Da was also apparent. This is believed to correspond to the protein monomer with a formyl group at the N-terminus of the protein.

Recent studies have suggested that *E. coli* peptide deformylase (EC 3.5.1.31), the enzyme that removes the formyl group from the N-terminal methionine in eubacteria is maximally active with both Fe^{2+} and Ni^{2+}, and binds a variety of other metals including Zn^{2+} although with reduced catalytic efficiency (Groche et al., 1998; Ragusa et al., 1998). At the time of writing the natural metal had not been clearly established. As *E. coli* GlxI also binds these metals it was speculated that when GlxI is overproduced in a culture with minimal metals there might be insufficient metals present for all the enzymes in the cell. In an attempt to counteract this potential problem, if in fact this is the case, additional $NiCl_2$ was added to the growth media and the amount of formylated protein monitored by ESMS. Based on the studies with *E. coli* DH93/pGL10, which indicated the concentration of $NiCl_2$ should be kept below 20 μM for growth in minimal media, low levels of metal were added to test cultures with a variety of M9 salt concentrations and samples taken at various induction time points. The time of addition of metal was also varied between addition at inoculation of the culture and induction of protein expression. SDS-PAGE analysis indicated that the level of GlxI expression was not significantly increased with induction times of greater than 6 hours, however the level of formylated GlxI did increase. This was not the expected relationship. A longer time period should give the deformylase enzyme additional time to react with the GlxI protein. However, there may be a maximal level of protein produced, after which the rate of protein degradation matches the rate of expression, explaining the steady level of GlxI produced from 6-12 hours. In this case there would continually be new proteins produced requiring deformylation, and peptide deformylase may not be able to keep up with the demand.

It was determined that addition of low levels of $NiCl_2$ (5 μM) at inoculation and additional $NiCl_2$ (7.5 μM) at induction, with a 6-8 hour induction time was optimal for

efficient protein expression, minimizing the amount of formylated protein. Under these conditions the level of SeMet incorporation varied between 85-100% fully incorporated (SeMet at all 3 Met positions), with 0-15% doubly incorporated protein. No unincorporated or singly incorporated SeMet protein was detected by ESMS. Figure 4.7 illustrates an example of the incorporation level with some residual formlyated protein also present.

Further studies are required to determine if in fact the additional metal affected the activity of the peptide deformylase activity, or if the results were just fortuitous.

Protein Purification

In most cases the SeMet-GlxI enzyme was effectively purified (Figure 4.8 and Table 4.1) with the protocol outlined for the wild-type GlxI enzyme (Section 2.2). As there are fewer cells and hence less protein when grown in M9 media versus LB, more than 1 L of SeMet-GlxI cell growth (generally 2-2.5 L of cell growth or ~4 g cells) was combined and utilized for protein purification. This gave sufficient levels of GlxI to obtain precipitated protein following the IEF step for crystallographic studies and well focused protein of high purity for all other analyses. When precipitated protein or well focused pure protein was not produced following the IEF step, a gel filtration column, Superdex 75, was employed for further purification of this protein. This column is described in more detail during the discussion of the H5Q mutant GlxI (Section 4.3). With this expression system between 5-50 mg of SeMet-GlxI were purified per litre of cell growth. It is not known why such a large variation in the expression occured.

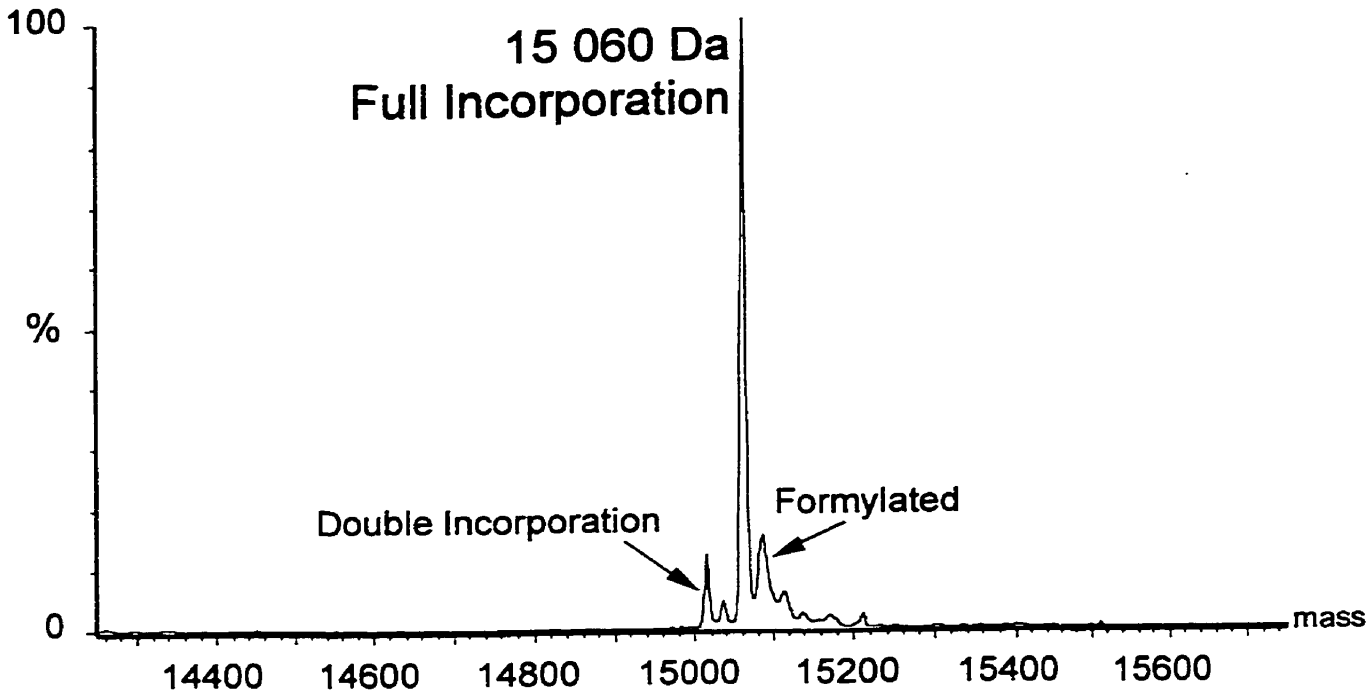

Figure 4.7: Reconstructed electrospray mass spectrum of the purified SeMet-GlxI, showing the fully incorporated (three SeMet) protein with minor levels of double incorporated protein and formylated fully incorporated protein.

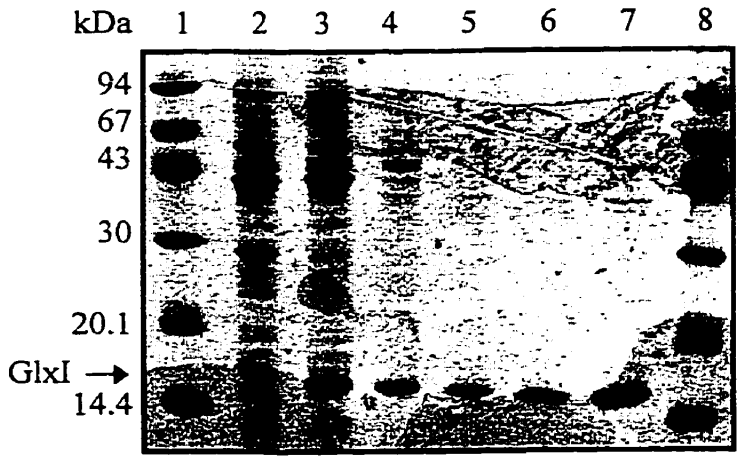

Lane:
1 LMW Standards
2 Uninduced Cells
3 Cell Break of Induced Cells
4 Q-Sepharose Fast Flow
5 Dialysis
6 IEF
7 Buffer Change and Concentration
8 LMW Standards

Figure 4.8: Stages of the purification of SeMet-GlxI. 20% Homogeneous SDS-PAGE with Coomassie staining.

Table 4.1: Summary of the stages of the purification of *E. coli* SeMet-GlxI from *E. coli* MG1655/pGL10 grown in minimal media with 0.3 mM SeMet.

Stage of Purification	Total Protein (mg)	Specific Activity (μmol/min/mg)		% Yield[†]	Fold Purification[‡]	Fold Increase in Activity with $NiCl_2$
Cell Break	149	Apo	36	100	1.00	7
		+$NiCl_2$	244			
Q-Sepharose Fast Flow	92	Apo	51	95	1.50	7
		+$NiCl_2$	365			
Post-Dialysis	85	Apo	48	87	1.53	8
		+$NiCl_2$	373			
IEF/Buffer Change	51	Apo	4.6	68	2.00	106
		+$NiCl_2$	487			

* Representative results from a purification of 2.1 g of cells from 2 x 0.7 L growth.
† Yield calculated by comparison of the total activity of the Ni^{2+}-activated enzyme.
‡ Purification factor calculated by comparison of the specific activity of the Ni^{2+}-activated enzyme at each stage to the activity at the cell break.

SeMet-GlxI Characterization

To be useful as a heavy atom derivative to aid in the solution of the x-ray crystal structure of a protein it is important that the protein containing SeMet be highly homologous structurally to the native enzyme. The kinetics and metal activation of SeMet-GlxI were measured to determine the effect of the SeMet incorporation on the properties of the enzyme. As outlined below, the characteristics of SeMet-GlxI are very similar to those for the native enzyme, making this a very useful form of the enzyme for crystallographic studies (Section 3.3.4).

Activation of the enzyme with 10 mole equivalents of metal to dimeric SeMet enzyme indicated that there is no difference in the relative activation of the enzyme with various metal chlorides compared to wild-type GlxI (Figure 4.9). In addition, activity titrations were performed to determine the ratio of metal binding. The activity reached a maximum with approximately 1 mole metal per mole of dimeric enzyme for both Ni^{2+} and Co^{2+} (Figure 4.10). This ratio of bound metal was confirmed by ICP analysis on the Ni^{2+}-substituted SeMet-GlxI enzyme (Appendix A). These results are consistent with those found for the native enzyme.

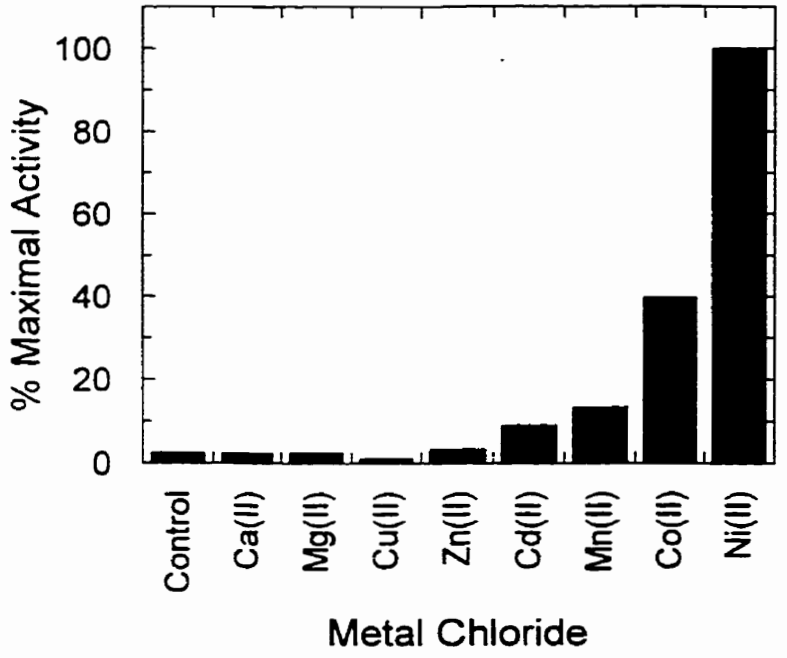

Figure 4.9: Activation of SeMet-GlxI with 10 mole equivalents of metal to dimeric enzyme. Activities are shown relative to the maximally activated Ni^{2+} form. Each point was measured in triplicate and the entire set of measurements performed in duplicate with 0.5 mM substrate and ~0.7 μg enzyme per assay.

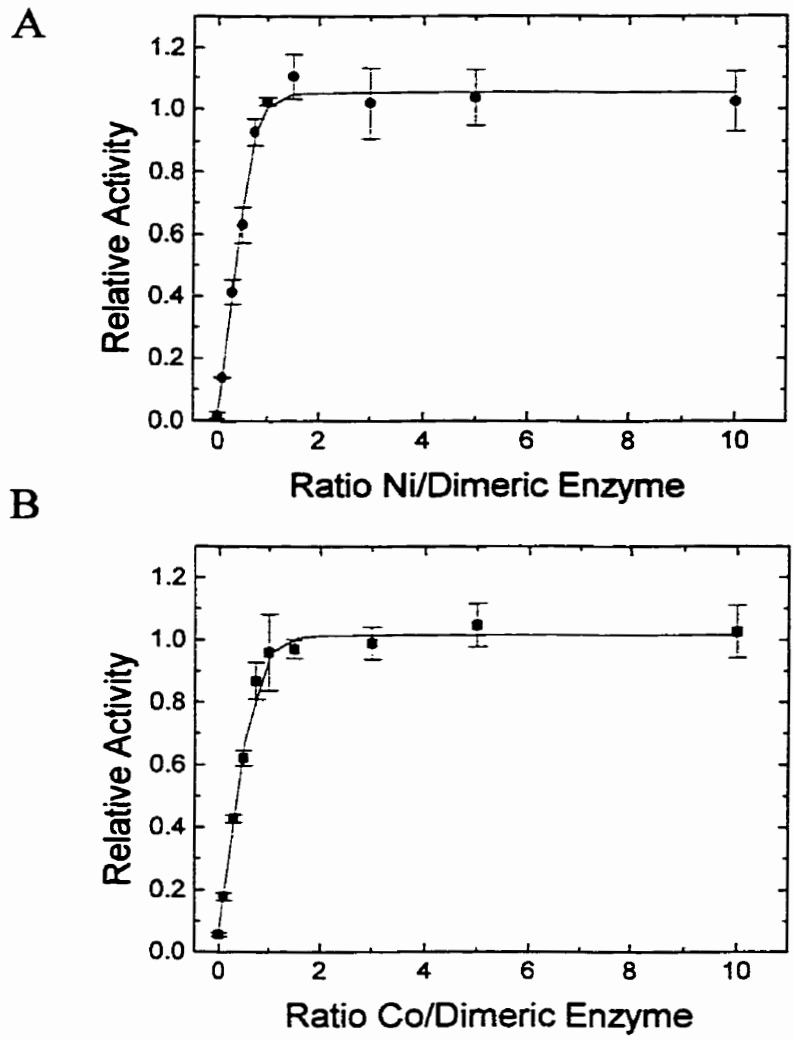

Figure 4.10: SeMet-GlxI activity titration curves. Activities are shown relative to the maximal activity measured for (A) $NiCl_2$ and (B) $CoCl_2$ addition. Each point was measured in duplicate and the entire curve determined twice with 0.5 mM substrate and ~0.7 μg enzyme per assay. The lines are arbitrary fits to show the trend in the data.

Table 4.2: Kinetic parameters[†] determined for SeMet-GlxI compared to the native *E. coli* enzyme.

		SeMet-GlxI	Native GlxI*
Ni^{2+}	V_{max} (μmol/min/mg)	487 ± 73	676 ± 17
	K_m (μM)	23 ± 1	27 ± 0.4
Co^{2+}	V_{max} (μmol/min/mg)	216 ± 19	213 ± 33
	K_m (μM)	13 ± 1	12 ± 2

[†]10 substrate concentrations from 0.005-2.0 mM were measured in triplicate with ~0.4 μg of enzyme per assay and each set of measurements performed twice on independent samples.
* From section 2.3.1 and Clugston et al., 1998a

The kinetic parameters were also determined for both Ni^{2+}- and Co^{2+}-activated SeMet-GlxI. In both cases the K_m measured was comparable to that determined for the native enzyme (Table 4.2). The V_{max} for SeMet-Co^{2+}-GlxI was not altered compared to the native enzyme, however the Ni^{2+}-activated SeMet enzyme was only about 70% as active as native GlxI (Table 4.2). This suggests that there may be a slight alteration of one of the ligands to the metal.

Examination of the crystal structure of *E. coli* GlxI reveals that Met7 is in the vicinity of the active site metal ligands (Figure 4.11). When Met7 is replaced with SeMet the added bulk of the selenium atom versus the sulfur atom may move one of the ligands slightly, resulting in a small change in the metal activity. The SeMet-GlxI crystals did not diffract to high enough resolution for detailed analysis of the protein side chains acting as metal ligands. Hence this hypothesis could not be tested.

Interestingly, during some of the protein purifications the activity of the SeMet-GlxI significantly decreased following the dialysis step. Addition of $NiCl_2$ produced protein with activity comparable to that prior to the dialysis, indicating that the bound metal, present from the cell growth, was lost. This was only found in some preparations. It is believed that the SeMet-GlxI has a slightly reduced affinity for the metal. As the dialysis is performed in 10% glycerol/H_2O, with no buffer, the pH does fluctuate. Alterations in the pH may affect the binding affinity of the protein for the metal, causing it to be lost for SeMet-GlxI in some instances. Studies are underway to examine the binding affinity by ITC, as described for the native enzyme.

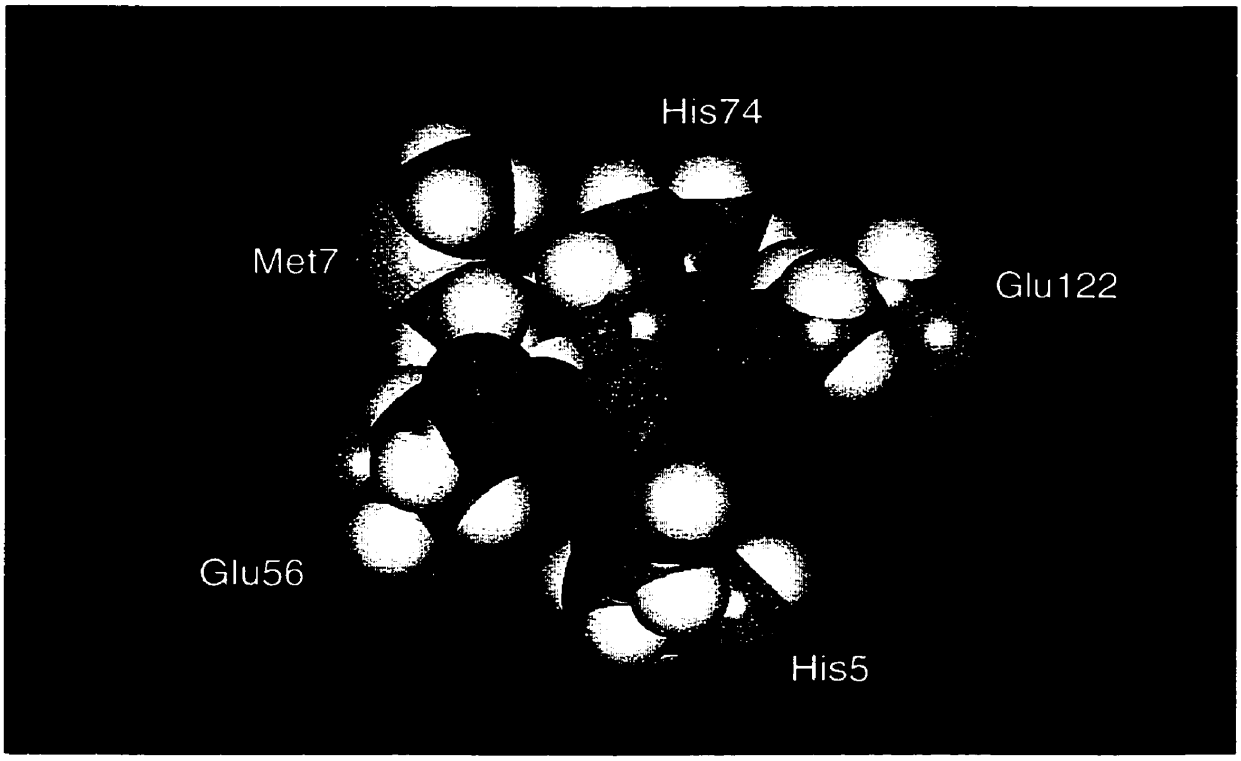

Figure 4.11: *E. coli* Ni^{2+}-GlxI active site showing the Ni^{2+} (green), two oxygen atoms of the aqua ligands (cyan, shown in half its diameter for clarity), the four metal binding ligands (His5, Glu56, His74, Glu122), and the proximal Met7. Graphics generated using WebLab ViewerPro, ver 3.7 (Molecular Simulations Inc.).

4.3.2 C-Terminal Truncated GlxI

During preliminary studies on the wild-type *E. coli* GlxI enzyme a C-terminal truncated protein was isolated (Barnard, 1997). The molecular weight of this protein (14 578 Da) corresponded to the removal of the C-terminal 4 residues (Gly132-Asn135), yet the protein was still active. Increase in the amount and frequency of the addition of protease inhibitors (PMSF) during the purification eliminated this problem with proteolytic degradation. As this suggested that these terminal residues were not critical for enzymatic activity we chose to remove this region to aid in cocrystallization attempts.

Construction of the Truncated Form of GlxI

In this system the 135 amino acid protein was prematurely truncated, eliminating the terminal 9 residues. This is more than the 4 residues removed by proteolytic degration without effect, but this mutation required a one base pair alteration and hence was a logical choice. Also, these terminal residues appear flexible in the crystal structure of the protein, without direct interactions with the protein or metal (Section 3.4).

Expression and Purification

Following the successful mutation of the GlxI gene, *gloA*, purification of the protein was attempted. Although small scale growth (<20 ml) and induction of protein expression initially indicated good expression of the mutant protein, numerous difficulties were encountered during large scale expression and purification attempts. The expression of the C-terminal truncated protein was quite variable. Some large scale growths (1 L) produced no apparent GlxI protein, based on SDS-PAGE, and others yielded moderate production. Numerous variables were tested. including growth with carbenicillin versus ampicillin, added $NiCl_2$, increased IPTG, and variable induction time. In addition, the plasmid was isolated and cells retransformed, starter cultures and small scale cultures were inoculated with single colonies from an LB_{Amp} plate as well as from freezer stocks in an attempt to produce good protein production, yet expression was not consistent (See Figure 4.12 for example). This is reminiscent of problems encountered when initial attempts were being made to create the expression system for the wild-type GlxI protein (Barnard, 1997).

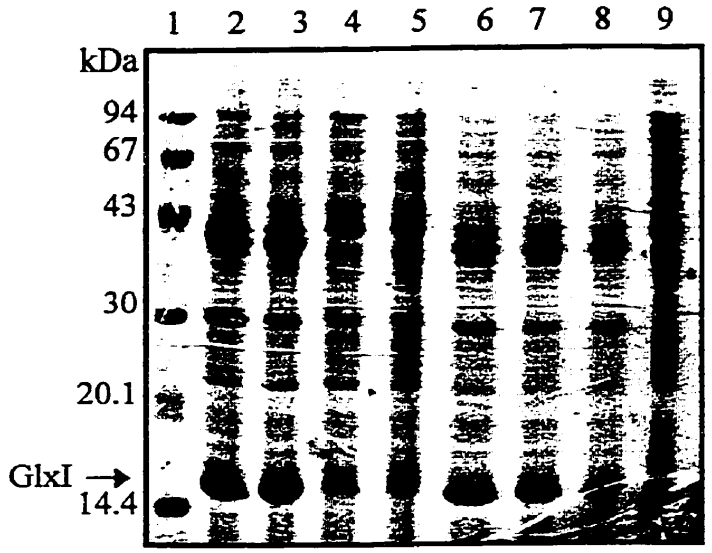

Lane:
1 LMW Standards
2 Colony A
3 Colony B
4 Colony C
5 Colony D
6 Colony E: 1 mM IPTG
7 0.5 mM IPTG + 1 mM $NiCl_2$
8 0.5 mM IPTG
9 Uninduced Cells

Figure 4.12: Examples of the variation in the level of protein production from select colonies of MG1655/pGL12, and the effect of increased IPTG and added $NiCl_2$ to the culture. 20% homogeneous SDS-PAGE PhastGel with Coomassie staining.

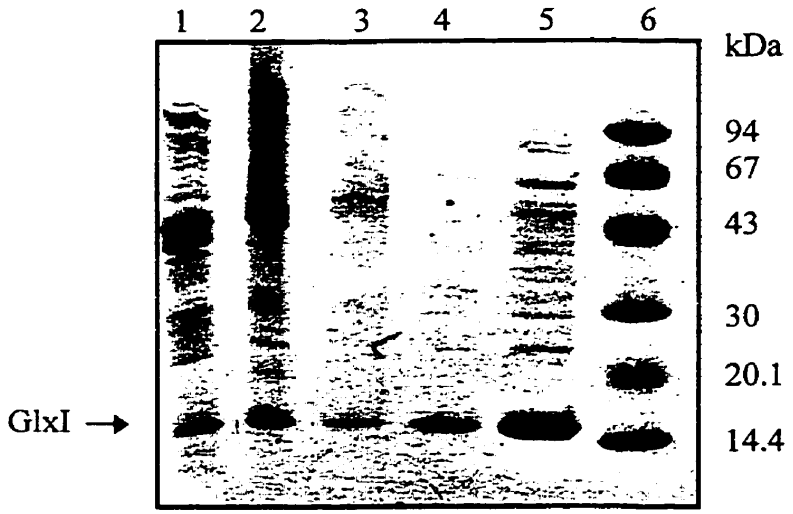

Lane:
1 Cell Break
2 Q-Sepharose Fast Flow
3 Dialysis
4 Isoelectric Focusing
5 Concentration and Buffer Change
6 LMW Standards

Figure 4.13: Stages of the purification of C-terminal truncated *E. coli* GlxI. 8-25% SDS-PAGE PhastGel with Coomassie staining.

Addition of $NiCl_2$ to the culture did not appear to affect the level of protein production, nor did an increase in the level of IPTG (0.5-1.0 mM). Figure 4.12 also illustrates the variation seen in truncated GlxI expression from different colonies randomly selected. Colonies C and D express much more poorly than other colonies, yet when one of the colonies that appears to express well under these conditions was also used to inoculate a starter culture for a large scale growth, poor expression resulted.

Several protein purification attempts were undertaken with the cultures producing a moderate level of truncated GlxI. However, as seen with the H5Q mutant GlxI, impure protein was obtained following the standard purification protocol. (See following section, 4.3.3, for possible reasons for this). Figure 4.13 illustrates the stages of purification of the C-terminal truncated GlxI. Clearly, even at the cell break stage there is significantly less GlxI produced than seen with the wild-type expression system. As evident from this gel, the protein appears pure following the IEF step, but after concentration during the buffer change, contaminating proteins were evident.

As the isolated protein was not homogeneous detailed kinetic analyses were not performed. However at each stage of the purification the enzymatic activity was tested and found to increase upon addition of $NiCl_2$. The specific activity for the partially purified enzyme, following the IEF step was 506 μmol/min/mg with the addition of excess $NiCl_2$, 2.4 μmol/min/mg with excess $ZnCl_2$, and 5.3 μmol/min/mg for the apoenzyme form. These results are consistent with those expected for a partially purified enzyme, suggesting that the removal of the terminal 9 residues does not affect enzymatic activity. The ESMS illustrated in Figure 4.14 indicates that the expressed protein exhibited the correct mass for the truncated GlxI, within standard error (14 051 Da predicted based on sequence).

While attempts were being made to troubleshoot the problems associated with inconsistent protein production, as well as protein impurities, crystals were obtained of the wild-type Ni^{2+}-GlxI in complex with several inhibitors (See section 3.3.4). With this crystallization success, the C-terminal truncated protein was no longer essential and hence further studies were not pursued.

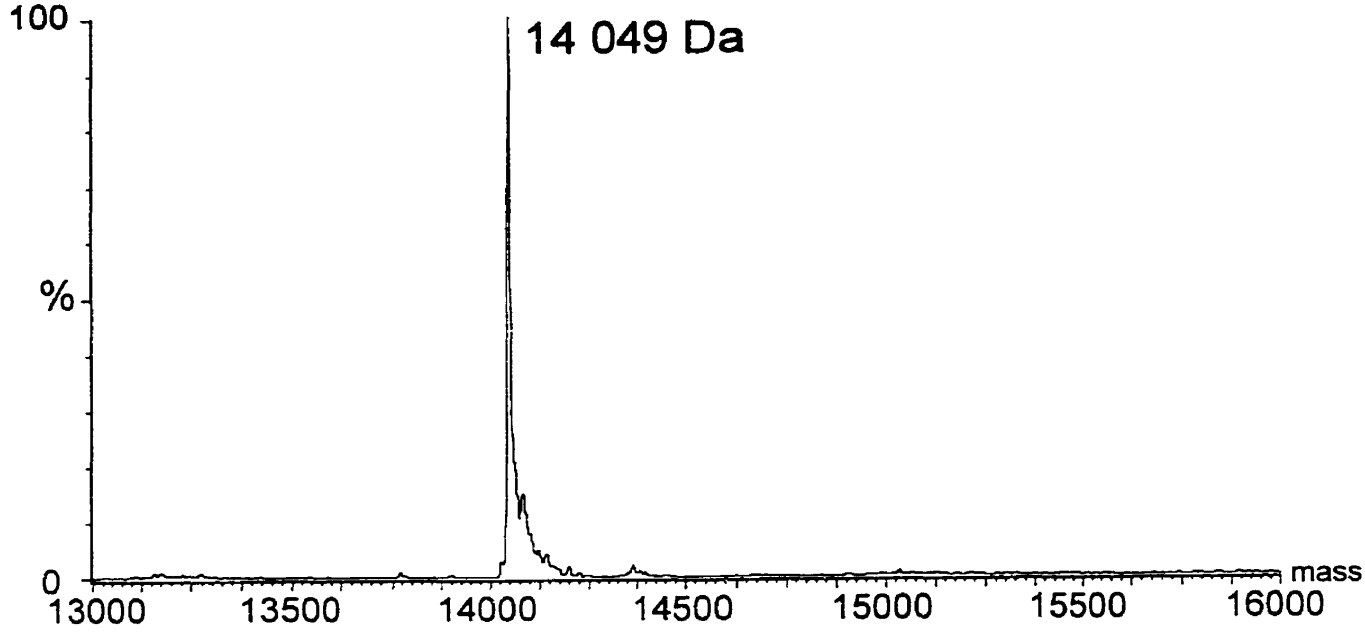

Figure 4.14: Reconstructed ESMS of the partially purified C-terminal truncated form of *E. coli* GlxI. Salt adducts are also evident.

4.3.3 H5Q Glyoxalase I

Mutagenesis

The PCR reaction containing 0.7 mM $MgSO_4$ appeared to produce the most efficient transformation.

Expression and Purification

There was no apparent effect on level of protein production with or without 1 mM $NiCl_2$ in the growth media. Although the expression of the protein appeared quite efficient based on the SDS-PAGE results (Figure 4.15), it was significantly less than that seen with the wild-type expression system. The same cell line is utilized (*E. coli* MG1655) as for the wild-type GlxI expression, and the entire plasmid was replicated with the mutation, preventing any change in the upstream or downstream regions of the protein, which may be important for translation. Hence, such a variation in the expression was not anticipated.

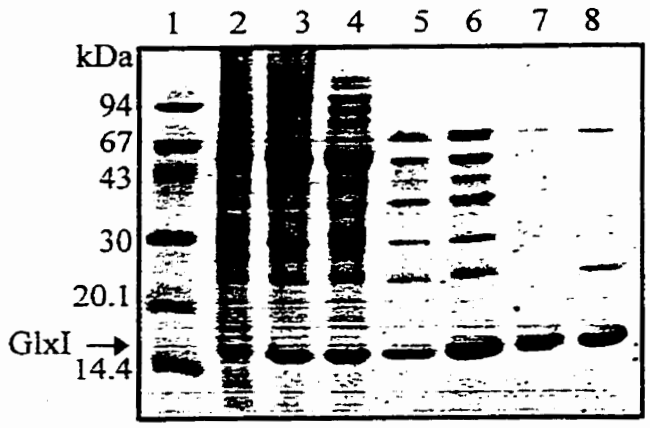

Lane:
1 LMW Standards
2 Cell Break
3 Q-Sepharose Fast Flow
4 Dialysis
5 Isoelectric Focusing
6 Concentration and Buffer Change
7 Precipitated Protein
8 Superdex 75

Figure 4.15: Purification of H5Q GlxI. 20% homogeneous SDS-PAGE with Coomassie staining.

The purification protocol designed for the wild-type GlxI enzyme produced impure protein after the preparative isoelectric focusing for the H5Q GlxI enzyme (Figure 4.15). There are a couple of explanations for this problem. The purification system utilizing preparative isoelectric focusing is ideal for the wild-type GlxI protein, as large amounts of pure apoenzyme are produced. However, this protocol is somewhat dependent upon the concentration of the desired protein. At high concentrations, GlxI will precipitate in the IEF cell when it is focused at its pI. This precipitated protein can be removed and resuspended in pH 7.0 buffer, producing active protein with no detectable impurities. The remaining soluble protein from the IEF is also >95% pure. In a system with reduced protein expression the ratio of GlxI to contaminants is much lower. With reduced GlxI, the high concentrations were not achieved in the IEF cell and GlxI precipitation did not always occur. In addition, there were often increased amounts of contaminating proteins that focused at either electrode in the IEF unit. This resulted in a large amount of precipitation and what appeared to be clumped, denatured protein, particularly at the basic electrode, which clogged the first two membranes.

It is suspected that this reduced the effective focusing during these separations. As such, protein of reduced purity resulted.

In an attempt to further purify the H5Q GlxI enzyme, several techniques were employed. First, since the protein is a dimer of 29 820 Da (29 838Da for wild-type GlxI), GlxI should be retained in a 10 kDa cutoff membrane but might pass through a 30, 50, and 100 kDa membrane. As some of the contaminating proteins were much larger than GlxI it was anticipated that these proteins would be retained by the membrane, efficiently purifying GlxI from the remaining contaminants. However, the 30 and 50 kDa Centricon spin columns both retained >90% of the GlxI protein as well as contaminating proteins. Although the 100 kDa cutoff unit did not retain GlxI, the contaminating proteins also passed through the membrane. Hence no purification was achieved by this simple method.

As the protein is known to bind metals, specifically Ni^{2+}, and metal affinity resins are currently in common use, it was of interest to determine whether GlxI, either the H5Q mutant or the wild-type enzyme, would bind to such a resin. This would provide a very rapid and simple technique to purify the enzyme without any modifications to the expression system, such as a His-tag generally required for the purification. A small scale (200 µl) trial was performed with Chelating Sepharose Fast Flow resin (gift from Dr. J. G. Guillemette), generated in the Ni^{2+} form. However, the majority of the glyoxalase I activity was detected in the initial buffer following incubation with the resin, indicating the protein did not bind to the resin. This is not completely unexpected. Although GlxI binds Ni^{2+}, and particularly tightly to the wild-type enzyme, the binding site is in the active site of the enzyme and may not be accessible to the metal which is bound to Sepharose resin.

Following these unsuccessful attempts to purify the H5Q GlxI enzyme, a gel filtration column was utilized, Superdex 75. Although only small amounts of protein can be applied for efficient separation (<500 µl) and hence numerous applications are required, the protein was effectively purified with this method. Examination of the elution profile (Figure 4.19) suggested the protein was not effectively separated by this method. However, if 0.5 ml fractions are collected and analyzed by SDS-PAGE (Figure 4.18) separation within the peak is evident. The fractions containing H5Q GlxI but with minimal contaminating proteins were selected for further analysis. Activity assays and the purity based on the gel separation were utilized to determine which fractions to collect.

Table 4.3 summarizes the purification of the H5Q GlxI enzyme. Figure 4.15 illustrates the level of protein expression and purification, with the stages of the purification indicated. Figures 4.16-4.19 present the column elution profiles and SDS-PAGE gel analyses of various steps in the purification protocol. As illustrated in Figure 4.17 the protein is focusing during the IEF run, but pure precipitated protein is not always produced. Other contaminating proteins are evidently focusing in the same region in this case. The precipitated protein from the IEF step was used when available. With excess protein on the gel, small levels of contaminating proteins can still be detected following the gel filtration separation. The protein is reasonably pure and was utilized for kinetic analyses.

Table 4.3: Summary of the stages of the purification of *E. coli* H5Q GlxI from *E. coli* MG1655/pGL11.

Stage of Purification	Total Protein (mg)	Specific Activity (μmol/min/mg)		% Yield[†]	Fold Purification[‡]	Fold Increase in Activity with $NiCl_2$
Cell Break	470	Apo	0.13	100	1.00	115
		+$NiCl_2$	15			
Q-Sepharose Fast Flow	240	Apo	0.22	85	1.57	114
		+$NiCl_2$	25			
IEF/Buffer Change	50	Apo	0.48	68	6.40	200
		+$NiCl_2$	96			
Precipitated Protein	6	Apo	0.73	12	9.07	186
from IEF		+$NiCl_2$	136			
Superdex 75[⊥]	24 (+6 from above for 30 mg overall yield)	Apo	0.70	42 (+12 from above for 54% overall yield	8.40	180
		+$NiCl_2$	126			

* Representative results from a purification of 4.1 g of cells.

† Yield calculated by comparison of the total activity of the Ni^{2+}-activated enzyme.

‡ Purification factor calculated by comparison of the specific activity of the Ni^{2+}-activated enzyme at each stage to the activity at the cell break.

⊥ Presuming the entire sample from the IEF step was passed through the gel filtration column, when in actual fact only that required for the enzymatic analysis was further purified, or half the volume.

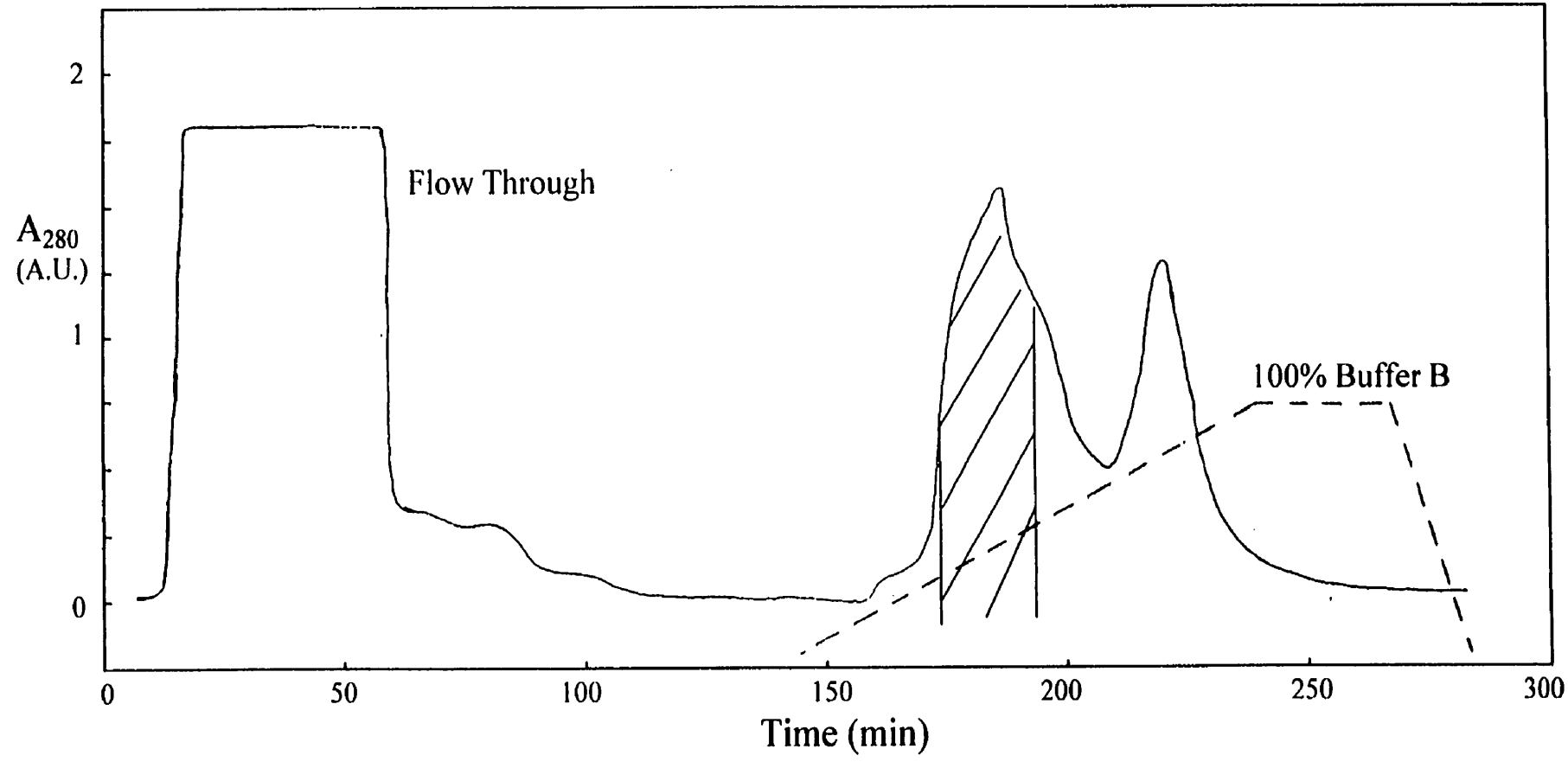

Figure 4.16: Elution profile of *E. coli* H5Q GlxI from the FPLC Q-Sepharose Fast Flow column. Dashed line represents the % buffer B (20 mM Tris, 30 % glycerol, 1M KCl, pH 7.0) and the solid line the absorbance at 280 nm. The elution region containing GlxI activity is shaded.

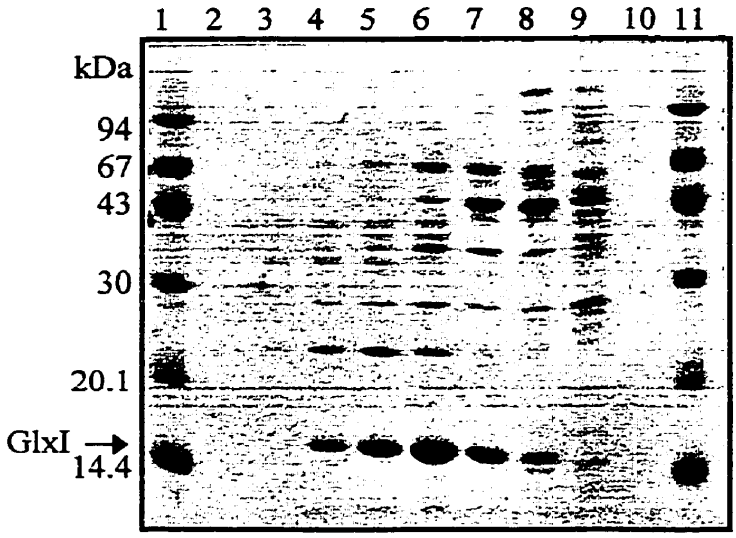

Lane:
1 LMW Standards
2 Fr. 3
3 Fr. 5
4 Fr. 6
5 Fr. 7
6 Fr. 9
7 Fr. 12
8 Fr. 13
9 Fr. 14
10 Fr. 19
11 LMW Standards

Figure 4.17: SDS-PAGE (20% homogeneous gel with Coomassie staining) illustrating the focusing of the *E. coli* H5Q GlxI protein in the Rotofor IEF unit from various fractions.

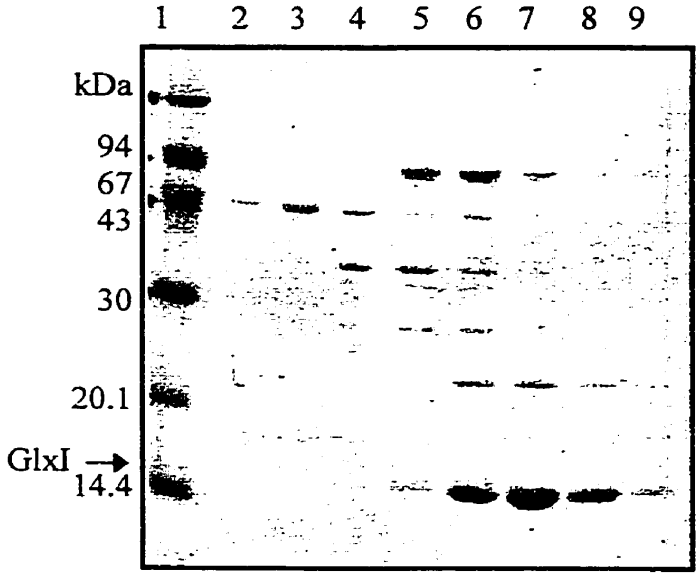

Lane:
1 LMW Standards
2 Min 22
3 Min 23
4 Min 24
5 Min 25
6 Min 26
7 Min 27
8 Min 28
9 Min 29

Figure 4.18: Purity of the H5Q GlxI in various fractions from the Superdex 75 gel filtration column, separated by SDS-PAGE (20% homogeneous gel with Coomassie staining). Fractions (0.5 ml) were collected at 1 minute intervals throughout the elution.

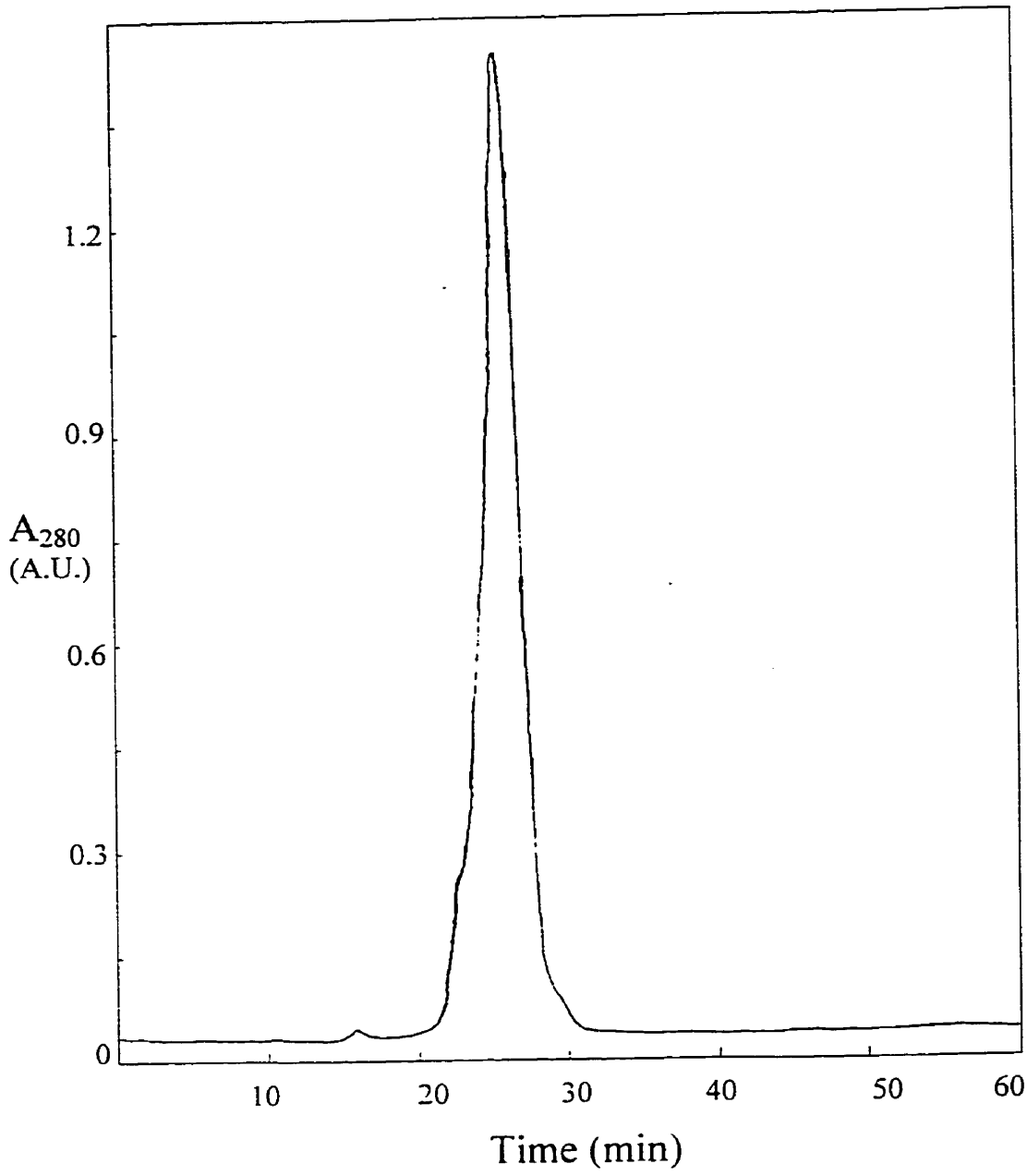

Figure 4.19: Superdex 75 elution profile. The solid line indicates the absorbance at 280 nm.

Protein Characterization and Metal Effects

Inductively couple plasma (ICP) metal analysis was performed on the purified H5Q GlxI and confirmed it was an apoenzyme, with only trace levels of metals detected (See Appendix A for table of results). ESMS indicated that a protein of the expected molecular weight (14 910 Da monomer predicted based on sequence) was produced (Figure 4.20). In addition, the mutant protein was eluted from the gel filtration column at the same time as the wild-type enzyme (Clugston, 1997) indicating that the H5Q GlxI is also a dimeric enzyme.

Preliminary experiments on a sample of crude cell extract indicated that the H5Q mutant GlxI was active with the addition of both $NiCl_2$ and $ZnCl_2$. This was an incredibly surprising result, as this was simply a one amino acid alteration, and a semi-conservative alteration which sequence analysis suggested would not affect the metal activation. This led to a detailed analysis of the metal activation in this mutated *E. coli* GlxI protein.

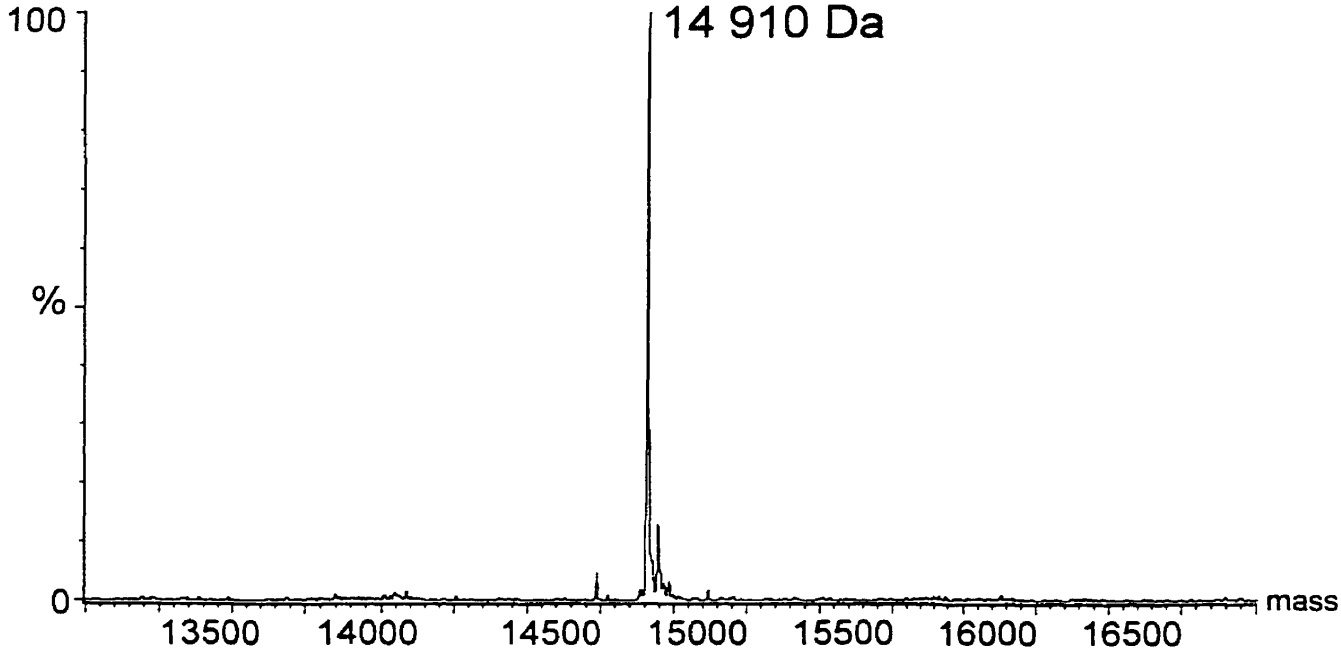

Figure 4.20: Reconstructed electrospray mass spectrum of the purified mutant *E. coli* H5Q GlxI.

Addition of increasing amounts of metal added to the enzyme stock did not result in a significant increase in the enzymatic activity. Upon addition of the enzyme to the assay solution, preincubated with high levels of metal (1-2 mM), the initial enzymatic activity (first 10 s) appeared much higher than the overall activity in the reaction. This suggests that the enzyme may bind the metal initially but when diluted into the assay buffer the metal dissociates relatively rapidly resulting in the reduced activity observed. However, if these levels of metal were added to the substrate solution there was a substantial increase in activity. The necessity for high levels of metal to observe increased activity suggests that although the protein is still activated by the metal, the affinity is very low. For this reason, the assays were performed with an equal concentration of the desired metal in the assay solution and preincubated with the enzyme. Therefore there will be no concentration difference, and hence no loss or gain in bound metal when the enzyme is added to the reaction mixture.

Mutation of the ligands to the metal in the *H. sapiens* GlxI enzyme also resulted in a decreased metal affinity in some instances. Mutation of Glu100→Gln (equivalent to Glu56 in *E. coli* GlxI) resulted in a protein with almost no metal bound. Further mutation of Gln34→Glu (His5 in the *E. coli* enzyme), Glu173→Gln (Glu122 in *E. coli*), and the double mutant Gln34→Glu/Glu100→Gln each was observed to contain only a small amount of bound catalytic zinc (Figure 4.21; Ridderström et al., 1998). However, the metal content was determined following standard purification of the enzyme. At no time were additional metal salts added to the protein after purification or during the enzymatic assays. As a result, these proteins may have had some residual metal binding properties and activity but it was not detected under the conditions examined.

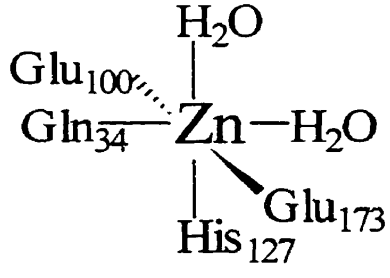

Figure 4.21: Active site structure in *H. sapiens* GlxI.

To determine the maximal enzymatic activity in *E. coli* H5Q GlxI and the required amount of metal to reach this activity, a metal activity titration was performed in which the enzymatic activity was monitored with increasing concentrations of metal. The maximal specific activity, 80 μmol/min/mg, for the Ni^{2+}-activated enzyme was observed at 5 mM metal. As apparent from Figure 4.22, the activity is steadily increased with increasing metal concentration. However, levels of metal at 5 mM and higher were found to breakdown the hemiacetal substrate making the analysis of the activity above 2 mM $NiCl_2$ (50 μmol/min/mg) unreliable. Furthermore, although initial studies indicated that the H5Q mutant GlxI was active with Ni^{2+}, Co^{2+}, Cd^{2+}, Zn^{2+}, and Mn^{2+} it was noted that higher levels of $ZnCl_2$ and $CdCl_2$ (>0.5 mM) added to the substrate assay solution resulted in precipitation of the metal.

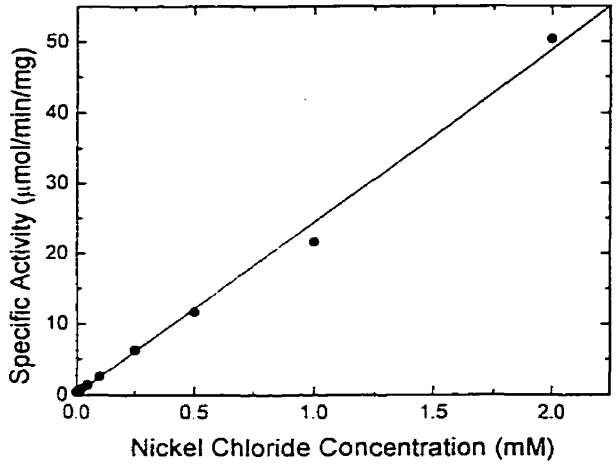

Figure 4.22: Activation of H5Q GlxI with increasing amounts of $NiCl_2$ in both the enzyme and substrate solution, measured in phosphate buffer pH 6.6 with 0.5 mM substrate. Each point was measured in triplicate with ~5 μg of enzyme. The line is a linear fit to illustrate the trend in the enzyme activity.

In an attempt to avoid the precipitation of these metals at concentrations below 0.5 mM the standard enzyme assay buffer was modified. The glyoxalase I enzyme is generally performed in 50 mM phosphate buffer pH 6.6 (Bergmeyer, 1983). For consistency the pH of the buffer was maintained but an alternative buffer employed. MES was chosen and utilized at a concentration of 50 mM, pH 6.6 (adjusted with KOH). The activity of the wild-type enzyme activated with Ni^{2+} at a substrate concentration of 0.5 mM was determined in both the standard phosphate buffer and in MES. There was no apparent difference in the activity and hence it was determined that the substrate equilibrium was not affected. In addition as outlined in Chapter 2, the K_m and V_{max} for wild-type Ni^{2+}-GlxI was later determined in MES and found to be consistent with that found when measured in the standard phosphate buffer.

The metal activity titration was repeated for the activation of H5Q GlxI with $NiCl_2$. Interestingly, the enzymatic activity was significantly increased (Figure 4.23). At a metal concentration of 2 mM the specific activity was 173 μmol/min/mg. This is nearly a 4-fold increase over the activity measured in phosphate buffer. This result can be rationalized by looking at the metal stability constants for the two buffers. Although phosphate does have a relatively low affinity for metals (Price, 1996), it may actually be higher than the affinity of the mutant protein for the metal. As a result the buffer may be chelating the metal making it inaccessible to the protein. MES however, has negligible metal affinity (Price, 1996) and hence would not interfere with the protein.

To ensure that there was no effect on the measured wild-type enzyme activity as all standard assays were performed in phosphate buffer, the activity of wild-type Ni^{2+}-GlxI was measure in MES with excess metals. No difference was seen on the enzyme activity in MES compared to previous results in potassium phosphate buffer. As the wild-type enzyme is known to have an extremely high metal affinity, the low affinity of the phosphate is most likely insignificant in these assays. It was noted however, that very high levels of $NiCl_2$ (>2 mM) did not breakdown the substrate as seen in phosphate buffer, however they did inhibit the wild-type GlxI activity. At 2 mM $NiCl_2$ the activity of the wild-type GlxI enzyme was 90% that seen with low levels of metal, and further reduced to 75% at 10 mM. The H5Q GlxI activity was only moderately increased at 5 mM and decreased at 10 mM $NiCl_2$. For this reason it was concluded that the enzymatic activity should not be measured above 2 mM.

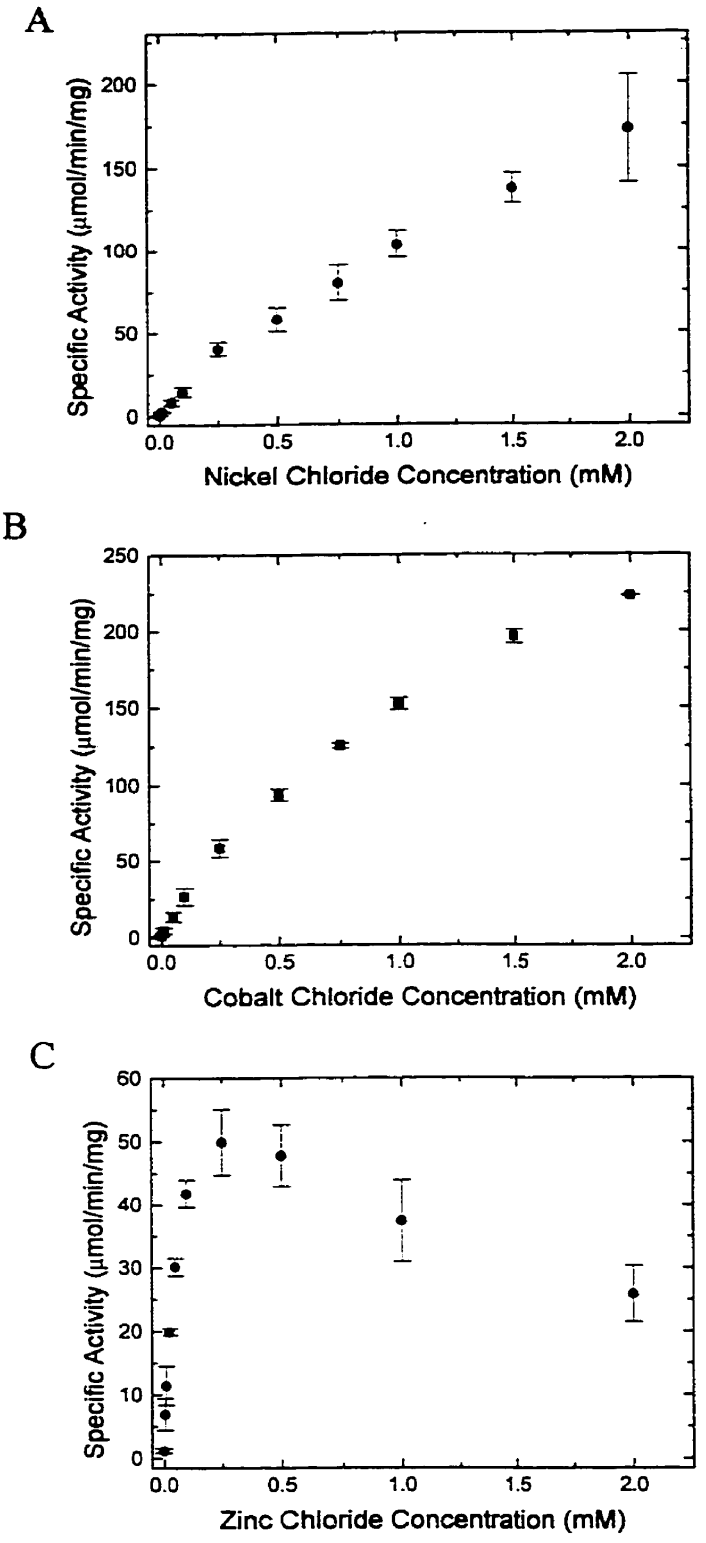

Figure 4.23: Activation of H5Q GlxI with increasing amounts of (A) $NiCl_2$, (B) $CoCl_2$, and (C) $ZnCl_2$, in both the enzyme and substrate solution, measured in **MES** buffer pH 6.6 with 0.5 mM substrate. Each point was measured in triplicate with ~2.5 µg of enzyme and each curve was measured in duplicate and the results averaged.

A similar activity titration was performed for $CoCl_2$ and $ZnCl_2$ (Figure 4.23B and C). In the case of $ZnCl_2$, the maximal enzymatic activity (50 μmol/min/mg) was observed at 0.25 mM metal, and a decrease in activity was noted above 0.5 mM. In addition, low levels of substrate breakdown were observed with $ZnCl_2$ at concentrations of 0.5 mM and above. The slopes of the uncatalyzed reactions were measured for each point and subtracted from the enzyme catalyzed reaction slope.

To ensure the apparent decrease in enzyme activity was not simply due to a breakdown of the reaction product, *S*-lactoylglutathione, the absorbance of 0.2 mM *S*-lactoylglutathione was monitored in the presence of 1, 5 and 10 mM $NiCl_2$ and 0.5, 1, and 2 mM $ZnCl_2$. No effect was seen on the absorbance at 240 nm. Also, there was no interference in the absorbance at 240 nm upon addition of either metal. Therefore, it appears that the high levels of metal are inhibiting the enzyme by an unknown mechanism, or somehow making the substrate unavailable.

As the enzyme has such a low metal affinity, ICP analysis can not be performed to determine the amount of metal bound. The metal would be lost upon dialysis to remove excess metals prior to the analysis. Also, as the affinity of H5Q GlxI appears weaker than that of phosphate buffer, it is most likely too low for accurate measurement by ITC.

Without a means of determining the amount of metal bound enzyme, and hence active enzyme, it is not possible to determine a meaningful V_{max} for the mutant enzyme. Figure 4.24 summarizes the maximal activities measured for each of the metals tested.

The observation that the enzyme is now active with $ZnCl_2$, although at low levels, is fascinating. A one amino acid change was not expected to create such a drastic effect on the metal affinity of the enzyme as well as the metal activation. The observation that *P. putida* and *S. cerevisiae* GlxI have the same four ligands as the *E. coli* enzyme, yet are active with Zn^{2+}, led to the speculation that the His versus Gln metal ligand was not a critical difference. These results clearly indicate that, although affecting the metal activation, this is not the only factor involved in the differential metal activation observed in the *E. coli* enzyme. There must be further alterations in the enzyme to produce such a drastic difference between two enzymes, which appear at first examination, very similar. Evidently, there are far more subtle changes causing drastic effects in the enzyme than could ever be predicted by sequence comparisons or even by a comparison of the crystal structure.

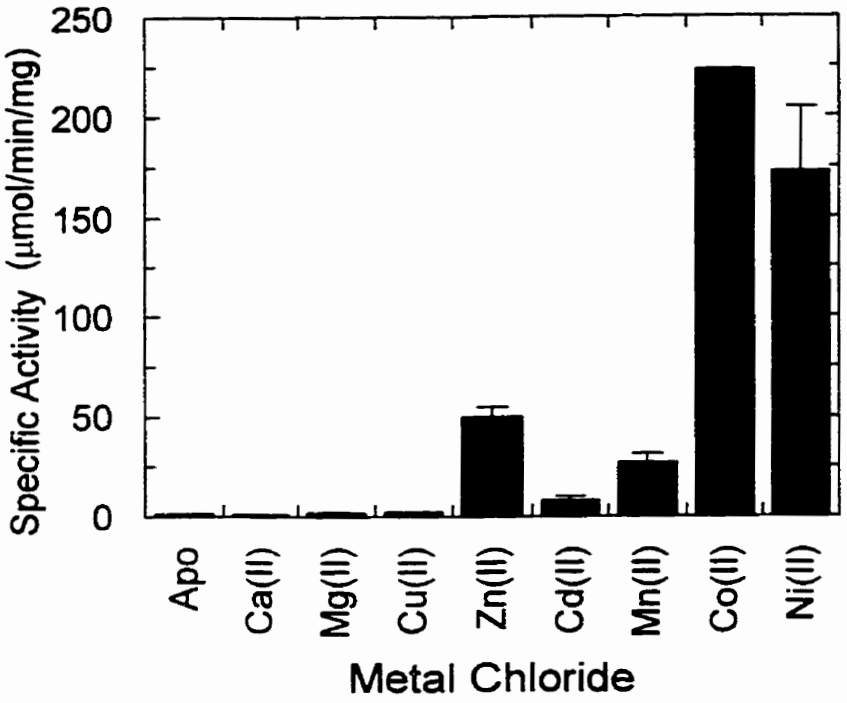

Figure 4.24: Activation of H5Q GlxI with various metal chlorides. Assays were performed in triplicate in MES buffer, pH 6.6 with 0.5 mM substrate, ~2.5 µg of enzyme, and the entire set of measurements duplicated. Three concentrations of each metal were tested and the maximal activity observed is displayed. Ca^{2+}, Mg^{2+}, Mn^{2+} were tested at 0.25, 1.0, 2.0 mM; Cu^{2+}, Cd^{2+} at 0.05, 0.1, 0.25 mM; Co^{2+}, Zn^{2+}, and Ni^{2+} data taken from titration curves. Precipitation of Cu^{2+} and Cd^{2+} precluded measurement above 0.25 mM.

One possible problem to note with this expression system is that the H5Q GlxI mutant was not expressed in a GlxI deficient cell line. The *E. coli* MG1655 utilized to express the wild-type enzyme was also employed here. As such, there could be contaminating low levels of wild-type GlxI from the *E. coli* chromosomal copy of the gene. This is believed not to be a factor for several reasons. There was no detectable wild-type enzyme in the ESMS when analyzed under the same conditions used for wild-type GlxI analysis. Also the activities measured and the affinity of the enzyme for the metals are drastically different to those seen for the wild-type enzyme. Even low levels of wild-type GlxI would be activated by trace amounts of metal and this activity would be detected. The fact that no activity is evident without a large excess of metal supports the fact that we are studying the mutant enzyme and that the activity measured is truly from the H5Q GlxI and not simply residual wild-type activity.

4.4 Conclusions

The expression and purification of *E. coli* GlxI containing selenomethionine at three positions in the protein aided in solving the x-ray crystal structure of the protein. In addition the enzyme exhibited slightly reduced activity in the presence of Ni^{2+}. Based on the location of the SeMet residues in the structure of the protein, it is thought that SeMet at position 7, which is adjacent to the active site, may slightly perturb the position of one of the metal ligands, resulting in the observation of a slightly reduced activity.

Surprisingly, the incorporation of SeMet into *E. coli* GlxI did not require plasmids to be placed into a methionine auxotrophic cell line or to use conditions that would inhibit methionine biosynthesis. SeMet was readily incorporated into the protein when expressed in wild-type *E. coli* cells in minimal media with added SeMet. A modification of the standard purification protocol was developed through numerous attempts to purify the SeMet-GlxI enzyme, C-terminal truncated GlxI enzyme, and the *E. coli* H5Q mutant GlxI. Following separation by isoelectric focusing, further purification of the enzyme was achieved by gel filtration chromatography. In addition, the standard assay protocol had to be altered for analysis of the H5Q GlxI enzyme. During analysis in phosphate buffer the metal ion was lost from the protein, as observed in the reduced enzyme activities. Utilizing MES as the buffer for the activity assays minimized this problem.

Analysis of the purified H5Q mutant *E. coli* GlxI revealed that the affinity of the protein for metal ions is greatly reduced. Furthermore, this mutation resulted in an enzyme that now has low levels of activity in the presence of Zn^{2+}. This is a very intriguing observation, as a change of this one ligand was not expected to have such a drastic effect. *S. cerevisiae* and *P. putida* GlxI are active with Zn^{2+} but both contain a histidine at this position, as in the *E. coli* enzyme (Aronsson et al., 1978; Saint-Jean et al., 1998). Therefore, alteration of this ligand to a glutamine, as found in the *H. sapiens* enzyme, was not expected to substantially affect the relative metal activation levels. Additional mutatagenesis of the metal ligands may help to elucidate the factors controlling this metal selectivity in *E. coli* GlxI.

CHAPTER 5

IDENTIFICATION OF GLYOXALASE I IN OTHER ORGANISMS

5.1 Introduction

Significant effort in recent years has been directed towards whole genome sequencing projects. The knowledge of a complete genome can not only lead to a better understanding of the particular organism under analysis but also permits vast comparisons of sequences to gain more detailed knowledge of the structure and function of particular genes and their gene products from various organisms. The latter is the focus of this chapter. Based on our previous genomic analyses of GlxI sequences performed during my M.Sc. studies and our biochemical studies on *E. coli* GlxI (Clugston, 1997; Clugston et al., 1997; Clugston et al., 1998a; Clugston et al., 1998b) a detailed sequence search and analysis was performed to determine if similarities have occurred over the evolution of this enzyme. Herein we report our findings with respect to sequence and possible structural alterations in GlxI.

5.1.1 Implications of Glyoxalase I as an Antibacterial Target

Due to its electrophilic nature, the glyoxalase I substrate, methylglyoxal (MG), can covalently modify cellular macromolecules (DNA, RNA, proteins), resulting in cell death (Ferguson et al., 1998). For this reason, MG concentrations are extremely well controlled and alteration in this balance with concomitant increase in MG levels can be cytotoxic (Ferguson et al., 1998). Inhibitors of GlxI that block the metabolism of MG, and hence take advantage of its toxic effects, have been studied as potential antitumor and antimalarial agents (Barnard et al., 1994; Thornalley, 1998; Kavarana et al., 1999). Selective inhibition of bacterial GlxI enzymes might also be advantageous for antibacterial therapy.

Multi-drug resistant bacteria have been increasingly prevalent in nosocomial infections. *Pseudomonas aeruginosa* is a leading cause of these infections, contributing 15-20% of all hospital-acquired pneumonias (Carmeli et al., 1999a; Chenoweth and Lynch, 1999). Increasing resistance to antipseudomonal agents is of growing concern (Carmeli et al., 1999b). In addition, frequent reports of necrotising fasciitis, caused by group A Streptococci

infections including *Streptococcus pyogenes*, have attracted much media attention in recent years. This bacterium is one of many shown to be increasingly resistant to current antimicrobial therapy (Blondeau et al., 1999). Even for cases in which vaccination has reduced the incidence of infection, such as *Bordetella pertussis*, the causitive agent of whooping cough, the diseases have not been eliminated (Yaari et al., 1999). In the case of *B. pertussis* immunized non-symptomatic adults are the main source for transmission of the disease (Yaari et al., 1999). Because of these continuing concerns, there is always a quest for new targets for antibacterial agents. As outlined in this chapter, we have identified nineteen postulated GlxI sequences from pathogenic organisms and nine additional sequences from other organisms (Clugston and Honek, 2000). The differences observed between the bacterial GlxI enzymes and those from other sources may be targeted for the development of inhibitors selective to the bacterial enzymes. Such GlxI inhibitors may prove to be a new class of effective antimicrobial agents, taking advantage of the toxicity of MG. As such, knowledge of the sequences of GlxI from a variety of organisms is quintessential to the possible development of new antibiotics as well as to increase our fundamental understanding of the evolution of this enzyme.

5.1.2 Expression of Postulated GlxI Sequences

To determine if the open reading frames postulated to encode GlxI enzymes in these organisms actually encode functional GlxI enzymes, we constructed vectors to express the proteins from two pathogenic organisms. As the predicted GlxI protein sequence from *Yersinia pestis* is very highly homologous to that of the *E. coli* protein (79%) we chose this for our first comparative analysis. The postulated *Pseudomonas aeurginosa* GlxI protein sequence is somewhat less homologous to the *E. coli* sequence (69%) and would provide an intermediate comparison to the *E. coli* protein, between the *Y. pestis* and the well studied *H. sapiens* protein with 36% homology. This study is also useful to see if the Ni^{2+}-activation is an anomaly or a general phenomenon with various GlxI enzymes.

5.2 Materials and Methods

5.2.1 Homology Searching

Sequence Identification

A BLAST search (tblastn program; Altschul et al., 1990; Altschul et al., 1997) of the National Center for Biotechnology Information (NCBI) Microbial Genome databases (http://www.ncbi.nlm.nih.gov/Microb_blast/unfinishedgenome.html), including the unfinished genome sequences, was performed using the full length *E. coli* GlxI sequence. The tblastn search compares the input protein sequence with each nucleotide sequence database, dynamically translated in all six reading frames. The DNA contigs containing the homologous regions identified in these searches were downloaded for analysis. As the search identified regions of DNA with homology regardless of reading frame, further analysis was required. PC/Gene® 6.85 (IntelliGenetics, Mountain View, CA) was utilized to identify the open reading frames in each DNA contig and its complement, which were translated and compared with the *E. coli* GlxI sequence. This ensured that the sequence obtained was a complete open reading frame, including both a start and stop codon.

It should be noted that this search was performed on a database of unfinished genomes which is regarded as preliminary and may still contain sequencing errors. The sequences presented here were the most up to date available at the time of writing. The last search was performed on September 8th, 2000. Further analysis prior to release into the NCBI GenBank may reveal some minor errors in the sequences presented here. These changes should not effect the overall alignment or relationship between the sequences presented in this work.

The full length *E. coli* GlxI protein sequence was also utilized to search the NCBI non-redundant GenBank database (http://www.ncbi.nlm.nih.gov/blast/blast.cgi) using the default parameters. This database contains confirmed or final sequencing data, as opposed to the incomplete genomes described above that have not undergone final checks and release. A BLAST search, both tblastn and blastp, comparison of protein to the nucleic acid database and to the protein database, respectively, were performed.

Sequence Analysis and Phylogenic Tree Construction

Pairwise comparisons were performed using the paired alignment program (Myers and Miller, 1988) from PC/Gene. Multiple sequence alignments were performed utilizing the ClustalW program, version 1.81 (Thompson et al., 1994) from the European Bioinformatics Institute (http://www2.ebi.ac.uk/clustalw/), with the default parameters. The unrooted phylogram based on the ClustalW sequence alignment was created utilizing the following programs from the PHYLIP phylogenetic analysis package, version 3.57c (Felsenstein, 1993), and references therein): SEQBOOT (1000 bootstrap analyses performed), PROTDIST (Dayhoff PAM matrix), NEIGHBOR (neighbor-joining algorithm), and CONSENSE. The branch lengths were determined by reanalyzing the aligned sequences with PROTDIST followed by NEIGHBOR, and combining this data with the bootstrap results from the consensus tree.

Preparation of Structure Illustrations

Structural illustrations of the *H. sapiens* GlxI crystal structure (PDB 1FRO; Cameron et al., 1997), the βαββββ motif, and members of the βαββββ structural superfamily were prepared using WebLab Viewer Pro, version 3.5 (Molecular Simulations Inc.).

5.2.2 Construction of Plasmids for the Expression of Putative Glyoxalase I Enzymes from Yersinia pestis and Pseudomonas aeruginosa

The genomic DNA from *Yersinia pestis* CO92 was obtained from K. Isherwood at the Biomedical Sciences Department at the Chemical and Biological Defence (CBD) establishment Porton Down (Wiltshire, UK). Dr. Elisabeth Daub created an expression plasmid, pYPG1, for the production of the postulated *Y. pestis* GlxI. *P. aeurginosa* (PA01) was a gift from Dr. J. Lam at the University of Guelph. The chromosomal DNA was isolated and the expression plasmid constructed and named pPAG1.

Primers and Sequencing

Primers were purchased from MOBIX (McMaster University, Hamilton, ON). The putative *gloA* DNA in each plasmid constructed was sequenced by MOBIX using the T7 promoter and terminator primers (Novagen, Madison, WI) to confirm the integrity of the construct.

DNA Amplification

The DNA postulated to encode GlxI in both *Y. pestis* and *P. aeruginosa*, based on the sequence analysis presented in this chapter, was amplified using the polymerase chain reactions (PCR), on a Thermolyne Amplitron II PCR machine. Primers homologous to the N- and C-terminal regions of the postulated GlxI DNA in each organism were designed (Figures 5.1 and 5.2), including restriction enzyme digestion sites for insertion into an appropriate expression vector. A "hot start" or "jump start", in which the PCR reaction solutions were heated to 85°C for 1 min prior to addition of the *Pwo* DNA polymerase enzyme (Boehringer Mannheim/Roche Diagnostics) was performed. The enzyme was then added and the DNA was amplified by PCR with the following protocol: 95°C 30 s; 55°C 60 s; 72°C 45 s; repeated for 10 cycles, then the 72°C step was extended by 20 s each round for each of 15 additional cycles, and ended with a 5 minute incubation at 72°C. For the *Y. pestis* DNA amplification several reaction mixtures were attempted with the concentration of $MgSO_4$ varied between 0.3-2.0 mM, and 0.7-2.5 mM for the *P. aeruginosa* DNA amplification.

The PCR products and the expression vector, pET22b (amp^R, T7 *lac* promoter, f1 origin of replication; Novagen, Madison, WI), were each digested with *Nde*I and *Bam*HI and the digestion products ligated. The resulting plasmids, pYPG1 and pPAG1, were transformed into *E. coli* DH5α. The structure of the plasmid was confirmed by isolation of the plasmid, digestion and analysis on an agarose gel. The plasmids were then each transformed into *E. coli* BL21 for protein expression and analysis.

Start

Pest-1 $^{5'}$CCA GAA TTC CAT **ATG** CGC TTA CTC CAT ACC ATG C$^{3'}$

*Eco*RI *Nde*I

Stop

Pest-2 $^{5'}$CCA AAG CTT GGA TCC **TCA** GTT TCC GAG GCA GTC ACC$^{3'}$

*Hind*III *Bam*HI

Figure 5.1: Primers for the PCR amplification of *Y. pestis* GlxI, with the restriction enzyme sites labelled.

Start

Pseudo-1 $^{5'}$CCA GAA TTC CAT **ATG** CGC ATT CTC CAT ACC ATG$^{3'}$

*Eco*RI *Nde*I

Stop

Pseudo-2 $^{5'}$CCA AAG CTT GGA TCC **TCA** GGA AGA CTT CTG GAT CAG$^{3'}$

*Hind*III *Bam*HI

Figure 5.2: Primers for the PCR amplification of *P. aeruginosa* GlxI, and restriction enzyme sites.

5.3 Results and Discussion

5.3.1 Sequence Identification and Analysis

Unfinished Databases

Of the 7 archaeal, 72 eubacterial, and 4 eukaryotic genomes searched in the incomplete genomes database, significant homology to the *E. coli* sequence was found in the DNA of sixteen organisms; *Enterococcus faecalis*, *Pasteurella multocida*, *Pseudomonas aeruginosa*, *Salmonella typhi*, *Shewanella putrefaciens*, *Streptococcus pyogenes*, *Streptococcus mutans*, *Streptococcus pneumoniae*, *Vibrio cholerae*, *Yersinia pestis*, *Bordetella pertussis*, *Neisseria gonorrhoeae*, *Haemophilus ducreyi*, *Legionella pneumophila*, *Caulobacter crescentus*, and *Thiobacillus ferrooxidans* (now classified as *Acidithiobacillus*; Kelly and Wood, 2000). In addition, known GlxI sequences from other organisms determined previously in unrelated studies, such as those from *E. coli* (Clugston et al., 1998a), and *Haemophilus influenzae* (Fleischmann et al., 1995), were identified in the search of this database of genome sequences.

Following the initial identification in the unfinished database and the time of writing, two sequences were finalized and released into GenBank, those from *P. aeruginosa* (Accession # AAG06912) and *V. cholerae* (AAF94171). The sequences remain unchanged in the final release. However, the postulated open reading frame for the *V. cholerae* GlxI is 46 amino acids longer at the N-terminus than predicted here. This N-terminal arm is not homologous to any of the known GlxI enzymes, including the N-terminal arm in the *H. sapiens* enzyme and hence the original protein start site was utilized in the analyses presented here, excluding this region.

Analysis of the sequence identified from *N. gonorrhoeae* revealed significant homology to the *E. coli* GlxI sequence from residue 8 to the end of the protein sequence. However, by removal of one residue, an adenine, in the DNA prior to the CTC encoding Leu8 (ATAGCTC), a stop codon is converted to a Met yielding the full length GlxI sequence, with residues 1-11 being identical to those in the *E. coli* enzyme. This modified sequence was used in the alignment and analyses. We believe that once the DNA in this region is re-

checked prior to its final release into the NCBI complete sequence database, this will be detected as a sequencing error and corrected to the sequence we have used here.

In addition to the sixteen new sequences we have identified in this work as putative GlxI sequences, other pathogenic organisms may prove to contain GlxI sequences with further sequence data. Fifty amino acids from *Pasteurella haemolytica* (Accession #AAB93470) show high homology to the N-terminal region of *E. coli* GlxI. Further sequencing in this region is required to identify the remainder of this enzyme sequence. Also, in the database of unfinished genomes additional partial sequences with high homology to GlxI were found. *Sinorhizobium meliloti* contains an apparent GlxI sequence but only the first two-thirds of the sequence is available to date. *Klebsiella pneumoniae* and *Salmonella paratyphi* both appear to contain GlxI sequences. However it appears that there are two sequencing errors in each resulting in a shift of reading frame, fragmenting the complete sequence. Further refinement of these unfinished databases will undoubtedly correct these errors, revealing the intact GlxI sequences in these organisms. The organization and funding source for each postulated sequence from the unfinished database are listed in Table 5.1.

As glutathione (GSH) is an essential cofactor in the glyoxalase reaction (Figure 1.1), GSH must be available for an organism to have a functional GlxI, similar to those previously identified. To further support our proposal that these sixteen open reading frames encode GlxI, a search was performed to ensure other GSH-utilizing enzymes were present. A search using the *E. coli* glutathione synthase (Accession #SYECGS) and glutathione reductase (Accession #RDECU) sequences identified high homology to one or both of these enzymes in *E. faecalis*, *H. ducreyi*, *L. pneumophila*, *P. multocida*, *P. aeruginosa*, *S. typhi*, *S. putreficiens*, *S. mutans*, *S. pneumoniae*, *S. pyogenes*, *T. ferrooxidans*, *V. cholerae*, and *Y. pestis*, and moderate similarity in *B. pertussis*, *N. gonorrhoeae*, and lower homology in *C. crescentus*. This suggests that the required GSH is available in these organisms for use by a putative glyoxalase system. This may not always be the case. GSH has not been detected in archaebacteria nor in several gram-positive organisms, including mycobacteria (Fahey and Sundquist, 1991; Newton et al., 1996). The absence of GSH may explain why no putative protein with high homology to the known GlxI enzymes has been detected in our searches of mycobacterial sequences, such as *Mycobacterium tuberculosis* Rv. It has been postulated that a recently identified unique thiol, termed mycothiol (Figure 5.3), may function similarly to

GSH in many of these organisms (Spies and Steenkamp, 1994; Patel and Blanchard, 1999; Newton et al., 2000). If present, the GlxI from mycobacteria may have diverged during its evolution in order that it may use mycothiol rather than GSH, or the mycobacterial system never converged to a glutathione-based glyoxalase system.

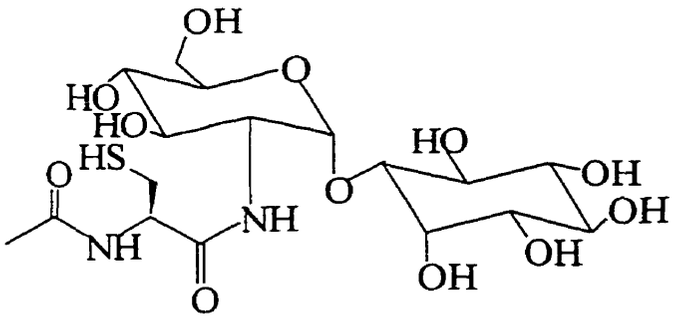

Figure 5.3: Mycothiol (1-D-*myo*-inositol-2-(*N*-acetyl-L-cysteinyl)amino-2-deoxy-α-D-glucopyranoside), a postulated alternative to glutathione in some organisms.

GenBank

From a search of the NCBI GenBank twelve additional putative GlxI sequences were identified from the pathogens *Neisseria meningitidis*, *Xylella fastidiosa*, *Enterococcus hirae*; the plants *Citrus X paradisi*, two sequences from *Arabidopsis thaliana*, *Oryza sativa*, *Triticum aestivum*, *Glycine max*, *Cicer arietinum*; and from the eukaryotes *Botryotinia fuckeiana*, and *Drosophila melanogaster*. Table 5.2 lists the accession numbers and associated references, where available, for these sequences as well as for the sequences known to encode GlxI and those previously predicted to be GlxI sequences (M.Sc. work and this work; Clugston et al., 1997, Clugston et al., 1998b).

Table 5.1: Sequencing organizations and funding sources for the sequences identified from the NCBI unfinished genome database.

Organism Containing GlxI	Sequencing Organization	Funding Source
B. pertussis	Sanger Centre (http://www.sanger.ac.uk)	Beowulf Genomics
C. crescentus	The Institute for Genomic Research (TIGR) (http://tigr.org)	Department of Energy (DOE)
E. faecalis	TIGR	National Institute of Allergy and Infectious Diseases (NIAID)
H. ducreyi	University of Washigton HTSC (http://www.htsc.washington.edu)	NIAID
L. pneumophila	Columbia Genome Center (http://genome3.cpmc.columbia.edu/~legion/)	NIAID
N. gonorrhoeae	University of Oklahoma, Advanced Center for Genome Technology (OU-ACGT) Gonococcal Genome Sequencing Project (http://www.genome.ou.edu/)	USPHS/NIH grant #AI38399
P. multocida PM70	University of Minnesota Computational Biology Center (http://www.cbc.umn.edu/ResearchProjects/AGAC/Pm/index.html)	USDA-NRI, Minnesota Agricultural Experiment Station, and Minnesota Turkey Research and Promotion Council
P. aeruginosa[†]	University of Washington Genome Center and PathoGenesis Corporation Pseudomonas Genome Project (PGP; http://www.pseudomonas.com/)	The Cystic Fibrosis Foundation and PathoGenesis Corporation
S. typhi	Sanger Centre	Beowulf Genomics
S. putrefaciens	TIGR	DOE

S. mutans	OU-ACGT *Streptococcal mutans* Genome Sequencing Project	USPHS/NIH grant from the Dental Institute
S. pneumoniae	TIGR	NIAID and the Merck Genome Research Institute (MGRI)
S. pyogenes	OU-ACGT Streptococcal Genome Sequencing Project	USPHS/NIH grant #AI38406
T. ferrooxidans	TIGR	DOE
V. cholerae‡	TIGR	NIAID
Y. pestis	Sanger Centre	Beowulf Genomics
Other Organisms with Incomplete GlxI Sequences		
K. pneumoniae	Washington University Genome Sequencing Center (http://genome.wustl.edu/gsc/Projects/bacteria.shtml)	N/A*
S. paratyphi A	Washington University Genome Sequencing Center	N/A
S. meliloti	Howard Hughes Medical Institute and the Stanford DNA Sequence and Technology Center (http://cmgm.stanford.edu/~mbarnett/lxgenome.htm)	DOE

* Funding source information not available.
† Sequence now available in GenBank (Acc. # AAG06912; Stover et al., 2000)
‡ Sequence now available in GenBank (Acc. # AAF94171; Heidelberg et al., 2000)

Table 5.2: Accession numbers and references for the known and postulated glyoxalase I sequences available in GenBank.

Organism		Accession Number	Contributors (Submission Date)	Reference
A. thaliana	*1*	2760327	J.R. Ecker (1997)	N/A*
	2	3157947	A. Theologis (1997)	N/A
B. fuckeiana		AL115292	F. Bitton, C. Levis, D. Fortini, J.M. Pradier, Y. Brygoo (1999)	N/A
B. juncea		Y13239	S.K. Sopory (1997)	Veena et al., 1999
B. oleracea		Z74962	R.D. Croy (1996)	N/A
C. arietinum		AJ224520	S. Romo, E. Labrador, F.J. Munoz, and B. Dopico (1998)	Romo et al., 1998
C. paradisi		Z97064	W.L. McKendree (1997)	McKendree et al., 1997
D. melanogaster		AAF59267	M.D. Adams, S.E. Celniker, R.A. Gibbs, G.M. Rubin, and C.J. Venter (2000)	Adams et al., 2000
E. hirae		D17462	Y. Kakinuma (1993)	N/A
E. coli		U57363	E. Daub, R. Kinach, D. Miedema, J.F.J. Barnard, S.L. Clugston, and J.F. Honek (1996)	Clugston et al., 1998a
G. max		AJ010423	M. Skipsey, C.J. Andrews, J.K. Townson, I. Jepson, and R. Edwards (1998)	N/A
H. influenzae		P44638	O. White (1995)	Fleishmann et al., 1995
H. sapiens		L07837	S. Ranganathan, E.S. Walsh, A.K. Godwin, and K.D. Tew (1994)	Kim et al., 1993; Ranganathan et al., 1993
L. esculentum		Z48183	J.M. Pardo (1995)	Espartero et al., 1995

N. meningitidis	Y14298	D.A.A. Ala'Aldeen and G. Kizil (1997)	Kizil et al., 2000
O. sativa	AB017042	M. Nakase, Y. Usui, A. Urisu, K. Kitajima, N. Aoki, and T. Matsuda (1998)	N/A
P. putida	L33880	T. Lu, D.J. Creighton, M. Antoine, C. Fenselau, and P.S Lovett (1994)	Rhee et al., 1988; Lu et al., 1994
S. cerevisiae	CAA89948	S. Gentles and S. Bowman B.G. Barrell, M.A. Rajandream, and S.V. Walsh (1995)	Inoue and Kimura, 1996
S. typhimurium	U57364	E. Daub, R. Kinach, D. Miedema, J.F.J. Barnard, S.L. Clugston, and J.F. Honek (1996)	Clugston et al., 1997
S. pombe	CAA90825	K. Devlin and C.M. Churcher B.G. Barrell, M.A. Rajandream, and S.V. Walsh (1995)	N/A
S. stapfianus	Y10782	C.K. Blomstedt, R.D. Gianello, A.D. Neale, J.D. Hamill, and D.F. Gaff (1997)	Blomstedt et al., 1998
Synechocystis sp.	BAA10101	S. Tabata (1995)	Kaneko et al., 1995
T. aestivum	AJ243528	K.S. Johansen, I. Svendsen, and S.K. Rasmussen (1999)	Johansen et al., 2000
V. parahaemolyticus	U06949	L.L McCarter (1994)	N/A
X. fastidiosa	AAF84208	A.J.G. Simpson, F.C. Reinach et al. (2000)	Simpson et al., 2000

* No published reference available.

5.3.2 Sequence Comparisons

Sequence Homology and Phylogenic Analysis

Comparison of the sixteen sequences from the unfinished genome databases and the three sequences from pathogenic organisms identified in GenBank, proposed here to encode GlxI enzymes, with the sequences of the well studied *E. coli*, *Homo sapiens*, *Pseudomonas putida*, and *Saccharomyces cerevisiae* GlxI enzymes reveal interesting similarities (Table 5.3).

Many of these sequences have extremely high homology to the *E. coli* sequence. Of particular interest is the very high similarity of the *E. coli* GlxI sequence to the sequence from *Y. pestis*, a severe pathogen responsible for the bubonic plague. These two protein sequences are almost 80% identical with an additional 6% similarity. The unrooted phylogenic tree (Figure 5.4) illustrates the evolutionary relationships among all the known and predicted GlxI sequences to date, including the twenty-eight identified in the present work. The *C. crescentus*, *L. pneumophila*, Enterococcus and Streptococcus sequences appear to have diverged from the other prokaryotic sequences in the evolution of the GlxI gene, as is evident in the paired comparisons (Table 5.3), yet key amino acids residues have been conserved, as discussed below. Appendix E contains sequence alignments of all the known and postulated GlxI sequences used in the construction of the phylogenic tree.

Although most of the bacterial sequences segregate together, the *P. putida* is more similar to that of the *H. sapiens*, as has been previously noted (Clugston et al., 1998b). In addition, the newly identified plant pathogen *X. fastidiosa* also appears to be more similar to the *P. putida* and many eukaryotic sequences than to the other bacterial GlxI sequences.

This phylogenic tree based on the glyoxalase I protein sequences differs in some cases from the universal phylogenic tree, which is based on 16S ribosomal RNA sequences (Fox et al., 1980; Ochman et al., 1987; Woese et al., 1990; Woese, 2000). For example, as mentioned the *P. putida* GlxI sequence does not group with other bacterial sequences. However, this tree only provides a summary of the similarities between the known and postulated GlxI protein sequences and a clear depiction of the sequence groupings among organisms. It is not intended to represent the evolution of the organisms.

Gene Duplication

We have previously reported a gene duplication event resulting in a fused dimer gene product in three plant sequences, *Citrus X paradisi*, *Sporobolus stapfianus*, and *Brassica oleracea* as well as in the yeast *S. cerevisiae* and *Schizosaccharomyces pombe* sequences (Clugston et al., 1997; Clugston et al., 1998b). The *Oryza sativa*, *Triticum aestivum*, and the two *Arabidopsis thaliana* GlxI sequences identified in this work, also appear to be the result of a gene duplication event producing a fused dimer. An alignment of the duplicated GlxI sequences is presented in Appendix E (Figure E.2). Interestingly the duplicated plant sequences segregate separately from the yeast sequences in the phylogenic tree. It is also of interest to note that although the *Brassica oleracea* sequence appears to be the result of a gene duplication event, the sequence from *Brassica juncea* does not. One may have expected sequences from the same genus to be more similar. The evolutionary implications of this apparent gene duplication event has been examined (Bergdoll et al., 1998) and is further discussed below.

Table 5.3: A pairwise comparison of the sequence identity (and identity plus similarity) between the four commonly studied glyoxalase I enzymes, from *E. coli*, *H. sapiens*, *P. putida*, and *S. cerevisiae*, with the recently identified sequences from pathogenic organisms.*

	Percentage Identity (Identity + Similarity)			
Organism	*E. coli*	*H. sapiens*	*P. putida*	*S. cerevisiae*
B. pertussis	67.18 (78.63)	44.27 (57.25)	41.22 (57.25)	39.69 (55.72)
C. crescentus	37.78 (53.34)	31.72 (42.06)	25.52 (40.69)	32.41 (49.65)
E. faecalis	36.29 (51.61)	25.00 (31.45)	43.55 (54.84)	40.32 (50.00)
E. hirae	34.96 (51.22)	39.02 (49.59)	42.28 (56.10)	40.65 (51.22)
H. ducreyi	69.63 (77.78)	38.52 (50.37)	37.78 (53.34)	34.81 (41.48)
L. pneumophila	23.70 (36.29)	36.69 (46.76)	21.58 (31.65)	26.62 (37.41)
N. gonorrhoeae	60.74 (74.81)	39.86 (50.00)	39.13 (51.45)	36.23 (44.20)
N. meningitidis	63.70 (77.77)	41.30 (50.72)	46.38 (56.52)	39.13 (46.38)
P. aeruginosa	68.75 (80.47)	42.97 (57.03)	32.81 (45.31)	35.94 (45.32)
P. multocida	69.63 (79.26)	38.52 (50.37)	35.56 (49.63)	36.30 (43.71)
S. putrefaciens	71.85 (75.55)	40.44 (54.41)	41.18 (56.62)	40.44 (48.53)
S. mutans	38.46 (53.08)	31.54 (38.46)	39.23 (47.69)	35.38 (47.69)
S. pneumoniae	34.92 (50.00)	25.40 (35.72)	33.33 (42.85)	28.57 (40.47)
S. pyogenes	38.40 (51.20)	31.20 (40.00)	30.40 (44.00)	40.00 (52.80)
S. typhi	91.85 (96.29)	39.26 (52.59)	37.78 (51.85	50.37 (60.74)
T. ferrooxidans	62.96 (71.85)	39.26 (51.11)	35.56 (48.15)	40.74 (53.33)
V. cholerae	67.41 (75.56)	39.13 (56.52)	40.58 (55.80)	42.03 (52.90)
X. fastidiosa	34.07 (47.40)	49.14 (59.43)	61.27 (71.10)	41.14 (53.71)
Y. pestis	79.26 (86.67)	37.78 (53.34)	38.52 (54.08)	42.22 (54.81)

* See Tables 5.1 and 5.2 for the sequence accession numbers and sequencing organization references.

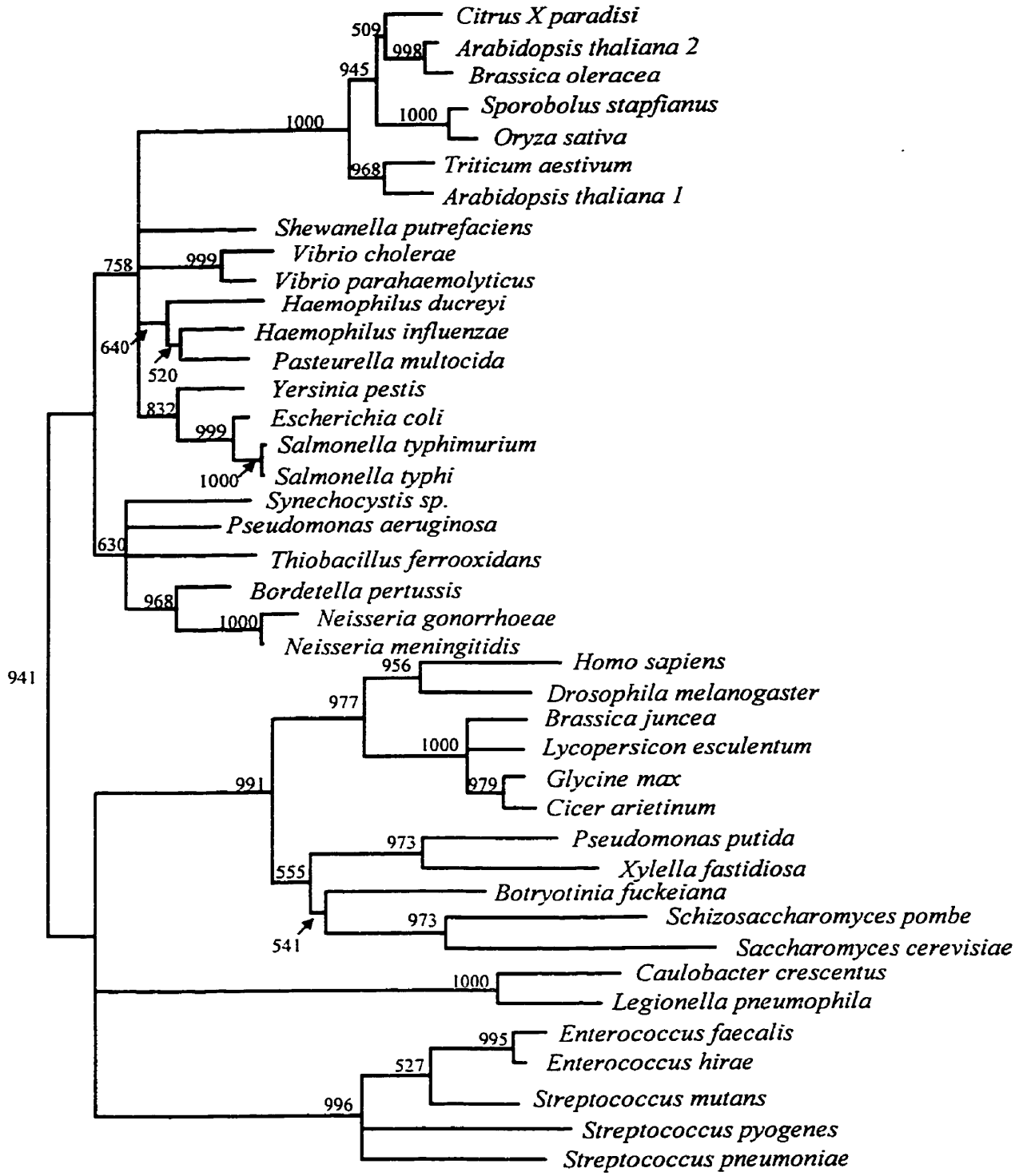

Figure 5.4: Phylogenic relationships among the known and predicted glyoxalase I sequences. This is an unrooted neighbor-joining tree. The numbers indicate the bootstrap confidence levels based on 1000 replications. Nodes with <50% support were collapsed. See Tables 1 and 2 for the sequence accession numbers and sequencing organization references.

5.3.3 Structural Implications

With the recent determination of a homodimeric GlxI crystal structure from both *E. coli* and *H. sapiens* (Cameron et al., 1997; He et al., 2000) we are now able to identify residues critical in binding the catalytic metal, as well as other important residues which are conserved in the sequence alignments (Clugston et al., 1997; Clugston et al., 1998b and this work, Figure 5.5). Many of our structural predications for *E. coli* GlxI were confirmed with the solution of the crystal structure of the *E. coli* GlxI enzyme, as discussed in Chapter 3. The similarity between the *E. coli* GlxI enzyme and the other bacterial enzymes identified in this work will be outlined with their relationship to the *H. sapiens* GlxI enzyme.

As is evident from the sequence alignment (Figure 5.5) there are four gaps in the *E. coli* GlxI sequence and sequences from the other pathogenic organisms identified in this work, when compared with the *H. sapiens* protein sequence. These gaps are also present in many of the previously identified GlxI sequences. The stereo view of the *H. sapiens* GlxI crystal structure in Figure 5.6 illustrates the regions not present in the GlxI sequences from *E. coli* and the pathogenic organisms discussed here. Region 1 (residues 1-29 of *H. sapiens* sequence) of each subunit is at the N-terminus and wraps around the other subunit. All of the microorganism sequences with the exception of those from *P. putida* and *X. fastidiosa*, are missing this region. Omission of this region should not have an effect on the overall enzyme structure. However, the second region (residues 81-95) in the *H. sapiens* enzyme, not present in the other sequences, forms an α-helix on one side of the active site. Removal of this segment may alter the size and shape of the active site in the bacterial GlxI enzymes presented. This was in fact observed in the structure of *E. coli* GlxI (Figure 3.10). The active site appears much more open than in the *H. sapiens* enzyme. Removal of the loops corresponding to regions 3 and 4 (residues ~110-114 and 120-123) of the *H. sapiens* enzyme may also have an indirect effect on the active site conformation. However, examination of the *E. coli* GlxI crystal structure revealed no obvious alterations. (Note: The location of region 3 varies by ~3 residues in the sequence alignments. Although the position of the gap in the sequences is altered, it is in the same region of the structure and expected to have the same effect.) Regions 2, 3, and 4 are missing in all of the known and predicted sequences, except the eleven sequences branching with the *H. sapiens* GlxI on the phylogenic tree (including *D. melanogaster*, *B. juncea*, *L. esculentum*, *G. max*, *C. arietinum*, *P. putida*, *X. fastidiosa*, *B.*

fuckeiana, *S. pombe*, *S. cerevisiae*). These changes in the active site structure may be used selectively in the design of inhibitors to target the bacterial enzymes.

The four ligands to the essential zinc in the *H. sapiens* enzyme, Gln34, Glu100, His127, and Glu173, are conserved in all GlxI sequences, including the sequences presented here from pathogenic sources, with the exception of the Gln34 which is a His in 35 of the 41 known and predicted GlxI sequences. As seen in the sequence alignment (Figure 5.5) and the active site structure (Figure 3.9), the first metal ligand in *E. coli* GlxI is a His. We have previously shown that this GlxI enzyme has no activity in the presence of Zn^{2+} but is maximally active with Ni^{2+} (Clugston et al., 1998a). However, *S. cerevisiae* and *P. putida* GlxI also contain this His ligand, rather than a Gln, yet are fully active with Zn^{2+} (Aronsson et al., 1978; Saint-Jean et al., 1998). Furthermore, mutation of this residue to a Gln in *E. coli* GlxI drastically reduced the affinity of the protein for metal ions. The H5Q mutant enzyme was still most active with Ni^{2+} yet displayed low levels of activity with Zn^{2+}. This residue is evidently not the determining factor in the metal activation. It would be interesting to determine whether other GlxI enzymes postulated in this work are active with Zn^{2+}, Ni^{2+}, or both.

Other residues (Thr35, Arg38, Val39, Tyr49, Leu70, Leu101, Thr102, Asn104, Tyr115, Gly118, Phe163, Pro167, and Asp168 in the *H. sapiens* GlxI sequence; Figure 5.5), although well conserved in the alignment between the *E. coli*, *H. sapiens* and the bacterial GlxI sequences presented, in some cases have undergone conservative mutations in some of the sequences from other organisms, most commonly those which are the result of a gene duplication event forming a fused dimer gene product. Several of these residues (Arg38, Asn104, Phe163) interact with a known inhibitor of *H. sapiens* GlxI, benzylglutathione, which was cocrystallized with the enzyme in the active site. Other residues shape the active site (Thr102, Tyr115), and some are at the dimer interface (Thr35, Gly118). These essential interactions with the cofactor have been maintained in the evolution of GlxI, as have others that may be required for the maintenance of the three-dimensional structure.

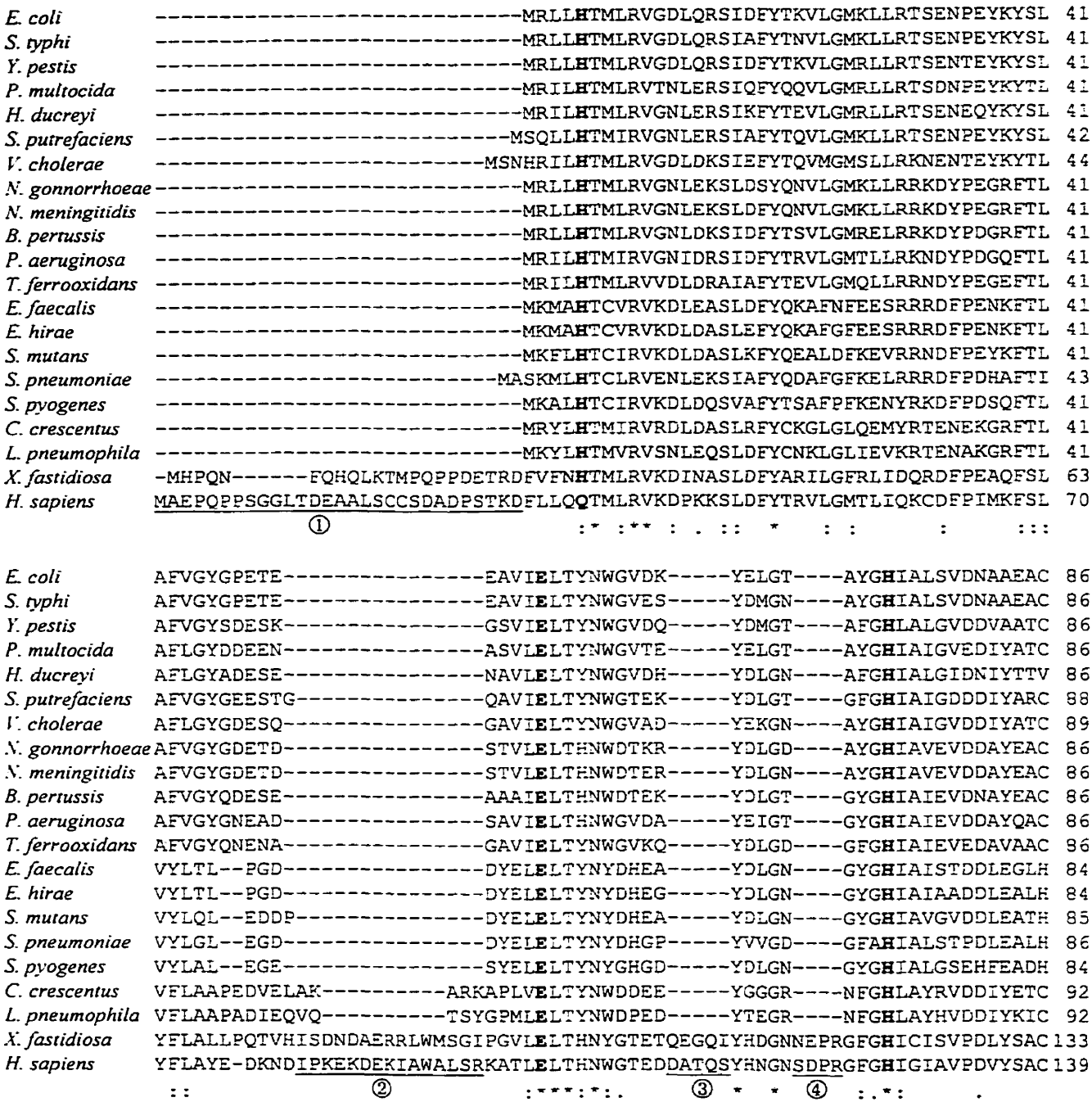
E. coli ----------MRLLHTMLRVGDLQRSIDFYTKVLGMKLLRTSENPEYKYSL 41
S. typhi ----------MRLLHTMLRVGDLQRSIAFYTNVLGMKLLRTSENPEYKYSL 41
Y. pestis ----------MRLLHTMLRVGDLQRSIDFYTKVLGMRLLRTSENTEYKYSL 41
P. multocida ----------MRILHTMLRVTNLERSIQFYQQVLGMRLLRTSDNPEYKYTL 41
H. ducreyi ----------MRILHTMLRVGNLERSIKFYTEVLGMRLLRTSENEQYKYSL 41
S. putrefaciens ----------MSQLLHTMIRVGNLERSIAFYTQVLGMKLLRTSENPEYKYSL 42
V. cholerae ----------MSNHRILHTMLRVGDLDKSIEFYTQVMGMSLLRKNENTEYKYTL 44
N. gonnorrhoeae ----------MRLLHTMLRVGNLEKSLDSYQNVLGMKLLRRKDYPEGRFTL 41
N. meningitidis ----------MRLLHTMLRVGNLEKSLDFYQNVLGMKLLRRKDYPEGRFTL 41
B. pertussis ----------MRLLHTMLRVGNLDKSIDFYTSVLGMRELRRKDYPDGRFTL 41
P. aeruginosa ----------MRILHTMIRVGNIDRSIDFYTRVLGMTLLRKNDYPDGQFTL 41
T. ferrooxidans ----------MRILHTMLRVVDLDRAIAFYTEVLGMQLLRRNDYPEGEFTL 41
E. faecalis ----------MKMAHTCVRVKDLEASLDFYQKAFNFEESRRRDFPENKFTL 41
E. hirae ----------MKMAHTCVRVKDLDASLEFYQKAFGFEESRRRDFPENKFTL 41
S. mutans ----------MKFLHTCIRVKDLDASLKFYQEALDFKEVRRNDFPEYKFTL 41
S. pneumoniae ----------MASKMLHTCLRVENLEKSIAFYQDAFGFKELRRRDFPDHAFTI 43
S. pyogenes ----------MKALHTCIRVKDLDQSVAFYTSAFPFKENYRKDFPDSQFTL 41
C. crescentus ----------MRYLHTMIRVRDLDASLRFYCKGLGLQEMYRTENEKGRFTL 41
L. pneumophila ----------MKYLHTMVRVSNLEQSLDFYCNKLGLIEVKRTENAKGRFTL 41
X. fastidiosa -MHPQN------FQHQLKTMPQPPDETRDFVFNHTMLRVKDINASLDFYARILGFRLIDQRDFPEAQFSL 63
H. sapiens MAEPQPPSGGLTDEAALSCCSDADPSTKDFLLQQTMLRVKDPKKSLDFYTRVLGMTLIQKCDFPIMKFSL 70
① :* :** : . :: * : : : :::
E. coli AFVGYGPETE----------EAVIELTYNWGVDK-----YELGT----AYGHIALSVDNAAEAC 86
S. typhi AFVGYGPETE----------EAVIELTYNWGVES-----YDMGN----AYGHIALSVDNAAEAC 86
Y. pestis AFVGYSDESK----------GSVIELTYNWGVDQ-----YDMGT----AFGHLALGVDDVAATC 86
P. multocida AFLGYDDEEN----------ASVLELTYNWGVTE-----YELGT----AYGHIAIGVEDIYATC 86
H. ducreyi AFLGYADESE----------NAVLELTYNWGVDH-----YDLGN----AFGHIALGIDNIYTTV 86
S. putrefaciens AFVGYGEESTG----------QAVIELTYNWGTEK-----YDLGT----GFGHIAIGDDDIYARC 88
V. cholerae AFLGYGDESQ----------GAVIELTYNWGVAD-----YEKGN----AYGHIAIGVDDIYATC 89
N. gonnorrhoeae AFVGYGDETD----------STVLELTHNWDTKR-----YDLGD----AYGHIAVEVDDAYEAC 86
N. meningitidis AFVGYGDETD----------STVLELTHNWDTER-----YDLGN----AYGHIAVEVDDAYEAC 86
B. pertussis AFVGYQDESE----------AAAIELTHNWDTEK-----YDLGT----GYGHIAIEVDNAYEAC 86
P. aeruginosa AFVGYGNEAD----------SAVIELTHNWGVDA-----YEIGT----GYGHIAIEVDDAYQAC 86
T. ferrooxidans AFVGYQNENA----------GAVIELTYNWGVKQ-----YDLGD----GFGHIAIEVEDAVAAC 86
E. faecalis VYLTL--PGD----------DYELELTYNYDHEA-----YDLGN----GYGHIAISTDDLEGLH 84
E. hirae VYLTL--PGD----------DYELELTYNYDHEG-----YDLGN----GYGHIAIAADDLEALH 84
S. mutans VYLQL--EDDP----------DYELELTYNYDHEA-----YDLGN----GYGHIAVGVDDLEATH 85
S. pneumoniae VYLGL--EGD----------DYELELTYNYDHGP-----YVVGD----GFAHIALSTPDLEALH 86
S. pyogenes VYLAL--EGE----------SYELELTYNYGHGD-----YDLGN----GYGHIALGSEHFEADH 84
C. crescentus VFLAAPEDVELAK----------ARKAPLVELTYNWDDEE-----YGGGR----NFGHLAYRVDDIYETC 92
L. pneumophila VFLAAPADIEQVQ----------TSYGPMLELTYNWDPED-----YTEGR----NFGHLAYHVDDIYKIC 92
X. fastidiosa YFLALLPQTVHISDNDAERRLWMSGIPGVLELTHNYGTETQEGQIYHDGNNEPRGFGHICISVPDLYSAC 133
H. sapiens YFLAYE-DKNDIPKEKDEKIAWALSRKATLELTHNWGTEDDATQSYHNGNSDPRGFGHIGIAVPDVYSAC 139
② ③ ④
:: :***:*:. * * :.*: .

```
E. coli          EKIRQNGGNVTREAGPVKGGTTVIAFVEDPDGYKIELIEEKDAGRGLGN---------- 135
S. typhi         ERIRQNGGNVTREAGPVKGGSTIIAFVEDPDGYKIELIEAKDAGRGLGN---------- 135
Y. pestis        DQIRQAGGKVTREAGPVKGGNTIIAFVEDPDGYKIELIENKSAGDCLGN---------- 135
P. multocida     DAVRQAGGKITREPGPVKGGKTVIAFVEDPDGYKIEFIENKHAQSGLGN---------- 135
H. ducreyi       EAVRLAGGKITREPGPVLGGKTVIAFAEDPDGYKIEFIENKNAQVALGN---------- 135
S. putrefaciens  EAIAAAGGKVTRAPGPVAGGTTEIAFVEDPDGYKIEFIQMKSATQGLG----------- 136
V. cholerae      DTIKAAGGIVTREPGPVKGGTTHIAFVKDPDGYMIELIQNKQAHAGLEG---------- 138
N. gonnorrhoeae  ERVKRQGGNVVREAGLMKHGTTVIAFVEDPDGCKIEFVQKKSGDDSVAYANT------- 138
N. meningitidis  ERVKRQGGNVVREAGPMKHGTTVIAFVEDPDGYKIEFIQKKSGDDSVAYQTA------- 138
B. pertussis     DKVKEKGGKVTREAGPMKHGTTVIAFVEDPDGYKIEFIQKKGRND-------------- 131
P. aeruginosa    DDIRYNGGQVTREAGPMKHGTTVIAFVTDPDGYKIELIQKSS----------------- 128
T. ferrooxidans  DGIRQRGGKVVREAGPMKHGNTVIAFVEDPDGYRIELIERKS--DFAEHPA-------- 135
E. faecalis      EKHQAAGFTVTDLKG-LPGTAPSYYFVVDPDGYKIEVIRER----------------- 124
E. hirae         EKHQAEGFNVTDLKG-LPGTAPSYYFVVDPDGYKIEVIRG------------------ 123
S. mutans        QAHQKAGYTVTDLSG-LPGKPKMYYFITDPDGYKIEVIRLKQFQEK------------ 130
S. pneumoniae    QEHSAKGYEVTEPNG-LPGTTPNYYFVKDPDGYKVEVIREK----------------- 126
S. pyogenes      KKHRQAGFPVTDIKE-LADKSARYYFIQDPDGYKIEVIDLNN----------------- 125
C. crescentus    QRLMDMGVTINRPPR-----DGHMAFVRSPDNISIELLQDGD-LPPAEPWVSMPNVGAW 145
L. pneumophila   QHLQECGVVINRPPR-----DGHMAFIRSPDNISIELLQKGEPLPKQEPWLS------- 139
X. fastidiosa    ARFDTLQVPYQKRLT--DGRMKNIAFIKDPDGYWVEIISNTPLP--------------- 175
H. sapiens       KRFEELGVKFVKKPD--DGKMKGLAFIQDPDGYWIEILNPNKMATLM------------ 184
                                  *  .**.  :*.:
```

Figure 5.5: Sequence alignment of the glyoxalase I sequences from *E. coli* and *H. sapiens* and the predicted glyoxalase I sequences from pathogenic organisms presented in this work, generated by ClustalW (Thompson et al., 1994). * indicates conserved residues; : highly homologous residues; . homologous residues. The underlined regions indicate the segments of the *H. sapiens* sequence not present in the other sequences and the residues in bold are the postulated metal ligands, based on the alignment with the known metal ligands in the *E. coli* GlxI enzyme. The numbers are used for identification of each region illustrated in Figure 5.6. See Tables 5.1 and 5.2 for the sequence accession numbers and sequencing organization references.

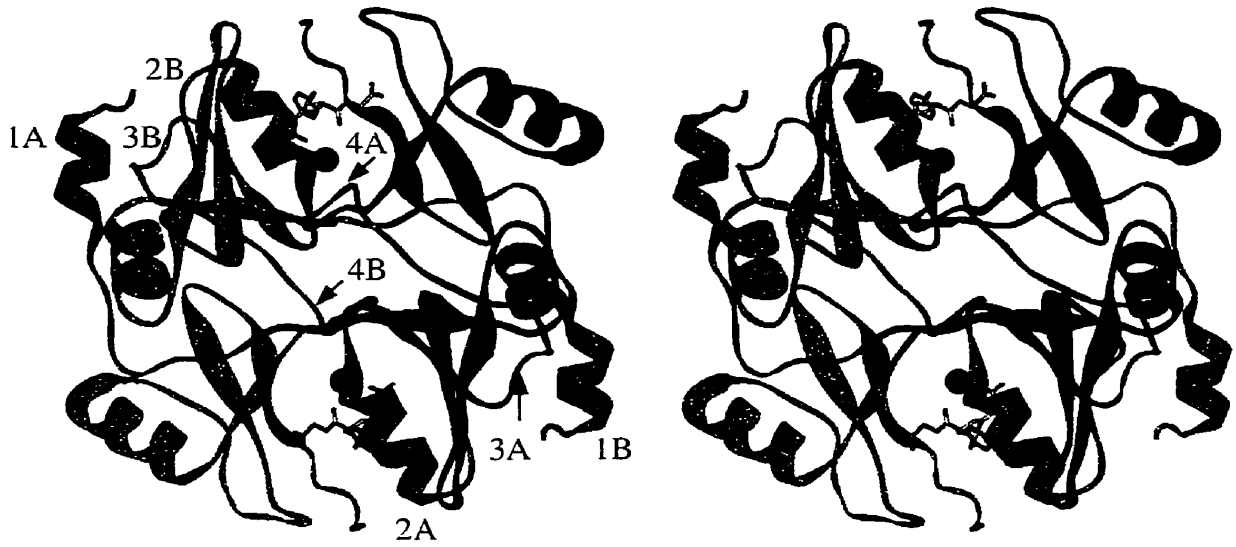

Figure 5.6: Stereo view of the homodimeric *H. sapiens* glyoxalase I crystal structure (Cameron et al., 1997). Subunit A is illustrated in blue, B in green, benzylglutathione is the stick structure, and the zinc atoms are in black spacefill. The red segments indicate the regions omitted in glyoxalase I from *E. coli* and the pathogenic organisms discussed in this work. The numbers are used for identification of the regions in the sequence alignment, and the letters indicate the subunit.

5.3.4 Evolutionary Analysis of Glyoxalase I and the βαββββ Superfamily

The recent determination of the crystal structure of the *H. sapiens* GlxI enzyme has indicated that glyoxalase I appears to be a member of a structural superfamily composed of a βαββββ motif (Bergdoll et al., 1998). As mentioned previously, the other members of this previously unrecognized superfamily include the bleomycin resistance protein (BRP) from *Streptoalloteichus hindustanus*, 2,3-dihydroxybiphenyl 1,2-dioxygenase (DHBD) from *Burkholderia cepacia*, and the Mn^{2+}-dependent fosfomycin resistance protein (FosA) (Dumas et al., 1994; Han et al., 1995; Bernat et al., 1997). Each of these enzymes is composed of repeats of the βαββββ motif (Figures 5.7 and 5.8). Each monomer of *E. coli* and *H. sapiens* GlxI contains two such βαββββ motifs (Chapter 3 and Cameron et al., 1997; He et al., 2000). Although not yet crystallized, the FosA protein is believed to also have the same structural pattern.

Figure 5.7: Representation of the βαββββ motif found in glyoxalase I and other members of the superfamily.

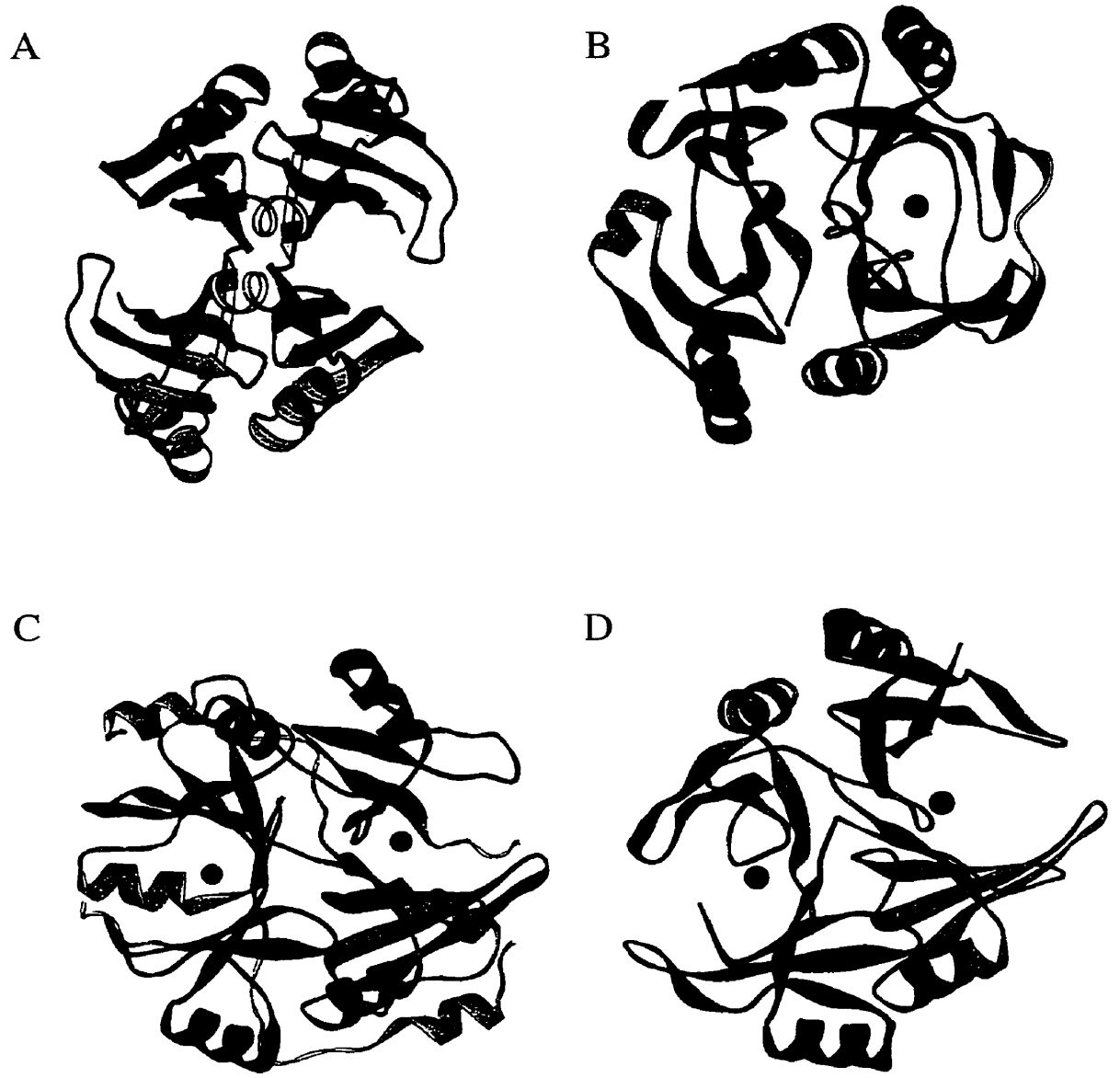

Figure 5.8: Structures of the βαββββ superfamily members currently known. (A) Bleomycin resistance protein from *S. hindustanus* (PDB 1BYL and Bergdoll et al., 1998), (B) extradiol dioxygenase from *B. cepacia* (PDB 1HAN), (C) *H. sapiens* glyoxalase I (PDB 1FRO), and (D) *E. coli* glyoxalase I (PDB 1F9Z). The four βαββββ motifs in each structure are illustrated in blue and red. The portions of the structure which are not part of this motif are illustrated in grey. The active site metals are in black space fill.

This group has also been called the "vicinal oxygen chelate superfamily" (Armstrong, 1998; Laughlin et al., 1998). The GlxI and DHBD enzymes have a metal ion in their active site with an octahedral coordination, with at least two water ligands to the metal. The substrate or intermediate in the reaction is believed to displace the water ligands. The common feature in the enzymes of this family is proposed to be the chelation of the vicinal oxygen ligands on the substrate with the metal to help promote the reaction (Laughlin et al., 1998). Although not yet established a similar involvement of the FosA substrate, fosfomyocin, with the active site Mn^{2+} is believed to occur through coordination of the phosphonate oxygens or the epoxide ring oxygen, or a combination of the two. As the BRP does not contain a metal center it does not fit with this classification of the superfamily. However, bleomycin itself is a metal-binding drug.

Structural comparisons made by Bergdoll and coworkers (1998) focus on the βαβββ motif and hence include the BRP in their analysis of the superfamily. In their analysis they suggest that each of the members of the superfamily arose from a common ancestor, a single βαβββ motif which underwent multiple gene duplication and fusion events, combined with accumulated mutations; divergent evolution from a common ancestral gene encoding the βαβββ motif. This yielded several groups of proteins that catalyze very distinct reactions, have relatively low sequence homology, and yet share a common ancestral protein fold. Figure 5.9 summarizes the proposed evolutionary history of this superfamily.

This analysis also presents a plausible explanation for the evolution of the two forms of GlxI enzymes, the smaller enzymes such as the *H. sapiens* and *E. coli* which function as dimers, and the larger enzyme observed in the *S. cerevisiae* that appears to be monomeric. We have reported that the two yeast sequences in addition to numerous plant sequences appear to be the result of a gene duplication event forming a fused dimer gene product (Ridderström and Mannervik, 1996; Clugston et al., 1997; Clugston et al., 1998b; and Section 5.3.2). Sequence analyses indicated that the shorter *E. coli* and *H. sapiens* GlxI sequences were homologous to both the N-and C-terminal halves of these apparent duplicated sequences (Clugston, 1997). It is proposed that after the first gene duplication and fusion event some of the enzymes evolved to function as dimers of the duplicated βαβββ motif whereas in other instances another duplication and fusion event occurred to form the large GlxI enzymes. In each case the active form of the enzyme consists of four βαβββ motifs. A similar evolution is

proposed to have occurred for the dioxygenase enzymes. No large forms of FosA or BRP have been identified to date and hence it appears that only one duplication and fusion event occurred in the evolution of these enzymes.

Further analysis of the structures and sequences of these enzymes suggest that the ultimate evolutionary link between these enzymes is in fact metal binding. Several of the metal ligands are conserved in the motifs of various enzymes and superposition of DHBD onto the *H. sapiens* GlxI structure shows that the Fe^{2+} in the active site of the DHBD is only 2.5 Å from one of the active site Zn^{2+} atoms in GlxI (Bergdoll et al., 1998). As mentioned there is no metal binding site in the BRP and for the most part the metal ligands are not conserved in the BRP sequences. The bleomycin is believed to bind in the same active site cavity as in the other enzymes, and interestingly bleomycin actually binds Fe^{2+} itself. The evolutionary explanation for this has not been established, but based on the high structural homology, the BRP is considered a member of this $\beta\alpha\beta\beta\beta$ superfamily. Further analysis and discussion of the evolution of the metal binding site and this superfamily in general can be found elsewhere (Bergdoll et al., 1998).

Our identification of additional plant sequences that are the result of an apparent duplication furthers our knowledge of the sequence similarity among the GlxI enzymes, and the superfamily. The four metal ligands are not conserved in both halves of all of the sequences suggesting that only one functional active site exists in several of these enzymes (illustrated in Appendix E). This is further supported by the observation that *S. cerevisiae* GlxI binds only one metal and one inhibitor molecule (Aronsson et al., 1978; Marmstål and Mannervik, 1979). Crystallization of one of these large GlxI enzymes would greatly enhance our knowledge of the evolution of this family, the metal binding site, and the gene fusion events.

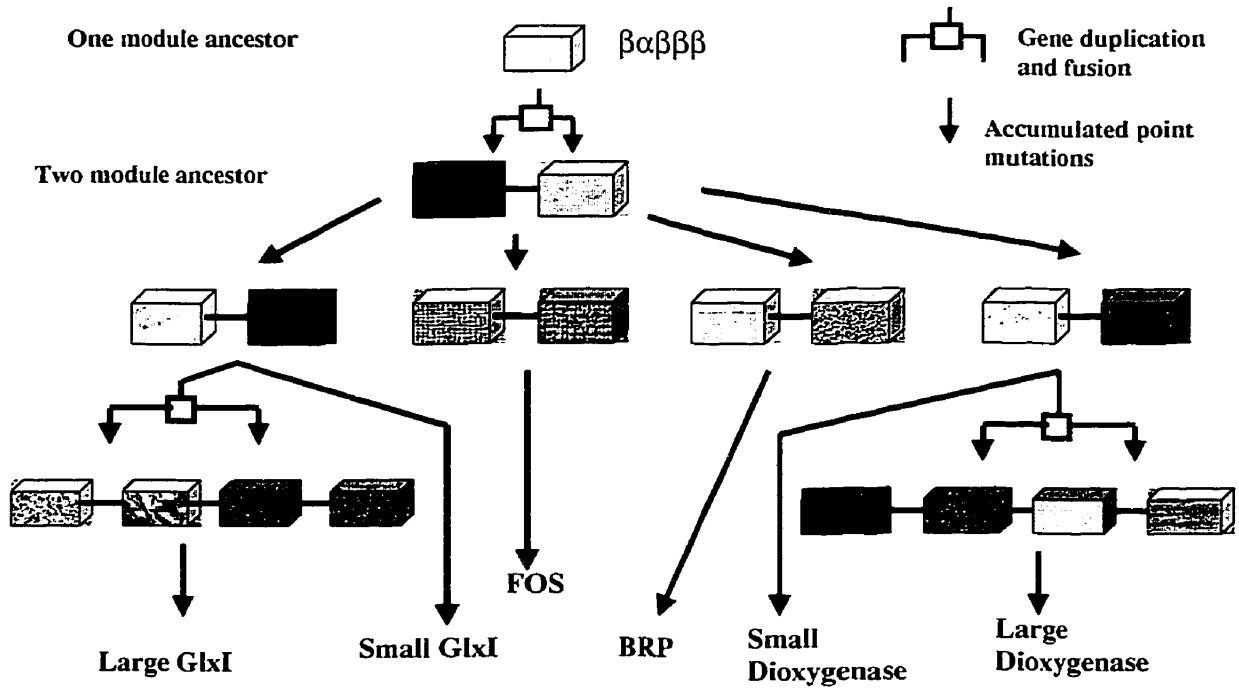

Figure 5.9: Scheme outlining the postulated evolution of the genes for the BRP, FosA, GlxI, and dioxygenase enzymes. Each square represents a βαβββ motif and the variation in colour depicts the distinctive forms of this motif resulting from various mutations during its evolution. (Adapted from Bergdoll et al., 1998)

5.3.5 Expression and Analysis of Glyoxalase I from Y. pestis and P. aeruginosa

To determine if in fact the postulated sequences encode a protein with glyoxalase I activity, and to gain further knowledge regarding bacterial GlxI enzymes and their metal activation, the genes from two organisms, *Y. pestis* and *P. aeruginosa* were amplified, placed in an overproduction plasmid and the expressed protein examined.

Based on the intensity of the band of DNA on an agarose gel, the 1.0-2.0 mM $MgSO_4$ conditions proved best for the PCR amplification of the putative *gloA* DNA from both the *Y. pestis* and *P. aeruginosa* chromosomal DNA. Growth of *E. coli* BL21/pYPG1 and BL21/pPAG1 in LB_{Amp}, induction of protein expression with IPTG (1 mM), and analysis by SDS-PAGE with Coomassie staining indicated that the plasmid constructs in pET22b successfully expressed both putative GlxI enzymes.

Preliminary analysis of a crude cell extract from each construct was performed. ESMS analyses indicates that a protein is produced of the molecular weight predicted based on the DNA and corresponding protein sequence (Figure 5.10 and 5.11) predicted to encode GlxI in both *Y. pestis* and *P. aeruginosa* (Figures 5.12 and 5.13). The *Y. pestis* GlxI protein sequence, encoding a 14 834 Da protein, is 79% identical to the sequence from *E. coli*. Only 28 of the 135 residues in this protein are altered from the *E. coli* sequence. The *P. aeruginosa* GlxI sequence encodes a 14 251 Da protein with 69% sequence identity to the *E. coli* protein sequence. There are 40 residues in this 128 amino acid protein that differ from the *E. coli* sequence.

Activity assays on the extract from each expression system indicated that the expressed protein did have glyoxalase I activity, confirming that the predicted DNA does in fact encode this enzyme. In addition the activity of the crude extract was significantly enhanced with the addition of $NiCl_2$ (20-fold in each case), but not $ZnCl_2$. This suggests that the unexpected activity enhancement seen for the *E. coli* GlxI enzyme with Ni^{2+} is not unique to the enzyme from this source but may actually be seen for many other GlxI enzymes.

Analysis of the protein expression from these two constructs and further detailed analysis of the purified *Y. pestis* GlxI enzyme, including its metal activation is presented in Appendix F.

A

```
      3         9        15        21        27        33        39        45
      |         |         |         |         |         |         |         |
  1 ATG CGC TTA CTC CAT ACC ATG CTC CGC GTC GGT GAC CTG CAA CGT
 46 TCT ATC GAT TTC TAC ACC AAG GTA TTA GGG ATG CGT TTA CTG CGT
 91 ACC AGC GAA AAT ACT GAA TAT AAA TAC TCG TTG GCA TTC GTA GGC
136 TAT AGC GAT GAA AGT AAA GGT TCG GTG ATT GAA CTG ACG TAT AAC
181 TGG GGC GTT GAC CAG TAC GAT ATG GGC ACC GCA TTC GGC CAT CTG
226 GCT CTG GGT GTT GAT GAT GTC GCC GCA ACG TGT GAT CAA ATT CGC
271 CAG GCA GGC GGT AAA GTC ACC CGC GAA GCT GGC CCG GTA AAA GGC
316 GGT AAT ACC ATT ATT GCT TTT GTT GAA GAT CCA GAT GGC TAC AAA
361 ATT GAG TTA ATT GAG AAT AAG AGC GCG GGT GAC TGC CTC GGA AAC
406 TGA
```

Total number of bases: 408
DNA sequence composition: A: 107; C: 88; G: 110; T: 103

B

```
          5         10        15        20        25        30
          |         |         |         |         |         |
  1 M R L L H T M L R V G D L Q R S I D F Y T K V L G M R L L R
 31 T S E N T E Y K Y S L A F V G Y S D E S K G S V I E L T Y N
 61 W G V D Q Y D M G T A F G H L A L G V D D V A A T C D Q I R
 91 Q A G G K V T R E A G P V K G G N T I I A F V E D P D G Y K
121 I E L I E N K S A G D C L G N
```

Number of residues: 135
Molecular weight (MW): 14 834

Amino acid composition:

9 A	2 C	2 H	4 M	9 T
7 R	4 Q	7 I	4 F	1 W
5 N	8 E	13 L	2 P	7 Y
11 D	16 G	7 K	7 S	10 V

Figure 5.10: *Y. pestis* glyoxalase I (A) DNA sequence and (B) corresponding protein sequence.

A

```
      3         9        15        21        27        33        39        45
      |         |         |         |         |         |         |         |
  1 ATG CGC ATT CTC CAT ACC ATG ATC CGG GTC GGA AAC ATC GAT CGC
 46 TCG ATC GAT TTC TAT ACC CGG GTG CTA GGC ATG ACC CTG CTC AGG
 91 AAG AAC GAC TAT CCC GAC GGC CAG TTC ACC CTC GCC TTC GTC GGC
136 TAT GGC AAC GAA GCG GAT TCC GCG GTG ATC GAG CTT ACC CAC AAC
181 TGG GGC GTG GAT GCC TAC GAG ATC GGC ACC GGC TAC GGC CAT ATC
226 GCC ATC GAG GTC GAC GAC GCC TAC CAG GCC TGC GAC GAC ATC CGC
271 TAC AAC GGC GGC CAG GTC ACC CGC GAA GCC GGG CCG ATG AAG CAC
316 GGT ACC ACC GTG ATC GCC TTC GTG ACC GAC CCG GAC GGC TAC AAG
361 ATC GAA CTG ATC CAG AAG TCT TCC TGA
```

Total number of bases: 387
DNA sequence composition: A: 85; C: 128; G: 106; T: 68

B

```
          5         10        15        20        25        30
          |         |         |         |         |         |
  1 M R I L H T M I R V G N I D R S I D F Y T R V L G M T L L R
 31 K N D Y P D G Q F T L A F V G Y G N E A D S A V I E L T H N
 61 W G V D A Y E I G T G Y G H I A I E V D D A Y Q A C D D I R
 91 Y N G G Q V T R E A G P M K H G T T V I A F V T D P D G Y K
121 I E L I Q K S S
```

Number of residues: 128
Molecular weight (MW): 14 251

Amino acid composition:

9 A	1 C	4 H	4 M	10 T
7 R	4 Q	12 I	4 F	1 W
5 N	6 E	7 L	3 P	8 Y
12 D	14 G	4 K	4 S	9 V

Figure 5.11: *P. aeruginosa* glyoxalase I (A) DNA sequence and (B) corresponding protein sequence.

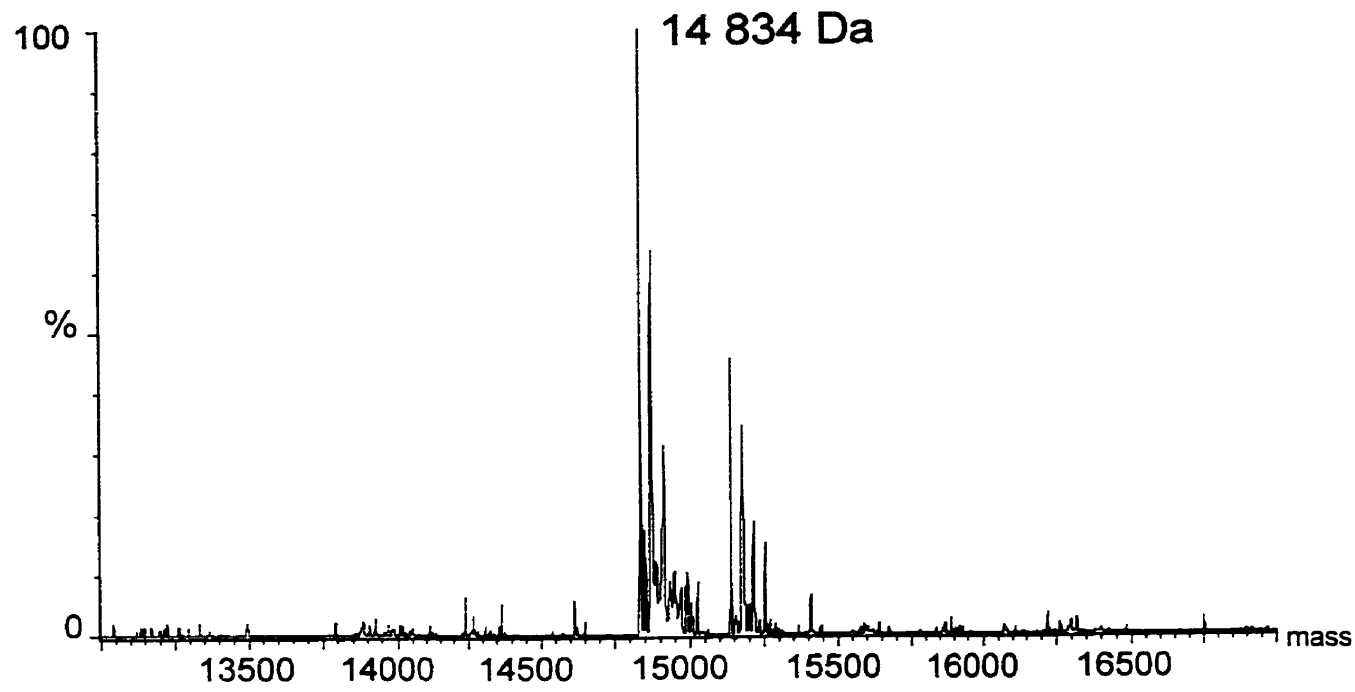

Figure 5.12: Reconstructed electrospray mass spectrum of a crude cell extract of *Y. pestis* GlxI, from *E. coli* BL21/pYPG1. The additional peaks observed correspond to adducts with buffer salts as well as other contaminating proteins.

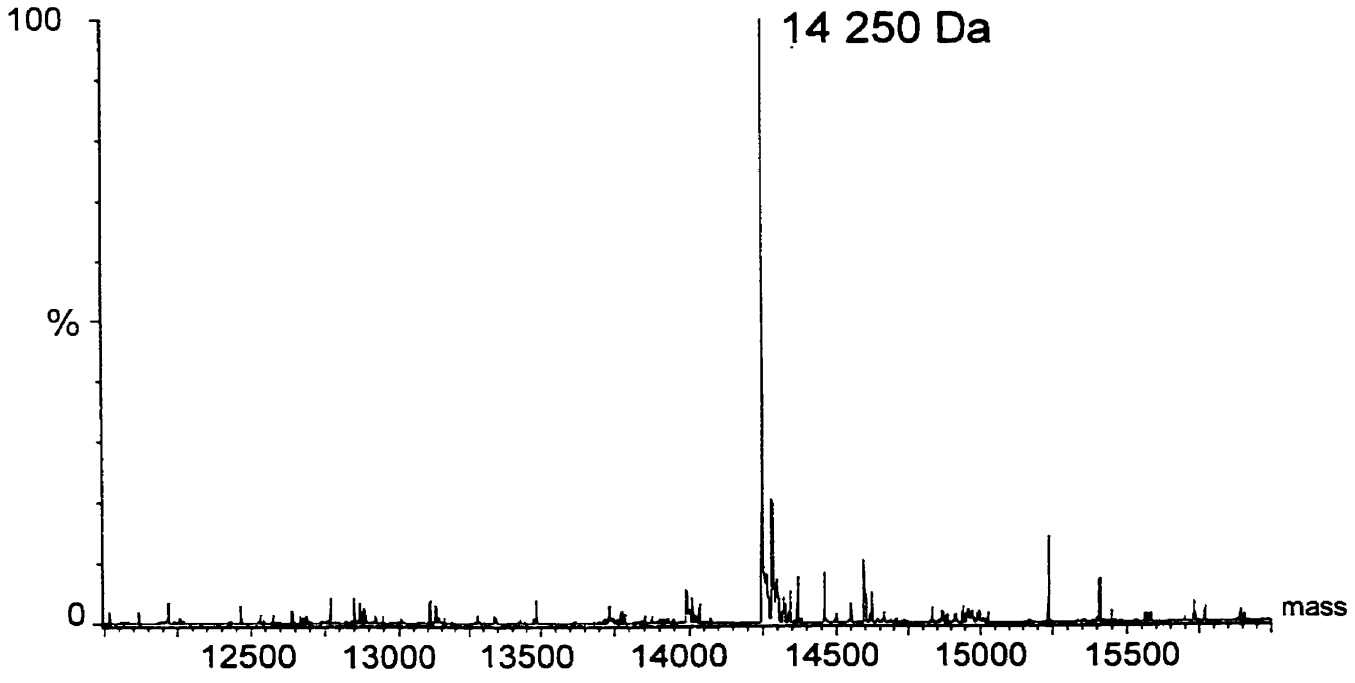

Figure 5.13: Reconstructed electrospray mass spectrum of a crude cell extract of *P. aeruginosa* GlxI, from *E. coli* BL21/pPAG1. Adducts with buffers salts are also present.

5.4 Conclusions

Utilizing the *E. coli* GlxI amino acid sequence, we have identified twenty-eight new putative GlxI sequences both from the unfinished databases of whole genome sequencing projects, and depositions in the GenBank sequence databases. Many of the bacterial sequences, in particular *Y. pestis*, have been shown to have high sequence similarity to the *E. coli* enzyme. Taken together it has been possible to identify consistent bacterial alterations compared to the *H. sapiens* enzyme, as well as absolutely conserved residues important in metal and cofactor binding and dimer interface interactions. These differences could be targeted in the development of novel antimicrobial agents.

One of the most intriguing features observed in the bacterial GlxI enzymes is its metal activation. We have examined the GlxI enzymes, from *E. coli*, *Y. pestis*, and *P. aeruginosa* and found activation with Ni^{2-} but not with Zn^{2+}, the native metal in the *H. sapiens* GlxI. The rat erythrocyte GlxI was tested in the presence of Ni^{2+} (Han et al., 1977). Although the enzyme was still active, the level of activity was not enhanced over that seen with Mg^{2+} (Han et al., 1977). There has been no report of the activity of the *H. sapiens* GlxI enzyme reconstituted with Ni^{2-} but it has been presumed that it would behave similarly to the rat enzyme. As such it would be of interest to determine if the activity with Ni^{2+} is restricted to the enzymes in the bacterial sequences grouping with the *E. coli* on the phylogenic tree (Figure 5.4) or also exists for enzymes in other groupings such as the plants. In addition, although the overall homology to the *E. coli* GlxI enzyme is lower, it is believed that the indicated sequences from the Enterococci and Streptococci encode GlxI. It would be of interest to express a representative of this grouping to confirm it is in fact a glyoxalase I sequence, and to determine its metal activation.

As previously mentioned it is essential to temper predictions based on sequence analysis with experimental results. It would be too easy to draw incorrect conclusions based on sequence alignments alone, with these GlxI sequences being a perfect example. Without the crystal structure data one may not have identified the first metal ligand as it is not universally conserved among the known and postulated GlxI sequences, being a Gln in *H. sapiens* GlxI versus a His in the *E. coli* enzyme. In addition, activation of the *E. coli*, *Y.*

pestis, and *P. aeruginosa* GlxI enzymes with Ni^{2+} would not have been predicted based on sequence analyses alone.

CHAPTER 6

SUMMARY AND FUTURE WORK

6.1 Summary

The glyoxalase system functions to remove cytotoxic methylglyoxal from the cell. The first enzyme in this system, glyoxalase I, has been of increased interest of late due to its potential as a novel drug target. Selective inhibition of GlxI could take advantage of the toxic effects of MG accumulation. This selective targeting of GlxI is beginning to show some promise in the area of anticancer research.

Although the glyoxalase system was identified 87 years ago, many aspects are still unknown. Recent crystallographic studies on *H. sapiens* GlxI have allowed for the identification of the ligands to the catalytic metal and led to a postulated reaction mechanism. GlxI has also recently been identified as a member of a structural superfamily composed of βαββββ motifs. To improve our knowledge of glyoxalase I and to identify any differences in the enzyme from a bacterial source, our studies have focused on GlxI from *E. coli*. These analyses have greatly enhanced our knowledge of the kinetics, structural features, and metal binding characteristics of this enzyme and have permitted the identification of other GlxI enzymes, as outlined below.

6.1.1 Kinetic Analyses and Metal Binding Characteristics

Kinetic studies have demonstrated that *E. coli* GlxI is maximally active with Ni^{2+} and with the following metals, each to a lower level of activity, Co^{2+}, Mn^{2+}, Fe^{2+}, and Cd^{2+}. No activity was observed in the presence of Zn^{2+}, Cu^{2+}, Mg^{2+}, or Ca^{2+}. Metal competition experiments using the change in enzymatic activity as a measure of the possible exchange in bound metal suggested that both Ni^{2+} and Zn^{2+} are stably bound to the enzyme, whereas metals such as Mn^{2+} and to a lesser extent Co^{2+} appear to exchange more rapidly with the competing metal. The apparent rate of exchange was dependent upon the amount of excess competing metal and the temperature at which the competition was occurring, in addition to the identities of the bound and competing metals.

Metal analysis was performed on the enzyme following reconstitution with each metal. Inductively coupled plasma analysis indicated that each of the activating metals, in addition to Zn^{2+} and Cu^{2+}, bind to the enzyme with a ratio of one mole of metal per mole of dimeric enzyme. Ca^{2+} and Mg^{2+} did not appear to bind to *E. coli* GlxI. Isothermal titration calorimetry confirmed these findings regarding the amount of bound metal. In addition ITC provided information regarding the thermodynamics of the interaction between apoGlxI and each metal. The metals were found to have a binding affinity (K_a) at the limits of detection ($>10^7$-10^8 M^{-1}) with the exception of Mn^{2+}, which had a weaker affinity of 3.9×10^6 M^{-1}. The thermal stability of GlxI was found to increase significantly upon addition of divalent metals, as determined by differential scanning calorimetry. Zn^{2+}-GlxI had a T_m 21°C higher than the apoenzyme, while the T_m of Ni^{2+}-GlxI was 17°C higher than the apoenzyme.

Electrospray mass spectrometry on non-covalent complexes of apoGlxI with several glutathione-based inhibitors as well as with a transition state analogue indicated that there are two possible binding sites on the enzyme. It is speculated based on the metal binding studies that perhaps only one active site may be functional. Combined with standard solution kinetic analysis on the level of inhibition imparted by these analogues, the transition state analogue and a vinyl-glutathione analogue were identified as the most potent *E. coli* GlxI inhibitors, and those with the greatest affinity based on the ESMS analysis.

6.1.2 Structural Studies and Metal Environment

Using ^{113}Cd NMR, EPR, and EXAFS analyses we have determined that the metal in the active site of *E. coli* GlxI is coordinated by five to six oxygen and nitrogen ligands. Expanding these studies to crystallographic analysis of the enzyme with various metal ions bound identified the protein residues that are involved in metal ligation. They are His5, Glu56, His74 and Glu122. Furthermore these studies indicated a clear correlation between the catalytic activity of the enzyme and the metal coordination. Each of the metal ions which produces an enzymatically active enzyme, Ni^{2+}, Co^{2+}, Mn^{2+}, and Cd^{2+}, has an octahedral geometry, with four ligands from the protein and two water molecules acting as ligands. In contrast, Zn^{2+} in the inactive form of the enzyme has only five ligands, the same four protein residues but only one water ligand, forming a trigonal bipyramidal coordination. *H. sapiens* GlxI, which contains Zn^{2+} in its active form, also appears to have an octahedral metal

coordination environment. These findings suggest than an octahedral coordination is essential for activity to either correctly position Glu122 (Glu173 in the *H. sapiens* enzyme) to function as a catalytic base or because two bound water molecules are important in some way in the reaction.

The finding that each of the two active sites in the protein crystal structure contains a metal ion contrasts with the observation that the *E. coli* GlxI enzyme is maximally active with only one metal ion. It is postulated that the high protein and hence metal concentrations utilized in the protein crystallization could account for this difference. If the second binding site has a much lower affinity the metal ions may not bind under the conditions in the metal analysis, titration, and kinetic analyses.

We have also successfully cocrystallized *E. coli* Ni^{2+}- and Zn^{2+}-GlxI with a GSH-based inhibitor and our transition state analogue. Upon solution of the diffraction data we should have more insights into the postulated mechanism of the catalyzed reaction. This information can be utilized to guide further investigations.

6.1.3 E. coli Glyoxalase I Variants

To aid in the solution of the x-ray structure of *E. coli* GlxI, the selenomethionine form of the protein was expressed, in which methionine 1, 7, and 26 were replaced with SeMet. This enzyme exhibited similar metal activation properties, however the enzyme reconstituted with Ni^{2+} was only 70% as active as the native enzyme. It is speculated that the proximity of SeMet7 to the active site may slightly perturb the metal ligands.

The first ligand to the essential metal, His5 in *E. coli* GlxI, was mutated to a glutamine, as found in the *H. sapiens* enzyme. Rather unexpectedly, the affinity of the protein for all metals was drastically reduced. Furthermore, activity was detected in the presence of Zn^{2+}, although the levels were extremely low and still much less than the activity seen with either Ni^{2+} or Co^{2+}. Evidently the change in this ligand to a histidine in the *E. coli* enzyme is not the sole factor determining the activation with Ni^{2+}, but it does influence the metal binding and activation. This was not predicted to be the determining feature as both the *P. putida* and *S. cerevisiae* GlxI enzymes are active with Zn^{2+} yet have the histidine ligand found in the *E. coli* enzyme. The drastic change in the metal affinity suggests that something within the enzyme active site has been perturbed. The affinity for the metal ions appears so weak

that it is unlikely a metal-bound form of the enzyme could be crystallized for examination of the active site metal environment.

6.1.4 Identification and Analysis of Other Glyoxalase I Sequences

Numerous putative glyoxalase I enzymes have been identified through extensive searches of the National Center for Biotechnology Information database, including the databases of unfinished genome sequences. Through analysis of these sequences and those known to encode functional GlxI enzymes, consistent alterations in the bacterial GlxI sequences compared to the *H. sapiens* GlxI enzyme were identified. With the elucidation of the crystal structure of *E. coli* GlxI, comparisons could be made with the *H. sapiens* GlxI structure. Combining this information we were able to identify the effects of the sequence alterations in the bacterial GlxI sequences. Most notable was the more open active site in the *E. coli* enzyme due to the absence of a region encoding an α-helix forming one side of the active site in the *H. sapiens* enzyme. These changes may explain the differences observed in the effectiveness of various glutathione-based inhibitors. Several of these analogues, which are potent inhibitors of the *H. sapiens* or *S. cerevisiae* GlxI enzymes, are not effective against *E. coli* GlxI, as determined here by IC_{50} measurements and the relative affinity as determined by analysis of non-covalent complexes by mass spectrometry.

Two of the putative GlxI sequences identified have been expressed and preliminary characterization of the proteins performed. The DNA predicted to encode GlxI proteins from *Yersinia pestis* and *Pseudomonas aeruginosa* does in fact encode enzymes with glyoxalase I activity based on kinetic analysis. Furthermore, preliminary studies on the crude proteins appear to indicate that these enzymes are active with Ni^{2+} but not Zn^{2+}, as seen for the *E. coli* enzyme. This is another intriguing development in GlxI research. This unexpected metal activation now observed in three glyoxalase I enzymes warrants further analysis to determine the factors affecting this metal selectivity.

6.2 Future Directions in Glyoxalase I Research

Our interest in GlxI is currently focused on the unusual metal activation and the details of the reaction mechanism. With the improved knowledge of *E. coli* GlxI provided in this work, and the identification of other GlxI enzymes, several additional questions remain unanswered and new questions have arisen.

6.2.1 Mutagenesis

Metal Ligands

Further analysis of the ligands to the essential metal may provide more information, not only on the reaction mechanism but perhaps the metal activation. Complementary mutations in the metal ligands, such as His5→Glu and Glu122→His would retain the same type of metal ligands yet place the putative catalytic glutamate in a different location. If the enzyme bound metal but displayed no catalytic activity it could imply that Glu122 plays a role in catalysis. Mutation of Glu122→Gln may also prove interesting to further examine the possible role of this ligand in the reaction. In each case the amount of bound metal must be determined. Conclusions on the reaction mechanism can not be made if the lack of catalytic activity is due to absence of a metal ion.

Substrate Binding

Mutation of residues postulated to play a role in substrate binding could also be informative. Upon completion of the structure of the enzyme with various inhibitors bound, residues that may be important in binding can be identified and their role explored further.

Insertion Mutations

The identification of several regions in the *H. sapiens* GlxI enzyme, not present in the *E. coli* enzyme begs the question as to the function or role of these regions in the other enzymes. It is possible that the absence of these regions may cause subtle changes in the protein structure resulting in the altered response to metal ions and GSH-based inhibitors, not evident from initial examination of the structures. The most obvious is the absence of region 2, which encodes an α-helix at the back of the active site of the *H. sapiens* enzyme (Chapters

3 and 5). Additionally omission of regions 3 and 4 may result in subtle perturbations of the protein structure. The absence of the N-terminal arm in the bacterial enzymes is not expected to be a critical difference. Although this arm wraps around the adjacent subunit in the *H. sapiens* structure, it does not interact with this subunit and is not expected to have a significant effect on the enzyme structure, activity, or stability.

To determine the influence of these regions on the response of the enzyme to various metals and GSH-analogues, these regions could be added to the *E. coli* GlxI sequence and the modified protein analyzed. Several reports are available describing techniques utilizing PCR to insert or delete segments of DNA (Grandori et al., 1997; Wang and Malcolm, 1999). Any possible effect on the enzyme active site could be analyzed by comparing the kinetics of the wild-type enzyme and these insertional mutant forms. Substrate analogues, such as phenylglyoxal could be tested as well as the level of enzyme inhibition with various GSH-based inhibitors to probe the enzyme active site.

6.2.2 Mechanistic Experiments

Substrate Stereoselectivity

NMR analyses have indicated that GlxI accepts both isomers of the hemiacetal substrate (Griffis et al., 1983; Creighton et al., 1988; Landro et al., 1992; Rae et al., 1994). These studies however were performed on GlxI from yeast and porcine erythrocyte. Although we have presumed this would not have changed, GlxI from *E. coli* may not behave in the same manner. To confirm *E. coli* GlxI is similar to other GlxI enzymes in this respect a similar experiment should be performed in which a stereochemically "locked" substrate such as *R*- and *S*-glutathiolactaldehyde are synthesized and utilized as the substrate in the reaction, while monitoring the conversion to glutathiohydroxyacetone by ^{1}H NMR.

Furthermore, it should also be reconfirmed that *E. coli* GlxI follows a reaction that proceeds through an enediol intermediate rather than a hydride shift mechanism. Monitoring the incorporation of deuterium from the media into the product of the reaction would confirm this aspect of the reaction.

Mutagenesis

As described, it would be beneficial to perform site-directed mutagenesis experiments on the metal ligands, to determine their effect not only on metal binding but also any role in the reaction itself.

Cocrystallization

Completion of the analysis of the x-ray diffraction data of Ni^{2+}- and Zn^{2+}-GlxI cocrystallized with GSH-based inhibitors and our putative transition state analogue should provide a clue as to whether the reaction in *E. coli* GlxI proceeds as postulated based on studies with *H. sapiens* GlxI. Once this data is analyzed, further crystallization experiments can be planned if required.

6.2.3 Metal Binding

Binding Affinity

Equilibrium dialysis can be employed to further examine the metal binding properties of *E. coli* GlxI. The binding affinities of various metals were determined for *H. sapiens* GlxI using equilibrium dialysis in which nitrilotriacetic acid was used as a metal chelator in order to establish low levels of the metal under analysis (Sellin and Mannervik, 1984). Alternatively, surface plasmon resonance could prove useful for determination of both the association and dissociation rate constant for the binding of each metal to the enzyme (Szabo et al., 1995).

Natural Metal

Determination of the metal ion in *E. coli* GlxI in a natural setting is of great interest. However, this is a difficult task. When the cells producing *E. coli* GlxI are grown in the presence of supplemental Ni^{2+}, the activity of the enzyme is increased, as is the amount of bound metal. This implies that the Ni^{2+} is transported into the cell and incorporated into the protein. Growth in the presence of ^{63}Ni would confirm this observation. Unfortunately this does not prove that the natural metal is Ni^{2+}, just that the enzyme can utilize Ni^{2+} when available.

If the media is not supplemented, the enzyme produced contains a variety of different metal ions at trace levels, including Zn, Ni, Cu, and Fe (Clugston, 1997). Even without supplementation there is a supply of metal from the media, and even the glass flask used in the cell growth would provide metal ions. As such, if the enzyme is grown in a laboratory setting the metal found in the enzyme active site may be the result of the artificial conditions under which it was grown. *E. coli* grown in a natural environment, such as an individual infected with a bacterial infection could provide a source of GlxI containing the naturally occurring metal. However, it may be difficult to obtain sufficient quantities of the enzyme, as the levels of GlxI normally in a cell are quite low. A previous study indicated that from 12 L of *E. coli* MG1655 cell growth 1 μg of GlxI was isolated (Barnard, 1997). It may be that *E. coli* GlxI uses several different metal ions as long as the enzyme is active and can remove toxic methylglyoxal.

APPENDIX A

INDUCTIVELY COUPLED PLASMA ANALYSES

The following tables supplied by the Solutions Analytical Laboratory (formerly Water Quality Lab), list the results from the inductively coupled analyses on the *E. coli* GlxI under the indicated conditions. The reference tested for each sample was 50 mM MOPS, pH 7.0 ± 10 % glycercol, matching the protein storage buffer, treated in the same manner as the protein. See Chapter 2 for details of the enzyme preparation for metal analysis.

Table A.1: Determination of the amount of metal incorporated into *E. coli* GlxI during protein expression with a variation in the metal added to the growth media

Analysis:		Al	As	B	Be	Ca	Cd	Co	Cr
Method:		ICP	ICP	ICP	ICP	ICP	ICP	ICP	ICP
Det. Limit:		0.20	0.10	0.02	0.02	0.05	0.02	0.10	0.02
Sample Name	WQL#	mg/L	mg/L	mg/L	mg/L	mg/L	mg/L	mg/L	mg/L
Reference #1	AOG001	<DL	<DL	0.18	<DL	<DL	<DL	<DL	<DL
Sample#1	AOG002	<DL	<DL	0.18	<DL	0.05	<DL	<DL	<DL
Reference #2	AOG003	<DL	<DL	0.09	<DL	<DL	<DL	<DL	<DL
Sample #2	AOG004	<DL	<DL	0.09	<DL	0.05	<DL	<DL	<DL

Analysis:		Cu	Fe	Hg	Mg	Mn	Mo	Na	Ni
Method:		ICP	ICP	ICP	ICP	ICP	ICP	ICP	ICP
Det. Limit:		0.02	0.10	1.00	0.05	0.05	0.10	0.50	0.05
Sample Name	WQL#	mg/L	mg/L	mg/L	mg/L	mg/L	mg/L	mg/L	mg/L
Reference #1	AOG001	<DL	<DL	<DL	<DL	<DL	<DL	606	<DL
Sample#1	AOG002	0.06	<DL	<DL	<DL	<DL	<DL	596	0.30
Reference #2	AOG003	<DL	<DL	<DL	<DL	<DL	<DL	223	<DL
Sample #2	AOG004	0.06	<DL	<DL	<DL	<DL	<DL	198	<DL

Analysis:		Pb	Se	Si	Sr	Ti	V	Zn	
Method:		ICP	ICP	ICP	ICP	ICP	ICP	ICP	
Det. Limit:		0.50	0.50	0.10	0.02	0.02	0.10	0.02	
Sample Name	WQL#	mg/L	mg/L	mg/L	mg/L	mg/L	mg/L	mg/L	
Reference #1	AOG001	<DL	<DL	1.51	<DL	<DL	<DL	<DL	
Sample#1	AOG002	<DL	<DL	1.52	<DL	<DL	<DL	0.43	
Reference #2	AOG003	<DL	<DL	0.71	<DL	<DL	<DL	<DL	
Sample #2	AOG004	<DL	<DL	0.68	<DL	<DL	<DL	1.63	

Sample	Water Quality Lab (WQL) ID Code	[Protein] (μM)
1. $NiCl_2$ in cell growth	AOG002	14
2. $ZnCl_2$ in cell growth	AOG004	50
Both purified to Pre-IEF		

Note: Na and K are from the buffer itself due to pH adjustments and Chelex treatment. Si was sometimes detected in the samples and is most likely from the glass syringe utilized during sample dilution by the WQL.

Table A.2: Determination of the amount of metal bound to *E. coli* GlxI following addition of zinc chloride to the apoenzyme.

Analysis:		Al	As	B	Ba	Ca	Cd	Co	Cr
Method:		ICP	ICP	ICP	ICP	ICP	ICP	ICP	ICP
Det. Limit:		0.20	0.10	0.02	0.01	0.05	0.02	0.10	0.02
Sample Name	WQL#	mg/L	mg/L	mg/L	mg/L	mg/L	mg/L	mg/L	mg/L
Reference #1	AQH001	<DL	<DL	0.09	<DL	<DL	<DL	<DL	<DL
Sample #1	AQH002	<DL	<DL	0.09	<DL	<DL	<DL	<DL	<DL

Analysis:		Cu	Fe	K	Mg	Mn	Mo	Na	Ni
Method:		ICP	ICP	ICP	ICP	ICP	ICP	ICP	ICP
Det. Limit:		0.02	0.10	1.00	0.05	0.05	0.10	0.50	0.05
Sample Name	WQL#	mg/L	mg/L	mg/L	mg/L	mg/L	mg/L	mg/L	mg/L
Reference #1	AQH001	<DL	<DL	<DL	<DL	<DL	<DL	464	<DL
Sample #1	AQH002	0.02	<DL	12.1	<DL	<DL	<DL	460	<DL

Analysis:		Pb	Se	Si	Sr	Ti	V	Zn	
Method:		ICP	ICP	ICP	ICP	ICP	ICP	ICP	
Det. Limit:		0.50	0.50	0.10	0.02	0.02	0.10	0.02	
Sample Name	WQL#	mg/L	mg/L	mg/L	mg/L	mg/L	mg/L	mg/L	mg/L
Reference #1	AQH001	<DL	3.09	0.71	<DL	<DL	<DL	<DL	
Sample #1	AQH002	<DL	2.94	0.87	<DL	<DL	<DL	1.3835	

Sample	Water Quality Lab (WQL) ID Code	[Protein] (μM)
1. ApoGlxI + $ZnCl_2$	AQH002	26

Table A.3: Determination of the amount of metal bound to *E. coli* GlxI following addition of cadmium or cobalt chloride to the apoenzyme.

Analysis:		Al	As	B	Ba	Ca	Cd	Co	Cr
Method:		ICP	ICP	ICP	ICP	ICP	ICP	ICP	ICP
Det. Limit:		0.20	0.20	0.02	0.01	0.05	0.02	0.10	0.02
Sample Name	WQL#	mg/L	mg/L	mg/L	mg/L	mg/L	mg/L	mg/L	mg/L
98/8/25									
Reference #1	ARP001	<DL	<DL	0.10	<DL	<DL	<DL	<DL	<DL
Sample #1	ARP002	<DL	<DL	0.08	<DL	<DL	3.06	<DL	<DL
Reference #2	ARP003	<DL	<DL	<DL	<DL	0.08	<DL	<DL	<DL
Sample #2	ARP004	<DL	<DL	0.06	<DL	<DL	<DL	1.72	<DL

Analysis:		Cu	Fe	K	Mg	Mn	Mo	Na	Ni
Method:		ICP	ICP	ICP	ICP	ICP	ICP	ICP	ICP
Det. Limit:		0.02	0.10	1.00	0.05	0.05	0.10	0.50	0.05
Sample Name	WQL#	mg/L	mg/L	mg/L	mg/L	mg/L	mg/L	mg/L	mg/L
98/8/25									
Reference #1	ARP001	<DL	<DL	43.0	<DL	<DL	<DL	723	<DL
Sample #1	ARP002	0.03	<DL	31.2	<DL	<DL	<DL	492	<DL
Reference #2	ARP003	<DL	<DL	142	0.05	<DL	<DL	276	<DL
Sample #2	ARP004	<DL	<DL	390	<DL	<DL	<DL	294	<DL

Analysis:		Pb	Se	Si	Sr	Ti	V	Zn	
Method:		ICP	ICP	ICP	ICP	ICP	ICP	ICP	
Det. Limit:		0.50	0.50	0.10	0.02	0.02	0.10	0.02	
Sample Name	WQL#	mg/L	mg/L	mg/L	mg/L	mg/L	mg/L	mg/L	mg/L
98/8/25									
Reference #1	ARP001	<DL	3.58	1.02	<DL	<DL	<DL	<DL	
Sample #1	ARP002	<DL	3.60	0.83	<DL	<DL	<DL	0.04	
Reference #2	ARP003	<DL	3.20	0.43	<DL	<DL	<DL	2.85	
Sample #2	ARP004	<DL	3.77	0.63	<DL	<DL	<DL	0.21	

Sample	Water Quality Lab (WQL) ID Code	[Protein] (μM)
1. ApoGlxI + $CdCl_2$	ARP002	29
2. ApoGlxI + $CoCl_2$	ARP004	37

Table A.4: Determination of the amount of metal bound to *E. coli* GlxI following addition of copper, manganese, calcium, or magnesium chloride to the apoenzyme.

Analysis:		Al	As	B	Ba	Ca	Cd	Co	Cr
Method:		ICP	ICP	ICP	ICP	ICP	ICP	ICP	ICP
Det. Limit:		0.20	0.10	0.02	0.01	0.05	0.02	0.10	0.02
Sample Name	SAL#	mg/L	mg/L	mg/L	mg/L	mg/L	mg/L	mg/L	mg/L
MOPS Reference	BFD001	<DL	<DL	<DL	0.02	<DL	<DL	<DL	<DL
Cu-GlxI #1	BFD002	<DL	<DL	<DL	0.01	0.08	<DL	<DL	<DL
Mn-GlxI #2	BFD003	<DL	<DL	<DL	0.01	0.13	<DL	<DL	<DL
Ca-GlxI #3	BFD004	<DL	<DL	<DL	<DL	0.10	<DL	<DL	<DL
Mg-GlxI #4	BFD005	<DL	<DL	<DL	0.01	0.10	<DL	<DL	<DL

Analysis:		Cu	Fe	K	Li	Mg	Mn	Mo	Na
Method:		ICP	ICP	ICP	ICP	ICP	ICP	ICP	ICP
Det. Limit:		0.02	0.10	1.00	0.05	0.05	0.05	0.10	0.50
Sample Name	SAL#	mg/L	mg/L	mg/L	mg/L	mg/L	mg/L	mg/L	mg/L
MOPS Reference	BFD001	<DL	<DL	1150	<DL	<DL	<DL	<DL	9.22
Cu-GlxI #1	BFD002	2.16	<DL	1110	<DL	<DL	<DL	<DL	24.2
Mn-GlxI #2	BFD003	0.04	<DL	1100	<DL	0.05	1.17	<DL	21.7
Ca-GlxI #3	BFD004	0.06	<DL	1070	<DL	<DL	<DL	<DL	22.5
Mg-GlxI #4	BFD005	0.06	<DL	1140	<DL	<DL	<DL	<DL	22.2

Analysis:		Ni	P	Pb	S	Se	Si	Sr	Zn
Method:		ICP	ICP	ICP	ICP	ICP	ICP	ICP	ICP
Det. Limit:		0.05	1.00	0.50	0.90	0.50	0.10	0.02	0.02
Sample Name	SAL#	mg/L	mg/L	mg/L	mg/L	mg/L	mg/L	mg/L	mg/L
MOPS Reference	BFD001	<DL	<DL	<DL	1790	<DL	0.11	<DL	<DL
Cu-GlxI #1	BFD002	<DL	<DL	<DL	1750	<DL	0.13	<DL	0.08
Mn-GlxI #2	BFD003	<DL	<DL	<DL	1770	<DL	0.13	<DL	0.09
Ca-GlxI #3	BFD004	<DL	<DL	<DL	1760	<DL	0.14	<DL	0.20
Mg-GlxI #4	BFD005	<DL	<DL	<DL	1850	<DL	0.16	<DL	0.18

Sample	Solutions Analytical Lab (SAL) ID Code	[Protein] (μM)
1. ApoGlxI + $CuCl_2$	BFD002	27
2. ApoGlxI + $MnCl_2$	BFD003	25
3. ApoGlxI + $CaCl_2$	BFD004	27
4. ApoGlxI + $MgCl_2$	BFD005	25

Table A.5: Determination of the effect of Chelex treatment on the amount of metal bound to *E. coli* GlxI reconstituted with nickel chloride. Metal analysis on standard LB_{Amp} media is also presented.

Analysis:		Al	As	B	Ba	Ca	Cd	Co	Cr
Method:		ICP	ICP	ICP	ICP	ICP	ICP	ICP	ICP
Det. Limit:		0.20	0.10	0.02	0.01	0.05	0.02	0.10	0.02
Sample Name	SAL#	mg/L	mg/L	mg/L	mg/L	mg/L	mg/L	mg/L	mg/L
LB Amp	BCY001	<DL	<DL	0.03	0.06	3.06	<DL	<DL	<DL
Reference A	BCY002	<DL	<DL	<DL	<DL	<DL	<DL	<DL	<DL
Reference B	BCY003	<DL	<DL	<DL	<DL	0.08	<DL	<DL	<DL
Sample A	BCY004	<DL	<DL	<DL	<DL	<DL	<DL	<DL	<DL
Sample B	BCY005	<DL	<DL	<DL	0.01	4.99	<DL	<DL	<DL

Analysis:		Cu	Fe	K	Li	Mg	Mn	Mo	Na
Method:		ICP	ICP	ICP	ICP	ICP	ICP	ICP	ICP
Det. Limit:		0.02	0.10	1.00	0.05	0.05	0.05	0.10	0.50
Sample Name	SAL#	mg/L	mg/L	mg/L	mg/L	mg/L	mg/L	mg/L	mg/L
LB Amp	BCY001	0.03	0.41	366	<DL	3.283	<DL	<DL	2570
Reference A	BCY002	<DL	<DL	3.34	<DL	<DL	<DL	<DL	645
Reference B	BCY003	<DL	<DL	796	<DL	<DL	<DL	<DL	169
Sample A	BCY004	0.04	<DL	9.94	<DL	<DL	<DL	<DL	591*
Sample B	BCY005	0.06	<DL	881*	<DL	<DL	<DL	<DL	184*

Analysis:		Ni	P	Pb	S	Se	Si	Sr	Zn
Method:		ICP	ICP	ICP	ICP	ICP	ICP	ICP	ICP
Det. Limit:		0.05	1.00	0.50	0.90	0.50	0.10	0.02	0.02
Sample Name	SAL#	mg/L	mg/L	mg/L	mg/L	mg/L	mg/L	mg/L	mg/L
LB Amp	BCY001	<DL	178	<DL	111	<DL	2.47	0.02	0.68
Reference A	BCY002	<DL	<DL	<DL	1640	<DL	0.65	<DL	<DL
Reference B	BCY003	<DL	<DL	<DL	1640	<DL	0.66	<DL	<DL
Sample A	BCY004	1.73	<DL	<DL	1530*	<DL	0.70	<DL	0.14
Sample B	BCY005	2.46	<DL	<DL	1110*	<DL	0.71	<DL	0.28

Sample	Water Quality Lab (WQL) ID Code	[Protein] (μM)
A. ApoGlxI + $NiCl_2$ Ran over Chelex resin	BCY004	26
B. ApoGlxI + $NiCl_2$ No Chelex treatment	BCY005	35

Table A.6: Further determination of the effect of Chelex treatment on the amount of metal bound to *E. coli* GlxI, which had been reconstituted with nickel chloride then concentrated with a Centricon (YM10), as performed in the preparation of the enzyme samples for EXAFS analyses. The levels of metal present in the buffer utilized for EXAFS analyses (50 mM MOPS, 25% glycerol pH 7.0 with tetraethyl ammonium hydroxide) is also presented.

Analysis:		Al	As	B	Ba	Ca	Cd	Co	Cr
Method:		ICP	ICP	ICP	ICP	ICP	ICP	ICP	ICP
Det. Limit:		1.00	0.50	0.10	0.05	0.25	0.10	0.50	0.10
Sample Name	SAL#	mg/L	mg/L	mg/L	mg/L	mg/L	mg/L	mg/L	mg/L
Sample #1	BER001	<DL	<DL	<DL	<DL	<DL	<DL	<DL	<DL
Sample #2	BER002	<DL	<DL	<DL	<DL	<DL	<DL	<DL	<DL
EXAFS Buffer	BER003	<DL	<DL	<DL	0.05	0.31	<DL	<DL	<DL
MOPS Reference	BER004	<DL	<DL	<DL	<DL	<DL	<DL	<DL	<DL

Analysis:		Cu	Fe	K	Li	Mg	Mn	Mo	Na
Method:		ICP	ICP	ICP	ICP	ICP	ICP	ICP	ICP
Det. Limit:		0.10	0.50	5.00	0.25	0.25	0.25	0.50	2.50
Sample Name	SAL#	mg/L	mg/L	mg/L	mg/L	mg/L	mg/L	mg/L	mg/L
Sample #1	BER001	<DL	<DL	1250	<DL	0.44	<DL	<DL	3.96
Sample #2	BER002	<DL	<DL	1210	<DL	<DL	<DL	<DL	<DL
EXAFS Buffer	BER003	<DL	<DL	<DL	<DL	<DL	<DL	<DL	7.63
MOPS Reference	BER004	<DL	<DL	1070	<DL	<DL	<DL	<DL	<DL

Analysis:		Ni	P	Pb	S	Se	Si	Sr	Zn
Method:		ICP	ICP	ICP	ICP	ICP	ICP	ICP	ICP
Det. Limit:		0.25	5.00	2.50	4.50	2.50	0.50	0.10	0.10
Sample Name	SAL#	mg/L	mg/L	mg/L	mg/L	mg/L	mg/L	mg/L	mg/L
Sample #1	BER001	1.44	<DL	<DL	1600	<DL	<DL	<DL	<DL
Sample #2	BER002	1.67	<DL	<DL	1600	<DL	<DL	<DL	0.13
EXAFS Buffer	BER003	<DL	<DL	<DL	1490	<DL	<DL	<DL	1.37
MOPS Reference	BER004	<DL	<DL	<DL	1500	<DL	<DL	<DL	<DL

Sample	Solutions Analytical Lab (SAL) ID Code	[Protein] (μM)
1. ApoGlxI + $NiCl_2$ Concentrated with a Centricon 10, ran over Chelex resin, and diluted	BER001	24
2. ApoGlxI + $NiCl_2$ As above but no Chelex treatment	BER002	24

Table A.7: Determination of the amount of metal bound to *E. coli* SeMet-GlxI following substitution of the apoenzyme with nickel chloride.

Sample Name	Code	Al	As	B	Ba	Be	Ca
MOPS Ref. 09/15/00	BIF001	<DL	<.168	0.018*	0.003*	<DL	0.074
SeMet Glx1 09/15/00	BIF002	<DL	<.168	0.024*	0.02*	<DL	3.84

Sample Name	Code	Cd	Ce	Co	Cr	Cu	Fe
MOPS Ref. 09/15/00	BIF001	<DL	<DL	<DL	<DL	0.009	<DL
SeMet Glx1 09/15/00	BIF002	<DL	<DL	<DL	<DL	0.04	<DL

Sample Name	Code	K	Li	Mg	Mn	Mo	Na
MOPS Ref. 09/15/00	BIF001	1000	<DL	0.008	0.022	<DL	62.5
SeMet Glx1 09/15/00	BIF002	1020	<DL	0.05	0.007	<DL	63.7

Sample Name	Code	Ni	P	Pb	S	Sb	Se
MOPS Ref. 09/15/00	BIF001	<DL	<DL	<DL	1590	<DL	<DL
SeMet Glx1 09/15/00	BIF002	0.768	<DL	<DL	1620	<DL	4.9

Sample Name	Code	SiO2	Sn	Sr	Ti	Tl	V
MOPS Ref. 09/15/00	BIF001	0.395	<DL	<DL	<DL	<DL	<DL
SeMet Glx1 09/15/00	BIF002	0.638	<DL	<DL	<DL	<DL	<DL

Sample Name	Code	Zn
MOPS Ref. 09/15/00	BIF001	<DL
SeMet Glx1 09/15/00	BIF002	0.297

Notes:

Concentrations reported in mg/L.
Samples diluted 1:2.
A white suspension formed in BIF002 soon after acidification with HNO3.
* denotes concentrations near detection limit.

Sample	Solutions Analytical Lab (SAL) ID Code	[Protein] (μM)
1. SeMet-GlxI	BIF002	12

Table A.8: Determination of the amount of metal bound to the H5Q mutant *E. coli* GlxI protein following purification. This provides confirmation that the enzyme is metal-free after isoelectric focusing, as observed for the wild-type enzyme.

Sample	Code	Al	As	B	Ba	Be	Ca
Ref. Buffer	BGB001	<detect.	<detect.	<detect.	<detect.	<detect.	0.938
H5Q Mutant	BGB002	<detect.	<detect.	<detect.	<detect.	<detect.	0.188

Sample	Code	Cd	Ce	Co	Cr	Cu	Fe
Ref. Buffer	BGB001	<detect.	<detect.	<detect.	<detect.	<detect.	<detect.
H5Q Mutant	BGB002	<detect.	<detect.	<detect.	<detect.	<detect.	0.042

Sample	Code	K	Li	Mg	Mn	Mo	Na
Ref. Buffer	BGB001	1040	<detect.	0.001	<detect.	<detect.	83.4
H5Q Mutant	BGB002	1100	<detect.	0.005	<detect.	<detect.	15.7

Sample	Code	Ni	P	Pb	S	Sb	Se
Ref. Buffer	BGB001	<detect.	1.17	<detect.	1540	<detect.	<detect.
H5Q Mutant	BGB002	<detect.	<detect.	<detect.	1640	<detect.	<detect.

Sample	Code	SiO2	Sn	Sr	Ti	Tl	V
Ref. Buffer	BGB001	0.6	<detect.	<detect.	<detect.	<detect.	<detect.
H5Q Mutant	BGB002	0.673	<detect.	<detect.	<detect.	<detect.	<detect.

Sample	Code	Zn
Ref. Buffer	BGB001	<detect.
H5Q Mutant	BGB002	0.035

Notes:

All sample concentrations are in mg/L.

Sample	Solutions Analytical Lab (SAL) ID Code	[Protein] (μM)
1. Apo H5Q GlxI	BGB002	34

APPENDIX B

ELECTRON PARAMAGNETIC RESONANCE

The following sample plot and listing of the typical settings for the EPR analysis on *E. coli* Mn^{2+}-GlxI were provided by Dr. G. D. Markham.

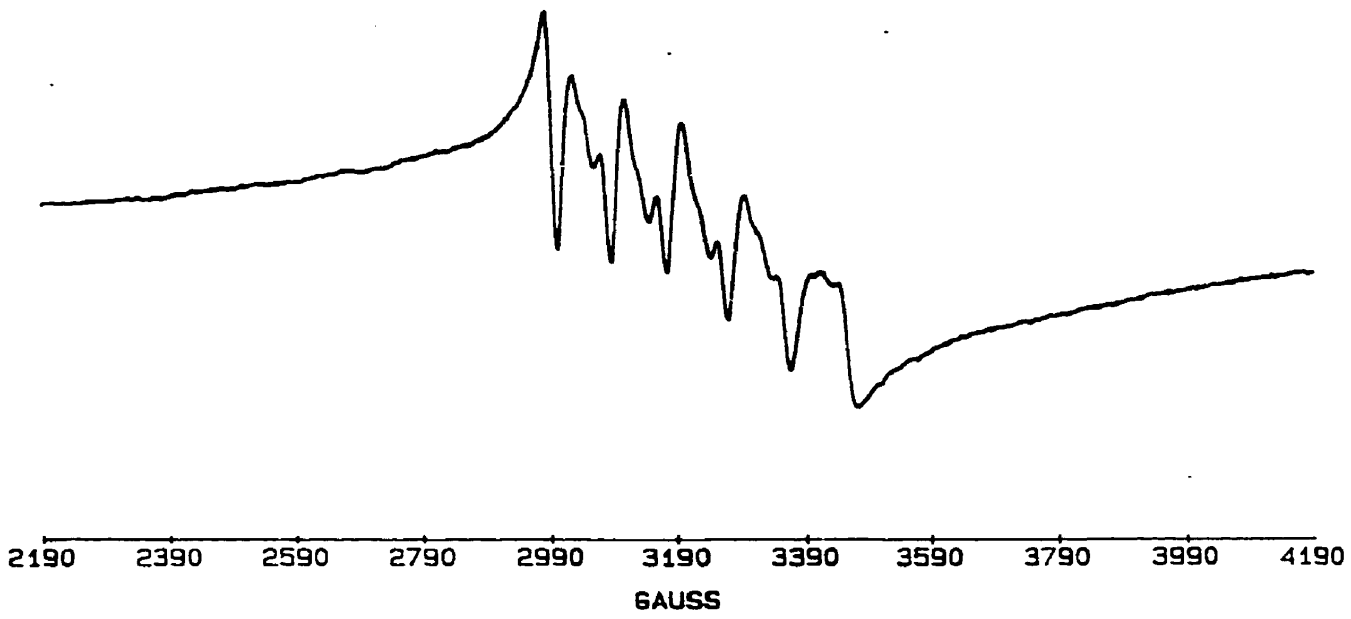

Figure B.1: EPR spectra of *E. coli* Mn^{2+}-GlxI. The sample was run in a 3 mm capillary tube with the following settings: Microwave Frequency = 9 GHz; Modulation Amplitude = 5; Temperature = -130°C.

APPENDIX C

EXTENDED X-RAY ABSORPTION FINE STRUCTURE

XAS data collection and analyses on *E. coli* GlxI reconstituted with Ni^{2+} and Zn^{2+} were performed by G. Davidson and Dr. M. J. Maroney at the University of Massachusetts. A summary of the data collection procedures and data fits are provided here. More details can be found elsewhere (Davidson et al., 2000a; Davidson et al., 2000b).

X-ray fluorescence data on frozen samples at 50 K were collected on beam line X9B at the National Synchrotron Light Source (2.8 GeV, 170 – 300 mA) with a Si[220] double crystal monochromator. The data were recorded using a 13-element Ge array detector (Canberra) and were calibrated to the first inflection points in metal foil spectra (Ni, 8331.6 eV, Zn, 9661.0 eV). The summed fluorescence data were then background corrected and normalized and the EXAFS fit using the program WinXAS (Ressler, 1997). XANES (x-ray absorption near-edge structure) data were obtained and analyzed as previously described (Colpas et al., 1991). EXAFS data were analyzed employing k^3-weighted Fourier-filtered data (FT limits = 2.0 – 12.5 $Å^{-1}$; Back-transform limits = 1.1 – 4.0 Å, uncorrected for phase shifts). Theoretical phases and amplitudes used in fitting the EXAFS for single and multiple scattering pathways were obtained from FEFF 6 calculations of crystallographically characterized model compounds (Rehr et al., 1992). Edge spectra monitored as a function of exposure time did not indicate any changes in the redox state or ligand environment of the metal sites during x-ray exposure.

The Ni K-edge XANES spectrum (Figure C.1) of *E. coli* GlxI reveals a small peak near 8332 eV assigned to a 1s→3d transition with an intensity (2.8(5) × 10^{-2} eV) that indicates a symmetric ligand environment. The absence of features associated with a 1s→4p_z transition rules out a four-coordinate planar geometry, indicating that the active site Ni is six-coordinate (Colpas et al., 1991). Analyses of the Ni K-edge EXAFS spectra are shown in Table C.1 and Figure C.1. Further information is available in the published article and supporting information (Davidson et al., 2000a). The supporting information contains a compilation of fits for Ni and Zn K-edge Fourier filtered EXAFS data for the *E. coli* GlxI samples. Data on

the analysis of *E. coli* GlxI with the TSA inhibitor and GSH-analogues bound has been submitted for publication (Davidson et al., 2000b).

Table C.1: Selected curve-fitting results of filtered EXAFS spectra for *E. coli* GlxI.[a]

Fit	*N* Ni-X	*R* (Å)	σ^2 (x 10^3 Å)[b]	GOF
Ni01	4 Ni - O	2.0691(2)	3.1	34.8
Ni02	1 Ni – O	1.9145(5)	0.2	29.2
	5 Ni – O	2.0827(2)	2.9	
Ni03	1 Ni – O	1.9138(5)	0.3	7.0
	5 Ni – O	2.0826(2)	2.9	
	2[Ni – C(His)]	2.9540(7) 3.246(2)	(5.4)	
	2[Ni – 2C/N(His)]	4.2052(9) 4.299(2)	(4.5)	
Ni04	1 Ni – O	1.9127(6)	1.5	5.8
	5 Ni – O	2.0813(2)	3.3	
	1 Ni – C	2.976(4)	6.1	
	2[Ni – 2C(His)]	2.9540(7) 3.277(2)	(5.4)	
	2[Ni – 2C/N(His)]	4.2052(9) 4.299(2)	(4.4)	
Zn01	4 Zn - O	1.9988(1)	8.5	38.5
Zn02	2 Zn – O	1.9022(2)	4.9	31.1
	3 Zn – O	2.0535(1)	4.0	
Zn03	2 Zn – O	1.9028(2)	5.2	8.9
	3 Zn – O	2.0523(1)	4.2	
	2[Zn – 2C(His)]	2.9962(4)	(8.2)	
		3.325(1)		
	2[Zn – 2C/N(His)]	4.2186(5) 4.521(2)	(*11.4*)	

[a] X is the scattering atom for each shell. *R* is the Ni-X distance. σ^2 is the root-mean-square disorder in the Ni-X distance. $GOF = 1/\sigma^2 \sum_{i=1}^{N} [y_{exp}(i) - y_{theo}(i)]^2$ (See Maroney et al., 1998). Accuracy of distances determined = ± 0.02 Å for atoms in the first coordination sphere of the meal and ±0.05 Å for second and third coordination sphere atoms. Precisions (indicated) are <0.02 Å for well-ordered shells; thus, differences are more accurate than the absolute distances.

[b] Italicized values are approaching physical insignificance. Large values of σ^2 indicate a coordination number that is too large or a badly disordered shell. Parentheses indicate that σ^2 for all atoms in that shell were constrained to a single value.

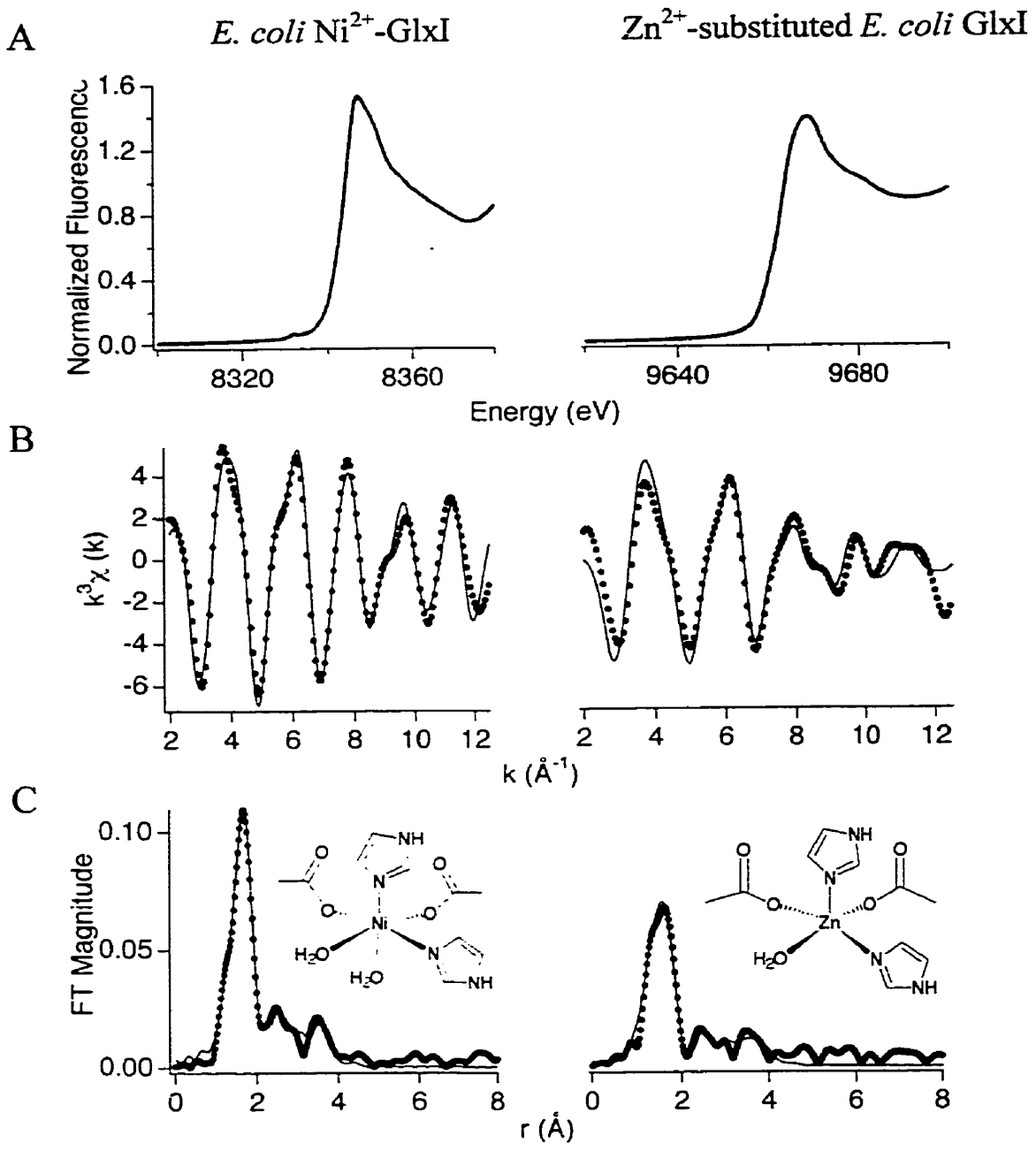

Figure C.1: Comparison of the Ni^{2+}- and Zn^{2+}-substituted *E. coli* GlxI metal sites. (A) Normalized Ni and Zn K-edges, (B) Fourier filtered (back-transform window, r = 1.1-4.0 Å) EXAFS, (C) Fourier transformed (k = 2-12.5 $Å^{-1}$) EXAFS. Data are shown as solid circles and the best fits as solid lines. r is uncorrected for phase shifts.

APPENDIX D

E. COLI GLYOXALASE I PROTEIN CRYSTALLOGRAPHY

The *E. coli* GlxI protein crystal structures were solved by Dr. M. M. He in Dr. B. W. Matthews lab at the University of Oregon (He et al., 2000). A summary of the methodology used and tables of structure data are provided here.

Structure Determination

All native GlxI data sets were integrated and scaled using the Mosflm and Scala package (CCP4, 1994; Leslie, 1999). The SeMet-Ni^{2+}-GlxI data sets were integrated and scaled using HKL2000 (Otwinowski and Minor, 1997). Data collection statistics can be seen in Table D.1. The space group of native GlxI crystals was determined to be $P2_1$ with two molecules per asymmetric unit. In contrast, the SeMet-Ni^{2+}-GlxI crystals grew in space group $P2_12_12_1$ with six molecules per asymmetric unit.

Attempts to determine the structure of the native *E. coli* enzyme in space group $P2_1$ using molecular replacement based on the *H. sapiens* enzyme (Cameron et al., 1997) were unsuccessful. This led to the use of the selenomethionine form, which as noted, crystallized in a different space group. The positions of the 12 Se sites were determined by Shake 'n Bake (Hauptman, 1997). The program SHARP (de La Fortelle and Bricogne, 1997) was used to refine the positions of the Se sites and to calculate the experimental electron density map. The phasing statistics can be seen in Table D.1.

Model Building, Refinement, and Analysis

The model of SeMet-Ni^{2+}-GlxI was built with the program O (Jones and Kjeldgaard, 1997; Jones et al., 1991). The noncrystallographic symmetry operators relating the three dimers in the asymmetric unit were determined using O and refined with CNS_Solve (Brunger et al., 1998). Refinement of the structure was first carried out using CNS_Solve (Brunger et al., 1998). This involved a combination of simulated annealing (Brunger et al., 1990) interspersed with manual rebuilding into maps averaged using RAVE (Kleywegt and Jones, 1994). Further refinement was carried out using TNT

(Tronrud, 1997). Five percent of the total reflections from thin shells were excluded from the refinement process and used to calculate *R*-free (Brunger, 1992). Strict non-crystallographic symmetry was maintained throughout, until *R* had dropped to 25% and *R*-free to 30%.

At this stage, the model was used in a molecular replacement search (Kissinger and Gehlhaar, 1997) leading to the successful determination of the GlxI structure in the $P2_1$ crystal form. This not only made it possible to refine (Tronrud, 1997) the structures of the various metal-substituted forms of the enzyme but also to take advantage of the higher resolution obtainable for these crystals. The structure validation program PROCHECK (Laskowski et al., 1993) shows that the final models for all structures have reasonable geometry, with good root mean square deviation from target values (Table D.2; Engh and Huber, 1992).

The presence and absence of the metal-bound water was confirmed by the calculation of omit-maps. Overlay of the structures were done by using program EDPDB on the basis of least square fitting (Zhang and Matthews, 1995).

Electrostatic potentials (Figure 3.10) were calculated and the molecular surfaces were displayed by using the program GRASP (Nicholls and Honig, 1991). The metal ions in both *E. coli* and *H. sapiens* GlxI proteins and the inhibitor ligand in the *H. sapiens* GlxI were excluded from these calculations. The density shown in the active site of Ni^{2+}- and Zn^{2+}-GlxI (Figure 3.8) shown is from a map calculated with amplitudes ($2F_o$-F_c) where F_o and F_c are, respectively, the observed structure amplitudes and those calculated from the final refined structure. The resolution is 1.5 Å for Ni^{2+}-GlxI and 1.8 Å for Zn^{2+}-GlxI. No distances or angle restrains were applied to the coordination geometry during refinement. These active site figures were prepared using Bobscript (Esnouf, 1997).

Table D.1: Data collection and phasing statistics.

Data Set	Ni^{2+}	Co^{2+}	Cd^{2+}	Zn^{2+}	Apo	SeMet-Ni^{2+}
Space Group	$P2_1$	$P2_1$	$P2_1$	$P2_1$	$P2_1$	$P2_12_12_1$
Cell Dimensions						
a (Å)	46.05	46.09	45.93	46.24	46.28	80.46
b (Å)	56.48	56.57	56.39	57.17	57.20	85.63
c (Å)	46.71	46.75	46.79	46.99	46.99	122.96
β (deg)	95.4	95.5	95.2	95.4	95.2	
Resolution Range (Å)	20-1.5	20-1.9	20-1.9	20-1.8	20-1.7	20-2.5
Measured Reflections	116 872	116 932	47 320	134 520	81 372	103 752
Unique Reflections	38 619	17 383	19 871	22 460	29 051	32 488
Completeness (%)[b]	98.9 (98.0)	90.0 (88.7)	90.3 (90.0)	98.3 (98.2)	97.8 (93.1)	94.2 (91.0)
R_{sym} (%)[c]	6.9 (28.9)	5.1 (11.0)	10.2 (27.6)	4.6 (5.2)	5.1 (24.1)	4.8 (26.2)
$\langle I/\sigma(I)\rangle$	12.8 (1.9)	33.2 (6.1)	8.7 (1.5)	38.9 (13.6)	11.5 (2.2)	19.2 (3.4)
Phasing Power[d]						3.2
R_{cullis}[e]						0.57

[a] The data statistics for SeMet- Ni^{2+}-GlxI are calculated from the data set collected at a remote wavelength (λ= 0.9665 Å).

[b] Numbers in parentheses are for the highest resolution bins.

[c] $R_{sym}(I) = (\sum_{hkl}\sum_i |I(i) - \langle I(hkl)\rangle|)/\sum_{hkl}\langle I(hkl)\rangle$.

[d] The phasing statistics are calculated from the data set collected at the peak wavelength (λ= 0.9792 Å). The phasing power, calculated for the acentric reflections, is the root-mean-square value of $(|F_H|/|F_{PH} - |F_P + F_H||)$.

[e] $R_{cullis} = \sum||F_{PH} - |F_P + F_H||/\sum|F_{PH} - F_H|$ and is calculated for the acentric reflections

Table D.2: Refinement statistics.

Protein[a]	Ni^{2+}	Co^{2+}	Cd^{2+}	Zn^{2+}	Apo
Resolution (Å)	20-1.5	20-1.9	20-1.9	20-1.8	20-1.7
R_{factor} (%)	20.5	16.9	17.7	18.6	18.8
R_{free} (%)	27.2	25.4	28.1	26.0	25.5
Δ_{bonds} (Å)[b]	0.01	0.005	0.007	0.007	0.006
Δ_{angles} (deg)[b]	1.987	1.439	1.580	1.603	1.483
Average B value ($Å^2$)					
Protein	19.5	22.0	18.2	18.5	23.5
Metal	17.6	25.6	15.1	18.0	
Overall	18.5	23.8	16.7	18.3	
No. of water molecules	266	263	273	235	288
Residues in disallowed regions of Ramachandran plot (%)[c]	0.0	0.0	0.0	0.0	0.0

[a] Values are for the dimer in the asymmetric unit.
[b] Discrepancies from ideal bond lengths and angles as defined by Engh and Huber (1992).
[c] Using a stringent boundary as defined by Kleywegt and Jones (1994).

APPENDIX E

GLYOXALASE I PROTEIN SEQUENCE ALIGNMENTS

All of the known and putative glyoxalase I sequences analyzed in Chapter 5 are presented and aligned in the following two figures.

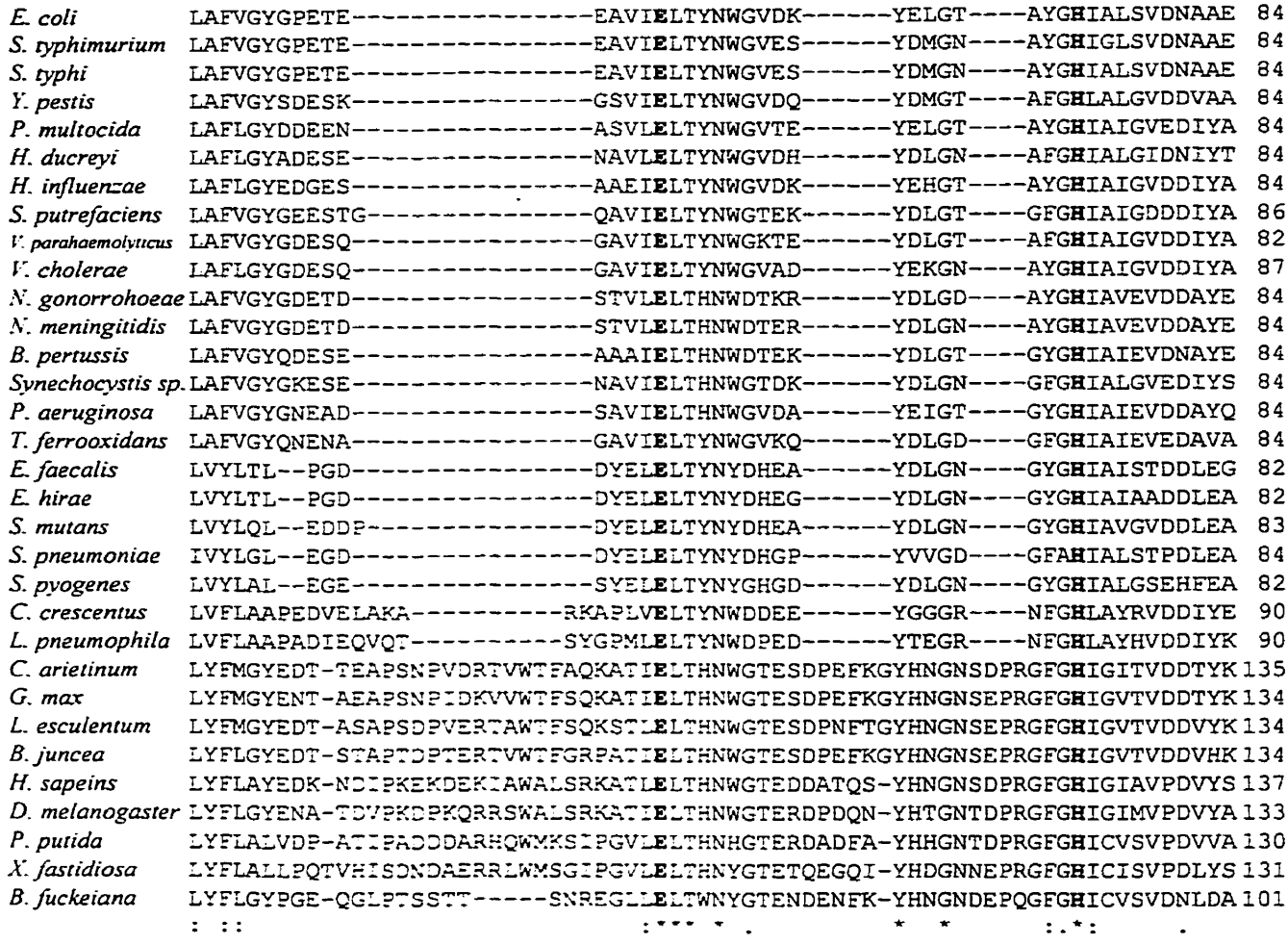
E. coli LAFVGYGPETE----------EAVIELTYNWGVDK------YELGT----AYGHIALSVDNAAE 84
S. typhimurium LAFVGYGPETE----------EAVIELTYNWGVES------YDMGN----AYGHIGLSVDNAAE 84
S. typhi LAFVGYGPETE----------EAVIELTYNWGVES------YDMGN----AYGHIALSVDNAAE 84
Y. pestis LAFVGYSDESK----------GSVIELTYNWGVDQ------YDMGT----AFGHLALGVDDVAA 84
P. multocida LAFLGYDDEEN----------ASVLELTYNWGVTE------YELGT----AYGHIAIGVEDIYA 84
H. ducreyi LAFLGYADESE----------NAVLELTYNWGVDH------YDLGN----AFGHIALGIDNIYT 84
H. influenzae LAFLGYEDGES----------AAEIELTYNWGVDK------YEHGT----AYGHIAIGVDDIYA 84
S. putrefaciens LAFVGYGEESTG----------QAVIELTYNWGTEK------YDLGT----GFGHIAIGDDDIYA 86
V. parahaemolyticus LAFVGYGDESQ----------GAVIELTYNWGKTE------YDLGT----AFGHIAIGVDDIYA 82
V. cholerae LAFLGYGDESQ----------GAVIELTYNWGVAD------YEKGN----AYGHIAIGVDDIYA 87
N. gonorrohoeae LAFVGYGDETD----------STVLELTHNWDTKR------YDLGD----AYGHIAVEVDDAYE 84
N. meningitidis LAFVGYGDETD----------STVLELTHNWDTER------YDLGN----AYGHIAVEVDDAYE 84
B. pertussis LAFVGYQDESE----------AAAIELTHNWDTEK------YDLGT----GYGHIAIEVDNAYE 84
Synechocystis sp. LAFVGYGKESE----------NAVIELTHNWGTDK------YDLGN----GFGHIALGVEDIYS 84
P. aeruginosa LAFVGYGNEAD----------SAVIELTHNWGVDA------YEIGT----GYGHIAIEVDDAYQ 84
T. ferrooxidans LAFVGYQNENA----------GAVIELTYNWGVKQ------YDLGD----GFGHIAIEVEDAVA 84
E. faecalis LVYLTL--PGD----------DYELELTYNYDHEA------YDLGN----GYGHIAISTDDLEG 82
E. hirae LVYLTL--PGD----------DYELELTYNYDHEG------YDLGN----GYGHIAIAADDLEA 82
S. mutans LVYLQL--EDDP----------DYELELTYNYDHEA------YDLGN----GYGHIAVGVDDLEA 83
S. pneumoniae IVYLGL--EGD----------DYELELTYNYDHGP------YVVGD----GFAHIALSTPDLEA 84
S. pyogenes LVYLAL--EGE----------SYELELTYNYGHGD------YDLGN----GYGHIALGSEHFEA 82
C. crescentus LVFLAAPEDVELAKA----------RKAPLVELTYNWDDEE------YGGGR----NFGHLAYRVDDIYE 90
L. pneumophila LVFLAAPADIEQVQT----------SYGPMLELTYNWDPED------YTEGR----NFGHLAYHVDDIYK 90
C. arietinum LYFMGYEDT-TEAPSNPVDRTVWTFAQKATIELTHNWGTESDPEFKGYHNGNSDPRGFGHIGITVDDTYK 135
G. max LYFMGYENT-AEAPSNPIDKVVWTFSQKATIELTHNWGTESDPEFKGYHNGNSEPRGFGHIGVTVDDTYK 134
L. esculentum LYFMGYEDT-ASAPSDPVERTAWTFSQKSTLELTHNWGTESDPNFTGYHNGNSEPRGFGHIGVTVDDVYK 134
B. juncea LYFLGYEDT-STAPTDPTERTVWTFGRPATIELTHNWGTESDPEFKGYHNGNSEPRGFGHIGVTVDDVHK 134
H. sapeins LYFLAYEDK-NDIPKEKDEKIAWALSRKATLELTHNWGTEDDATQS-YHNGNSDPRGFGHIGIAVPDVYS 137
D. melanogaster LYFLGYENA-TDVPKDPKQRRSWALSRKATIELTHNWGTERDPDQN-YHTGNTDPRGFGHIGIMVPDVYA 133
P. putida LYFLALVDP-ATIPADDDARHQWMKSIPGVLELTHNHGTERDADFA-YHHGNTDPRGFGHICVSVPDVVA 130
X. fastidiosa LYFLALLPQTVHISDNDAERRLWMSGIPGVLELTHNYGTETQEGQI-YHDGNNEPRGFGHICISVPDLYS 131
B. fuckeiana LYFLGYPGE-QGLPTSSTT-----SNREGLLELTWNYGTENDENFK-YHNGNDEPQGFGHICVSVDNLDA 101

```
E. coli              ACEKIRQNGGNVTREAGPVKGGTTVIAFVEDPDGYKIELIEEKDAGRGLGN---------- 135
S. typhimurium       ACERIRQNGGNVTREAGPVKGGSTIIAFVEDPDGYKIELIEAKDAGRGLGN---------- 135
S. typhi             ACERIRQNGGNVTREAGPVKGGSTIIAFVEDPDGYKIELIEAKDAGRGLGN---------- 135
Y. pestis            TCDQIRQAGGKVTREAGPVKGGNTIIAFVEDPDGYKIELIENKSAGDCLGN---------- 135
P. multocida         TCDAVRQAGGKITREPGPVKGGKTVIAFVEDPDGYKIEFIENKHAQSGLGN---------- 135
H. ducreyi           TVEAVRLAGGKITREPGPVLGGKTVIAFAEDPDGYKIEFIENKNAQVALGN---------- 135
H. influenzae        TCEAVRASGGNVTREAGPVKGGSTVIAFVEDPDGYKIEFIENKSTKSGLGN---------- 135
S. putrefaciens      RCEAIAAAGGKVTRAPGPVAGGTTEIAFVEDPDGYKIEFIQMKSATQGLG---------- 136
V. parahaemolyticus  TCDAIKAAGGNVTREAGPVKGGTTHIAFVKDPDGYMIELIQNKQASAGLEG---------- 133
V. cholerae          TCDTIKAAGGIVTREPGPVKGGTTHIAFVKDPDGYMIELIQNKQAHAGLEG---------- 138
N. gonorrohoeae      ACERVKRQGGNVVREAGLMKHGTTVIAFVEDPDGCKIEFVQKKSGDDSVAYANT------- 138
N. meningitidis      ACERVKRQGGNVVREAGPMKHGTTVIAFVEDPDGYKIEFIQKKSGDDSVAYQTA------- 138
B. pertussis         ACDKVKEKGGKVTREAGPMKHGTTVIAFVEDPDGYKIEFIQKKGRND------------- 131
Synechocystis sp.    TCDKIRDKGGKVVREPGPMKHGTTVIAFVEDPDGYKIELIQTSSKKD------------- 131
P. aeruginosa        ACDDIRYNGGQVTREAGPMKHGTTVIAFVTDPDGYKIELIQKSS---------------- 128
T. ferrooxidans      ACDGIRQRGGKVVREAGPMKHGNTVIAFVEDPDGYRIELIERKSDFAEHPA---------- 135
E. faecalis          LHEKHQAAGFTVTDLKG-LPGTAPSYYFVVDPDGYKIEVIRER----------------- 124
E. hirae             LHEKHQAEGFNVTDLKG-LPGTAPSYYFVVDPDGYKIEVIRG------------------ 123
S. mutans            THQAHQKAGYTVTDLSG-LPGKPKMYYFITDPDGYKIEVIRLKQFQEK------------ 130
S. pneumoniae        LHQEHSAKGYEVTEPNG-LPGTTPNYYFVKDPDGYKVEVIREK----------------- 126
S. pyogenes          DHKKHRQAGFPVTDIKE-LADKSARYYFIQDPDGYKIEVIDLNN---------------- 125
C. crescentus        TCQRLMDMGVTINRPPR-----DGHMAFVRSPDNISIELLQDGD-LPPAEPWVSMPNVGAW 145
L. pneumophila       ICQHLQECGVVINRPPR-----DGHMAFIRSPDNISIELLQKGEPLPKQEPWLS------- 139
C. arietinum         ACERFQNLGVEFVKKPD--DGKMKGIAFIKDPDGYWIELFDRKTIGNVTEGNA-------- 186
G. max               ACERFQNLGVEFVKKPE--DGKMKGIAFIKDPDGYWIEIFDRKTIGNVTQTAA-------- 185
L. esculentum        ACERFESLGVEFVKKPL--DGKMKGIAFIKDPDGYWIEIFDTKIIKDAAGSAS-------- 185
B. juncea            ACERFEQLGVEFVKKPH--DGKMKNIAFIKDPDGYWIEIFDLKTIGTTAGNAA-------- 185
H. sapeins           ACKRFEELGVKFVKKPD--DGKMKGLAFIQDPDGYWIEILNPNKMATLM------------ 184
D. melanogaster      ACQRFQELGVDFVKKPD--DGRMKGLAFIKDPDGYWIEIFNAHSV---------------- 176
P. putida            ACERFEALQVPFQKRLS--DGRMNHLAFIKDPDGYWVEVIQPTPL---------------- 173
X. fastidiosa        ACARFDTLQVPYQKRLT--DGRMKNIAFIKDPDGYWVEIISNTPLP--------------- 175
B. fuckeiana         ACERFEKMGVNWKKRLT--DGRMKHVAFVLDPDNYWIEVIQNEKLKERANW---------- 150
                                        *  .**.  :*..
```

Figure E.1: Alignment of the *E .coli* glyoxalase I protein sequence with the known and postulated glyoxalase I sequences (excluding those which appear to be the result of a gene duplication event forming a fused dimer). The alignment was generated by ClustalW (Thompson et al., 1994). * indicates conserved residues; : highly homologous residues; . homologous residues. The residues in bold are the postulated metal ligands based on alignment with the *E. coli* and *H. sapiens* glyoxalase I sequences. See Tables 5.1 and 5.2 for the sequencing organization references and accession numbers.


E. coli
T. aestivum
A. thaliana 1
A. thaliana 2
B. oleracea
C. paradisi
S. stapfianus
O. sativa
S. cerevisiae
S. pombe
MVRIIPMAASSIRPSLACFSDSPRFPISLLSRNLSRTLHVPQSQLFGLTSHKLLRRSVNCLGVAESGKAA
SFSSN---DEAFTWAKKDNRRLLHVVYRVGDIDRTIKFYTECLGMKLLRKRDIPEEKYTNAFLGYGPE--
QATTQ---DDLLTWVKNDKRRMLHVVYRVGDMDRTIKFYTECLGMKLLRKRDIPEEKYTNAFLGYGPE--
A-------SDLLEWPKKDNRRFLHVVYRVGDLDRTIEFYTEVFGMKLLRKRDIPEEKYSNAFLGFGPE--
N-------ADLVEWPKKDKRRFLHVVYRVGDLDRTIQFYTECFGMKVLRKRDVPEEKYSNAFLGFGPE--
ASPAAAN-AELLEWPKKDKRRFLHAVYRVGDLDRTIKFYTECFGMKLLRKRDVPEEKYSNAFLGFGPE--
GSDA------VLEWHKQDKKRMLHAVYRVGDLDRTIKCYTECFGMKLLRKRDVPEEKYTNAFLGYGPE--
GSEAEKSPEVVLEWPKKDKKRLLHAVYRVGDLDRTIKCYTECFGMKLLRKRDVPEEKYTNAFLGFGPE--
STDSTRYPIQIEKASNDPTLLLNHTCLRVKDPARTVKFYTEHFGMKLLSRKDFEEAKFSLYFLSFPKDDI
----------MASTTDMSTYKLNHTMIRVKDLDKSLKFYTEVFGMKLIDQWVFEENEFSLSFLAFDG---
-----------TEEAVIELTYNWGVDK----------YELGTAYGHIALSVDNAAEACEKIRQNGG-NVT
-----------ETNFAIELTYNYGVDS----------YDIGAGFGHFGIATDDVAKTVELIRAKGG-KVT
-----------DSHFVIELTYNYGVDK----------YDIGAGFGHFGIAVDDVAKTVELVKAKGG-KVS
-----------TSNFVVELTYNYGVSS----------YDIGTGFGHFAISTQDVSKLVENVRAKGG-NVT
-----------TSNFVVELTYNYGVSS----------YDIGTGFGHFAISTQDVSKMVEAVRAKGG-NVT
-----------QSHFVVELTYNYGVTS----------YDIGTGFGHFAIATEDVYKLVENIRAKGG-NVT
-----------DKNFALELTYNYGVDK----------YDIGEGFGHFAIATEDINKIAEAVKSSGCCKIT
-----------DTNFALELTYNYGVDK----------YDIGAGFGHFAIATEDVYKLAEKIKSSCCCKIT
PKNKNGEPDVFSAHGVLELTHNWGTEKNPDYKINNGNEEPHRGFGHICFSVSDINKTCEELESQGVKFKK
PGALNHGVERSKREGILELTYNFGTEKKEGPVYINGNTEPKRGFGHICFTVDNIESACAYLESKGVSFKK

Figure E.2: Alignment of the *E .coli* glyoxalase I protein sequence with the known and postulated glyoxalase I sequences which appear to be the result of a gene duplication event forming a fused dimer. The alignment was generated by ClustalW (Thompson et al., 1994). * indicates conserved residues; : highly homologous residues; . homologous residues. The residues in bold are the postulated metal ligands based on alignment with the *E. coli* sequence. Note the postulated ligands are not conserved in all of the C-terminal halves of the sequences. See Table 5.2 for the sequence accession numbers.

APPENDIX F

CHARACTERIZATION OF *YERSINIA PESTIS* GLYOXALASE I

The construction of an *E. coli* expression system for both *Y. pestis* GlxI and *P. aeruginosa* GlxI has been described in Chapter 5, in addition to the initial characterization of these enzymes. Following this work, induction time courses were performed for each of these protein expression systems and the purified *Y. pestis* GlxI enzyme was characterized in more detail, as outlined below.

Induction Time Course for Y. pestis and P. aeruginosa Glyoxalase I

The level of protein production was monitored for both *Y. pestis* GlxI, expressed from *E. coli* BL21/pYPG1, and *P. aeruginosa* GlxI, expressed in *E. coli* BL21/pPAG1. A cell culture in LB_{Amp} was induced with 0.5 mM IPTG when the optical density (OD) reached 0.5. The OD was monitored at 600 nm to determine the relative cell density. In addition a sample of cells was taken each hour for 6 hours, the cells disrupted by sonication and the protein activity monitored with 0.5 mM substrate and 1.0 mM $NiCl_2$ utilizing the standard enzymatic assay outlined in Chapter 2. Protein electrophoresis was also performed to monitor the amount of protein produced (Figure F.1).

From these analyses a four hour induction time with 0.5 mM IPTG was determined to be optimal for the expression of *Y. pestis* GlxI from this construct. Similar results were observed for the expression of *P. aeruginosa* GlxI. An increase in the level of IPTG to 1.0 mM did not appear to affect the overall protein production in either construct.

Cell Growth and Protein Purification

Y. pestis GlxI expressed in *E. coli* BL21/pYPG1 was growth in LB_{Amp} media, induced for 4 hr with 0.5 mM IPTG. From 1 L of growth with no added metals, 3.9 g of cells resulted. The protein was purified as described in Chapter 2 for *E. coli* GlxI. Following cell disruption utilizing the French Press, the sample was separated by anion exchange chromatography on the Q-Sepharose Fast Flow column, followed by preparative isoelectric focusing. Table F.1 summarizes the amount and activity of the protein at each stage of the purification.

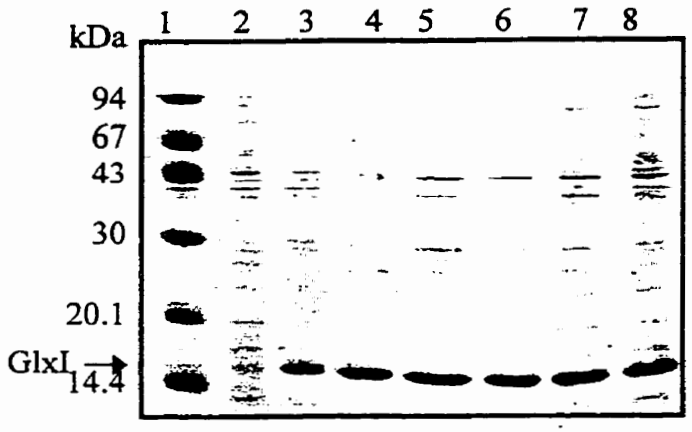

Figure F.1: Level of *Y. pestis* GlxI expressed in *E. coli* BL21/pYPG1 during an induction time course (0.5 mM IPTG). 20 % homogeneous SDS-PAGE with Comassie staining.

The protein separated into two main fractions during the isoelectric focusing, centering around fractions 8 and 13. The protein was active in each case and ran the same on denaturing SDS-PAGE. ESMS analyses indicated that the samples had the same molecular weight. However, there were two components to each sample, the expected monomer and an apparent dimer (Figure F.2). Analysis by native PAGE suggests that the samples contain a dimeric enzyme as well as an apparent tetramer. It is speculated that a disulfide bond has formed between subunits of two different dimeric enzymes, forming this apparent dimer of dimers. The ESMS was performed under denaturing conditions, hence the non-covalent interactions forming the native dimer would be disrupted in this form of analysis. The addition of dithiolthreitol to the protein appears to reverse this disulfide bond formation, monitored by native PAGE. Analysis of the *Y. pestis* GlxI protein sequence (Figure 5.10) reveals that there is a second cysteine in the C-terminus of the protein at position 132, not present in the *E. coli* enzyme. This is most likely the location of the disulfide bond formation. This region appeared quite flexible and mobile in the *E. coli* GlxI protein structure (Chapter 3), and therefore could readily form the observed disulfide bonds.

Table F.1: Summary of the stages of the purification of *Y. pestis* GlxI from *E. coli* BL21/pYPG1 grown with no supplemental metal.

Stage of Purification	Total Protein (mg)	Specific Activity (μmol/min/mg)		% Yield[†]	Fold Purification[‡]	Fold Increase in Activity with $NiCl_2$[⊥]
Cell Break	368	Apo	4.0	100	1.00	121
		+$NiCl_2$	486			
Q-Sepharose Fast Flow	256	Apo	8.8	85	1.22	67
		+$NiCl_2$	591			
IEF/Buffer Change	123	Apo	3.8	46	1.38	176
		+$NiCl_2$	669			
Precipitated Protein from IEF	13 (+ 123 from above for 136 mg overall yield)	Apo	7.2	5.2 (+46 from above for 51% overall yield	1.47	99
		+$NiCl_2$	715			

* Results from a purification of 2.5 g of cells from 3.9 g in 1 L cell growth.

† Yield calculated by comparison of the total activity of the Ni^{2+}-activated enzyme (0.5 mM $NiCl_2$ added to enzyme sample).

‡ Purification factor calculated by comparison of the specific activity of the Ni^{2+}-activated enzyme at each stage to the activity at the cell break.

⊥ Increase with added $NiCl_2$ varies due to variation in the low apoenzyme level.

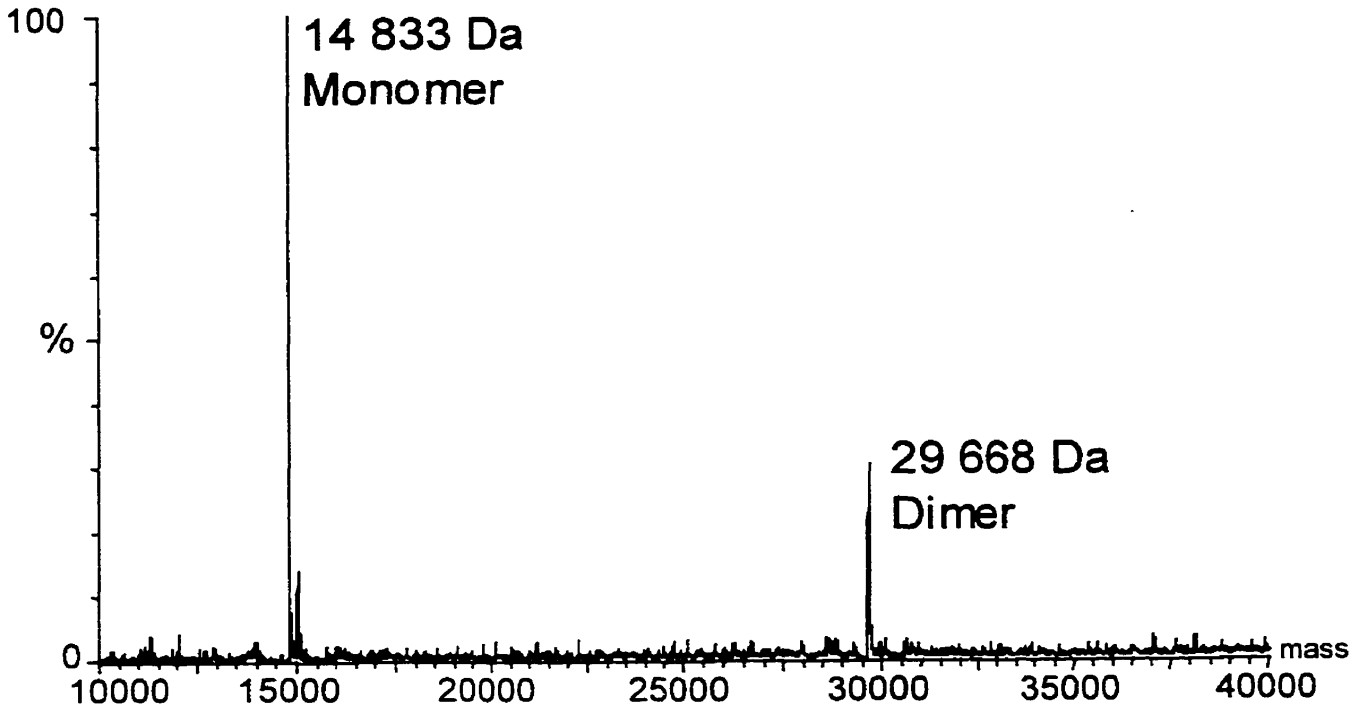

Figure F.2: Reconstructed electrospray mass spectrum of purified *Y. pestis* GlxI. The monomeric subunit is indicated, as is the apparent dimer.

The separation of the protein into two regions during the isoelectric focusing was most likely a result of the formation of disulfide bonds in the protein solution during the run, disrupting the protein focusing. As the two samples appear the same, their protein levels were combined for simplicity in the purification summary presented in Table F.1. The precipitated protein from the IEF was utilized in the metal activation studies. Based on these results this expression system for *Y. pestis* GlxI appears to produce a large quantity of protein (~200 mg/L), similar to that observed for the *E. coli* GlxI expression.

Enzymatic Activation with Divalent Metals

The activation of the apo *Y. pestis* GlxI with various divalent metal chlorides was studied, as described for the *E. coli* wild-type, SeMet, and H5Q GlxI enzymes (Chapters 2 and 4). The results of these analyses are presented in Figure F.3. As observed for the *E. coli* enzyme, *Y. pestis* GlxI is also maximally active with Ni^{2+} and displays no apparent activity in the presence of Zn^{2+}. Furthermore, this enzyme appears even more selective for Ni^{2+} over the other activating metals, Co^{2+}, Mn^{2+}, and Cd^{2+}, than the *E. coli* enzyme.

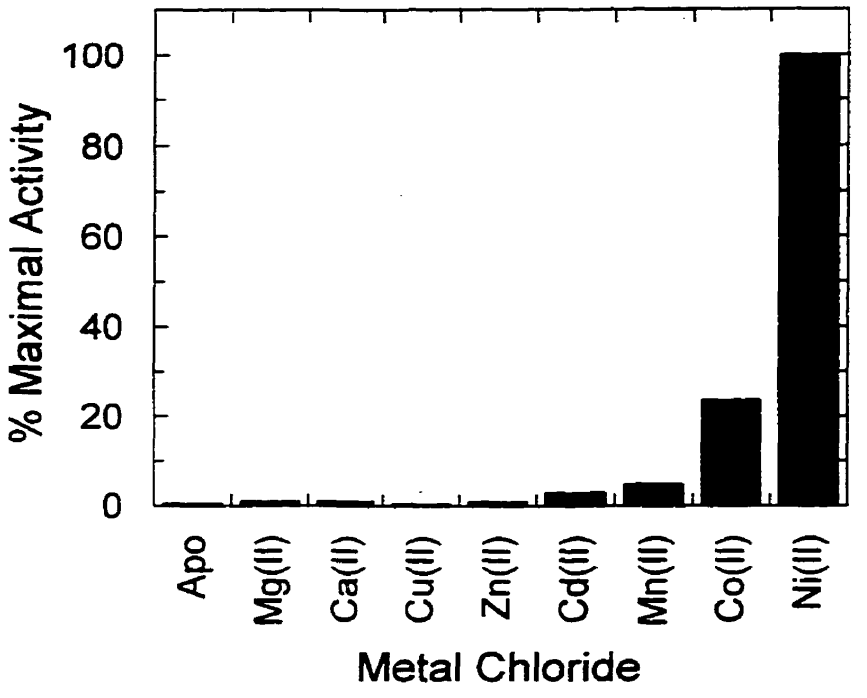

Figure F.3: Activation of *Y. pestis* GlxI with 10 mole equivalents of metal to dimeric enzyme. The activities are shown relative to the maximally activated Ni^{2+} form. Each point was measured in triplicate with 0.5 mM substrate and 0.2-0.4 μg enzyme per assay. The assays with Mn^{2+} were performed in MES buffer whereas all others were performed in phosphate buffer.

REFERENCES

Aceto, A., Dragani, B., Melino, S., Principato, G., Saccucci, F., Gualtieri, G. and Petruzzelli, R. (1998) Structural characterization of human glyoxalase II as probed by limited proteolysis. *Biochem. Mol. Biol. Int.*, **44**, 761-769.

Adams, M.D., Celniker, S.E., Holt, R.A., Evans, C.A., Gocayne, J.D., Amanatides, P.G., Scherer, S.E., Li, P.W., Hoskins, R.A., Galle, R.F., George, R.A., Lewis, S.E., Richards, S., Ashburner, M., Henderson, S.N., Sutton, G.G., Wortman, J.R., Yandell, M.D., Zhang, Q., Chen, L.X., Brandon, R.C., Rogers, Y.H., Blazej, R.G., Champe, M., Pfeiffer, B.D., Wan, K.H., Doyle, C., Baxter, E.G., Helt, G., Nelson, C.R., et al. (2000) The genome sequence of *Drosophila melanogaster*. *Science*, **287**, 2185-2195.

Ahmed, M.U., Brinkmann Frye, E., Degenhardt, T.P., Thorpe, S.R. and Baynes, J.W. (1997) N^{ε}-(Carboxyethyl)lysine, a product of the chemical modification of proteins by methylglyoxal, increases with age in human lens proteins. *Biochem. J.*, **324**, 565-570.

Altschul, S.F., Gish, W., Miller, W., Myers, E.W. and Lipman, D.J. (1990) Basic local alignment search tool. *J. Mol. Bio.*, **215**, 403-410.

Altschul, S.F., Madden, T.L., Schäffer, A.A., Zhang, J., Zhang, Z., Miller, W. and Lipman, D.J. (1997) Gapped BLAST and PSI-BLAST: A new generation of protein database search programs. *Nucleic Acids Res.*, **25**, 3389-3402.

Anderson, M.E., Powrie, F., Puri, R.N. and Meister, A. (1985) Glutathione monoethyl ester: Preparation, uptake by tissues, and conversion to glutathione. *Arch. Biochem. Biophys.*, **239**, 538-548.

Angleton, E.L. and Van Wart, H.E. (1988) Preparation and reconstitution with divalent metal ions of class I and class II *Clostridium histolyticum* apocollagenases. *Biochemistry*, **27**, 7406-7412.

Ankel-Fuchs, D. and Thauer, R.K. (1988) Nickel in biology: Nickel as an essential trace element. In Lancaster Jr., J.R. (ed.) *The Bioinorganic Chemistry of Nickel*. YCH Publishers Inc., NY, pp. 93-110.

Armstrong, R.N. (1998) Mechanistic imperatives for the evolution of glutathione transferases. *Curr. Opin. Chem. Biol.*, **2**, 618-623.

Aronsson, A.C., Marmstål, E. and Mannervik, B. (1978) Glyoxalase I, a zinc metalloenzyme of mammals and yeast. *Biochem. Biophys. Res. Commun.*, **81**, 1235-1240.

Aronsson, A.C., Tibbelin, G. and Mannervik, B. (1979) Purification of glyoxalase I from human erythrocytes by the use of affinity chromatography and separation of the three isoenzymes. *Anal. Biochem.*, **92**, 390-393.

Aronsson, A.C., Sellin, S., Tibbelin, G. and Mannervik, B. (1981) Probing the active site of glyoxalase I from human erythrocytes by use of the strong reversible inhibitor *S-p*-bromobenzylglutathione and metal substitutions. *Biochem. J.*, **197**, 67-75.

Atamna, H. and Ginsburg, H. (1997) The malaria parasite supplies glutathione to its host cell-Investigation of glutathione transport and metabolism in human erythrocytes infected with *Plasmodium falciparum*. *Eur. J. Biochem.*, **250**, 670-679.

Avaeva, S., Kurilova, S., Nazarova, T., Rodina, E., Vorobyeva, N., Sklyankina, V., Grigorjeva, O., Harutyunyan, E., Oganessyan, V., Wilson, K., Dauter, Z., Huber, R. and Mather, T. (1997) Crystal structure of *Escherichia coli* inorganic pyrophosphatase complexed with $SO4^{2-}$. Ligand-induced molecular asymmetry. *FEBS Lett.*, **410**, 502-508.

Ayed, A., Krutchinsky, A.N., Ens, W., Standing, K.G. and Duckworth, H.W. (1998) Quantitative evaluation of protein-protein and ligand-protein equilibria of a large allosteric enzyme by electrospray ionization time-of-flight mass spectrometry. *Rapid Commun. Mass Spectrom.*, **12**, 339-344.

Ayi, K., Cappadoro, M., Branca, M., Turrini, F. and Arese, P. (1998) *Plasmodium falciparum* glutathione metabolism and growth are independent of glutathione system of host erythrocyte. *FEBS Lett.*, **424**, 257-261.

Ayoub, F.M., Zaman, M.A., Thornalley, P.J. and Masters, J.R.W. (1993) Glyoxalase activity in human tumor cell lines *in vitro*. *Anticancer Res.*, **13**, 151-156.

Babine, R.E. and Bender, S.L. (1997) Molecular recognitition of protein-ligand complexes: Applications to drug design. *Chem. Rev.*, **97**, 1359-1472.

Barnard, J.F.J. (1997) Isolation and Characterization of Glyoxalase I from *Escherichia coli*. *Ph. D. Thesis*, Department of Chemistry. University of Waterloo, Waterloo.

Barnard, J.F. and Honek, J.F. (1989) Investigation on glyoxalase I inhibitors. *Biochem. Biophys. Res. Commun.*, **165**, 118-124.

Barnard, J.F., Vander Jagt, D.L. and Honek, J.F. (1994) Small molecule probes of glyoxalase I and glyoxalase II. *Biochim. Biophys. Acta*, **1208**, 127-135.

Baskaran, S. and Balasubramanian, K.A. (1987) Purification and active site modification studies on glyoxalase I from monkey intestinal mucosa. *Biochim. Biophys. Acta*, **913**, 377-385.

Bergdoll, M., Eltis, L.D., Cameron, A.D., Dumas, P. and Bolin, J.T. (1998) All in the family: Structural and evolutionary relationships among three modular proteins with diverse functions and variable assembly. *Protein Sci.*, **7**, 1661-1670.

Bergmeyer, H.U. (ed.) (1983) Glyoxalase I. *Methods of Enzymatic Analysis* 3rd ed. Verlag Chemie, Deerfield Beach, Vol. 2, pp. 217-218.

Bergmeyer, H.U. (ed.) (1984) Methylglyoxal. *Methods of Enzymatic Analysis* 3rd ed. Verlag Chemie, Deerfield Beach, Vol. 6, pp. 593-596.

Bernat, B.A., Laughlin, L.T. and Armstrong, R.N. (1997) Fosfomycin resistance protein (FosA) is a manganese metalloglutathione transferase related to glyoxalase I and the extradiol dioxygenases. *Biochemistry*, **36**, 3050-3055.

Biemann, H.P. and Koshland, D.E. (1994) Aspartate receptors of *Escherichia coli* and *Salmonella typhimurium* bind ligand with negative and half-of-the-sites cooperativity. *Biochemistry*, **33**, 629-634.

Bito, A., Haider, M., Hadler, I. and Breitenbach, M. (1997) Identification and phenotypic analysis of two glyoxalase II encoding genes from *Saccharomyces cerevisiae*, *GLO2* and *GLO4*, and intracellular localization of the corresponding proteins. *J. Biol. Chem.*, **272**, 21509-21519.

Blomstedt, C.K., Gianello, R.D., Gaff, D.F., Hamill, J.D. and Neale, A.D. (1998) Differential gene expression in desiccation-tolerant and desiccation-sensitive tissue of the resurrection grass, *Sporobolus stapfianus*. *Aust. J. Plant Physiol.*, **25**, 937-946.

Blondeau, J.M., Church, D., Yaschuk, Y. and Bjarnason, J. (1999) *In vitro* activity of several anitmicrobial agents against 1003 isolates of *Streptococcus pyogenes* collected from Western Canada. *Int. J. Antimicrob. Agents*, **12**, 67-70.

Bradford, M.M. (1976) A rapid and sensitive method for the quantitation of microgram quantities of protein utilizing the principle of protein-dye binding. *Anal. Biochem.*, **72**, 248-254.

Brandts, J.F., Lin, J.N., Wiseman, T., Williston, S. and Yang, C.P. (1990) An instrument for rapid determination of binding constants for biomolecules. *Amer. Laboratory*, **22**, 30-35.

Brayman, T.G. and Hausinger, R.P. (1996) Purification, characterization, and functional analysis of a truncated *Klebsiella aerogenes* UreE urease accessory protein lacking the histidine-rich carboxyl terminus. *J. Bacteriol.*, **178**, 5410-5416.

Briggner, L.E. and Wadsö, I. (1991) Test and calibration processes for microcalorimeters, with special reference to heat conduction instruments used with aqueous systems. *J. Biochem. Biophys. Methods*, **22**, 101-118.

Brown, C., Douglas, K.T. and Ghobt-Sharif, J. (1981) Direct demonstration by ^{1}H NMR spectrometry of the stereoselectivity of yeast glyoxalase I towards the diasteromeric forms of the α-ketoaldehyde-glutathione hemithioacetal. *J. Chem. Soc. Chem. Comm.*, **18**, 944-946.

Brünger, A.T. (1992) Free *R* value: A novel statistical quantity for assessing the accuracy of crystal structures. *Nature*, **355**, 472-475.

Brünger, A.T., Adams, P.D., Clore, G.M., DeLano, W.L., Gros, P., Grosse-Kunstleve, R.W., Jiang, J.S., Kuszewski, J., Nilges, M., Pannu, N.S., Read, R.J., Rice, L.M., Simonson, T. and Warren, G.L. (1998) Crystallography & NMR system: A new software suite for macromolecular structure determination. *Acta Crystallogr.*, **D54**, 905-921.

Brünger, A.T., Krukowski, A. and Erickson, J.W. (1990) Slow-cooling protocols for crystallographic refinement by simulated annealing. *Acta Crystallogr.*, **A46**, 585-593.

Cameron, A.D., Olin, B., Ridderström, M., Mannervik, B. and Jones, T.A. (1997) Crystal structure of human glyoxalase I--Evidence for gene duplication and 3D domain swapping. *EMBO J.*, **16**, 3386-3395.

Cameron, A.D., Ridderström, M., Olin, B., Kavarana, M.J., Creighton, D.J. and Mannervik, B. (1999a) Reaction mechanism of glyoxalase I explored by an X-ray crystallographic analysis of the human enzyme in complex with a transition state analogue. *Biochemistry*, **38**, 13480-13490.

Cameron, A.D., Ridderström, M., Olin, B. and Mannervik, B. (1999b) Crystal structure of human glyoxalase II and its complex with a glutathione thiolester substrate analogue. *Structure*, **7**, 1067-1078.

Camilleri, P. and Haskins, N.J. (1993) Investigating the non-covalent interaction of cytidylic acids, with ribonuclease A by electrospray mass spectrometry. *Rapid Comm. Mass Spec.*, **7**, 603-604.

Campbell, I.D. and Dwek, R.A. (1984) *Biological Spectroscopy*. Benjamin/Cummings Publishing Company Inc., Menlo Park, pp. 179-213.

Cantor, C.R. and Schimmel, P.R. (1980) *Biophysical chemistry Part II: Techniques for the study of biological structure and function*. W.H. Freeman & Company, NY, pp. 525-537.

Carmeli, Y., Troillet, N., Eliopoulos, G.M. and Samore, M.H. (1999a) Emergence of anitibotic-resistant *Pseudomonas aeruginosa*: Comparion of risks associated with different antipseudomonal agents. *Antimicrob. Agents Chemother.*, **43**, 1379-1382.

Carmeli, Y., Troillet, N., Karchmer, A.W. and Samore, M.H. (1999b) Health and economic outcomes of antibiotic resistance in *Pseudomonas aeruginosa*. *Arch. Intern. Med.*, **159**, 1127-1132.

CCP4, Collaborative Computational Project Number 4 (1994) *Acta Crystallogr.*, **D50**, 760-763.

Chenoweth, C.E. and Lynch, J.P. (1999) Hospital-acquired pneumonia: Antimicrobials for specific pathogens. *J. Respir. Dis.*, **20**, 381-391.

Chivers, P.T. and Sauer, R.T. (2000) Regulation of high affinity nickel uptake in bacteria. Ni^{2+}-Dependent interaction of NikR with wild-type and mutant operator sites. *J. Biol. Chem.*, **275**, 19735-19741.

Choudhury, S.B., Lee, J.W., Davidson, G., Yim, Y.I., Bose, K., Sharma, M.L., Kang, S.O., Cabelli, D.E. and Maroney, M.J. (1999) Examination of the nickel site structure and reaction mechanism in *Streptomyces seoulensis* superoxide dismutase. *Biochemistry*, **38**, 3744-3752.

Cliffe, E.E. and Waley, S.G. (1961) The mechanism of the glyoxalase I reaction, and the effect of opthalmic acid as an inhibitor. *Biochem. J.*, **79**, 475-482.

Clugston, S.L. (1997) A Detailed Analysis of the Glyoxalase I Metalloenzyme from *Escherichia coli*. *M. Sc. Thesis*, Department of Chemistry, University of Waterloo, Waterloo.

Clugston, S.L., Barnard, J.F.J., Kinach, R., Miedema, D., Ruman, R., Daub, E. and Honek, J.F. (1998a) Overproduction and characterization of a dimeric non-zinc glyoxalase I from *Escherichia coli*: Evidence for optimal activation by nickel ions. *Biochemistry*, **37**, 8754-8763.

Clugston, S.L., Daub, E. and Honek, J.F. (1998b) Identification of glyoxalase I sequences in *Brassica oleracea* and *Sporobolus stapfianus*: Evidence for gene duplication events. *J. Mol. Evol.*, **47**, 230-234.

Clugston, S.L., Daub, E., Kinach, R., Miedema, D., Barnard, J.F.J. and Honek, J.F. (1997) Isolation and sequencing of a gene coding for glyoxalase I activity from *Salmonella typhimurium* and comparison with other glyoxalase I sequences. *Gene*, **186**, 103-111.

Clugston, S.L. and Honek, J.F. (2000) Identification of sequences encoding the detoxification metalloisomerase glyoxalase I in microbial genomes from several pathogenic organisms. *J. Mol. Evol.*, **50**, 491-495.

Coleman, J.E. (1993) Cadmium-113 nuclear magnetic resonance applied to metalloproteins. *Methods Enzymol.* **227**, 16-43.

Collier, H.B. (1973) A note on the molar absorptivity of reduced Ellman's reagent, 3-carboxylato-4-nitrothiophenolate. *Anal. Biochem.*, **56**, 310-311.

Colpas, G.J. and Hausinger, R.P. (2000) *In vivo* and *in vitro* kinetics of metal transfer by the *Klebsiella aerogenes* urease nickel metallochaperone, UreE. *J. Biol. Chem.*, **275**, 10731-10737.

Colpas, G.J., Maroney, M.J., Bagyinka, C., Kumar, M., Willis, W.S., Suib, S.L., Baidya, N. and Mascharak, P.K. (1991) X-ray spectroscopic studies of nickel complexes, with application to the structure of nickel sites in hydrogenases. *Inorg. Chem.*, **30**, 920-928.

Cooper, R.A. (1984) Metabolism of methylglyoxal in microorganisms. *Ann. Rev. Microbiol.*, **38**, 49-68.

Creighton, T.E. (ed.) (1989) *Protein Structure: A practical approach.* IRL Press, Oxford, pp. 157.

Creighton, D.J., Hamilton, D.S., Kavarana, M.J., Sharkey, E.M. and Eiseman, J.L. (2000) Glyoxalase enyzme system as a potential target for antitumor drug development. *Drugs Fut.*, **25**, 385-392.

Creighton, D.J., Migliorini, M., Pourmotabbed, T. and Guha, M.K. (1988) Optimization of efficiency in the glyoxalase pathway. *Biochemistry*, **27**, 7376-7384.

Crowder, M.W., Maiti, M.K., Banovic, L. and Makaroff, C.A. (1997) Glyoxalase II from *A. thaliana* requires Zn(II) for catalytic activity. *FEBS Lett.*, **418**, 351-354.

Dakin, H.D. and Dudley, H.W. (1913a) *J. Biol. Chem.*, **14**, 155-157.

Dakin, H.D. and Dudley, H.W. (1913b) *J. Biol. Chem.*, **14**, 423-431.

Davenport, R.C., Bash, P.A., Seaton, B.A., Karplus, M., Petsko, G.A. and Ringe, D. (1991) Structure of the triosephosphate isomerase-phosphoglycolohydroxamate complex: An analogue of the intermediate on the reaction pathway. *Biochemistry*, **30**, 5821-5826.

Davidson, S.D., Cherry, J.P., Choudhury, M.S., Tazaki, H., Mallouh, C. and Konno, S. (1999) Glyoxalase I activity in human prostate cancer: A potential marker and importance in chemotherapy. *J. Urol.*, **161**, 690-691.

Davidson, G., Clugston, S.L., Honek, J.F. and Maroney, M.J. (2000a) XAS investigation of the nickel active site structure in *Escherichia coli* Glyoxalase I. *Inorg. Chem.*, **39**, 2962-2963.

Davidson, G., Clugston, S.L., Honek, J.F. and Maroney, M.J. (2000b) An XAS investigation of product and inhibitor complexes of Ni-containing GlxI from *E. coli*: Mechanistic implications. *Biochemistry*, Submitted.

Davis, R.W., Botstein, D. and Roth, J.R. (1980) *Advanced Bacterial Genetics*. Cold Spring Harbor Laboratory, Cold Spring Harbor, NY.

Davis, K.A. and Williams, G.R. (1969) Glyoxalase I, a lyase or an oxidoreductive isomerase. *Can. J. Biochem.*, **47**, 553-556.

de La Fortelle, E. and Bricogne, G. (1997) Maximum-likelihood heavy-atom parameter refinement for multiple isomorphous replacement and multiwavelength anomalous diffraction methods. *Methods Enzymol.*, **276**, 472-494.

Deswal, R. and Sopory, S.K. (1991) Purification and partial characterization of glyoxalase I from a higher plant *Brassica juncea*. *FEBS Lett.*, **282**, 277-280.

Deswal, R. and Sopory, S.K. (1998) Biochemical and immunochemical characterization of *Brassica juncea* glyoxalase I. *Phytochemistry*, **49**, 2245-2253.

Deswal, R. and Sopory, S.K. (1999) Glyoxalase I from *Brassica juncea* is a calmodulin stimulated protein. *Biochim. Biophys. Acta*, **1450**, 460-467.

Di Ilio, C., Angelucci, S., Pennelli, A., Zezza, A., Tenaglia, R. and Sacchetta, P. (1995) Glyoxalase activities in tumor and non-tumor human urogenital tissues. *Cancer Lett.*, **96**, 189-193.

Diekert, G. (1988) Carbon monoxide dehydrogenase of acetogens. In Lancaster Jr., J.R. (ed.) *The Bioinorganic Chemistry of Nickel*. VCH Publishers Inc., NY, pp. 299-309.

DiMarco, A.A., Bobik, T.A. and Wolfe, R.S. (1990) Unusual coenzymes of methanogenesis. *Ann. Rev. Biochem.*, **59**, 355-394.

Doublié, S. (1997) Preparation of selenomethionyl proteins for phase determination. *Methods Enzymol.*, **276**, 523-530.

Douglas, K.T. and Shinkai, S. (1985) Chemical basis of the action of glyoxalase I, an anticancer target enzyme. *Angew. Chem. Int. Ed.*, **24**, 31-43.

Doyle, M.L. (1997) Characterization of binding interactions by isothermal titration calorimetry. *Curr. Opin. Biotech.*, **8**, 31-35.

Doyle, M.L. and Hensley, P. (1997) Experimental dissection of protein-protein interactions in solution. *Adv. Mol. Cell Biol.*, **22A**, 279-337.

Drake, H.L. (1988) Biological transport of nickel. In Lancaster Jr., J.R. (ed.) *The Bioinorganic Chemistry of Nickel*. YCH Publishers Inc., NY, pp. 111-139.

Drake, H.L., Hu, S.I. and Wood, H.G. (1980) Purification of carbon monoxide dehydrogenase, a nickel enzyme from *Clostridium thermoaceticum*. *J. Biol. Chem.*, **255**, 7174-7180.

Dumas, P., Bergdoll, M., Cagnon, C. and Masson, J.M. (1994) Crystal structure and site-directed mutagenesis of a bleomycin resistance protein and their significance for drug sequestering. *EMBO J.*, **13**, 2483-2492.

Együd, L.G. and Szent-Györgyi, A. (1966a) Cell division, SH, ketoaldehydes, and cancer. *Proc. Natl. Acad. Sci.*, **55**, 388-393.

Együd, L.G. and Szent-Györgyi, A. (1966b) On the regulation of cell division. *Proc. Natl. Acad. Sci.*, **56**, 203-207.

Eitinger, T., Wolfram, L., Degen, O. and Anthon, C. (1997) A Ni^{2+} binding motif is the basis of high affinity transport of the *Alcaligenes eutrophus* nickel permease. *J. Biol. Chem.*, **272**, 17139-17144.

Ekwall, K. and Mannervik, B. (1970) Inhibition of yeast *S*-lactylglutathione lyase (glyoxalase 1) by sulfhydryl reagents. *Arch. Biochem. Biophys.*, **137**, 128-132.

Elliott, W.H. (1959) Amino-acetone: Its isolation and role in metabolism. *Nature*, **183**, 1051-1052.

Ellman, G.L. (1959) Tissue sulfhydryl groups. *Arch. Biochem. Biophys.*, **82**, 70-77.

Engh, R.A. and Huber, R. (1991) Accurate bond and angle parameters for X-ray protein structure refinement. *Acta Crystallogr.*, **A47**, 392-400.

Esnouf, R.M. (1997) An extensively modified version of MolScript that includes greatly enhanced coloring capabilities. *J. Mol. Graphics*, **15**, 132-134.

Espartero, J., I., Sánchez-Aguayo, I. and Pardo, J.M. (1995) Molecular characterization of glyoxalase-I from a higher plant; upregulation by stress. *Plant Mol. Biol.*, **29**, 1223-1233.

Fahey, R.C. and Sundquist, A.R. (1991) Evolution of glutathione metabolism. *Adv. Enzymol. Relat. Areas Mol. Biol.*, **64**, 1-53.

Felsenstein, J. (1993) PHYLIP (Phylogeny Inference Package) Version 3.5c. Distributed by the author. Department of Genetics, University of Washington, Seattle.

Ferguson, G.P., Tötemeyer, S., MacLean, M.J. and Booth, I.R. (1998) Methylglyoxal production in bacteria: Suicide or survival? *Arch. Microbiol.*, **170**, 209-219.

Fersht, A. (1999) *Structure and Mechanism in Protein Science: A guide to enzyme catalysis and protein folding*. W.H. Freeman and Company, NY.

Fleischmann, R.D., Adams, M.D., White, O., Clayton, R.A., Kirkness, E.F., Kerlavage, A.R., Bult, C.J., Tomb, J.F., Dougherty, B.A., Merrick, J.M., McKenney, K., Sutton, G., FitzHugh, W., Fields, C., Gocayne, J.D., Scott, J., Shirley, R., Liu, L.I., Glodek, A., Kelley, J.M., Weidman, J.F., Phillips, C.A., Spriggs, T., Hedblom, E., Cotton, M.D., Utterback, T.R., Hanna, M.C., Nguyen, D.T., Saudek, D.M., Brandon, R.C., Fine, L.D., Fritchman, J.L., Fuhrmann, J.L., Geoghagen, N.S.M., Gnehm, C.L., McDonald, L.A., Small, K.V., Fraser, C.M., Smith, H.O. and Venter, J.C. (1995) Whole-genome random sequencing and assembly of *Haemophilus influenzae* Rd. *Science*, **269**, 496-512.

Fox, G.E., Stackebrandt, E., Hespell, R.B., Gibson, J., Maniloff, J., Dyer, T.A., Wolfe, R.S., Balch, W.E., Tanner, R.S., Magrum, L.J., Zablen, L.B., Blakemore, R., Gupta, R., Bonen, L., Lewis, B.J., Stahl, D.A., Luehrsen, K.R., Chen, K.N. and Woese, C.R. (1980) The phylogeny of prokaryotes. *Science*, **209**, 457-463.

French, F.A. and Freedlander, B.L. (1958) Carcinostatic action of polycarbonyl compounds and their derivatives. *Cancer Res.*, **18**, 172-175.

Fulkerson, J.F., Garner, R.M. and Mobley, H.L.T. (1998) Conserved residues and motifs in the NixA protein of *Helicobacter pylori* are critical for the high affinity transport of nickel ions. *J. Biol. Chem.*, **273**, 235-241.

Gao, J., Cheng, X., Chen, R., Sigal, G.B., Bruce, J.E., Schwartz, B.L., Hofstadler, S.A., Anderson, G.A., Smith, R.D. and Whitesides, G.M. (1996) Screening derivatized peptide libraries for tight binding inhibitors to carbonic anhydrase II by electrospray ionization-mass spectrometry. *J. Med. Chem.*, **39**, 1949-1955.

Garcia-Iniguez, L., Powers, L., Chance, B., Sellin, S., Mannervik, B. and Mildvan, A.S. (1984) X-ray absorption studies of the Zn^{2+} site of glyoxalase I. *Biochemistry*, **23**, 685-689.

Gardner, K.H. and Coleman, J.E. (1994) ^{113}Cd-^{1}H heteroTOCSY: A method for determining metal-protein connectivities. *J. Biomol. NMR*, **4**, 761-774.

Gill, S.C. and von Hippel, P.H. (1989) Calculation of protein extinction coefficients from amino acid sequence data. *Anal. Biochem.*, **182**, 319-326.

Gomis-Rüth, F.X., Grams, F., Yiallouros, I., Nar, H., Küsthardt, U., Zwilling, R., Bode, W. and Stöcker, W. (1994) Crystal structures, spectroscopic features, and catalytic properties of cobalt (II), copper(II), nickel(II), and mercury(II) derivatives of zinc endopeptidase astacin. A correlation of structure and proteolytic activity. *J. Biol. Chem.*, **269**, 17111-17117.

Goodfellow, B.J., Lima, M.J., Ascenso, C., Kennedy, M., Sikkink, R., Rusnak, F., Moura, I. and Moura, J.J.G. (1998) The use of ^{113}Cd NMR chemical shifts as a structural probe in tetrathiolate metalloproteins. *Inorg. Chim. Acta*, **273**, 279-287.

Grandori, R., Struck, K., Giovanielli, K. and Carey, J. (1997) A three-step PCR protocol for construction of chimeric proteins. *Protein Eng.*, **10**, 1099-1100.

Green, B.N., Bordoli, R.S., Hanin, L.G., Lallier, F.H., Toulmond, A. and Vinogradov, S.N. (1999) Electrospray ionization mass spectrometric determination of the molecular mass of the ~200-kDa globin dodecamer subassemblies in hexagonal bilayer hemoglobins. *J. Biol. Chem.*, **274**, 28206-28212.

Green, M.L. and Elliott, W.H. (1964) The enzymic formation of aminoacetone from threonine and its further metabolism. *Biochem. J.*, **92**, 537-549.

Griffis, C.E.F., Ong, L.H., Buettner, L. and Creighton, D.J. (1983) Nonstereospecific substrate utilization by glyoxalase I. *Biochemistry*, **22**, 2945-2951.

Groche, D., Becker, A., Schlichting, I., Kabsch, W., Schultz, S. and Wagner, A.F.V. (1998) Isolation and crystallization of functionally competent *Escherichia coli* peptide

deformylase forms containing either iron or nickel in the active site. *Biochem. Biophys. Res. Commun.*, **246**, 342-346.

Hall, S.S., Doweyko, A.M. and Jordan, F. (1976) Glyoxalase I enzyme studies. 2. Nuclear magnetic resonance evidence for an enediol-proton transfer mechanism. *J. Am. Chem. Soc.*, **98**, 7460-7461.

Hall, S.S., Doweyko, A.M. and Jordan, F. (1978) Glyoxalase I enzyme studies. 4. General base catalyzed enediol proton transfer rearrangement of methyl- and phenylglutathionylhemithiol acetal to *S*-lactoyl- and *S*-mandeloylglutathione followed by hydrolysis. A model for the glyoxalase enzyme system. *J. Am. Chem. Soc.*, **100**, 5934-5939.

Hamilton, D.S. and Creighton, D.J. (1992) Inhibition of glyoxalase I by the enediol mimic *S*-(*N*-hydroxy-*N*-methylcarbamoyl)glutathione. The possible basis of a tumor-selective anticancer strategy. *J. Biol. Chem.*, **267**, 24933-24936.

Hamilton, D.S., Kavarana, M.J., Sharkey, E.M., Eiseman, J.L. and Creighton, D.J. (1999) A new method for rapidly generating inhibitors of glyoxalase I inside tumor cells using *S*-(*N*-Aryl-*N*-hydroxycarbamoyl)ethylsulfoxides. *J. Med. Chem.*, **42**, 1823-1827.

Han, L.P.B., Schimandle, C.M., Davison, L.M. and Vander Jagt, D.L. (1977) Comparative kinetics of Mg^{2+}-, Mn^{2+}-, Co^{2+}-, and Ni^{2+}-activated glyoxalase I. Evaluation of the role of the metal ion. *Biochemistry*, **16**, 5478-5484.

Han, S., Eltis, L.D., Timmis, K.N., Muchmore, S.W. and Bolin, J.T. (1995) Crystal structure of the biphenyl-cleaving extradiol dioxygenase from a PCB-degrading Pseudomonad. *Science*, **270**, 976-980.

Harp, J.M., Hanson, B.L., Timm, D.E. and Bunick, G.J. (1999) Macromolecular crystal annealing: Evaluation of techniques and variables. *Acta Crystallogr.*, **D55**, 1329-1334.

Harp, J.M., Timm, D.E. and Bunick, G.J. (1998) Macromolecular crystal annealing: Overcoming increased mosaicity associated with cryocrystallography. *Acta Crystallogr.*, **D54**, 622-628.

Hauptman, H.A. (1997) Shake-and-Bake: An algorithm for automatic solution *ab initio* of crystal structures. *Methods Enzymol.*, **277**, 3-13.

Hausinger, R.P. (1987) Nickel utilization by microorganisms. *Microbiol. Rev.*, **51**, 22-42.

Hausinger, R.P. (1994) Nickel enzymes in microbes. *Sci. Total Environ.*, **148**, 157-166.

Hausinger, R.P. (1997) Metallocenter assembly in nickel-containing enzymes. *J. Biol. Inorg. Chem.*, **2**, 279-286.

Hay, R.W. (1984) *Bio-Inorganic Chemistry*. Ellis Horwood Ltd., West Sussex, pp. 51-57.

He, M.M., Clugston, S.L., Honek, J.F. and Matthews, B.W. (2000) Determination of the structure of *Escherichia coli* glyoxalase I suggests a structural basis for differential metal activation. *Biochemistry*, **39**, 8719-8727.

Heidelberg, J.F., Eisen, J.A., Nelson, W.C., Clayton, R.A., Gwinn, M.L., Dodson, R.J., Haft, D.H., Hickey, E.K., Peterson, J.D., Umayam, L., Gill, S.R., Nelson, K.E., Read, T.D., Tettelin, H., Richardson, D., Ermolaeva, M.D., Vamathevan, J., Bass, S., Qin, H.,

Dragoi, I., Sellers, P., McDonald, L., Utterback, T., Fleishmann, R.D., Nierman, W.C. and White, O. (2000) DNA sequence of both chromosomes of the cholera pathogen *Vibrio cholerae*. *Nature*, **406**, 477-483.

Hendrickson, W.A., Horton, J.R. and LeMaster, D.M. (1990) Selenomethionyl proteins produced for analysis by multiwavelength anomalous diffraction (MAD): A vehicle for direct determination of three-dimensional structure. *EMBO J.*, **9**, 1665-1672.

Hensley, P. (1996) Defining the structure and stability of macromolecular assemblies in solution: the re-emergence of analytical ultracentrifugation as a practical tool. *Structure*, **4**, 367-373.

Hernandez Valladares, M., Felici, A., Weber, G., Adolph, H.W., Zeppezauer, M., Rossolini, G.M., Amicosante, G., Frère, J.M. and Galleni, M. (1997) Zn(II) dependence of the *Aeromonas hydrophila* AE036 metallo-β-lactamase activity and stability. *Biochemistry*, **36**, 11534-11541.

Ho, S.N., Hunt, H.D., Horton, R.M., Pullen, J.K. and Pease, L.R. (1989) Site-directed mutagenesis by overlap extension using the polymerase chain reaction. *Gene*, **77**, 51-59.

Homewood, C.A. and Neame, K.D. (1980) Biochemistry of malarial parasites. In Kreier, J.P. (ed.) *Malaria: Epidemology, Chemotherapy, Morphology, and Metabolism*. Academic Press, NY, Vol. 1, pp. 345-405.

Hopkins, F.G. and Morgan, E.J. (1948) *Biochem. J.*, **42**, 23-27.

Hopper, D.J. and Cooper, R.A. (1971) The regulation of *Escherichia coli* methylglyoxal synthase: A new control site in glycolysis? *FEBS Lett.*, **13**, 213-216.

Hopper, D.J. and Cooper, R.A. (1972) The purification and properties of *Escherichia coli* methylglyoxal synthase. *Biochem. J.*, **128**, 321-329.

Hou, S.M., Nori, P., Fang, J.L. and Vaca, C.E. (1995) Methylglyoxal induces *hprt* mutation and DNA adducts in human T-lymphocytes *in vitro*. *Environ. Mol. Mutagen.*, **26**, 286-291.

Huang, C.C., Lesburg, C.A., Kiefer, L.L., Fierke, C.A. and Christianson, D.W. (1996) Reversal of the hydrogen bond to zinc ligand histidine-119 dramatically diminishes catalysis and enhances metal equilibration kinetics in carbonic anhydrase II. *Biochemistry*, **35**, 3439-3446.

Hughes, T.R. and Klotz, I.M. (1956) Analysis of metal-protein complexes. In Glick, D. (ed.) *Methods of Biochemical Analysis*. Interscience Publishing Inc., NY, Vol. 3, pp. 265-325.

Hunt, J.A. and Fierke, C.A. (1997) Selection of carbonic anhydrase variants displayed on phage. Aromatic residues in zinc binding site enhance metal affinity and equilibration kinetics. *J. Biol. Chem.*, **272**, 20364-20372.

Hunt, J.B., Neece, S.H., Schachman, H.K. and Ginsburg, A. (1984) Mercurial-promoted Zn^{2+} release from *Escherichia coli* aspartate transcarbamoylase. *J. Biol. Chem.*, **259**, 14793-14803.

Inoue, Y. and Kimura, A. (1992) Purification and characterization of glyoxalase II from *Hansenula mrakii*. *J. Ferment. Bioeng.*, **73**, 271-276.

Inoue, Y. and Kimura, A. (1995) Methylglyoxal and regulation of its metabolism in microorganisms. *Adv. Microb. Physiol.*, **37**, 177-227.

Inoue, Y. and Kimura, A. (1996) Identification of the structural gene for glyoxalase I from *Saccharomyces cerevisiae*. *J. Biol. Chem.*, **271**, 25958-25965.

Inoue, Y., Tran, L.T., Yoshikawa, K., Murata, K. and Kimura, A. (1991) Purification and characterization of glyoxalase I from *Hansenula mrakii*. *J. Ferment. Bioeng.*, **71**, 131-133.

Iyengar, R. and Rose, I.A. (1981) Concentration of activated intermediates of the fructose-1,6-bisphosphate aldolase and triosephosphate isomerase reactions. *Biochemistry*, **20**, 1223-1229.

Izard, T. and Geerlof, A. (1999) The crystal structure of a novel bacterial adenylyltransferase reveals half of sites reactivity. *EMBO J.*, **18**, 2021-2030.

Jabri, E., Carr, M.B., Hausinger, R.P. and Karplus, P.A. (1995) The crystal structure of urease from *Klebsiella aerogenes*. *Science*, **268**, 998-1004.

Johansen, K.S., Svendsen, I. and Rasmussen, S.K. (2000) Purification and cloning of the two domain glyoxalase I from wheat bran. *Plant Sci.*, **155**, 11-20.

Jones, T.A. and Kjeldgaard, M. (1997) Electron-density map interpretation. *Methods Enzymol.*, **277**, 173-208.

Jones, T.A., Zou, J.Y., Cowan, S.W. and Kjeldgaard, M.O. (1991) Improved methods for binding protein models in electron density maps and the location of errors in these models. *Acta Crystallogr.*, **A47**, 110-119.

Jørgensen, T.J.D., Roepstorff, P. and Heck, A.J.R. (1998) Direct determination of solution binding constants for noncovalent complexes between bacterial cell wall peptide analogues and vancomycin group antibiotics by electrospray ionization mass spectrometry. *Anal. Chem.*, **70**, 4427-4432.

Joseph, D., Petsko, G.A. and Karplus, M. (1990) Anatomy of a conformational change: Hinged "lid" motion of the triosephosphate isomerase loop. *Science*, **249**, 1425-1428.

Jowett, M. and Quastel, J.H. (1933) *Biochem. J.*, **27**, 486-498.

Kalapos, M.P. (1999) On the promine/retine theory of cell division: Now and then. *Biochim. Biophys. Acta*, **1426**, 1-16.

Kaneko, T., Tanaka, A., Sato, S., Kotani, H., Sazuka, T., Miyajima, N., Sugiura, M. and Tabata, S. (1995) Sequence analysis of the genome of the unicellular cyanobacterium *Synechocystis* sp. strain PCC6803. I. Sequence feature in the 1 Mb region from map positions 64% to 92% of the genome. *DNA Res.*, **2**, 153-166.

Kavarana, M.J., Kovaleva, E.G., Creighton, D.J., Wollman, M.B. and Eiseman, J.L. (1999) Mechanism-based competitive inhibitors of glyoxalase I: Intracellular delivery, *in vitro* antitumor activities, and stabilities in human serum and mouse serum. *J. Med. Chem.*, **42**, 221-228.

Keating, K.M., Ghosaini, L.R., Giedroc, D.P., Williams, K.R., Coleman, J.E. and Sturtevant, J.M. (1988) Thermal denaturation of T4 gene 32 protein: Effects of zinc removal and substitution. *Biochemistry*, **27**, 5240-5245.

Kelly, D.P. and Wood, A.P. (2000) Reclassification of some species of *Thiobacillus* to the newly designated genera *Acidithiobacillus* gen. nov., *Halothiobacillus* gen. nov. and *Thermithiobacillus* gen. nov. *Int. J. Syst. Evol. Microbiol.*, **50**, 511-516.

Kermack, W.O. and Matheson, N.A. (1957) The effects of some analogues of glutathione on the glyoxalase system. *Biochem. J.*, **65**, 48-58.

Kester, M.V. and Norton, S.J. (1975) Isolation and characterization of mouse liver glyoxalase I. *Biochim. Biophys. Acta*, **391**, 212-221.

Kiefer, L.L., Paterno, S.A. and Fierke, C.A. (1995) Hydrogen bond network in the metal binding site of carbonic anhydrase enhances zinc affinity and catalytic efficiency. *J. Am. Chem. Soc.*, **117**, 6831-6837.

Kim, E.J., Kim, H.P., Hah, Y.C. and Roe, J.H. (1996) Differential expression of superoxide dismutases containing Ni and Fe/Zn in *Streptomyces coelicolor*. *Eur. J. Biochem.*, **241**, 178-185.

Kim, N.S., Sekine, S., Kiuchi, N. and Kato, S. (1995) cDNA cloning and characterization of human glyoxalase I isoforms from HT-1080 cells. *J. Biochem.*, **117**, 359-361.

Kim, N.S., Umezawa, Y., Ohmura, S. and Kato, S. (1993) Human glyoxalase I. cDNA cloning, expression, and sequence similarity to glyoxalase I from *Pseudomonas putida*. *J. Biol. Chem.*, **268**, 11217-11221.

Kissinger, C.R. and Gehlhaar, D.K. (1997) EPMR Users' manual. Agouron Pharmaceuticals Inc., San Diego.

Kizil, G., Wilks, K., Wells, D. and Ala'Aldeen, D.A.A. (2000) Detection and characterisation of the genes encoding glyoxalase I and II from *Neisseria meningitidis*. *J. Med. Microbiol.*, **49**, 669-673.

Kleywegt, G. and Jones, T. (1994) In Bailey, S., Hubbard, R. and Waller, D. (eds.), *From First Map to Final Model*. EPSRC Daresbury Laboratory, Daresbury, UK, pp. 59-66.

Knell, A.J. (ed.) (1991) *Malaria: A publication of the tropical programme of the Wellcome Trust*. Oxford University Press, NY.

Koshland, D.E. (1996) The structural basis of negative cooperativity: Receptors and enzymes. *Curr. Opin. Struc. Biol.*, **6**, 757-761.

Kozarich, J.W. and Deegan, J.L. (1979) 7-Methylguanosine-dependent inhibition of globin mRNA translation by methylglyoxal. *J. Biol. Chem.*, **254**, 9345-9348.

Kraulis, P.J. (1991) MOLSCRIPT: a program to produce both detailed and schematic plots of protein structures. *J. Appl. Crystallogr.*, **24**, 946-950.

Kreier, J.P. (ed.) (1980) *Malaria: Epidemology, Chemotherapy, Morphology, and Metabolism*. Academic Press, NY, Vol. 1.

Kurasawa, S., Takeuchi, T. and Umezawa, H. (1976) The reaction mechanism of rat liver glyoxalase I and its inhibition by MS-3. *Agric. Biol. Chem.*, **40**, 559-566.

Lan, Y., Lu, T., Lovett, P.S. and Creighton, D.J. (1995) Evidence for a (triosephosphate isomerase-like) "catalytic loop" near the active site of glyoxalase I. *J. Biol. Chem.*, **270**, 12957-12960.

Ladbury, J.E. and Chowdhry, B.Z. (1996) Sensing the heat: The application of isothermal titration calorimetry to thermodynamic studies of biomolecular interactions. *Chem. Biol.*, **3**, 791-801.

Ladbury, J.E. and Chowdhry, B.Z. (eds.) (1998) *Biocalorimetry: Applications of calorimetry in the biological sciences*. John Wiley & Sons Ltd., England.

Landro, J.A., Brush, E.J. and Kozarich, J.W. (1992) Isomerization of (*R*)- and (*S*)-glutathiolactaldehydes by glyoxalase I: The case for dichotomous stereochemical behavior in a single active site. *Biochemistry*, **31**, 6069-6077.

Laskowski, R.A., MacArthur, M.W., Moss, D.S. and Thornton, J.M. (1993) PROCHECK: a program to check the stereochemical quality of protein structures. *J. Appl. Crystallogr.*, **26**, 283-291.

Laughlin, L.T., Bernat, B.A. and Armstrong, R.N. (1998) Mechanistic imperative for the evolution of a metalloglutathione transferase of the vicinal oxygen chelate superfamily. *Chem. Biol. Interact.*, **111-112**, 41-50.

Leslie, A.G.W. (1999) Mosflm 6.0 Users' manual 6.0 edit. MRC Laboratory of Molecular Biology, Cambridge.

Live, D.H., Kojiro, C.L., Cowburn, D. and Markley, J.L. (1985) Identification of protein NMR signals from the metal ligands in cadmium-substituted plastocyanin via two-dimensional multiple-quantum detection in the absence of explicitly resolved ^{1}H-^{113}Cd Coupling. *J. Am. Chem. Soc.*, **107**, 3043-3045.

Lo, T.W.C., Selwood, T. and Thornalley, P.J. (1994a) The reaction of methylglyoxal with aminoguanidine under physiological conditions and prevention of methylglyoxal binding to plasma proteins. *Biochem. Pharmacol.*, **48**, 1865-1870.

Lo, T.W.C. and Thornalley, P.J. (1992) Inhibition of proliferation of human leukemia 60 cells by diethyl esters of glyoxalase inhibitors *in vitro*. *Biochem. Pharmacol.*, **44**, 2357-2363.

Lo, T.W.C., Westwood, M.E., McLellan, A.C., Selwood, T. and Thornalley, P.J. (1994b) Binding and modification of proteins by methylglyoxal under physiological conditions. *J. Biol. Chem.*, **269**, 32299-32305.

Lohmann, K. (1932) *Biochem Z.*, **254**, 332-354.

Loo, J.A. (1997) Studying noncovalent protein complexes by electrospray ionization mass spectrometry. *Mass Spectrom. Rev.*, **16**, 1-23.

Lu, T., Creighton, D.J., Antoine, M., Fenselau, C. and Lovett, P.S. (1994) The gene encoding glyoxalase I from *Pseudomonas putida*: cloning, overexpression, and sequence comparisons with human glyoxalase I. *Gene*, **150**, 93-96.

Ly, H.D., Clugston, S.L., Sampson, P.B. and Honek, J.F. (1998) Syntheses and kinetic evaluation of hydroxamate-based peptide inhibitors of glyoxalase I. *Bioorg. Med. Chem. Lett.*, **8**, 705-710.

Lyles, G.A. and Chalmers, J. (1995) Aminoacetone metabolism by semicarbazide-sensitive amine oxidase in rat aorta. *Biochem. Pharm.*, **49**, 416-419.

MacLean, M.J., Ness, L.S., Ferguson, G.P. and Booth, I.R. (1998) The role of glyoxalase I in the detoxification of methylglyoxal and in the activation of the KefB K^+ efflux system in *Escherichia coli. Mol. Microbiol,*. **27**, 563-571.

Maiti, M.K., Krishnasamy, S., Owen, H.A. and Makaroff, C.A. (1997) Molecular characterization of glyoxalase II from *Arabidopsis thaliana. Plant Mol. Biol.*, **35**, 471-481.

Mannervik, B., Lindstrom, L. and Bartfai, T. (1972) Partial purification and characterization of glyoxalase I from porcine erythrocytes. *Eur. J. Biochem.*, **29**, 276-281.

Marmstål, E., Aronsson, A.C. and Mannervik, B. (1979) Comparison of glyoxalase I purified from yeast (*Saccharomyces cerevisiae*) with the enzyme from mammalian sources. *Biochem. J.*, **183**, 23-30.

Marmstål, E. and Mannervik, B. (1978) Subunit structure of glyoxalase I from yeast. *FEBS Lett.*, **85**, 275-278.

Marmstål, E. and Mannervik, B. (1979) Binding of the competitive inhibitor *S*-(*p*-bromobenzyl)-glutathione to glyoxalase I from yeast. *FEBS Lett.*, **102**, 162-164.

Maroney, M.J. (1999) Structure/function relationships in nickel metallobiochemistry. *Curr. Opin. Chem. Biol.*, **3**, 188-199.

Maroney, M.J., Davidson, G., Allan, C.B. and Figlar, J. (1998) The structure and function of nickel sites in metalloproteins. *Struct. Bonding*, **92**, 1-65.

McKendree, W.L., Doostdar, H., T.G., M. and Mayer, R.T. (1997) cDNA cloning and expression of a gene (Acession No. Z97064) from *Citrus paradisi* roots similar to bacterial YRN1 and HEAHIO protein and an mRNA from *Brassica oleracea* that is wound and dark inducible (PGR97-127). *Plant Physiol.*, **115**, 314.

McLellan, A.C., Thornalley, P.J., Benn, J. and Sonksen, P.H. (1994) Glyoxalase system in clinical diabetes mellitus and correlation with diabetic complications. *Clin. Sci.*, **87**, 21-29.

Melino, S., Capo, C., Dragani, B., Aceto, A. and Petruzzelli, R. (1998) A zinc-binding motif conserved in glyoxalase II, β-lactamase and arylsulfatases. *Trends Biochem. Sci.*, **23**, 381-382.

Merritt, E.A. and Bacon, D.J. (1997) Raster3D: Photorealistic molecular graphics. *Methods Enzymol.*, **277**, 505-524.

Misra, K., Banerjee, A.B., Ray, S. and Ray, M. (1995) Glyoxalase III from *Escherichia coli*: A single novel enzyme for the conversion of methylglyoxal into D-lactate without reduced glutathione. *Biochem. J.*, **305**, 999-1003.

Mobley, H.L.T., Island, M.D. and Hausinger, R.P. (1995) Molecular biology of microbial ureases. *Microbiol. Rev.*, **59**, 451-480.

Murata, K., Inoue, Y., Rhee, H.I. and Kimura, A. (1989) 2-Oxoaldehyde metabolism in microorganisms. *Can. J. Microbiol.*, **35**, 423-431.

Murata, K., Inoue, Y., Watanabe, K., Fukuda, Y., Saikusa, T., Shimosaka, M. and Kimura, A. (1986a) Metabolism of α-ketoaldehydes in yeasts: Purification and characterization of glyoxalase II from *Saccharomyces cerevisiae*. *Agric. Biol. Chem.*, **50**, 135-142.

Murata, K., Saikusa, T., Fukuda, Y., Watanabe, K., Inoue, Y., Shimosaka, M. and Kimura, A. (1986b) Metabolism of 2-oxoaldehydes in yeast. Possible role of glycolytic bypath as a detoxification system in L-threonine catabolism by *Saccharomyces cerevisiae*. *Eur. J. Biochem.*, **157**, 297-301.

Murata, K., Saikusa, T., Watanabe, K., Inoue, Y., Fukuda, Y., Shimosaka, M. and Kimura, A. (1986c) Complete purification of yeast glyoxalase I and its activation by ferrous ions and polyamines. *Agric. Biol. Chem.*, **50**, 2381-2383.

Murthy, N.S.R.K., Bakeris, T., Kavarana, M.J., Hamilton, D.S., Lan, Y. and Creighton, D.J. (1994) *S*-(*N*-Aryl-*N*-hydroxycarbamoyl)glutathione derivatives are tight-binding inhibitors of glyoxalase I and slow substrates for glyoxalase II. *J. Med. Chem.*, **37**, 2161-2166.

Myers, E.W. and Miller, W. (1988) Optimal alignments in linear space. *Comput. Appl. Biosci.*, **4**, 11-17.

Navarro, C., Wu, L.F. and Mandrand-Berthelot, M.A. (1993) The *nik* operon of *Escherichia coli* encodes a periplasmic binding-protein-dependent transport system for nickel. *Mol. Microbiol.*, **9**, 1181-1191.

Nettleton, E.J., Sunde, M., Lai, Z., Kelly, J.W., Dobson, C.M. and Robinson, C.V. (1998) Protein subunit interactions and structural integrity of amyloidogenic transthyretins: Evidence from electrospray mass spectrometry. *J. Mol. Biol.*, **281**, 553-564.

Neuberg, C. (1913a) *Biochem. Z*, **49**, 502-506.

Neuberg, C. (1913b) *Biochem Z*, **51**, 484-508.

Newton, G.L., Arnold, K., Price, M.S., Sherrill, C., Delcardayre, S.B., Aharonowitz, Y., Cohen, G., Davies, J., Fahey, R.C. and Davis, C. (1996) Distribution of thiols in microorganisms: Mycothiol is a major thiol in most actinomycetes. *J. Bacteriol.*, **178**, 1990-1995.

Newton, G.L., Av-Gay, Y. and Fahey, R.C. (2000) A novel mycothiol-dependent detoxification pathway in mycobacteria involving mycothiol *S*-conjugate amidase. *Biochemistry*, **39**, 10739-10746.

Nicholls, A. and Honig, B. (1991) *J. Comput. Chem.*, **12**, 435-445.

Norton, S.J., Talesa, V., Yuan, W.J. and Principato, G.B. (1990) Glyoxalase I and glyoxalase II from *Aloe vera*: Purification, characterization and comparison with animal glyoxalases. *Biochem. Int.*, **22**, 411-418.

Ochman, H. and Wilson, A.C. (1987) Evolution in bacteria: Evidence for a universal substitution rate in cellular genomes. *J. Mol. Evol.*, **26**, 74-86.

Omburo, G.A., Kuo, J.M., Mullins, L.S. and Raushel, F.M. (1992) Characterization of the zinc binding site of bacterial phosphotriesterase. *J. Biol. Chem.*, **267**, 13278-13283.

Oray, B. and Norton, S.J. (1980) Purification and characterization of mouse liver glyoxalase II. *Biochim. Biophys. Acta*, **611**, 168-173.

Otwinowski, Z. and Minor, W. (1997) Processing of x-ray diffraction data collected in oscillation mode. *Methods Enzymol.*, **276**, 307-326.

Oya, T., Hattori, N., Mizuno, Y., Miyata, S., Maeda, S., Osawa, T. and Uchida, K. (1999) Methylglyoxal modification of protein: Chemical and immunochemical characterization of methylglyoxal-arginine adducts. *J. Biol. Chem.*, **274**, 18492-18502.

Pallen, C.J. and Wang, J.H. (1986) Stoichiometry and dynamic interaction of metal ion activators with calcineurin phosphatase. *J. Biol. Chem.*, **261**, 16115-16120.

Papoulis, A., Al-Abed, Y. and Bucala, R. (1995) Identification of N^2-(1-carboxy)guanine (CEG) as a guanine advanced glycosylation end product. *Biochemistry*, **34**, 648-655.

Park, I.S. and Hausinger, R.P. (1995) Requirement of carbon dioxide for *in vitro* assembly of the urease nickel metallocenter. *Science*, **267**, 1156-1158.

Patel, M.P. and Blanchard, J.S. (1999) Expression, purification, and characterization of *Mycobacterium tuberculosis* mycothione reductase. *Biochemistry*, **38**, 11827-11833.

Pauling, L. (1960) *The Nature of the Chemical Bond.* Cornell University Press, Ithaca, NY.

Paulus, C., Köllner, B. and Jacobsen, H.J. (1993) Physiological and biochemical characterization of glyoxalase I, a general marker for cell proliferation, from a soybean cell suspension. *Planta*, **189**, 561-566.

Penninckx, M.J., Jaspers, C.J. and Legrain, M.J. (1983) The glutathione-dependent glyoxalase pathway in the yeast *Saccharomyces cerevisiae*. A vital defense line against methylglyoxal produced during glycerol catabolism. *J. Biol. Chem.*, **258**, 6030-6036.

Phillips, S.A., Mirrlees, D. and Thornalley, P.J. (1993) Modification of the glyoxalase system in streptozotocin-induced diabetic rats. Effect of the aldose reductase inhibitor Statil. *Biochem. Pharmacol.*, **46**, 805-811.

Phillips, S.A. and Thornalley, P.J. (1993) The formation of methylglyoxal from triose phosphates. Investigation using a specific assay for methylglyoxal. *Eur. J. Biochem.*, **212**, 101-105.

Pompliano, D.L., Peyman, A. and Knowles, J.R. (1990) Stabilization of a reaction intermediate as a catalytic device: Definition of the functional role of the flexible loop in triosephosphate isomerase. *Biochemistry*, **29**, 3186-3194.

Potier, N., Barth, P., Tritsch, D., Biellmann, J.F. and Van Dorsselaer, A. (1997) Study of non-covalent enzyme-inhibitor complexes of aldose reductase by electrospray mass spectrometry. *Eur. J. Biochem.*, **243**, 274-282.

Price, N.C. (ed.) (1996) *Protein LabFax*. BIOS Scientific Publishers, Academic Press, San Diego, pp. 22-23.

Przybylski, M. and Glocker, M.O. (1996) Electrospray mass spectrometry of biomacromolecular complexes with noncovalent interactions-New analytical perspectives for supramolecular chemistry and molecular recognition processes. *Agnew. Chem. Int.*, **35**, 806-826.

Racker, E. (1951) The mechanism of action of glyoxalase. *J. Biol. Chem.*, **190**, 685-696.

Racker, E. (1954) In Colowick, S. and Lazarow, A. (eds.), *Glutathione*. Academic Press, NY, p. 208.

Rae, C., O'Donoghue, S.I., Bubb, W.A. and Kuchel, P.W. (1994) Stereospecificity of substrate usage by glyoxalase 1: Nuclear magnetic resonance studies of kinetics and hemithioacetal substrate conformation. *Biochemistry*, **33**, 3548-3559.

Ragsdale, S.W. (1998) Nickel biochemistry. *Curr. Opin. Chem. Biol.*, **2**, 208-215.

Ragusa, S., Blanquet, S. and Meinnel, T. (1998) Control of peptide deformylase activity by metal cations. *J. Mol. Biol.*, **280**, 515-523.

Ranganathan, S., Walsh, E.S., Godwin, A.K. and Tew, K.D. (1993) Cloning and characterization of human colon glyoxalase-I. *J. Biol. Chem.*, **268**, 5661-5667.

Ranganathan, S., Walsh, E.S. and Tew, K.D. (1995) Glyoxalase I in detoxification: Studies using a glyoxalase I transfectant cell line. *Biochem. J.*, **309**, 127-131.

Ratliff, D.M., Vander Jagt, D.J., Eaton, R.P. and Vander Jagt, D.L. (1996) Increased levels of methylglyoxal-metabolizing enzymes in mononuclear and polymorphonuclear cells from insulin-dependent diabetic patients with diabetic complications: Aldose reductase, glyoxalase I, and glyoxalase II - A clinical research study. *J. Clin. Endocrin.*, **81**, 488-492.

Ray, M. and Ray, S. (1984) Purification and partial characterization of a methylglyoxal reductase from goat liver. *Biochim. Biophys. Acta*, **802**, 119-127.

Ray, M. and Ray, S. (1987) Aminoacetone oxidase from goat liver. Formation of methylglyoxal from aminoacetone. *J. Biol. Chem.*, **262**, 5974-5977.

Ray, S. and Ray, M. (1982) Purification and characterization of NAD and NADP-linked α-ketoaldehyde dehydrogenases involved in catalyzing the oxidation of methylglyoxal to pyruvate. *J. Biol. Chem.*, **257**, 10566-10570.

Ray, S. and Ray, M. (1987) A reinvestigation of inhibitors of glyoxalase I. *J. Biosci.*, **12**, 405-414.

Rehr, J.J., Albers, R.C., and Zabinsky, S.I. (1992) High-order multiple-scattering calculations of x-ray-absorption fine structure. *Phys. Rev. Lett.*, **69**, 3397-3400.

Ressler, R. (1997) WinXAS: A new software package not only for the analysis of energy-dispersive XAS data. *J. Phys. IV*, 7, C2 269-270.

Rhee, H.I., Murata, K. and Kimura, A. (1986) Purification and characterization of glyoxalase I from *Pseudomonas putida*. *Biochem. Biophys. Res. Commun.*, **141**, 993-999.

Rhee, H.I., Sato, N., Murata, K. and Kimura, A. (1988) Nucleotide sequence of the glyoxalase I gene of *Pseudomonas putida*. *Agric. Biol. Chem.*, **52**, 2243-2246.

Rhodes, G. (1993) *Crystallography made crystal clear: A guide for users of macromolecular models*. Academic Press Inc., San Diego.

Richard, J.P. (1991) Kinetic parameters for the elimination reaction catalyzed by triosephosphate isomerase and an estimation of the reaction's physiological significance. *Biochemistry*, **30**, 4581-4585.

Ridderström, M., Cameron, A.D., Jones, T.A. and Mannervik, B. (1997) Mutagenesis of residue 157 in the active site of human glyoxalase I. *Biochem. J.*, **328**, 231-235.

Ridderström, M., Cameron, A.D., Jones, T.A. and Mannervik, B. (1998) Involvement of an active-site Zn^{2+} ligand in the catalytic mechanism of human glyoxalase I. *J. Biol. Chem.*, **273**, 21623-21628.

Ridderström, M. and Mannervik, B. (1996) Optimized heterologous expression of the human zinc enzyme glyoxalase I. *Biochem. J.*, **314**, 463-467.

Ridderström, M. and Mannervik, B. (1996) The primary structure of monomeric yeast glyoxalase I indicates a gene duplication resulting in two similar segments homologous with the subunit of dimeric human glyoxalase I. *Biochem. J.*, **316**, 1005-1006.

Ridderström, M. and Mannervik, B. (1997) Molecular cloning and characterization of the thiolesterase glyoxalase II from *Arabidopsis thaliana*. *Biochem. J.*, **322**, 449-454.

Ridderström, M., Saccucci, F., Hellman, U., Bergman, T., Principato, G. and Mannervik, B. (1996) Molecular cloning, heterologous expression, and characterization of human glyoxalase II. *J. Biol. Chem.*, **271**, 319-323.

Riddles, P.W., Blakeley, R.L. and Zerner, B. (1983) Reassessment of Ellman's reagent. *Methods in Enzymol.*, **91**, 49-60.

Robinson, J.W. (1996) *Atomic Spectroscopy*. Marcel Dekker, Inc., NY.

Roepstorff, P. (1997) Mass spectrometry in protein studies from genome to function. *Curr. Opin. Biotechnol.*, **8**, 6-13.

Romo, S., Labrodor, E. and Dopico, B. (1998) Isolation and characterizaiton of a cDNA encoding a glyoxalase-I (Accession No. AJ224520) from *Cicer arietinum* L. epicotyls up-regulated by stress (PGR 98-074). *Plant Physiol.*, **117**, 331.

Rose, I.A. (1957) Mechanism of the action of glyoxalase I. *Biochim. Biophys. Acta*, **25**, 214-215.

Rostom, A.A., Sunde, M., Richardson, S.J., Schreiber, G., Jarvis, S., Bateman, R., Dobson, C.M. and Robinson, C.V. (1998) Dissection of multi-protein complexes using mass spectrometry: Subunit interactions in transthyretin and retinol-binding protein complexes. *Proteins*, **2**, 3-11.

Saadat, D. and Harrison, D.H.T. (1998) Identification of catalytic bases in the active site of *Escherichia coli* methylglyoxal synthase: Cloning, expression, and functional characterization of conserved aspartic acid residues. *Biochemistry*, **37**, 10074-10086.

Saadat, D. and Harrison, D.H.T. (1999) The crystal structure of methylglyoxal synthase from *Escherichia coli*. *Structure*, **7**, 309-317.

Saikusa, T., Rhee, H.I., Watanabe, K., Murata, K. and Kimura, A. (1987) Metabolism of 2-oxoaldehydes in bacteria: Purification and characterization of methylglyoxal reductase from *Escherichia coli*. *Agric. Biol. Chem.*, **51**, 1893-1899.

Saint-Jean, A.P., Phillips, K.R., Creighton, D.J. and Stone, M.J. (1998) Active monomeric and dimeric forms of *Pseudomonas putida* glyoxalase I: Evidence for 3D domain swapping. *Biochemistry*, **37**, 10345-10353.

Sakamoto, H., Mashima, T., Kizaki, A., Dan, S., Hashimoto, Y., Naito, M. and Tsuruo, T. (2000) Glyoxalase I is involved in resistance of human leukemia cells to antitumor agent-induced apoptosis. *Blood*, **95**, 3214-3218.

Sambrook, J., Fritsch, E.F. and Maniatis, T. (1989) *Molecular Cloning: A Laboratory Manual*. Cold Spring Harbor Laboratory Press, Plainsview, NY.

Schimandle, C.M. and Vander Jagt, D.L. (1979) Isolation and kinetic analysis of the multiple forms of glyoxalase-I from human erythrocytes. *Arch. Biochem. Biophys.*, **195**, 261-268.

Sellin, S., Aronsson, A.C., Eriksson, L.E.G., Larsen, K., Tibbelin, G. and Mannervik, B. (1983a) Properties and catalytic function of glyoxalase I. In Larsson, A. (ed.) *Functions of Glutathione: Biochemical, Physiological, Toxicological, and Clinical Aspects*. Raven Press, NY, pp. 187-197.

Sellin, S., Eriksson, L.E.G., Aronsson, A.C. and Mannervik, B. (1983b) Octahedral metal coordination in the active site of glyoxalase I as evidenced by the properties of Co(II)-glyoxalase I. *J. Biol. Chem.*, **258**, 2091-2093.

Sellin, S., Eriksson, L.E.G. and Mannervik, B. (1982a) Fluorescence and nuclear relaxation enhancement studies of the binding of glutathione derivatives to manganese-reconstituted glyoxalase I from human erythrocytes. A model for the catalytic mechanism of the enzyme involving a hydrated metal ion. *Biochemistry*, **21**, 4850-4857.

Sellin, S., Eriksson, L.E.G. and Mannervik, B. (1987) Electron paramagnetic resonance study of the active site of copper-substituted human glyoxalase I. *Biochemistry*, **26**, 6779-6784.

Sellin, S. and Mannervik, B. (1984) Metal dissociation constants for glyoxalase I reconstituted with Zn^{2-}, Co^{2-}, Mn^{2-}, and Mg^{2+}. *J. Biol. Chem.*, **259**, 11426-11429.

Sellin, S., Rosevear, P.R., Mannervik, B. and Mildvan, A. (1982b) Nuclear relaxation studies of the role of the essential metal in glyoxalase I. *J. Biol. Chem.*, **257**, 10023-10029.

Sharkey, E.M., O'Neill, H.B., Kavarana, M.J., Wang, H., Creighton, D.J., Sentz, D.L. and Eiseman, J.L. (2000) Pharmacokinetics and antitumor properties in tumor-bearing mice of an enediol analogue inhibitor of glyoxalase I. *Cancer Chemother. Pharmacol.*, **46**, 156-166.

Sherman, I.W. (1979) Biochemistry of *Plasmodium* (Malarial parasites). *Microbiol. Rev.*, **43**, 453-495.

Shih, M.J., Edinger, J.W. and Creighton, D.J. (1997) Diffusion-dependent kinetic properties of glyoxalase I and estimates of the steady-state concentrations of glyoxalase-pathway intermediates in glycolyzing erythrocytes. *Eur. J. Biochem.*, **244**, 852-857.

Shinohara, M., Thornalley, P.J., Giardino, I., Beisswenger, P., Thorpe, S.R., Onorato, J. and Brownlee, M. (1998) Overexpression of glyoxalase-I in bovine endothelial cells inhibits intracellular advanced glycation endproduct formation and prevents hyperglycemia-induced increases in macromolecular endocytosis. *J. Clin. Invest.*, **101**, 1142-1147.

Silver, S. (1996) Transport of inorganic cations. In Neidhardt, F.C. (ed) *Escherichia coli and Salmonella: Cellular and molecular biology* 2nd Ed. ASM Press, Washington, Vol. 1, pp. 1091-1102.

Simpson, A.J., Reinach, F.C., Arruda, P., Abreu, F.A., Acencio, M., Alvarenga, R., Alves, L.M., Araya, J.E., Baia, G.S., Baptista, C.S., Barros, M.H., Bonaccorsi, E.D., Bordin, S., Bove, J.M., Briones, M.R., Bueno, M.R., Camargo, A.A., Camargo, L.E., Carraro, D.M., Carrer, H., Colauto, N.B., Colombo, C., Costa, F.F., Costa, M.C., Costa-Neto, C.M., Coutinho, L.L., Cristofani, M., Dias-Neto, E., Docena, C., El-Dorry, H. et al., (2000) The genome sequence of the plant pathogen *Xylella fastidiosa*. The *Xylella fastidiosa* Consortium of the Organization for Nucleotide Sequencing and Analysis. *Nature*, **406**, 151-157.

Skipsey, M., Andrews, C.J., Townson, J.K., Jepson, I. and Edwards, R. (2000) Cloning and characterization of glyoxalase I from soybean. *Arch. Biochem. Biophys.*, **374**, 261-268.

Smith, J.L. (1991) Determination of three-dimensional structure by multiwavelength anomalous diffraction. *Curr. Opin. Struc. Biol.*, **1**, 1002-1011.

Smith, J.L. and Thompson, A. (1998) Reactivity of selenomethionine-Dents in the magic bullet? *Structure*, **6**, 815-819.

Snavely, M.D., Florer, J.B., Miller, C.G. and Maguire, M.E. (1989) Magnesium transport in *Salmonella typhimurium*: $^{28}Mg^{2+}$ transport by the CorA, MgtA, and MgtB systems. *J. Bacteriol.*, **171**, 4761-4766.

Spano, L., Poma, A. and Amicarelli, F. (1998) Glyoxalase I activity in two lines of corn (*Zea mays*) with different sensitivity to cold stress. *Maydica*, **43**, 301-303.

Spies, H.S.C. and Steenkamp, D.J. (1994) Thiols of intracellular pathogens. Identification of ovothiol A in *Leishmania donovani* and structural analysis of a novel thiol from *Mycobacterium bovis*. *Eur. J. Biochem.*, **224**, 203-213.

Stark, M.J.R. (1987) Multicopy expression vectors carrying the *lac* repressor gene for regulated high-level expression of genes in *Escherichia coli*. *Gene*, **51**, 255-267.

Stokvis, E., Clugston, S.L., Honek, J.F. and Heck, A.J.R. (2000) Characterization of Glyoxalase I (*E. coli*) - Inhibitor interactions by electrospray time-of-flight mass spectrometry and enzyme kinetic analysis. *J. Prot. Chem.*, In press.

Stover, C.K., Pham, X.Q., Erwin, A.L., Mizoguchi, S.D., Warrener, P., Hickey, M.J., Brinkman, F.S., Hufnagle, W.O., Kowalik, D.J., Lagrou, M., Garber, R.L., Goltry, L., Tolentino, E., Westbrock-Wadman, S., Yuan, Y., Brody, L.L., Coulter, S.N., Folger,

K.R., Kas, A., Larbig, K., Lim, R., Smith, K., Spencer, D., Wong, G.K., Wu, Z. and Paulsen, I.T. (2000) Complete genome sequence of *Pseudomonas aeruginosa* PA01, an opportunistic pathogen. *Nature*, **406**, 959-964.

Summers, M.F. (1988) ^{113}Cd NMR spectroscopy of coordination compounds and proteins. *Coordination Chem. Rev.*, **86**, 43-134.

Szabo, A., Stolz, L. and Granzow, R. (1995) Surface plasmon resonance and its use in biomolecular interaction analysis (BIA). *Curr. Opin. Str. Biol.*, **5**, 699-705.

Szent-Györgyi, A. (1965) Cell division and cancer. *Science*, **149**, 34-37.

Szent-Györgyi, A., Együd, L.G. and McLaughlin, J.A. (1967) Keto-aldehydes and cell division. *Science*, **155**, 539-541.

Talesa, V., Rosi, G., Bistoni, F., Marconi, P., Norton, S.J. and Principato, G.B. (1990) Presence of a plant-like glyoxalase II in *Candida albicans*. *Biochem. Int.*, **21**, 397-403.

Tew, K.D., Monks, A., Barone, L., Rosser, D., Akerman, G., Montali, J.A., Wheatley, J.B. and Schmidt, D.E., Jr. (1996) Glutathione-associated enzymes in the human cell lines of the National Cancer Institute Drug Screening Program. *Mol. Pharmacol.*, **50**, 149-159.

Thompson, J.D., Higgins, D.G. and Gibson, T.J. (1994) CLUSTAL W: improving the sensitivity of progressive multiple sequence alignment through sequence weighting, position-specific gap penalties and weight matrix choice. *Nucleic Acids Res.*, **22**, 4673-4680.

Thornalley, P.J. (1991) Population genetics of human glyoxalases. *Heredity*, **67**, 139-142.

Thornalley, P.J. (1995) Advances in glyoxalase research. Glyoxalase expression in malignancy, anti-proliferative effects of methylglyoxal, glyoxalase I inhibitor diesters and *S*-D-lactoylglutathione, and methylglyoxal-modified protein binding and endocytosis by the advanced glycation endproduct receptor. *Crit. Rev. Oncol. Haematol.*, **20**, 99-128.

Thornalley, P.J. (1998) Glutathione-dependent detoxification of α-oxoaldehydes by the glyoxalase system: Involvement in disease mechanisms and antiproliferative activity of glyoxalase I inhibitors. *Chem. Biol. Interact.*, **111-112**, 137-151.

Thornalley, P.J., Edwards, L.G., Kang, Y., Wyatt, C., Davies, N., Ladan, M.J. and Double, J. (1996a) Antitumor activity of *S*-*p*-bromobenzylglutathione cyclopentyl diester *in vitro* and *in vivo*. Inhibition of glyoxalase I and induction of apoptosis. *Biochem. Pharmacol.*, **51**, 1365-1372.

Thornalley, P.J., Ladan, M.J., Ridgway, S.J.S. and Kang, Y. (1996b) Antitumor activity of *S*-(*p*-bromobenzyl)glutathione diesters *in vitro*: A structure-activity study. *J. Med. Chem.*, **39**, 3409-3411.

Thornalley, P.J., Langborg, A. and Minhas, H.S. (1999) Formation of glyoxal, methylglyoxal and 3-deoxyglucosone in the glycation of proteins by glucose. *Biochem. J.*, **344**, 109-116.

Thornalley, P.J., Strath, M. and Wilson, R.J.M. (1994) Antimalarial activity *in vitro* of the glyoxalase I inhibitor diester, *S-p*-bromobenzylglutathione diethyl ester. *Biochem. Pharmacol.*, **47**, 418-420.

Tötemeyer, S., Booth, N.A., Nichols, W.W., Dunbar, B. and Booth, I.R. (1998) From famine to feast: The role of methylglyoxal production in *Escherichia coli*. *Mol. Microbiol.*, **27**, 553-562.

Tronrud, D.E. (1997) TNT refinement package. *Methods Enzymol.*, **277**, 306-319.

Uchida, K., Khor, O.T., Oya, T., Osawa, T., Yasuda, Y. and Miyata, T. (1997) Protein modification by a Maillard reaction intermediate methylglyoxal. Immunochemical detection of fluorescent 5-methylimidazolone derivatives *in vivo*. *FEBS Lett.*, **410**, 313-318.

van Berkel, W.J.H., van den Heuvel, R.H.H., Versluis, C. and Heck, A.J.R. (2000) Detection of intact megaDalton protein assemblies of vanillyl-alcohol oxidase by mass spectrometry. *Protein Sci.*, **9**, 435-439.

van Dongen, W.D. and Heck, A.J.R. (2000) Binding of selected carbohydrates to apo-concanacalin A studies by electrospray ionization mass spectrometry. *Analyst*, **125**, 583-589.

Vander Jagt, D.L. (1975) Growth inhibitory properties of aromatic α-ketoaldehydes toward bacteria and yeast. Comparison of inhibition and glyoxalase I activity. *J. Med. Chem.*, **18**, 1155-1158.

Vander Jagt, D.L. (1989) The glyoxalase system. In Dolphin, D., Poulson, R. and Avramovic, O. (eds.), *Coenzymes and Cofactors VIII: Glutathione Part A*. John Wiley and Sons Inc., New York, pp. 597-641.

Vander Jagt, D.L. and Han, L.P.B. (1973) Deuterium isotope effects and chemically modified coenzymes as mechanism probes of yeast glyoxalase-I. *Biochemistry*, **12**, 5161-5167.

Vander Jagt, D.L., Han, L.P.B. and Lehman, C.H. (1972) Kinetic evaluation of substrate specificity in the glyoxalase-I-catalyzed disproportionation of α-ketoaldehydes. *Biochemistry*, **11**, 3735-3740.

Vander Jagt, D.L., Hunsaker, L.A., Campos, N.M. and Baack, B.R. (1990) D-Lactate production in erythrocytes infected with *Plasmodium falciparum*. *Mol. Biochem. Parasitol.*, **42**, 277-284.

Vander Jagt, D.L., Robinson, B., Taylor, K.K. and Hunsaker, L.A. (1992) Reduction of trioses by NADPH-dependent aldo-keto reductases. Aldose reductase, methylglyoxal, and diabetic complications. *J. Biol. Chem.*, **267**, 4364-4369.

Veena, Reddy, V.S. and Sopory, S.K. (1999) Glyoxalase I from *Brassica juncea*: Molecular cloning, regulation and its over-expression confer tolerance in transgenic tobacco under stress. *Plant J.*, **17**, 385-395.

Vince, R. and Daluge, S. (1971) Glyoxalase inhibitors. A possible approach to anticancer agents. *J. Med. Chem.*, **14**, 35-37.

Vince, R., Daluge, S. and Wadd, W.B. (1971) Studies on the inhibition of glyoxalase I by *S*-substituted glutathiones. *J. Med. Chem.*, **14**, 402-404.

Vince, R. and Wadd, W.B. (1969) Glyoxalase inhibitors as potential anticancer agents. *Biochem. Biophys. Res. Commun.*, **35**, 593-598.

Volbeda, A., Fontecilla-Camps, J.C. and Frey, M. (1996) Novel metal sites in protein structures. *Curr. Opin. Struct. Biol.*, **6**, 804-812.

Wackett, L.P., Honek, J.F., Begley, T.P., Shames, S.L., Niederhoffer, E.C., Hausinger, R.P., Orme-Johnson, W.H. and Walsh, C.T. (1988) Methyl-*S*-Coenzyme-M Reductase: A nickel-dependent enzyme catalyzing the terminal redox step in methane biogenesis. In Lancaster Jr., J.R. (ed.) *The Bioinorganic Chemistry of Nickel*. VCH Publishers, NY, pp. 249-274.

Wang, W. and Malcolm, B.A. (1999) Two-stage PCR protocol allowing introduction of multiple mutations, delections and insertions using QuikChange™ site-directed mutagenesis. *BioTechniques*, **26**, 680-682.

Watt, R.K. and Ludden, P.W. (1999) Nickel-binding proteins. *Cell. Mol. Life Sci.*, **56**, 604-625.

Westwood, M.E., Argirov, O.K., Abordo, E.A. and Thornalley, P.J. (1997) Methylglyoxal-modified arginine residues-A signal for receptor-mediated endocytosis and degradation of proteins by monocytic THP-1 cells. *Biochim. Biophys. Acta*, **1356**, 84-94.

Westwood, M.E. and Thornalley, P.J. (1995) Molecular characteristics of methylglyoxal-modified bovine and human serum albumins. Comparison with glucose-derived advanced glycation endproduct-modified serum albumins. *J. Prot. Chem.*, **14**, 359-372.

White, J.S. and Rees, K.R. (1982) Inhibitory effects of methylglyoxal on DNA, RNA and protein synthesis in cultured guinea pig keratocytes. *Chem. Biol. Interac.*, **38**, 339-347.

Wiseman, T., Williston, S., Brandts, J.F. and Lin, L.N. (1989) Rapid measurement of binding constants and heats of binding using a new titration calorimeter. *Anal. Biochem.*, **179**, 131-137.

Woese, C.R. (2000) Interpreting the universal phylogenetic tree. *Proc. Natl. Acad. Sci.*, **97**, 8392-8396.

Woese, C.R., Kandler, O. and Wheelis, M.L. (1990) Towards a natural system of organisms: Proposal for the domains Archaea, Bacteria, and Eucarya. *Proc. Natl. Acad. Sci.*, **87**, 4576-4579.

Wu, L.F., Navarro, C., de Pina, K., Quénard, M. and Mandrand, M.A. (1994) Antagonistic effect of nickel on the fermentative growth of *Escherichia coli* K-12 and comparison of nickel and cobalt toxicity on the aerobic and anaerobic growth. *Environ. Health Perspect.*, **102**, 297-300.

Wülfing, C., Lombardero, J. and Plückthun, A. (1994) An *Escherichia coli* protein consisting of a domain homologous to FK506-binding proteins (FKBP) and a new metal binding motif. *J. Biol. Chem.*, **269**, 2895-2901.

Yaari, E., Yafe-Zimerman , Y., Schwartz, S.B., Slater, P.E., Shvartzman, P., Andoren, N., Branski, D. and Kerem, E. (1999) Clinical manifestations of *Bordetella pertussis* infection in immunized children and young adults. *Chest*, **115**, 1254-1258.

Yachandra, V.K. (1995) X-ray absorption spectroscopy and applications in structural biology. *Methods Enzymol.*, **246**, 638-675.

Yamazoye, S. (1936) *J. Biochem. (Toyko)*, **23**, 319-334.

Youn, H.D., Kim, E.J., Roe, J.H., Hah, Y.C. and Kang, S.O. (1996) A novel nickel-containing superoxide dismutase from *Streptomyces* spp. *Biochem. J.*, **318**, 889-896.

Zhang, X.J. and Matthews, B.W. (1995) EDPDB: a multifunctional tool for protein structure analysis. *J. Appl. Crystallogr.*, **28**, 624-630.